AORTIC VALVE MECHANOBIOLOGY –

THE EFFECT OF CYCLIC STRETCH

A Dissertation
Presented to
The Academic Faculty

by

Kartik Balachandran

In Partial Fulfillment
Of the Requirements for the Degree
Doctor of Philosophy in Bioengineering

Department of Biomedical Engineering
Georgia Institute of Technology
May 2010

AORTIC VALVE MECHANOBIOLOGY –

THE EFFECT OF CYCLIC STRETCH

Approved by:

Dr. Ajit P. Yoganathan, Advisor
Georgia Institute of Technology

Dr. Robert M. Nerem
Georgia Institute of Technology

Dr. Hanjoong Jo
Georgia Institute of Technology and Emory University

Dr. Michael S. Sacks
University of Pittsburgh

Dr. Adrian H. Chester
Imperial College, London

Dr. Stephen L. Hilbert
Children's Mercy Hospital

Date Approved: Jan 13, 2010

To my family,

ACKNOWLEDGEMENTS

This dissertation represents more than five years of work and it would not have been possible without the support and encouragement of several people. First and foremost, I would like to thank my advisor Dr. Ajit Yoganathan for taking me on as a student. I am thankful that he had enough confidence in me to put a person with a Mechanical Engineering background into the exciting world of heart valve biology. Apart from research, he has given me the opportunity to mentor students, to travel the world to present my work, and to collaborate with different research groups. These opportunities have definitely provided me a great foundation to begin my academic career.

I would also like to thank Drs. Bob Nerem, Hanjoong Jo, Stephen Hilbert, Michael Sacks and Adrian Chester for being part of my thesis committee. Their critical input has constantly refined and molded my thesis over the last five years. I am especially thankful to Dr. Chester for mentoring and training me during my visit to HHSC in 2007, to Dr. Jo, for allowing me to use the resources of his lab, and to Dr. Sacks for the initial design of the stretch bioreactor.

I would like to acknowledge Holifield Farms, Covington, GA for donating the porcine hearts for this study. This thesis work was supported by the National Science Foundation through the ERC program at Georgia Institute of Technology under award number EEC-9731643, and by the American Heart Association Predoctoral Fellowship award number 09PRE2060605.

Sanity was maintained in the crazy, fast-paced world of the Cardiovascular Fluid Mechanics Laboratory with the help and support of great friends and colleagues. Udayan,

Karan, Nishi, Vivek, Vasudha, Anish, Shruti,Vik and Cecilia, you guys made these last two years normal again. Kartik S, Murali and Philippe, thank you for the enriching conversations on research, sports, XBOX, philosophy and everything else. I will never forget the good times we had together in the lab. Yash, Ayona, Rahul and the rest of the pot-luck gang, thank you for the great food and company. Everyone knows that good research only is possible with good food. Yap, Erin, Hiroumi, Diane, Hélène, Prasad, Jorge, Dr. Boz, Ismail, David, Chris, JP, Brandon, Andrew, Neela, Shiva, Kerem, Zhaoming, Suchitra, Yun, James, Resmi, and Anna, it was amazing working with all of you. I could not have asked for a better set of colleagues and friends here. Chrissy, Christina, Darshin, Kaitlyn, Samiya, Patrick, Mike, Brian, and Phillip, thank you for assisting me in my research. Randy and Casey, thank you for your help in training me in western blotting and RNA extraction. Michelle, Colly, LaKeisha, Gail and Cosetta, thank you all for your assistance in the administrative tasks.

Last, but definitely not least, I am very grateful to my family for providing me with encouragement and loving support. Thank you amma and appa! Amma, I knew you always wanted me to do a PhD and have always pushed me academically. I hope I have made you proud. Thank you Smitha. You have been a constant source of strength and support, and kept me motivated and going even when it seemed like things were not working out. I also appreciate the patience of both our parents and siblings as we went through this journey in Georgia Tech. This thesis is dedicated to them.

TABLE OF CONTENTS

LIST OF TABLES

LIST OF FIGURES

LIST OF SYMBOLS AND ABBREVIATIONS

5-HT	5-hydroxytryptamine
5-HTT	5-hydroxytryptamine transporter
ALP	Alkaline phosphatase
α-SMA	Alpha smooth muscle cell actin
AVEC	Aortic valve endothelial cell
AVIC	Aortic valve interstitial cell
BMP	Bone morphogenic protein
BrdU	5-Bromo-2'-deoxyuridine
BSA	Bovine serum albumin
DAPI	4',6-Diamidino-2-phenylindole
DH_2O	Deionized water
DMEM	Dulbecco's modified eagle medium
DNA	Deoxyribonucleic acid
DPBS	Dulbecco's phosphate buffered saline
EC	Endothelial cells
ECM	Extracellular matrix
F	Fibrosa
GAG	Glycosaminoglycan
H & E	Hematoxylin and Eosin
HSP47	Heat Shock protein 47
IC	Interstitial cell
ICAM-1	Intercellular adhesion molecule 1
IHC	Immunohistochemistry
LDV	Laser doppler velocimetry

MMP	Matrix metalloproteinase
mRNA	Messenger ribonucleic acid
μRNA	Micro ribonucleic acid
OST	Osteocalcin
PVDF	Polyvinylidene fluoride
S	Spongiosa
SDS-PAGE	Sodium dodecyl sulfate polyacrylamide gel electrophoresis
SEM	Scanning electron microscopy
TGF-β1	Transforming growth factor β1
TIMP	Tissue inhibitor of metalloproteinase
TUNEL	Terminal deoxynucleotidyl transferase mediated dUTP Nick End Labeling
V	Ventricularis
VCAM-1	Vascular cell adhesion molecule 1
vWF	von Willebrand Factor

SUMMARY

The aortic valve is a dynamic, elegant structure that functions in a complex mechanical environment interacting with this environment to drive critical cell-extracellular matrix interactions. Altered mechanical forces are believed to trigger changes in valve biology but the cellular and molecular events involved in these processes are not well characterized. The particular phenotypes of aortic valvular endothelial and interstitial cells appear to be dependent on a combination of intrinsic genetically programmed biology and the influence of the local mechanical factors. Studies indicate that pathological mechanical loading experienced by the valve cusps lead to degenerative disease, which is characterized among other things by inflammation, calcification, stenosis, regurgitation and ultimate valve failure.

The objective of the current thesis work was to understand the effects of cyclic stretch on valve mechanobiology with a focus on the key questions that are relevant in understanding degenerative aortic valve disease. An *ex vivo* bioreactor system was built, validated and utilized to subject valve cusp samples to controlled waveforms of cyclic stretch representing normal and pathological conditions. The following aspects of degenerative aortic valve disease were studied. 1) Extracellular matrix remodeling; 2) Aortic valve calcification; and 3) Serotonin-related valvular degeneration via stretch-sensitive receptors in the aortic valve.

Normal physiological magnitude of cyclic stretch was observed to maintain normal extracellular matrix composition and synthesis in aortic valve cusps. Aortic valve remodeling was maximum at 15% stretch, but did not increase with further increases in cyclic stretch magnitude. At 20% stretch, cell apoptosis and proliferation were significantly higher than at the lower magnitudes of cyclic stretch. These results imply

that the valve cells are quiescent at 10% stretch; activated, in a synthetic phenotype at 15% stretch, and in a proliferative phenotype at 20% stretch.

Specific aim 2 sought to elucidate the effects of cyclic stretch on aortic valve calcification. Aortic valve cells were observed to differentiate into an osteoblast-like phenotype resulting in rapid mineralization of the cusp tissue under elevated cyclic stretch (15%). These responses were demonstrated to be strongly BMP dependent, and were also positively correlated with cyclic stretch magnitude. BMP expression was primarily in the endothelial cells, leading to speculation that the endothelial cells are a key mechanotransducer in the valve cusp and effecting downstream signaling and activation of the valve interstitial cell. All stretch responses could be inhibited by the BMP antagonist noggin in a dose-dependent manner, further demonstrating the importance of this cytokine in valve calcification.

In specific aim 3, 5-HT dependent degenerative aortic valve disease was studied. This type of degenerative valvulopathy is observed to occur along with valve thickening, increased cellular proliferation and changes in valve geometry. 5-HT induced valve remodeling was shown to occur via a 5-HT_{2A} receptor-dependent mechanism, increasing collagen synthesis and crosslinking resulted due to the combined effects of 5-HT administration and cyclic stretch. These responses were more prominent at 15% stretch compared to 10% stretch implying that the 5-HT_{2A} receptor subtype is mechanosensitive. Mechanical testing revealed that these changes in collagen biochemistry resulted in transition to the stiffer regime of the valve stress-strain curve at a lower level of strain. This can be mostly attributed to the increased collagen crosslinking as evidenced by increased expression of lysyl oxidase. In addition, increases in collagen synthesis appeared to occur independent of the increased cellular proliferation that was observed. Cell proliferation was in fact primarily influenced by stretch magnitude, but not 5-HT administration.

In conclusion, the importance of cyclic stretch in altering valve remodeling and degenerative disease has been demonstrated in this thesis work. It is hoped that this thesis will inspire further study into the specific mechanobiological mechanisms of different degenerative valvulopathies. This knowledge can then be used to develop treatments that target degenerative valve disease. In addition, the valve tissue responses to elevated cyclic stretch of collagen synthesis and crosslinking can be used as starting points for preconditioning and testing regimes for tissue engineered valve constructs.

CHAPTER 1

INTRODUCTION

Heart valve disease is a serious condition that affects a significant percentage of the population both in the United States and worldwide. According to the American Heart Association, valvular diseases cause nearly 20,000 deaths per year and are related to 42,000 deaths, with aortic valve disease contributing to 63% (222). Worldwide, aortic valve disease is a serious clinical condition, resulting in 170,000 valve replacements per year (9). Aortic valve pathology may be caused by inflammation or increasingly by degenerative valve disease, and also by increasing longevity coupled with rheumatic and infective endocarditis (278). It is also a strong risk factor for other cardiac related deaths (159, 181). Degenerative aortic valve disease is characterized by structural changes such as increased thickness, stiffness and calcification of the leaflets leading to altered function of the entire valve manifesting as aortic stenosis, regurgitation or both (184).

Treatment for heart valve disease depends on the type and severity of the diagnosis. In some cases, such as bicuspid valve disease, only careful monitoring is needed, while in others, medication such as statins can control the symptoms and slow or halt the progression of the disease (199). However, more serious cases require surgery to repair or replace defective valves. Every year, surgeons perform more than 225,000 heart valve operations worldwide, and this number is expected to triple by 2050 (279). Repair options include aortic valve sparing, and aortic root remodeling. Currently, there are multiple options for aortic valve replacement such as mechanical valves, bioprosthetic valves, allograft and autograft valves. Despite the advantages and high success rates of valve surgery, major drawbacks include the need to be on anti-coagulant therapy, the possibility of immune rejection, the ability and skill of the surgeon (in the case of the

Ross procedure), and most importantly, the inability of the replacement valve to grow and remodel *in vivo*. This last point makes it especially disadvantageous for the pediatric population, which requires a "living" valve that is capable of adapting and remodeling itself to humoral and hemodynamic cues *in vivo*.

Recent advances in tissue engineering have spurred the development of tissue engineered valves. The ideal tissue engineered replacement valve is expected be non-immunogenic, since the cells will be harvested from the recipient. Ideally these valves should be manufactured on a commercial scale ensuring "off-the-shelf" availability. Most crucially, they will have the ability to grow and remodel once implanted as they are composed of viable cells. A significant gap in achieving this ideal tissue engineered valve is in the understanding of the proper preconditioning protocols, which are accepted as being required for the development of a durable tissue engineered construct. *In vitro* or *ex vivo* preconditioning has been shown to result in constructs with superior mechanical properties compared to simple static culture or direct implantation (168, 169).

In the context of the aortic valve there is still a relatively poor understanding of the optimum mechanical preconditioning conditions. For this purpose, understanding of the native hemodynamics and the corresponding biological response is critical. Firstly, this information will allow characterization of how a normal valve responds to these mechanical factors will help predict the responses of a tissue engineered construct. Secondly, and perhaps of more importance in the short-term, this will provide insight into the physiological development and pathological remodeling processes of a native aortic valve.

The aortic valve is a dynamic, sophisticated structure which interacts closely with its harsh hemodynamic environment to achieve its elegant function. More specifically, aortic valves stretch during diastole, and flex, stretch and shear during systole (250). Earlier studies have indicated that abnormal hemodynamics (especially hypertension)

experienced by the valve leaflets cause tissue inflammation, which can lead to calcification, stenosis, and ultimate valve failure (72, 159, 162, 205). The expression of particular phenotypes of aortic valvular endothelial and interstitial cells appears to depend on a combination of intrinsic genetically programmed biology and the influence of local hemodynamic environmental factors (164). This dissertation will focus on understanding the effects of cyclic stretch on valve biological responses which has so far been understudied.

Cyclic stretch is one of the forces experienced by the aortic valve during the cardiac cycle which allows the valve cusps to extend and form a coaptive seal with each other during diastole (251, 255, 256). The valve, under normal physiologic conditions, experiences approximately 10% stretch during diastole (141, 250). Preliminary studies in our laboratory using an *in vitro* flow loop and a native porcine aortic valve have also shown that for every 40 mmHg increase in pressure, there is a 5% increase in cyclic stretch (280). Apart from mechanical stimuli, chemical mediators such as 5-hydroxytryptamine (5-HT) or serotonin have been linked to aortic valve disease following reports of valve dysfunction secondary to the appetite suppressants fenfluramine and phentermine (46, 121). In addition, increased circulating levels of 5-HT in the carcinoid syndrome most often lead to valve disease (194). Although structural changes are the main focus of attention in these disease processes, little is known about the changes in the intrinsic biomechanical and biosynthetic properties of the valves secondary to the humoral imbalance caused by these agents. In addition, it is unclear as to how altered mechanical environment will synergize and influence the response of valve cusps to changes in the biochemical environment of the valve.

This thesis research will attempt to understand the effects of cyclic stretch on valve mechanobiology with a focus on the key questions that are relevant in the field today. An *ex vivo* bioreactor system will be built, validated and utilized to subject valve

cusp samples to controlled waveforms of cyclic stretch representing normal and pathological conditions. The following aspects of degenerative aortic valve disease will be studied. 1) Extracellular matrix remodeling; 2) Aortic valve calcification; and 3) Serotonin-related valvular degeneration via stretch-sensitive receptors in the aortic valve.

To provide a proper background and rationale for this thesis, a thorough literature review is presented in CHAPTER 2 leading to the hypothesis and specific aims in CHAPTER 3. The methodology employed in this thesis research is presented in CHAPTER 4 and the results for each of the specific aims are compiled in CHAPTER 5. CHAPTER 6 discusses the results, attempting to synthesize and explain the responses of aortic valves to cyclic stretch on the cellular level, as well as the significance and limitations of the study. The discussion chapter will end with a section on future directions which areas for future exploration. Finally, the dissertation concludes with a summary of the major findings from this study and their implications.

CHAPTER 2

BACKGROUND AND SIGNIFICANCE

This chapter presents the background and clinical rationale for this thesis research. The first few sub-sections will present a literature review of the physiology and anatomy of the heart, the aortic valve and its cellular components. A brief overview of the relation between aortic valve structure, function and mechanics will be included. The next sub-sections will outline aortic valve pathology, the current treatment options available, and current gaps in treating patients with aortic valve disease. The final section will present an overview of aortic valve mechanobiology in relation to degenerative valve disease.

2.1 The Heart and the Cardiac Cycle

The heart (**Figure 2-1**) is a crucial organ in the human body. The primary function of the heart is to pump the deoxygenated blood from the right side of the heart to the lungs and eject the oxygenated blood returned from the lungs to the rest of the circulatory system. A normal heart has four chambers – the left and right atria, and the left and right ventricles (**Figure 2-1**).

The right (deoxygenated) and left (oxygenated) sides of the heart are separated by a muscular wall known as the septum. The right atrium collects oxygen-depleted blood from the vena cavae and pumps it via the right ventricle and the pulmonary arteries to the lungs, where the blood is oxygenated. The oxygenated blood returns to the left atrium via the pulmonary veins and is pumped to the systemic circulation when the left ventricle contracts during systole.

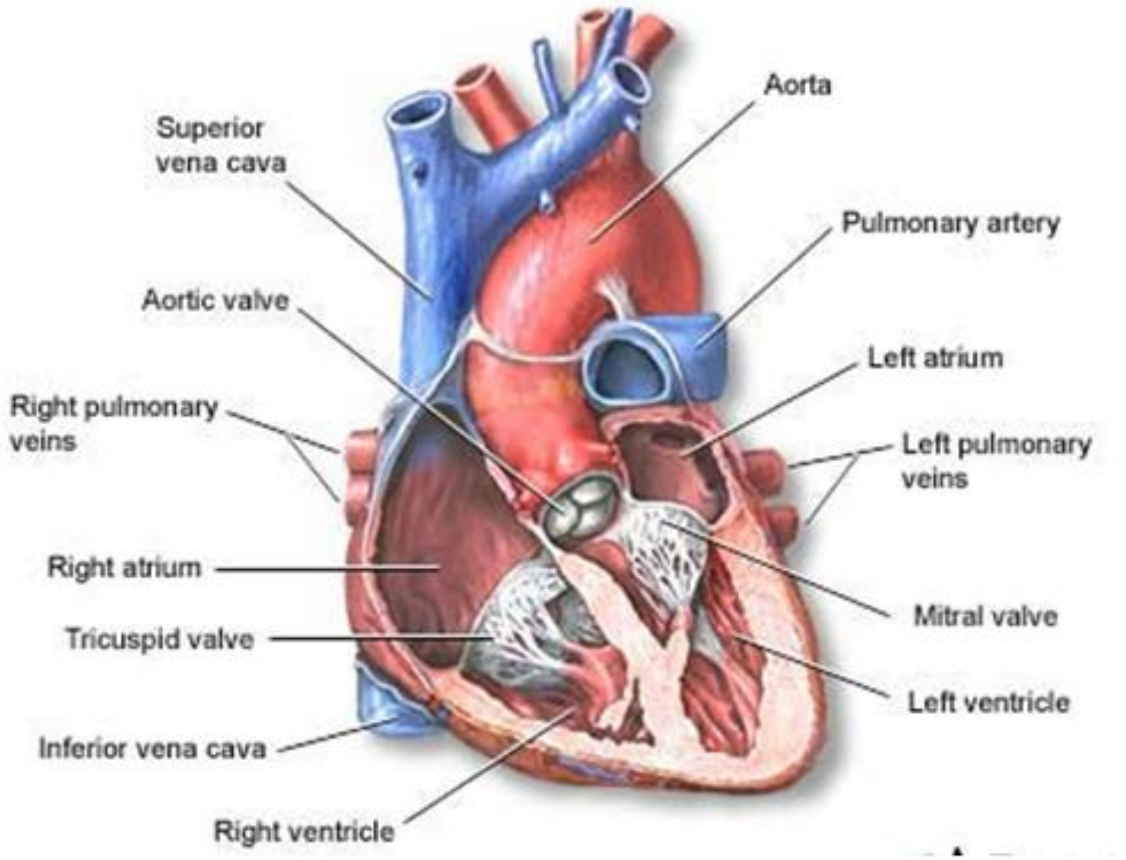

Figure 2-1: Schematic depicting a long axis section of the heart and its various components. Schematic adapted from http://www.nih.gov.

The heart has four valves (**Figure 2-2**): two on each side of the heart in order to maintain unidirectional flow of blood through the heart. These valves can be classified into two types based on their anatomical location: atrioventricular valves (mitral and tricuspid valve) and semilunar or outflow tract valves (aortic and pulmonary valve) (107). The atrioventricular valves have chordae tendinae that attach to papillary muscles on the ventricular walls. This structural feature is absent in the outflow tract valves.

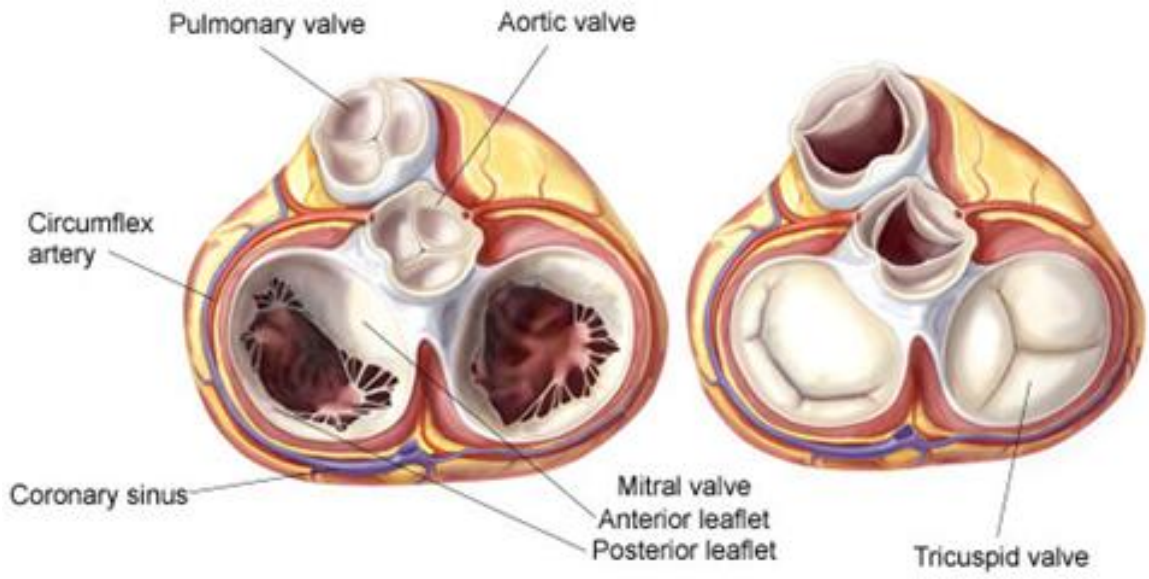

Figure 2-2: Superior, short-axis view of the heart showing the heart valves and their anatomies. Schematic adapted from http://www.mitralvalverepair.org.

The events during a normal cardiac cycle can be divided into seven phases. During **(1) atrial contraction** or atrial systole, the atria contract ejecting blood into the ventricles resulting in a rise in ventricular pressure. A fourth heart sound may be heard at this juncture. At the onset of systole, which is typically 1/3 of the cardiac cycle, **(2) ventricular isovolumic contraction** occurs with the closing of the atrioventricular valves first followed by all the valves. As the name suggests, the ventricular volume remains constant. In the **(3) rapid ejection phase**, as soon as the pressure in the left ventricle exceeded the pressure in the aorta, the aortic valve opens and blood flows rapidly from the ventricle into the aorta. Following rapid ejection, the rate of outflow from the ventricle decreases, and the ventricular and aortic pressures start to decrease in the **(4) reduced ejection phase**. At the end of systole, during the **(5) isovolumic relaxation** phase, the ventricular ejection decreases to zero. The left ventricle pressure falls below the pressures in the aorta and pulmonary artery, which causes the aortic and pulmonary valves to close (beginning of diastolic phase). Once the ventricular pressure falls below the atrial pressure the atrioventricular valves open and **(6) rapid ventricular filling**

begins. During this period, the flow of blood from the aorta to the peripheral arteries continues, and the aortic pressure slowly decreases. This rapid ventricular filling phase is followed by the **(7)** reduced ventricular filling phase in which a large portion of filling occurs. These events are depicted graphically in **Figure 2-3**.

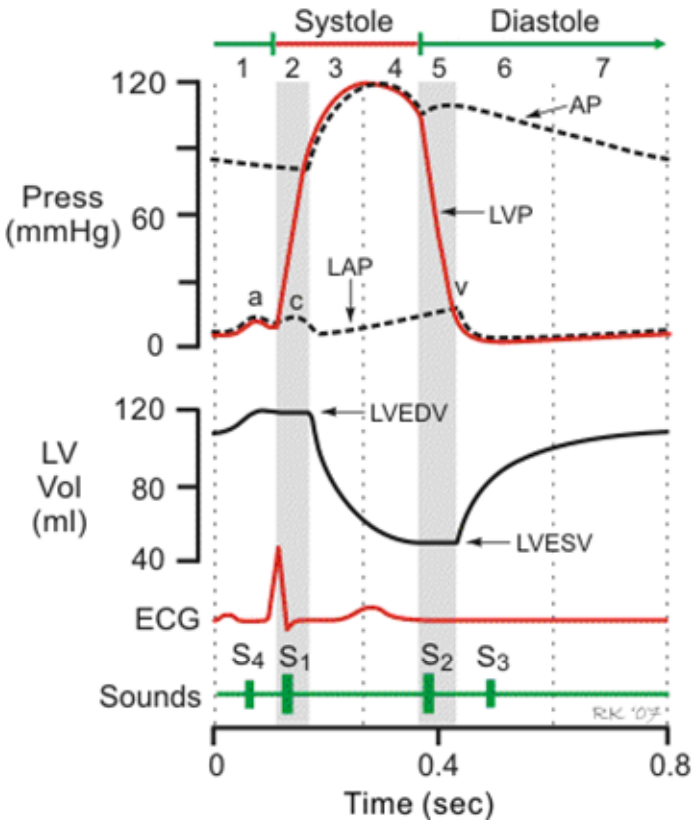

Figure 2-3: The cardiac cycle. The seven phases of the cardiac cycle are labeled here and one can observe the relationship between hemodynamic pressures, ventricular volume, electrocardiogram signals and heart sounds S_1 through S_4 (phonocardiogram). Graph adapted from http://www.ctsnet.org.

2.2 The Aortic Valve - Anatomy

The aortic valve (**Figure 2-4**), which is the focus of this dissertation, is situated at the aortic root and regulates blood flow between the left ventricle and the aorta. It is comprised of three semilunar cusps (interchangeably referred to as valve leaflets in this dissertation) attached to a fibrous annulus embedded within the left ventricle and the septum. The three cusps are attached at the commissures and are named for their anatomical positions within the heart.

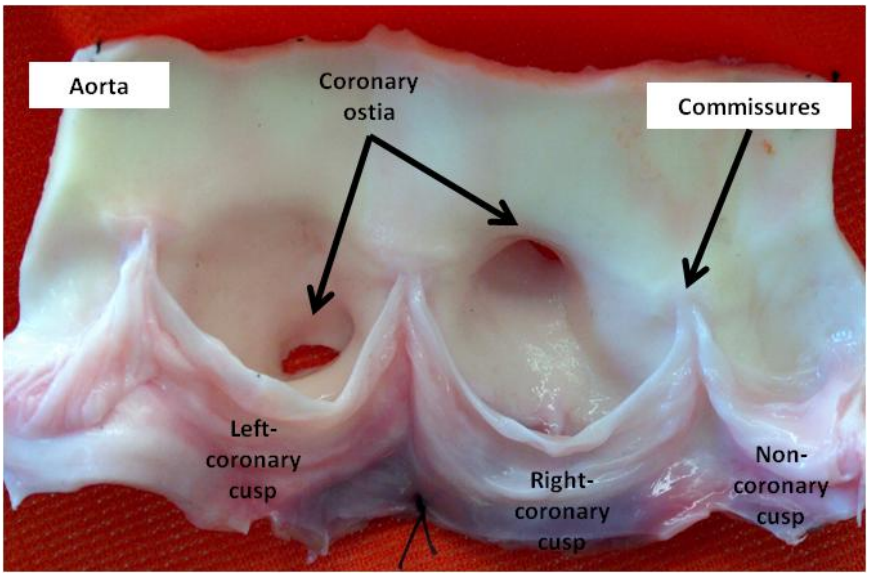

Figure 2-4: An excised porcine aortic valve showing (from left to right) the left-coronary, right-coronary and non-coronary cusps. Other relevant anatomical features are also clearly visible. Of note are the sinuses of Valsalva, and the ostia leading to the coronary arteries.

The sinuses of Valsalva are three elliptical depressions behind each cusp (**Figure 2-5**), which together with the cusps form the functional unit of the aortic valve. The left and right sinuses contain ostia that lead into the left and right main coronary arteries. The third sinus does not feed a coronary artery and is named the non-coronary sinus. A cross-section of the aorta at the sinuses reveals a cloverleaf pattern and a thinner wall thickness compared to regions distal to the sinuses. The sinuses of Valsalva are bounded at the

inferior edge by the basal attachment of the aortic valve leaflet and by the sinotubular junction at the superior edge (**Figure 2-5**).

The aortic annulus is a fibrous ring-like structure composed primarily of collagen that is part of the continuous fibrous skeleton of the heart. It functions to support the aortic valve and the root from the high pressures experienced during systole. It is arranged as three arches in a "crown-like" configuration. The distal part of each arch blends with the fibro-elastic tissue of the aortic valve sinuses. The part that faces the lumen of the aorta blends with the lamina fibrosa of the aortic valve cusps.

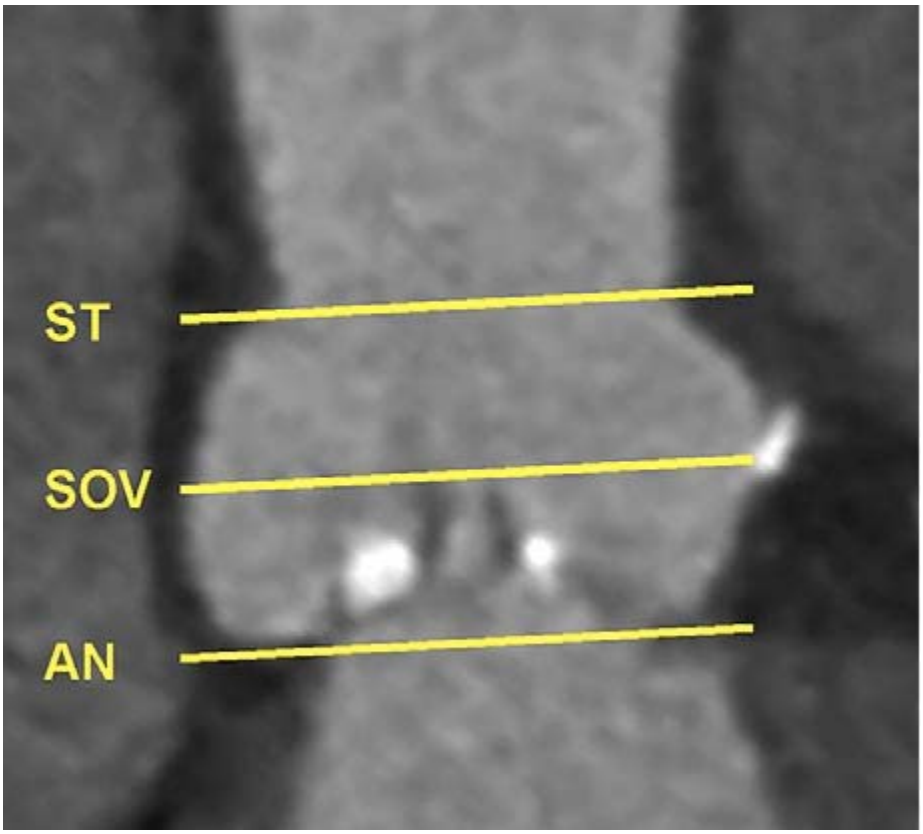

Figure 2-5: Long axis view of the aortic valve depicting the anatomical positions of the sinotubular junction (ST), the sinus of Valsalva (SOV), and the annulus (AN). Coapted valve leaflets are clearly visible. Figure adapted from (4).

2.3 Aortic Valve Cusp Structure

The aortic valve cusps or leaflets are thin, flexible structures that come together and close the valve opening during diastole. Valvular endothelial cells line the aortic and ventricular surfaces of each cusp, so named for the anatomical structures the cusp faces when the valve is closed. These endothelial cells are oriented circumferentially on both the aortic and ventricular surfaces, and form a continuum with the aortic and ventricular endothelium respectively (54). Interestingly, the orientation of these endothelial cells is perpendicular to the direction of flow (54).

Each cusp consists of an ordered arrangement of connective extracellular matrix tissue organized in three distinct layers – the fibrosa, spongiosa, and the ventricularis (217, 250) (**Figure 2-6**). These layers vary in thickness and in the amount and organization of the extracellular components (primarily collagen and elastin) radially across the valve cusp, while being relatively consistent in the circumferential direction (261).

The fibrosa is located immediately below the endothelial layer on the aortic surface of the valve cusp. It is composed of collagen fibers aligned in the circumferential-direction in parallel sheets and bundles, with some interspersed radially-aligned elastin fibers (261). Collagen forms long uninterrupted fibrils that are composed mainly of proline, hydroxyproline and glycine in a triple helical structure. The primary collagens subtypes present in the fibrosa are collagen I, III, and V in an approximate 85:10:5 ratio (250). The matrix of elastin surrounds the collagen bundles to maintain the microstructure of the valve during unloading, and the spaces between the fibers are filled with hydrated proteoglycans or protein polysaccharides. The fibrosa is mechanically the strongest part of the leaflet (239), and is thought to be the major stress-bearing layer within the cusp.

Directly beneath the endothelial cells of the ventricular side of the cusp lies the ventricularis layer of the aortic valve. The main component of the ventricularis is an elastin layer two to several fibers thick, oriented principally in the radial direction, with some collagen interspersed. Elastin is considerably less stiff than collagen (262). It is a coiled hydrophobic structure consisting mainly of the amino acids alanine, valine, leucine, and glycine. As elastin molecules are hydrophobic they are able to slide over one another or stretch to provide for effective coaptation, maintain structural integrity and provide recoil (201). It should be noted that the fibers in the ventricularis have much less directionality than those in the fibrosa (220).

The spongiosa is a loose and watery connective tissue located between the fibrosa and the ventricular. This component is of varying thickness, forming the core of the cusp near the base, proximal to the attachment point at the aortic wall. In contrast, this layer is prominently absent near the free edge. The semi-fluid nature of this layer gives the cusp its deformability, and it is thought that the layer allows the collagen and elastin fibers of the cusp to easily slide over each other as the leaflet deforms during the cardiac cycle. Another function of the spongiosa is to dampen the vibrations in the fibrosa associated with leaflet deformation during diastole (83, 84, 86). The spongiosa consists of radially-oriented collagen fibers and cells. Since the fibers and cells of the core tissue are sparse, its bulk consists of connective tissue, principally glycosaminoglycans and water. Glycosaminoglycans are unbranched heteropolysaccharides consisting of n-acetylgalactoseamine or n-acetylglucoseamine and uronic acid. There are four types of glycosaminoglycans, namely, hyaluronan, the chondroitin/dermatin sulfates, keratan sulfates and the heparan sulfate/heparan, with hyaluronan and the chondroitin/dermatin sulfates representing 90% of total valvular glycosaminoglycans. All except hyaluronan, are covalently linked to core proteins to form proteoglycans. The major types of structurally associated proteoglycans found in cardiac valve extracellular matrix are the

large proteoglycans such as versican and the small proteoglycans such as biglycan and decorin. The large proteoglycans are trapped within the collagen meshwork of tissues as large macromolecular complexes formed through their non-covalent association with hyaluronan (85).

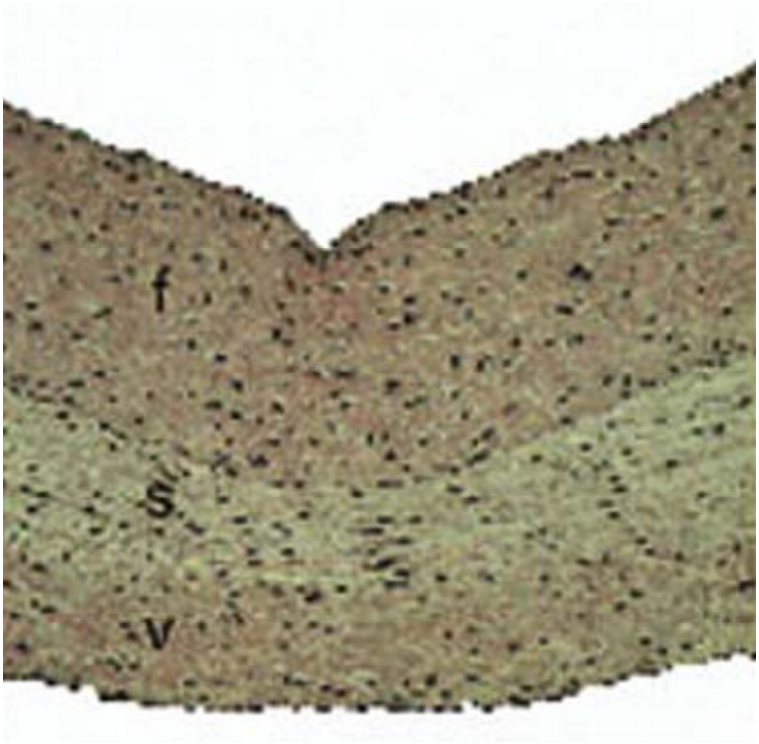

Figure 2-6: Characteristic histologic appearance of a native aortic valve. Three distinct regions are present: the ventricularis (v), the spongiosa (s), and the fibrosa (f). Note the layer of endothelial cells on the two surfaces of the valve and the ridges surface of the fibrosa side compared to the relatively flat, contoured surface of the ventricularis side. Micrograph adapted from (100).

2.4 Aortic valve mechanics and Function

2.4.1 In vivo Tissue Mechanics of the Valve Cusp

The mechanics of soft tissues such as the aortic valve are highly complex: they exhibit highly non-linear stress–strain behavior, undergo large deformations, complex viscoelasticity and axial coupling behaviors that defy simple experiments and material models (212). Much of this behavior is due to strain-induced changes in the internal configuration of the fiber network continuously changing the isotropy of the different layers of the cusp. This involves both straightening of highly crimped collagen fibers and rotation of these fibers towards the axis of stretch (212).

The majority of the stresses and strains experienced by the leaflets occur during diastole and early opening of the valve, and occur because of the complex interplay between the surrounding blood and the valve cusp tissue. Thubrikar *et al* approximated the stresses *in vivo* by assuming that the majority of the pressure load is supported by a combination of bending and membrane stretching (251, 254, 257). They concluded that the total stresses in the leaflet in systole were on the order of 50 kPa during systole and 500 kPa during diastole. The aortic surface of the leaflet appeared to bear the diastolic load, while the ventricular surface bore the systolic load. From their calculations of membrane stress, they determined that the leaflet stretches approximately 10% circumferentially from peak systole to peak diastole. More careful considerations of the geometry of the load bearing surfaces during systole and diastole have generated estimates of maximum physiological leaflet stress between 200 - 400 kPa (42). Using similar methods, Brewer *et al* (22), Thubrikar *et al* (252) and Missirlis *et al* (39, 157) have calculated average *in vivo* leaflet strains to be approximately 10% in the circumferential direction and 40% in the radial direction. In general, the data is pretty consistent across different species.

2.4.2 Material Properties of Aortic Valve Cusps

Considerable study, both experimental and computational, has focused on understanding the mechanical properties of valve cusps. It should be pointed out that the ultimate tensile strength of the aortic and pulmonary valves are on the same order of magnitude at about 1.5 MPa despite the large differences in transvalvular pressures experienced *in vivo* (43, 80). Typical loads experienced by the cusp are about one-tenth of this load. It is clear that these semilunar valves have been designed with a very large "safety factor".

Most material property characterization to date has relied on uniaxial mechanical testing (129, 262). Tests on thin tissue strips, however, cannot mimic the heterogeneous multi-axial deformation fields, combined loading sequences and native fiber kinematics found *in vivo* (212). In addition, valves rarely fail acutely, and of more concern is the ability of the valve to remain sufficiently compliant and coapt efficiently. This phenomenon is typical for materials that must endure many loading cycles without fatigue. As a result, uniaxial failure tests are not necessary and biaxial studies are much more preferable. Flexure studies such as those performed by the Sacks lab (64, 65, 150, 155) provide information on the bending stiffness of the valve cusp, which is directly related to the ability of the valve to coapt effectively. In addition, small angle light scattering studies can be used to study the directionality of the collagen architecture of the valve under different transvalvular pressure loads, and these approaches have also been pioneered by the Sacks lab (210, 211).

Both pseudoelastic and viscoelastic properties of the valve cusp have been studied extensively. The typical pseudoelastic behavior for the aortic valve is depicted in **Figure 2-7**. In the circumferential direction, there is first a very brief initial elastic phase with very low modulus for elasticity that represents the uncrimping of the collagen fibers in the cusp. A transition region follows, occurring at a strain typically representing the

complete uncrimping of collagen fibers. Finally, there is an inelastic tangent modulus phase that represents the complete uncrimping of all collagen fibers and the extension of these same fibers. This extremely stiff circumferential response serves to effectively support the large transvalvular pressure during diastole (42, 43). Radially, there is a much more gradual response since this axis has fewer aligned collagen fibers and mostly elastin fibers. Initially, there is a large toe region where strain increases with little appreciable stress. Then there is a transition leading to a rise in stress where the tissue reaches maximum extensibility. The high compliance exhibited in this initial radial direction toe region represents the ability of the tissue to coapt in response to the diastolic pressures (212).

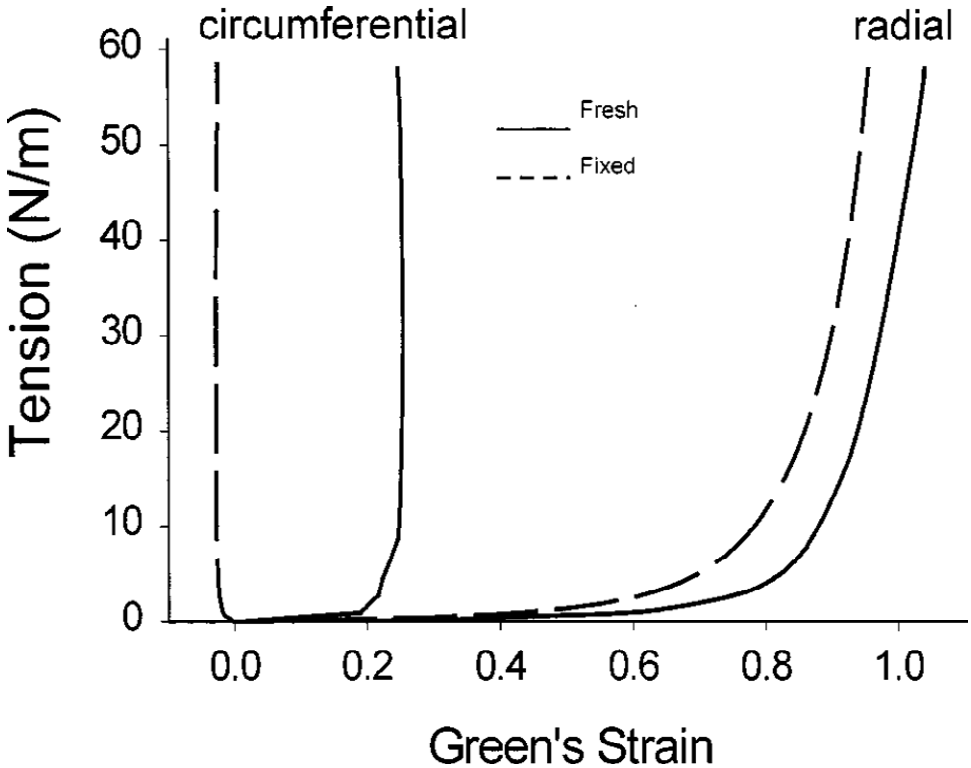

Figure 2-7: Representative circumferential and radial tension–strain curves from a fresh and fixed AV cusp, demonstrating the biphasic pseudoelastic behavior of the aortic valve cusp. The differences in material behavior in the circumferential and radial directions are evident. Adapted from (16).

Early work by Missirlis (156, 157), Barratt-Boyes and Christie (42, 148) reported considerable strain-rate dependence of aortic valve material properties. Later biaxial studies by Sacks and colleagues demonstrated that the valve is indeed strain-rate independent (212). The first set of complete biaxial mechanical data for the constitutive modeling of the aortic valve leaflet was developed by Billiar *et al* (16). Stella *et al* studied the biaxial properties of the different layers of the aortic valve (239). Their results indicated that both layers exhibited very different nonlinear, highly anisotropic mechanical behaviors. The fibrosa layer dominated the tissue mechanical response. However, the ventricularis contributed significantly to radial tension.

Several studies have characterized stress relaxation in porcine leaflets. Notable among those are studies by Vesely (27, 262), Grande-Allen (240)Lee (129) and Sacks (87, 238). These studies reported the relaxation time constants to be approximately 5%/s in both the radial and circumferential directions. Stress relaxation is important because it characterizes the ability of the leaflet to transmit diastolic stress to the aortic root. This property highlights the ability of the leaflet tissue to dynamically reorganize its microstructure. The level of stress remaining in the tissue prior to opening of the leaflets must be carried by the flexion of the leaflet base. Thus it is critical that adequate stress relaxation occur in diastole to ensure long-term function of the leaflets.

2.5 Aortic valve cell biology

The cells contained within the aortic valve play a crucial role in the durability and function of the aortic valve (35). There are two broad categories of cells found in the aortic valve: (i) endothelial cells on the surface of the cusps, and (ii) interstitial cells that populate the body of the valve cups and form an integral network along with the extracellular matrix. Recent studies have demonstrated the important role of the endothelial and interstitial cells in modulating and regulating valve structure and function.

2.5.1 Aortic Valve Endothelial Cells

Aortic valve endothelial cells populate the surface of the aortic valve cusp, and are responsible for maintaining a non-thrombogenic blood contact surface, as well as transmit nutrient, biochemical and mechanical signals to the interstitial cells (23, 73). Aortic valve endothelial cells form single cell monolayers on both cusp surfaces, express von Willebrand factor (132), produce vasoactive agents such as endothelin-1 (77) and nitric oxide (230), exhibit prostacyclin activity (145), and possess cell junctions similar to arterial endothelial cells (145). Another study reported that valvular endothelial cells are oriented circumferentially across leaflets, perpendicular to the direction of blood flow, in contrast to vascular endothelium, which aligns parallel to flow (54). This difference is attributed to the difference in stress pattern in the two tissue types: circumferential in the leaflets and radial in the vessel. This differential alignment was also demonstrated in an *in vitro* setting by Butcher *et al* (24).

Endothelial cells of the aortic valve appear to originate from different sources than either arterial endothelial or ventricular endocardial cells in development (110), which suggests potential reasons the difference in the behavior of these cells compared to other endothelial cell types. In addition, the cells from the outflow and inflow surfaces of

the valve are also thought to originate from different progenitor sources. Intriguingly, Peter Davies and Craig Simmons demonstrated that gene expression profile differs between the endothelial cells on the fibrosa surface and those on the ventricularis surface (53, 227, 228). This can point to potential differences in disease propensity of the two surfaces of the valve cusp. Indeed, one observes a predominantly sclerotic or calcific pathology on the fibrosa surface of the valve cusp, and an endocarditic pathology on the inflow or ventricularis surface (23).

Recent evidence by Jo *et al*, Davies *et al* and others has also pointed to dysfunction in aortic valve endothelial cells as being an important initiator of inflammatory responses related to the initiation of valvular disorders (82, 101, 190, 229). This will be further elaborated in the sub-section on aortic valve disease pathology (**2.8**). In addition, we have shown in our laboratory that endothelial cells can actively regulate the mechanical properties of valve cusps (62).

2.5.2 Aortic Valve Interstitial Cells

Aortic valve interstitial cells are a heterogeneous and dynamic population of specific cell types that have several unique characteristics (132). These cells are responsible for constant renewal and turnover of the extracellular matrix "scaffold", and therefore have a key role in regulating the mechanical characteristics of the valve that are vital for continued valve function (**Figure 2-8**). Indeed, researchers have demonstrated the role of the valve interstitial cell in regulating valve pathology (140). In particular, researchers at the Harefield Heart Science Centre (Imperial College, London) have published several key papers on the different phenotypes of the aortic valve interstitial cell (35, 247-249).

Several cellular phenotypes can be distinguished in the valve interstitial cell population: some are sparsely arranged throughout the valve leaflets, whilst others are

arranged in thin bundles. Three cellular phenotypes have been demonstrated by electron microscopy and immunocytochemistry, both *in situ* and in cells cultured from valves. The myofibroblast, is characterized by prominent stress fibers associated with α-smooth muscle actin expression (164, 247), primarily localized to the ventricularis side of the valve cusp (7, 248). This myofibroblast phenotype is thought to be contractile, proliferative, migratory, and capable of remodeling the extracellular matrix (5). The fibroblast phenotype is characterized by prominent synthetic and secretory organelles and is involved in matrix regulation and production. This phenotype is strongly associated with the expression of prolyl hydroxylase, providing further evidence toward their role in collagen synthesis (35). Apart from these two, a smooth muscle-like cell phenotype has also been observed, with these cells occurring either singly or in thin bundles, and positive for the classic smooth muscle markers of calponin and caldesmon (248). Valve interstitial cells respond to vasoactive mediators such as endothelin-1 and 5-hydroxytryptamine (33-35), further demonstrating behavior similar to smooth muscle cells. Recent electron microscopy images show nerve endings near a valve cell, implying a potential "active" modulation of valve contraction (63).

Among the three cell phenotypes, myofibroblasts are likely to account for a large percent of the interstitial cell population and play an important role in valve function. As mentioned before, this cell type has characteristics of both fibroblasts and smooth muscle cells and can perform the functions of both. They display a highly plastic and diverse phenotype, and can exist as an "active" phenotype in pathological tissue (3). This has been postulated by Aikawa *et al* and the London group. Indeed, the role of the myofibroblast may be critical in ensuring the long term function and viability of the valve cusp. Its role is currently poorly understood.

Liu *et al* further alluded to the phenotypes of interstitial cells as being quiescent, activated, osteoblastic or of progenitor types, with the ability to switch phenotype from

one to the other (138). This review paper suggests that it is important to study phenotype-function relationships and suggests that valve interstitial cells become activated through activation of valve endothelial cells and by inflammation and associated cytokine and chemokine signaling. In pathology, interstitial cells may respond to endothelial denuding injuries by increased proliferation, as has been reported with valve interstitial cells (133). In addition, aortic valve interstitial cellular dysfunction and secretion of TGF-β1 have been implicated in the pathogenesis of valvular calcification (113) and serotonin disorders (113). It is therefore clear that the valve interstitial cell plays a crucial role in the normal function of the aortic valve, and also in the initiation and progression of valve pathology.

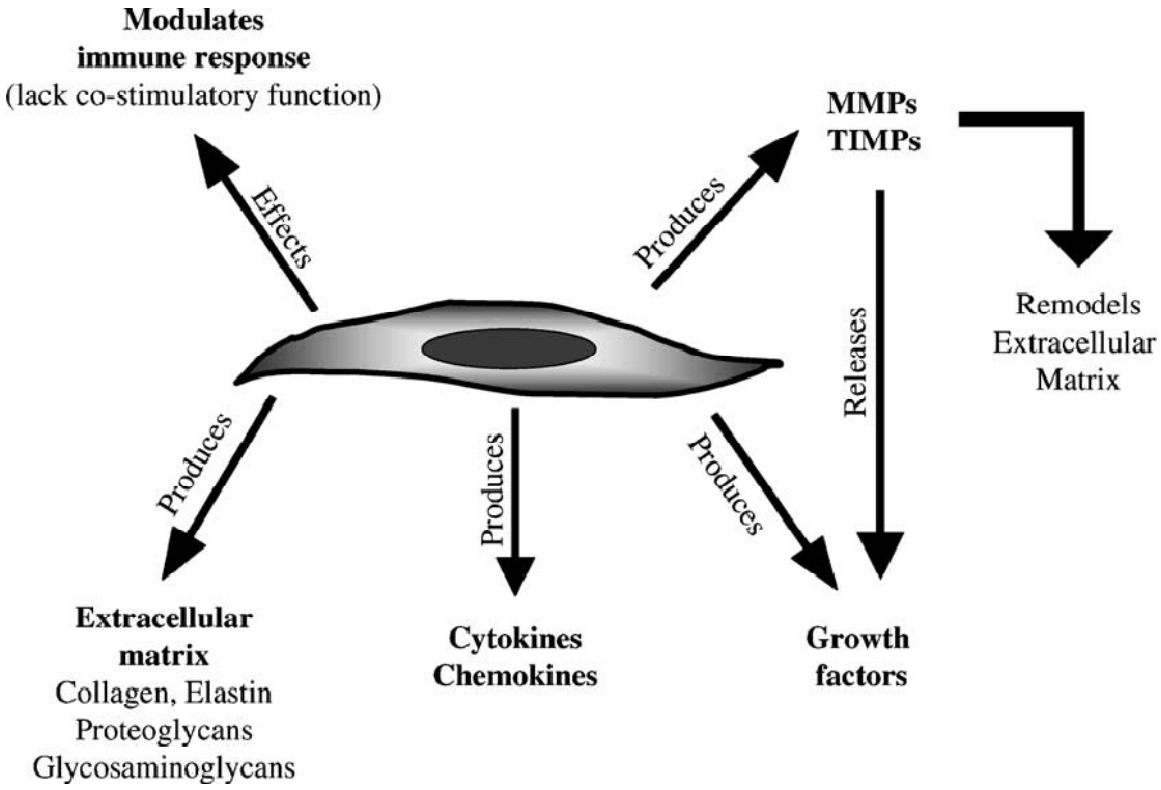

Figure 2-8: Schematic depicting the various cellular roles of the aortic valve interstitial cell. Adapted from (248).

2.6 Degenerative Aortic Valve Disease

2.6.1 Aortic Valve Disease

Aortic valve disease is a significant source of morbidity and mortality. According to the American Heart Association, heart valve disease is responsible for nearly 20,000 deaths per year and is a contributing factor in 42,000 deaths, with aortic valve disease contributing to about 63 percent (222). Worldwide, aortic valve disease is a serious clinical condition as well, resulting in 300,000 valve replacements per year, a number which is expected to triple by the year 2050 (279). It is also a strong risk factor for other cardiac related deaths (159, 181).

While some forms of valve disease can be genetic, and be either inherited or occurring during cardiogenesis, other forms of valve disease are completely epigenetic. Some valvular diseases are acquired as a consequence of other pathologies, such as in chronic renal failure (143, 236). Degenerative aortic valve disease is characterized by structural changes such as increased thickness, stiffness and calcification of the leaflets leading to altered function of the entire valve manifesting as aortic stenosis, regurgitation or both. Although these changes occur in the extracellular matrix, they are a result of active cellular processes leading to collagen synthesis and lipid and calcium deposition (159). Although these structural changes have been thoroughly studied, little is known about the intrinsic regulation of the mechanical and biological properties of the aortic valve leaflets, which ultimately lead to valvular dysfunction. Aortic valve disease can be broadly categorized into two categories: (i) aortic valve stenosis, and (ii) aortic valve regurgitation (**Figure 2-9**).

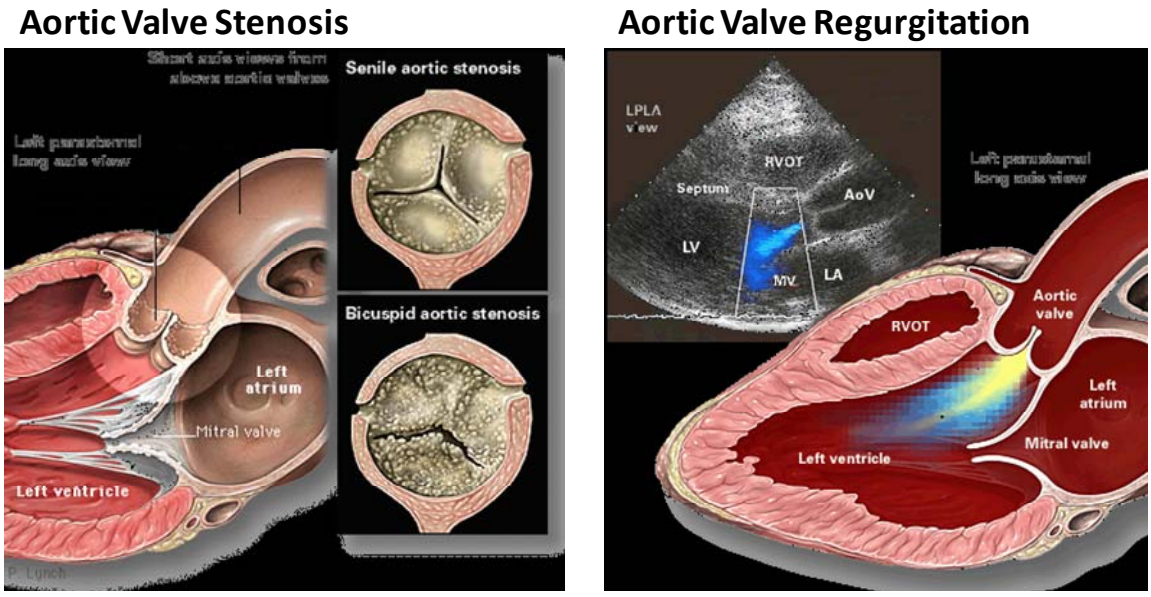

Figure 2-9: Schematics depicting aortic valve stenosis and regurgitation respectively. In stenosis, the cause could be either senile or bicuspid, and the valve is unable to open completely during systole. In valve regurgitation, improper coaptation results in backflow of blood into the left ventricle during diastole. Picture adapted from http://www.med.yale.edu.

2.6.1.1 Aortic Valve Stenosis

Aortic valve stenosis occurs when the valve opening is reduced during systole resulting in a larger pressure gradient between the ventricle and the aorta. That is, the left ventricle has to generate an increased pressure in order to overcome the increased afterload caused by the stenotic aortic valve and eject blood out of the ventricle at the same cardiac output. Indeed, aortic valve stenosis is characterized by the left ventricular pressure being much greater than aortic pressure during left ventricular ejection (shaded region in **Figure 2-10**).

Normally, the pressure gradient across the normal aortic valve is only a few mm Hg. The more severe the stenosis, the higher the gradient between the left ventricular and aortic systolic pressures. For instance, with a mild stenosis, the gradient may be 20 mmHg. However, the pressure gradient can become quite high during severe stenosis

(>100 mmHg). The pressure gradient across the stenotic lesion results from increased fluid resistance and distal turbulence resulting in increased power losses. In fact, aortic valve stenosis is associated with a mid-systolic systolic murmur because of this turbulence. The magnitude of the pressure gradient is determined by the severity of the stenosis and the flow rate across the valve, and can be used as a metric to determine severity of valve stenosis.

Severe aortic stenosis results in i) reduced ventricular stroke volume due to increased afterload (which decreases ejection velocity); ii) increased end-systolic volume, and iii) a compensatory increase in end-diastolic volume and pressure. Due to the increased pressures generated by the left ventricle, the myocardium of the ventricle undergoes hypertrophy. This is seen as thickening of the walls of the left ventricle (162, 170). Usually symmetric, concentric hypertrophy is observed. If the stenosis is severe, aortic valve repair or replacement is a necessity.

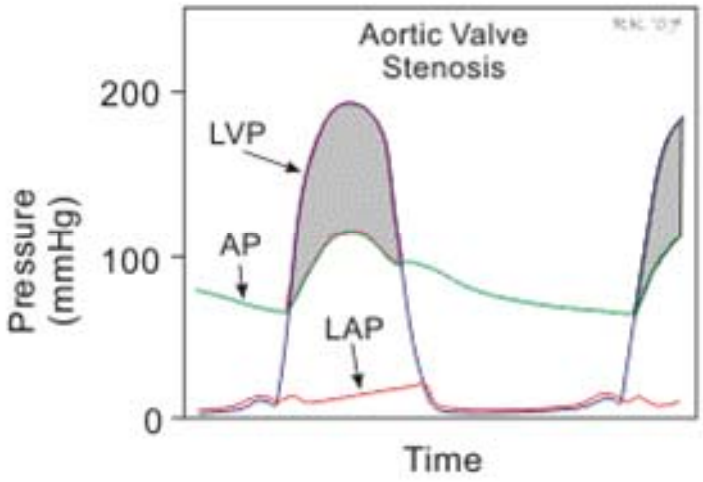

Figure 2-10: Typical pressure curves in the case of aortic valve stenosis. Note the extremely high left ventricular pressure (LVP) during left ventricular ejection. AP – atrial pressure; LAP – left atrial pressure. Picture adapted from http://www.cvphysiology.com/Heart%20Disease/HD004.htm.

2.6.1.2 Aortic Valve Regurgitation

The second category of aortic valve disease is aortic valve regurgitation or insufficiency. In patients with aortic valve insufficiency, there is backflow of blood during diastole from the aorta to the left ventricle due to improper coaptation of the valve cusps. About half of the cases of aortic insufficiency are due to the dilatation of the aortic root, which is idiopathic in over 80% of cases, but otherwise occurs with aging and hypertension, Marfan syndrome, aortic dissection, and syphilis. In about 15% of the regurgitation cases, the cause is innate bicuspid aortic valve, while another 15% of the cases are due to retraction of the cusps as part of post-inflammatory processes of endocarditis in rheumatic fever and various collagen vascular diseases (170).

Aortic regurgitation occurs when the aortic valve fails to close completely and blood flows back into the left ventricle after ejection into the aorta is complete (after heart sound S_2). Normally, there is a brief period of isovolumic relaxation after the aortic valve closes (the mitral valve is also closed at this point). However, when the aortic valve is leaky, the ventricle begins to fill from the aorta after the incomplete closure of the aortic valve. This leads to an increase in ventricular volume prior to the opening of the mitral valve and normal ventricular filling. As blood is leaving the aorta in two directions (back into the heart as well as down the aorta), the aortic diastolic pressure falls more rapidly thereby leading to a decrease in arterial diastolic pressure (**Figure 2-11**). As the ventricle fills from both the aorta and the left atrium, there is a large increase in left ventricular volume and pressure (increased preload). The increased preload causes the left ventricle to contract more forcefully as explained by the Frank-Starling mechanism, thereby increasing ventricular (and aortic) systolic pressure and increasing stroke volume to help compensate for the regurgitation. The increase in ventricular end-diastolic pressure, however, also leads to an increase in left atrial pressure, which can result in pulmonary congestion and edema. Regurgitation, coupled with enhanced left ventricular

stroke volume, results in a characteristic widening of the aortic pulse pressure and can be detected this way. The backward flow of blood into the ventricular chamber during diastole results in a diastolic murmur between S_2 and S_1 (**Figure 2-3**).

Early in the course of aortic valve regurgitation, there is a large increase in left ventricular end-diastolic pressure and left atrial pressure. The ventricle and atria function on a stiffer portion of their compliance curves so that the increased volume results in a large rise in pressure. With long-standing regurgitation, the ventricles and atria dilate so that the increased volume does not result in an exceptionally large increase in pressure. As with aortic stenosis, patients with severe aortic insufficiency must undergo valve replacement therapy or repair.

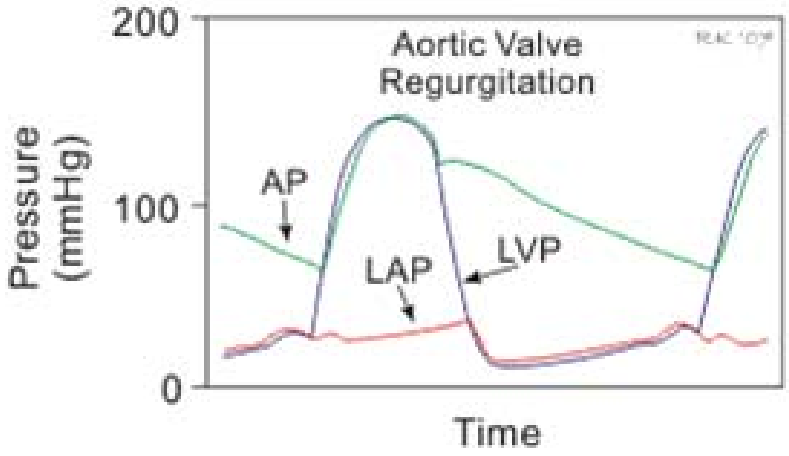

Figure 2-11: During the latter half of ventricular ejection, blood flows backward from the aorta into the left ventricle. Note the higher aortic pressure (AP) compared to the left ventricular pressure (LVP) curve. Aortic systolic pressure increases, aortic diastolic pressure increases, and pulse pressure increases. LAP – left atrial pressure. Picture adapted from http://www.cvphysiology.com/Heart%20Disease/HD005.htm.

2.7 Treatment Options for Aortic Valve Disease

Initial approaches for heart valve pathology aimed at salvaging left ventricular function, and correcting the compromised valve function. However, there was little understanding about the actual implications of these surgeries on valve function. The slow progression of valve disease implies that most patients are unaware of serious valvular complications until it is too late. Therapies include valve repair via sparing surgery, replacement, and sometimes a combination of both. As understanding of the complex functions of the aortic valve grew, so also did advances in surgical techniques and prosthetic designs to preserve valvular structure and prosthetic valve design to mimic valvular hemodynamics. The following section outlines several treatment options used in the clinic today.

2.7.1.1 Valve Replacement

Prosthetic aortic valve replacement has existed since the early 1950's and 60's, beginning with the successful implantation of a mechanical valve in the subcoronary sinus by Dr. Dwight Harken (96). Till today, mechanical replacement valves account for approximately half of the replacement market. Initial designs from the 1950s and 60s were caged-ball type valves, which have a high tendency to forming blood clots, so the patient must have a high degree of anti-coagulation. Tilting disc valves and bileaflet mechanical valves are more popularly utilized today, with more than 200,000 in use currently, as they have better effective orifice area (EOA) and anti-coagulant potential compared to the caged-ball valves. Besides mechanical valves, three other options exist for replacement valves: bioprosthetic, homograft, and pulmonary autograft. Each of these options has their advantages and limitations, and is matched by the surgeon to the particular clinical condition of the patient. The major drawback for these valves is the

need for lifelong anticoagulant therapy to prevent thrombus formation, which could spontaneously clog the valve and lead to sudden cardiac death.

Bioprosthetic (or xenograft) valves were first developed in an attempt to potentially avoid anticoagulant therapy. With the discovery of glutaraldehyde fixation, non-immunogenic xenografts with acceptable shelf-lives became more commonplace (28). Porcine aortic valve tissue and bovine/equine pericardial tissue are normally used, with the former being preferred due to its similarity to the human aortic valve cusps. These valves can come in stented or stentless versions, with the stented versions being easier to manufacture and implant, and with the stentless versions having much better functionality (185). Common failure modes include tissue wear (210) and calcification due to the presence of glutaraldehyde and/or cellular residues (218).

Homograft (or allograft) valves are human aortic or pulmonary valves that are obtained at autopsy, disinfected, and stored until needed for implantation. These valves are generally preferred over other valves because they are identical to the valve being replaced. The obvious disadvantage for these valves is that they are in extremely short supply. Advances in collection, sterilization and storage techniques have dramatically extended the "shelf life" of these valves, and with the advent of cryopreservation, have some cell viability at implantation (174, 175).

2.7.1.2 Valve Repair

In some pathologies, such as aortic root dilatation, the valve cusps themselves are not affected (104). In such situations it would significantly benefit patients to preserve native sinus and cusp tissue. In this regard, a number of aortic valve cusp sparing and repair surgeries have been developed specifically for cases of aortic regurgitation caused by root dilatation or dissection, which are typically conditions that cannot easily accommodate a prosthetic replacement. Techniques used include root remodeling and

aortic valve reimplantation, with techniques mainly pioneered by Magdi Yacoub (214) and Tirone David (52), respectively. Post-operative mortality and long term survivability are generally good, with recurrence of dilatation being a common failure mode (104). The experience and expertise of the surgeon is critical for such surgeries and as such are only practiced at few centers worldwide (104).

2.7.1.3 Ross Procedure

The pulmonary autograft or Ross procedure (**Figure 2-12**) was first developed by surgeons and researchers who recognized the similarity in morphology between the aortic and pulmonary valves. The pulmonary circulation experiences transvalvular pressures on the order of 15 mmHg and would therefore tolerate a replacement valve much better than one in the aortic position. The pulmonary circulation is the higher pressure side of the heart throughout cardiovascular development, so it was thought that this valve would function well in the high pressure aortic position in adults. Indeed, pulmonary valves cultured under aortic valve mechanical conditions show the potential to remodel their matrix to better withstand the higher pressure conditions (109). First developed by Dr. Ross, it is preferred as it provides a living valve in the critical aortic position. However, this procedure because it demands extreme technical expertise and failure would then result in two damaged valves. As a result, this surgery is performed in only a few centers around the world, albeit with highly favorable results (30).

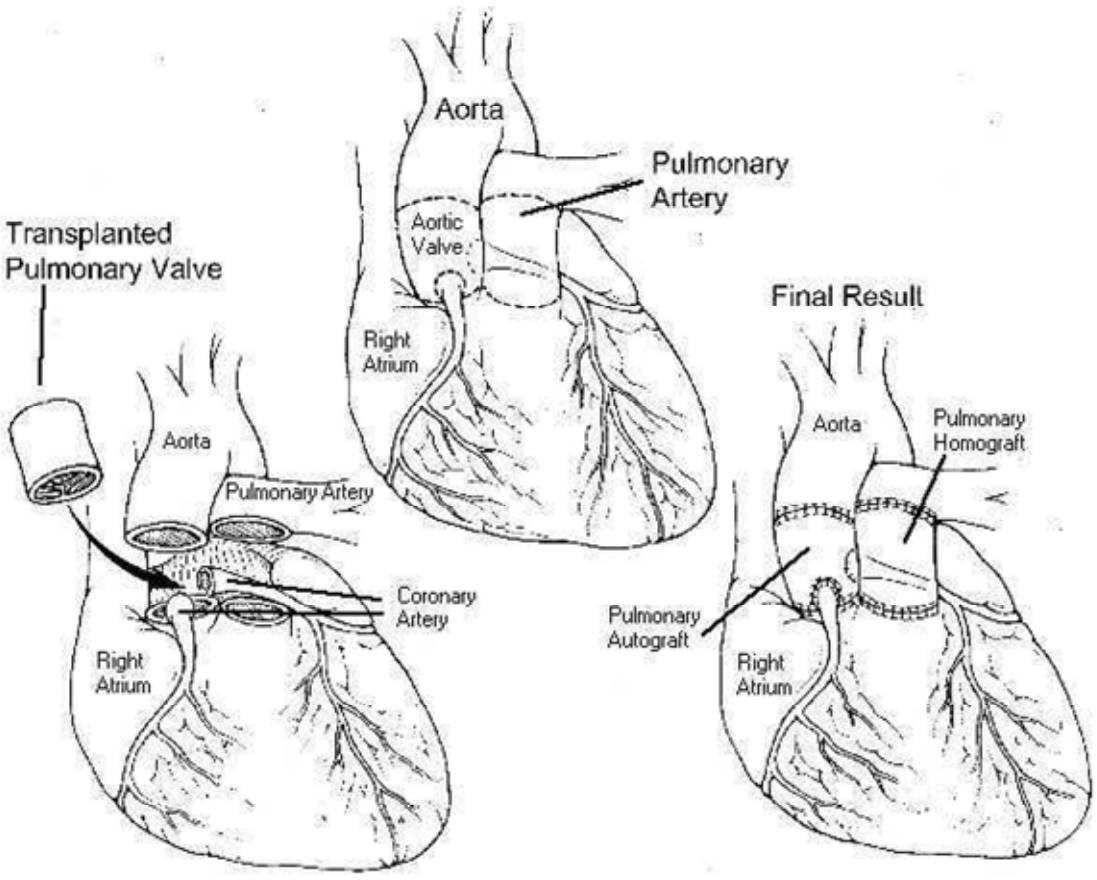

Figure 2-12: The Ross procedure replaces a diseased aortic valve with the patient's own pulmonic valve. The pulmonic valve is in turn replaced by a homograft valve or a mechanical valve. This is well tolerated as the pulmonary valve is under lower pressure load compared to the aortic system. However, success is very dependent on the skill of the surgeon. Adapted from http://www.csmc.edu.

2.7.1.4 Limitations of Current Treatment Methods

While the abovementioned solutions can treat valve disease and help preserve cardiac function in the short-term, they tend to fail over time due to a variety of reasons. Mechanical valves have superior durability, but suffer from incidents relating to thrombus and coagulation. As mentioned earlier, tissue valves suffer from tissue degeneration and calcification. Continued root and valve degeneration and subsequent redilatation are common failure modes for the repair procedures. In addition, all prosthetic valves are at an increased susceptibility to bacterial infection (263).

2.7.1.5 The Ideal Replacement: Heart Valve Tissue Engineering?

There are several characteristics of an ideal replacement aortic valve. It should be durable enough to thrive and be functional long-term in the harsh mechanical environment of the aortic position. It should be non-thrombogenic, and it should be able to remodel according to the needs of the patient. The ultimate goal is for a tissue engineered valve to mimic and even become identical to the valve it is replacing (224, 231, 232). This field involves the optimization of combining living cells, a matrix-like scaffold and mechanical or biochemical stimulation factors to create a living tissue (128). Ideally, this tissue would be preconditioned to a certain level of mechanical strength and functionality, and implanted, where it will be able to remodel according to the organ's needs and integrate itself seamlessly over time (89, 128).

With respect to aortic valve tissue engineering, the field has seen tremendous progress over the last decade. While most research has focused on the development of appropriate scaffold materials and cell types (224, 231, 232, 237, 242), crucial aspects of research include understanding the biology and more importantly the mechanobiology of valve disease progression. In particular, the effect of mechanical forces on valve biology cannot be ignored in the quest for an optimum tissue engineered valve replacement.

2.8 Degenerative Aortic Valve Disease Pathobiology

As mentioned earlier, valvular degeneration is characterized by the development of stenosis and/or insufficiency, and by the time it has clinically manifested it is usually only treatable by surgical repair or prosthetic valve replacement (11). Early intervention, and pharmacological or molecular treatment would require a very thorough understanding of the key molecules involved in the progression of valve disease.

Studies of diseased valves reveal a wide spectrum of pathology, including inflammation, sclerotic and calcific lesions, thrombus formations, bacterial vegetations, and fractured matrix fibers (95, 180, 183). Aortic valve disease was originally thought to be a passive process of fatigue over time, but recent evidence suggests that it is an active biological and pathophysiological response of the valves, involving inflammation, oxidation, cell differentiation, fibrosis, possible calcification and ossification (130, 197, 246). Several studies (55, 120, 158, 162, 241, 254) suggest correlations between hemodynamics and valve structure to pro-calcific probability, such as in congenital bicuspid occurrences (202, 204). Strong associations between atherosclerotic risk factors and valve disease suggest that atherosclerotic processes may be involved (59). Finally it has been demonstrated that valvular calcification can be induced by agents that accelerate vascular calcification (such as 25-hydroxycholesterol) (162).

The following sub-sections will outline a review of the degenerative disease pathways explored in this dissertation, namely, elevated matrix remodeling, calcific aortic stenosis and serotonin-related aortic valve degeneration. **Figure 2-13** depicts the potential interplay between various atherogenic and genetic factors that can lead to ultimate valve disease. The close link between matrix remodeling and ultimate valve disease can be observed here.

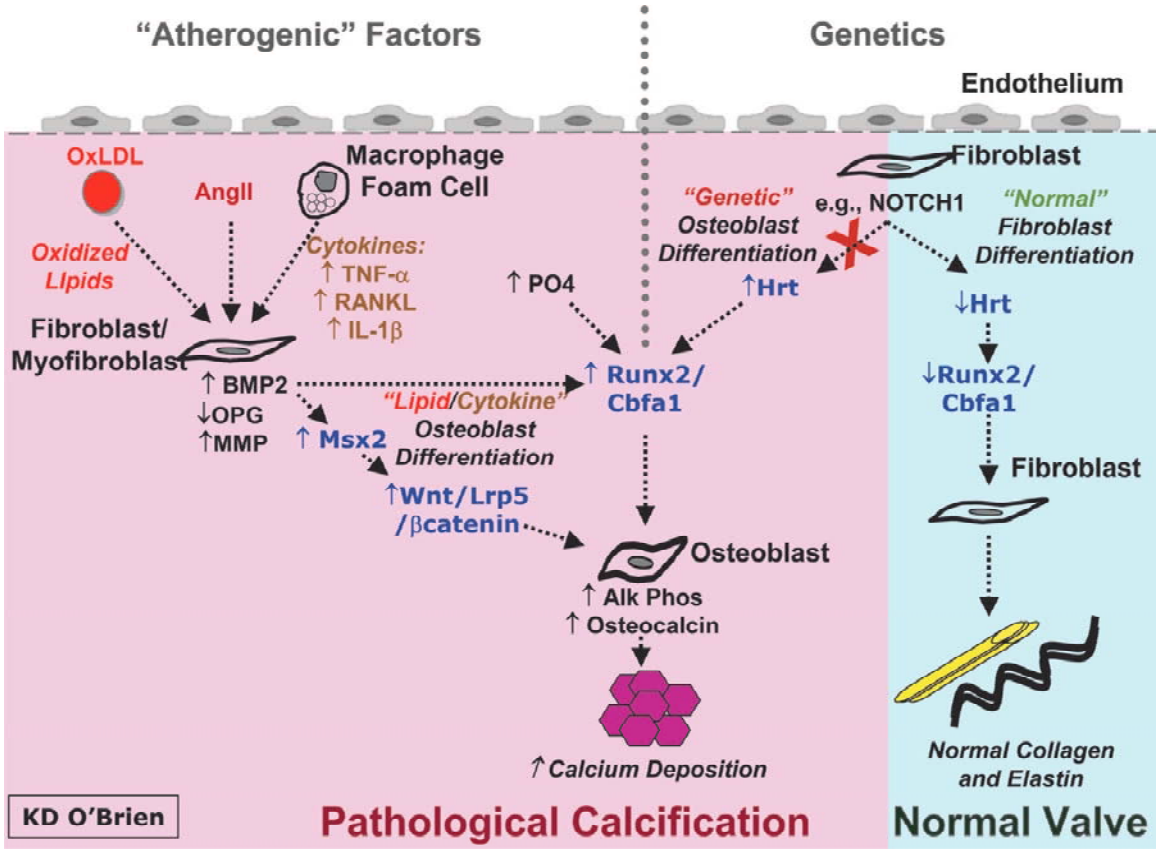

Figure 2-13: Potential interplay between genetic and atherogenic factors in the pathogenesis of valve calcification. Potential mechanisms include upregulation of MMPs and BMPs leading to activation of Wnt/Lrp5 or Runx2/Cbfa1 pathway leading to differentiation of the valve interstitial cell to an osteoblast-like phenotype. Schematic adapted from (171).

2.8.1 Elevated Extracellular Matrix Remodeling and Inflammation

Aortic stenosis and regurgitation, which are clinical manifestations of aortic valve disease, have been correlated in several patients with over-expression of proteolytic enzymes such as matrix metalloproteinases (MMPs), their tissue inhibitors (TIMPs) and cathepsins (71). During normal homeostasis in the aortic valve, there is balance between extracellular matrix biosynthesis and degradation maintained by these enzymes (17). A perturbation of this delicate equilibrium can lead to pathological remodeling of the tissue matrix and compromised valve function (71). A number of these cathepsins, MMPs and

TIMPs, are also involved in key cellular processes such as apoptosis, proliferation, and cell differentiation, and have demonstrated roles in valve disease pathways (57). Cathepsins K, L, and S, which are potent elastolytic proteases, have been associated with atherosclerotic plaque progression (245), and myxomatous heart valves (191) as demonstrated by Aikawa *et al*.

It is also thought that macrophages can potentially infiltrate the valve endothelium and release cytokines that act on valvular fibroblasts to promote elevated cellular proliferation and extracellular matrix remodeling (74, 180, 181). A subset of valvular fibroblasts within the fibrosa layer then differentiate into "activated" myofibroblasts. Low density lipoprotein that is taken into the sub-endothelial layer is oxidatively modified and taken up by macrophages to become foam cells. Angiotensin converting enzume is colocalized with apolipoprotein B and facilitates conversion of angiotensin II (AngII), which acts on angiotensin 1 receptors, expressed on valvular myofibroblasts. A subset of valvular myofibroblasts then further differentiate into an osteoblast-like phenotype that is capable of promoting calcium nodule and bone formation. These pathways are described in the schematic in **Figure 2-14**.

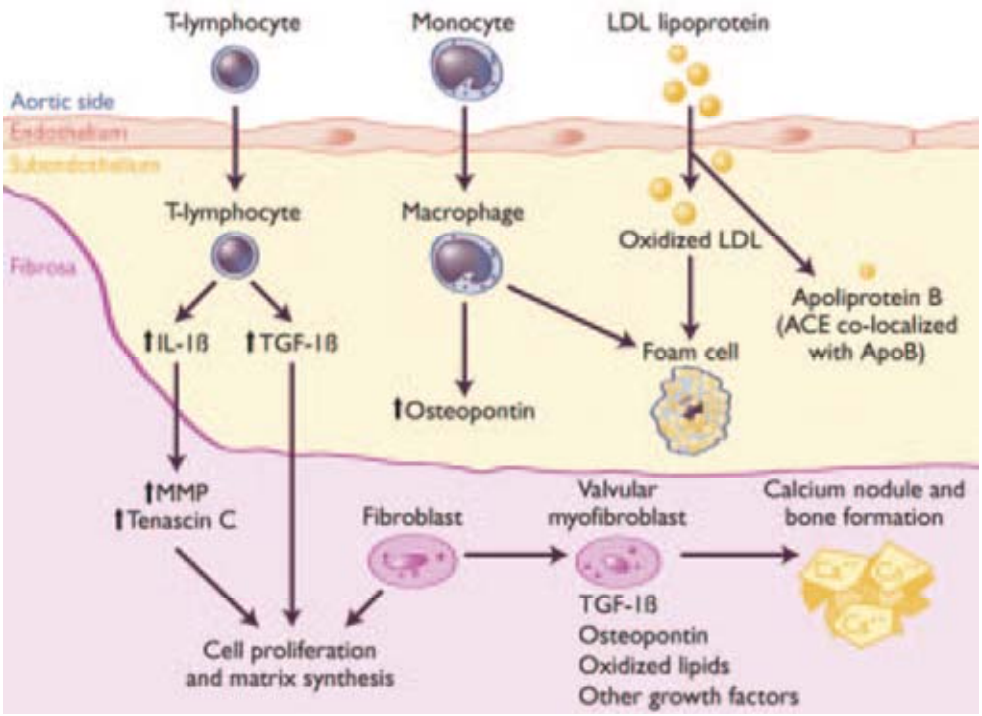

Figure 2-14: Potential pathways depicting inflammation and matrix remodeling leading to ultimate valvular calcification. IL – interleukin; TGF – transforming growth factor; MMP – matrix metalloproteinase. Schematic adapted from (74).

2.8.2 Calcific aortic stenosis

Interstitial valvular calcification is characterized by accumulation of extracellular matrix proteins such as collagen (183), excessive tissue remodeling, the presence of bone-related factors including tenascin-C, osteopontin, osteonectin, matrix gla protein-1 (MGP-1), bone morphogenic protein (BMP)-2/-4, transforming growth factor (TGF)-β (112, 113, 161, 173), the frequent appearance of osteoblast-like cells (161, 197), focal calcification and lamellar bone formation in the fibrosa. The presence of ectopic bone and bone-related proteins in calcified valves suggests calcification can occur through active induction of bone formation via valvular interstitial cells. Aortic valve interstitial cells have been shown to spontaneously form calcified bone nodules in culture (160). The nodules are composed of apoptotic cells and hydroxyapatite mineral. They are

surrounded by viable osteoblast-like cells that express alkaline phosphatase, BMP-2/4, osteopontin, and osteocalcin. Nodule formation is stimulated by TGF-β1 and 25-hydroxycholesterol, and is inhibited by statins (273). Factors regulating the phenotypic conversion of aortic valve interstitial cells to osteoblast-like cells *in situ* are largely unknown.

In humans (173, 183) and pigs (227), calcific lesions tend to occur in the fibrosa, below the endothelium that lines the aortic surface of the leaflet, where they are exposed to complex and unstable hemodynamic conditions (172, 182, 226). In contrast, the ventricular side of the leaflets, which is exposed to relatively stable hemodynamic conditions, is spared from the diseases (226). The findings that BMP-2/4 expression, reactive oxygen species (ROS) production, accumulation of inflammatory cells, and calcification occurring in close proximity to each other in the fibrosa side suggest that factors such as BMP produced in endothelium by the *unfavorable hemodynamic and mechanical conditions* may be a paracrine mediator leading to side-specific lesion development. Both Peter Davies' group and Hanjoong Jo's group using porcine aortic valves and aortic valve endothelial cells have found that BMP-4 mRNA and protein expressions are higher in the aortic side of the valve cusp than that of ventricular side (26, 227). This distinctive side-specific phenotypic difference of aortic valve endothelium *in vivo* further supports the hypothesis that BMP-4 is a mechanosensitive gene product, which may be involved in the side-specific inflammation and calcification of the leaflets.

2.8.2.1 Bone Morphogenic Proteins and their Antagonists

The bone morphogenic protein (BMP) was originally discovered as a bone-formation inducing protein (136). The BMPs are the members of transforming growth factor-β (TGF-β) super family. This super family consists of TGF-βs, inhibins, bone morphogenetic proteins, growth differentiation factors, anti-mullerian hormone, activins,

and myostatin (146). More than thirty BMP proteins have been identified, and the BMP-2/4 and BMP-5/6/7 classes are the best characterized members. BMPs have critical and diverse role that now include embryonic development, patterning, cartilage formation, and cell differentiation (103, 146).

BMPs (-2 and -4) are mechanosensitive, pro-inflammatory, pro-oxidative, pro-osteogenic and atherogenic cytokines. Recent studies from Jo *et al* and others have shown that BMP-2 and -4 are produced from endothelial cells in response to high pressure and oscillatory shear, respectively (50, 234, 235). Once produced, both then stimulate NADPH oxidases and ROS production, which eventually lead to ICAM-1 induction and monocyte adhesion (49, 117, 234, 235). The importance of BMPs including BMP-2 and -4 in aortic endothelial cells and atherosclerosis have been demonstrated by its findings in calcified atherosclerotic plaques (56), in endothelium overlying foam cell lesions and in cultured endothelial cells exposed to oscillatory shear stress (234, 235). Exposure of cultured endothelial cells to oscillatory shear induces BMP-4 expression at the transcriptional level (235). Secreted BMP-4 is then believed to bind to the cognate receptors, activating signaling pathways (235). The signaling pathways result in induction of NADPH oxidase components nox1, which is responsible for reactive oxygen species (ROS) production (108, 235). Although the detailed pathways still need to be defined, shear- and BMP-4-induced ROS production leads to activation of smad- and NFkB-pathways, which in turn is responsible for ICAM-1 induction and increase in monocyte adhesion (234).

BMP-4 has been identified as a protein that induces ectopic bone and cartilage formation when implanted in rats (146). Unlike TGF-β, BMPs are secreted as active proteins and their activities are counterbalanced by secreted antagonists such as chordin and noggin (147). BMP-4 directly binds with high affinity to chordin (K_d= 300 pM) or noggin (K_d= 20 pM) (285). Binding of BMP-4 to its antagonist prevents it from binding

to its cognate receptor. Although BMP-7 can also interact with noggin, it does so with a very low affinity (51). Furthermore, noggin and chordin do not bind TGF-β1 or activin (67). Due to its relatively specific effect, noggin has been used as a valuable tool to dissect BMP function in cells and tissues (234). In addition, Jo and colleagues have been successful using synthetic siRNA duplexes to specifically knockdown BMP-4 expression and function in endothelial cells (234). Pharmacological methods using noggin will be explored in this thesis in order to understand if BMPs are important mechanosensitive mediators of aortic valve disease.

2.8.3 Serotonin-Related Valve Degeneration

2.8.3.1 Serotonin, Serotonin Receptors and the Serotonin Transporter

Serotonin or 5-hydroxytryptamine (5-HT) is a neurotransmitter synthesized in serotonergic neurons in the central nervous system (33). Outside the central nervous system, where 95% of the total 5-HT content of the body is found (97), 5-HT is localized mainly in the enterochromaffin cells of the gut and participates in the regulation of intestinal motility, fluid secretion, and regional blood flow (81). The major breakdown product of 5-HT is 5-Hydroxyindoleacetic acid (5 HIAA), which is excreted in the urine. The entire process of 5-HT synthesis to reuptake is depicted in **Figure 2-15**. Various cell culture studies have shown the mitogenic effects of 5-HT on smooth muscle cells, osteoblasts, fibroblasts and endothelial cells (97, 166). It also has diverse cardiovascular effects which can be attributed to the existence of multiple different receptor subtypes that can control both vasoconstriction ($5\text{-}HT_2$) as well as vasodilation ($5\text{-}HT_1$) (76).

There are a total of fifteen 5-HT receptor subtypes which can be further divided into seven subfamilies ($5\text{-}HT_1$ – $5\text{-}HT_7$) (277). Of these, the $5\text{-}HT_3$ receptor is a ligand-gated ion channel while the others belong to the family of G-protein coupled receptors. These receptors work via activating intracellular second messenger cascades (277). Studies have reported that the $5\text{-}HT_{1B/IC}$ and $5\text{-}HT_{2A/2B}$ receptors are expressed in human, porcine and canine aortic valves (70, 207).

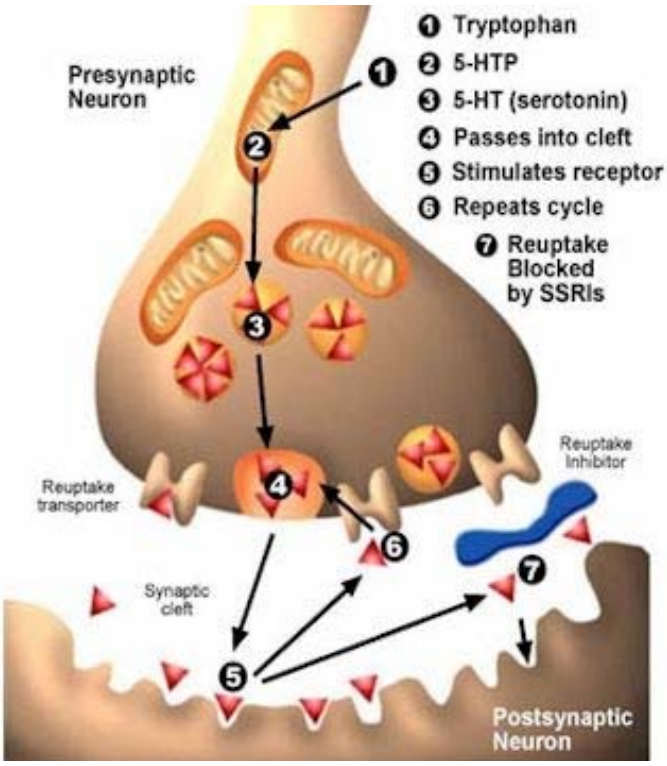

Figure 2-15: Illustration of 5-HT and its transport. **1:** Tryptophan enters system; **2:** Converts to 5-hydrohytryptophan (5-HTP); **3:** 5-HTP converts to 5-HT; **4:** 5-HT passes into synaptic cleft; **5:** 5-HT acts and stimulates its receptor; **6:** 5-HT joins with 5-HT reuptake transporter (5-HTT); **7:** Reuptake inhibitors (i.e. selective serotonin reuptake inhibitors) increase systemic levels of 5-HT by inhibiting reuptake. (Image from www.vrp.com)

After release and action, 5-HT is rapidly taken up by an active transport mechanism into a number of cell types, with platelets serving as the major reservoir (91). The 5-HT transporter (5-HTT/SERT) is a monoamine transporter transmembrane protein that transports serotonin from synaptic spaces into presynaptic neurons (105). It is also present in platelets and pulmonary vascular cells (149). There has been evidence that 5-HTT and other neurotransmitter transporters are tightly regulated via activation of protein kinase C (92). 5-HTT is responsible for 5-HT uptake and subsequent inactivation of the amine passing through the lung (149). Most crucially, 5-HT reuptake inhibitors, also known as selective serotonin reuptake inhibitors (SSRIs) can increase synaptic and systemic levels of 5-HT by inhibiting the reuptake of 5-HT. This mechanism has been

utilized in drugs that treat depression (e.g.: fluoxetine) (44, 200). It should be noted that the 5-HTT is also present in valvular cells (149).

2.8.3.2 5-HT Mechanisms – Relevance to Valve Disease

5-HT overproduction is known to cause valvular heart disease in patients with carcinoid tumors (47). Left-sided carcinoid disease is reported in about 15% of total carcinoid population (47). This can be primarily attributed to the clearing of 5-HT by the reservoir of 5-HTT in the pulmonary vascular cells (149). However, it remains important to study these in the context of left-sided valves due to the often severe hemodynamic consequences of the disease (i.e. valve insufficiency) (12, 13). Indeed, valve replacement surgery is often the only option for these patients (13).

The development of certain anti-depressants and appetite suppressant drugs have utilized 5-HT mechanisms due to the role of 5-HT in regulating modulation of anger, aggression, mood, sleep, appetite, and metabolism (135). Recent clinical and *in vitro* studies however have reported that there are significant cardiovascular risks associated with pharmacological agents acting via 5-HT and 5-HTT mechanisms.

1. Severe (grade 3 or 4) aortic regurgitation was observed in patients being treated with ergot-derived dopamine receptor antagonists, compared to patients on non-ergot derived dopamine antagonists (106).
2. Individuals treated with the diet drug combination of fenfluramine-phentermine (Fen/Phen) developed aortic insufficiency and valve fibrosis and plaque-like encasement comparable to that of carcinoid disease and ergotamine-induced valve disease (46). These patients also demonstrate symptoms of pulmonary hypertension and cardiac arrhythmias (69, 165).

3. A recent study on rats has shown that daily injection of serotonin resulted in elevated serum 5-HT levels as well as left- and right-heart valvulopathies (91).
4. Levy *et al* reported that 5-HT addition to cultured sheep aortic valve interstitial cells resulted in increased TGF-β1 mRNA expression and activity, which may potentially result in calcific valve degeneration (114). This same study also demonstrated that 5-HT results in increased collagen biosynthesis on cultured sheep aortic valve endothelial cells.
5. A mouse study demonstrated that those 5-HTT-knockout mice develop collagen accumulation, cardiac fibrosis and myocardial dysfunction (149). This study in particular demonstrates that inefficiencies in 5-HTT reuptake can increase risk of 5-HT associated valve disease.

As mentioned earlier, 5-HT-mediated responses occur via the 5-HT receptor and the 5-HTT protein. It is therefore important to analyze the relation between 5-HT receptors and the 5-HT transporter for any 5-HT related pathologies. In the case of Fen/Phen, it was originally thought that 5-HT levels would increase in patients. However, the opposite was the case (135). Fenfluramine (Fen) was known to behave as a 5-HT receptor agonist as well as a 5-HTT protein substrate (135). Phentermine (Phen) on the other hand is a monoamine oxidase inhibitor, and therefore would result in delayed breakdown on 5-HT (206). It is therefore possible that the combined effect of this drug is to prevent 5-HT transmembrane transport and breakdown, thereby increasing the number of 5-HT-to-receptor interactions, thus increasing the observed mitogenic and synthetic effects of 5-HT.

2.8.3.3 5-HT Receptors and their Mechanosensitivity

Previous studies have demonstrated the presence of 5-$HT_{1B/1C}$ and 5-$HT_{2A/2B}$ receptor subtypes present in human and porcine aortic valve cells (70, 207). The 5-HT_2 subtype was initially hypothesized to be the primary target of 5-HT agonists such as Fen. Indeed, Xu *et al* (277) demonstrated that the 5-HT_2 receptor is involved in 5-HT-mediated G-protein signal transduction and extracellular signal-regulated kinase (ERK 1/2) signaling. Protein kinase inhibitors and Src inhibitors resulted in attenuation of ERK signaling, while a 5-HT_{2A} receptor antagonist resulted in reduction in phospholipase C (PLC) upregulation, but not ERK 1/2. This result points to the potential involvement of other serotonin receptor subtypes. Another study showed that inhibition of 5-$HT_{1B/1D}$ receptor signaling did not affect 5-HT mediated collagen synthesis in human valve myofibroblasts (149). This phenomenon could be attributed to the interactions at the 5-HT_2 receptors which were not inhibited in the above study. Indeed, it was demonstrated that mice overexpressing 5-HT_{2B} receptors demonstrated mitochondrial proliferation and myocardial hypertrophy.

Recently, studies have demonstrated that some 5-HT receptors are mechanosensitive. This is of particular relevance to the cardiac valve, which is under continuous mechanical stimulation (212). It has been shown before the G-protein coupled receptors as well as ion-gated channels are mechanoresponsive to stretch (208, 216). Liang *et al* reported that mechanical stress enhanced 5-HT_{2R} signaling thereby implicating this receptor subtype with pressure-induced cardiomyopathy (137). Additionally, Brattelid and colleagues demonstrated that 5-HT responsiveness through 5-HT_{2A} and 5-HT_4 receptors is differentially regulated in the hypertrophic rat ventricle (19). The 5-HT_{2A}-mediated positive inotropic response was linearly correlated with the degree of hypertrophy while the 5-HT_4-mediated response seemed to increase with LV dilatation.

2.8.3.4 Effect on Valve Function and Clinical Relevance

Chester (33, 34) has reported that 5-HT administration on aortic valves resulted in and increased rate of leakage in a 5-HT concentration dependent manner. El-Hamamsy and colleagues have shown that 5-HT mediates valve contractility and relaxation in an endothelium dependent manner (62). This further highlights the importance on 5-HT receptors and the potential role of 5-HT mediated signaling on valve function and competence.

The clinical studies and reports alluded to so far, while highlighting potential issues with 5-HT related pharmacological therapies have not completely elucidated the link between 5-HT, 5-HT receptor signaling and ultimate valve disease (46, 283). However, the *in vitro* and *in vivo* studies clearly report an increase in cell proliferation and collagen biosynthesis in response to 5-HT administration – all classic hallmarks of valve disease (114, 149, 277). The 5-HTT knockout mouse studies demonstrate the potential importance of SSRIs and 5-HT receptor antagonists with regards to 5-HT-related valve disease (149). The presence of 5-HT receptor subtypes in aortic valve cusps, and the responsiveness of these receptors to specific antagonists and mechanical stretch therefore merit further study.

2.9 Effect of Mechanical Forces on Aortic Valve Biology

2.9.1 Mechanical Environment of the Aortic Valve

The aortic valve functions in a complex mechanical environment (**Figure 2-16**) that includes fluid shear stresses, pulsatile pressures, bending and tensile stresses. These forces translate to shear stress, tension and compression on the aortic valve cells. Altered or non-physiological hemodynamics are often implicated in the initiation and progression of aortic valve disease (180), leading to severely compromised valve structure and function (140). Understanding the effects of these forces is therefore crucial in elucidating the mechanisms of aortic valve disease and also in the design of a tissue engineered valve substitute. The subsequent section will outline the various experimental studies that have been performed to quantify the mechanical environment of the aortic valve cusp. This will be followed by a brief section on the mechanisms by which these mechanical forces may be transmitted to the cells populating the tissue. The final section will provide a literature review of studies linking mechanical forces to valve biology and more specifically, valve degeneration.

2.9.1.1 Pressure

In a healthy human heart, the heart beats at a frequency of about 1 to 1.167 Hz, and during diastole the aortic valve experiences a transvalvular pressure of about 100 mmHg. If the patient is hypertensive, the pressure can be as high as 200 mmHg (275, 276). *In vivo* the pressure on the cusp varies throughout the cardiac cycle, thereby changing the stress and the length of the leaflet. Under normal hemodynamic conditions, the closed valve supports a transvalvular pressure of 80-120 mmHg acting perpendicular to the leaflet area. This normal force is supported by the lamina fibrosa layer of the leaflet and is transmitted from the collagen fibers to the cells within the tissue that are aligned with the collagen fibers. The pressure acting on the leaflets is usually estimated in terms

of stresses assuming the tissue to be homogeneous, which is not an ideal assumption as the leaflet is inhomogeneous, anisotropic, nonlinear, and viscoelastic with a complex geometry (250, 253).

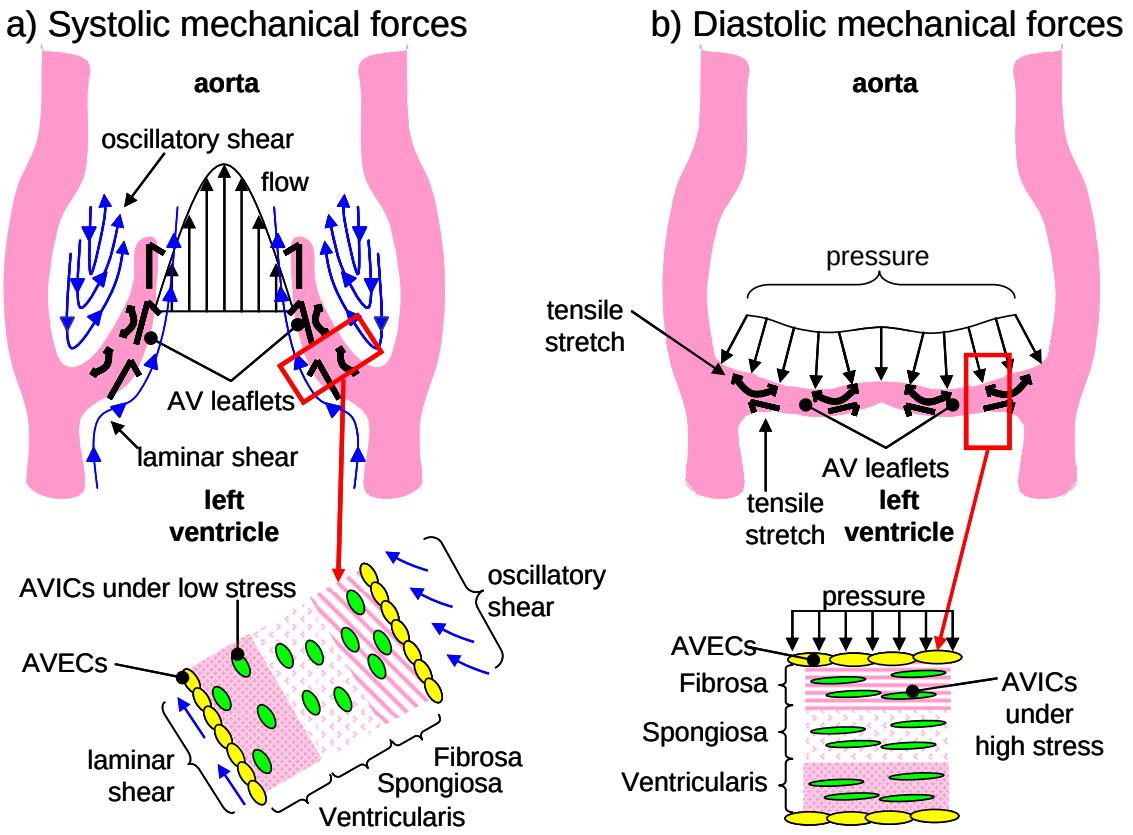

Figure 2-16: Overview of systolic and diastolic mechanical forces acting on the aortic valve cusp. Of note are the differences in forces acting on the two sides of the aortic valve. In addition, it should be noted that aortic valve interstitial cells are under high stress during diastole, due to the stretch and transvalvular pressure. AVIC – aortic valve interstitial cell; AVEC – aortic valve endothelial cell.

Thubrikar *et al* first performed studies using a marker-fluoroscopy technique with radiopaque markers placed on canine aortic valve cusps (252, 253). The stresses were estimated from the change in position of these markers using Laplace's equations assuming a cylindrical geometry. This is in contrast to the assumption of Sacks that the valve has a spherical geometry (212). Both assumptions yield reasonable estimates of the stress in the valve cusp. Thubrikar reported the membrane stresses in the circumferential

direction to be 1.7 g/mm^2 during systole and 24.5 g/mm^2 during diastole. In another study, finite element modeling was used to analyze the stresses. Based on a pressure of 114.7 mmHg and a human aortic valve leaflet thickness of 0.6 mm, the maximum principle stress was found to be 22.35 g/mm^2 (29), which was comparable to the data from Thubrikar's *in vivo* study.

2.9.1.2 Fluid Shear Stresses

Fluid shear stresses are experienced by the endothelial cells of the valve cusp, and are an important factor in the synthetic activity of the valvular cells and also in cell-cell and cell-matrix adhesions. Shear stress is experienced by the ventricular surface of the leaflets during systole when blood flows past the leaflets and on the aortic surface during diastole when blood pools into the sinuses. It is thought that the valve endothelial cell experiences shear which gets transduced to the integrins and cadherins on the inner surface of these cells (23, 25). An estimate of these stresses aids in understanding effect of stresses on leaflet cellular function and in elucidating cellular responses (270). Experimental techniques such as laser doppler velocimetry (LDV), and hot film anemometry (HFA) have been used to estimate the wall shear stresses on the surface of mechanical and bioprosthetic valve cusps.

LDV measurements were performed using a polymeric trileaflet valve under pulsatile conditions (61). Shear stress on the leaflet surface at peak systole was found to be 800–1800 dyn/cm^2. In a recent study by Weston *et al* (270), two-component LDV measurements were conducted on a polymeric valve. Measurements were taken at the location of the valve cusps as well as downstream of the valve. The maximum wall shear stress inside the valve was found to be 79 dyn/cm^2 while the wall shear stress measured 83 mm downstream of the valve was 10-17 dyn/cm^2 at a flow rate of 7.5 L/min. At a flow

rate of 22.5 L/min the shear stress was 52-104 dyn/cm^2. These values are an order of magnitude less than those found in earlier investigations.

Average shear stresses felt by the ventricular surface of the aortic valve are approximately 20 dyn/cm^2 (270). In contrast, there are few experimental studies that have been able to accurately quantify the shear stress profiles on the aortic side of the valve cusp. Ge et al have developed computational models, but these models average the wall shear stresses across the entire leaflet surface (79, 282). Current efforts are being directed toward estimating the wall shear stresses on the aortic surface of the native aortic valve cusp.

Shear stresses on the valve can change with developing pathology. As the aortic valve becomes diseased, the diameter of the valve decreases, and the shear stresses experienced by the valve do indeed become altered (170). By virtue of the unique mechanics of valve and root motion, the fibrosa is under compression and experiences oscillatory shear stresses during systole, while the ventricularis is under tension and experiences pulsatile shear stresses (260).

2.9.1.3 Bending Stresses

Thubrikar reported that the change in three dimensional leaflet curvature during the cardiac cycle gives rise to bending stresses, shearing, or buckling (250). Bending stress is both tensile and compressive with the inflow side experiencing tensile stress while the outflow side experiences compressive stress. During bending, the belly of the leaflet undergoes large changes in curvature due to loading and unloading of the valve while the zone of attachment acts as a hinge facilitating leaflet movement. Indeed, the curvature of the leaflet is integral in ensuring proper coaptation and long term functionality and viability of the valve cusp.

Thubrikar used the radio-opaque marker technique to calculate the bending strains *in vivo* in canine aortic valves. The bending strains, calculated from modulus of elasticity, thickness and radius of the leaflet, were found to be 2% during systole and 2.2% during diastole in the circumferential direction (250). *In vitro* experiments using dip-cast polyurethane trileaflet valves were performed to determine values for bending strain and stress at the free edge of the cusp under physiological pulsatile conditions. The bending stains were greatest during systole, corresponding to a maximum strain and stress of 14.5% and 1.22 MPa, respectively. During diastole, the maximum strain and stress were 8.3% and 0.71MPa, respectively (48).

2.9.1.4 Cyclic Stretch

Cyclic stretch, which is the main focus of this dissertation, is one of the forces experienced by the aortic valve during the cardiac cycle which allows the valve cusps to extend and form a coaptive seal with each the other cusps during diastole (251, 255, 256). It is also required for the maintenance of an adequate coaptation area. Leaflet stretch may be lost at a relatively rapid rate with age as the tissues become less extensible with increasing age. This is primarily because continued collagen fibrillogenesis increases the diameter of some of the constituent fibrils, requiring greater force to produce the same extension (250). The first and most rapid change starts in late adolescence. The maximum radial stretch during this period is halved from 80% to 40% over a time span of 15 to 25 years. Between the ages of 25 and 40 the stretch remains approximately constant at a value of about 40%. After age 40, the stretch continues to decline at a slower linearized rate of about 1% per year (41).

The first studies on characterizing *in vivo* in-plane strains or stretch on the valve cusps were performed by Thubrikar on canines, by measuring the change in cusp length in both the radial and circumferential directions. The leaflets elongate by 11% in the

circumferential direction and 31% in the radial direction from systole to diastole (250). This is because the collagen in the circumferential direction provides greater tensile strength than that in the radial direction, which is mainly composed of elastic fibers. Missirlis *et al* reported strains on the leaflets to be to be 33% and 60% in the circumferential and radial directions, respectively (157).

More recently, Yap *et al* measured the strains on valve cusps under different pressure conditions in an *in vitro* flow loop system (280). This study reported that the stretch on the valve increases by 5% for a change in pressure of 40 mmHg. This is highly interesting as it points to a potential link between altered mechanical loading and valve pathology, and as such warrants further study. This particular finding is used as justification for the different levels of stretch studied in this dissertation.

2.9.2 Cellular Mechanisms for Mechanotransduction

The mechanisms by which cultured cells or tissues sense changes in pressure forces remains unresolved. Several force-transducer systems can be hypothesized. Stretch and pressure might induce morphological changes in aortic valve endothelial and interstitial cells through compression (for pressure) resulting in dilatational stress. This dilatational stress may cause reorganization of the cytoskeleton (213) and opening or closing of ion channels (60, 144), resulting in intracellular responses. Studies on obligate barophiles (i.e., animals and bacteria that live in high hydrostatic pressure environments) have provided insights on how changes in pressure could result in biologic responses in the absence of motion (10, 233). Although the mechanisms by which hydrostatic pressure affects cells are not fully understood, there is growing evidence showing that factors including alpha V integrin, basic fibroblast growth factor (FGF) and vascular endothelial growth factor C (VEGF-C) are involved in pressure-induced cellular processes, while TGF-β and interleukin-1 (IL-1) have been excluded (219, 223). Other recent studies showed that sustained hydrostatic pressure induced protein tyrosine phosphorylation, activation of extracellular signal-regulated kinase (ERK)1/2, enhanced expression of c-fos (68), and that nitric oxide (NO) might be involved in the pressure-induced proliferation of smooth muscle cells (258).

Transduction of shear stress into gene regulation is now an active area of research and has been recently reviewed (98, 225). Fluid flow might act directly upon trans-membrane proteins or the lipid bilayer itself. In addition, the plasma membrane contains structures that are capable of both transmitting forces to the cytoskeleton and transducing forces into biochemical signals. Under static conditions, the mechanosensitive integrins are in an inactive conformation and various signaling molecules are not phosphorylated or assembled as a signaling complex. Shear stress activates the integrins by switching them to an active conformation which increases their affinity and avidity for cognating

extracellular matrix proteins. Through specific interaction of the α and β subunits on the activated integrins, the focal adhesion kinase (FAK)/c-Src and the Cav-1/Fyn pathways are activated to elicit cascades of phosphorylation on various downstream effectors and their assembly through SH2 and SH3 interactions. The two pathways converge at the level of Raf-MEK-ERK in aortic valve endothelial cells in response to shear stress. Additionally, the force signal can also be transmitted to the nucleus and cell-cell junctions in the membrane via tension of the cytoskeleton, resulting in intracellular events. Support for transmission through intracellular junctions mainly comes from the molecular interactions between these junctions and the cytoskeleton.

2.9.3 Effect of Mechanical Forces on Aortic Valve Degeneration

As mentioned earlier, aortic valves experience a myriad of mechanical forces during the cardiac cycle. The close correlations between mechanical stresses and heart valve biology to gene and protein expression have been evidenced by clinical observations, animal studies, as well as in the laboratory (7, 8, 124, 215, 243, 267, 268, 271, 272, 275, 276). According to these studies, the structural components of the aortic valve undergo constant renewal in response to mechanical loading and the sites of protein and matrix synthesis in the leaflets are correlated with focal regions of functional stresses. Similarly, alterations in mechanical loading affect biosynthetic behavior of valve cells. A selection of these studies most relevant to this dissertation is reviewed in this sub-section. Discussion is limited to cell types of strongest relevance to this dissertation, namely, cardiac cells.

Mechanical forces modulate cell physiology and have been shown to affect the biosynthetic activity of cells in tissue matrices (153, 272, 275). Initial studies focused on the effects of hydrostatic pressure on cell proliferation. Increased transvalvular pressure can result in both increased cellular compression as well as stretching and elongation of

the cell (250, 280). Tokunaga *et al* reported that exposure of human umbilical vein endothelial cells to constant pressure of 80 mmHg resulted in significant increases in cell proliferation as compared to atmospheric controls (259). In contrast, pressures of approximately 160 mmHg appeared to have an inhibitory effect on cell proliferation (259).

Due to its apparent relevance to atherosclerosis, the effects of shear stress on vascular endothelial cells have been extensively studied (127, 176, 284). One of the earliest recognized effects of shear stress is the elongation and realignment of endothelial cells. Porcine aortic valve endothelial cells exposed to 20 dyn/cm^2 of steady laminar shear stress showed an organization of focal adhesion complexes and cytoskeletal alignment different than that in static endothelial cell culture, suggesting that valvular endothelial cells exhibit altered responses to mechanical forces (24). Valvular endothelial alignment was dependent on Rho-kinase signaling, whereas vascular endothelial alignment was dependent on both Rho-kinase and phosphatidylinositol 3-kinase signal pathways. When exposed to fluid forces in a parallel plate flow system, native porcine aortic valve leaflets retained synthetic activity of the valve cells at native levels. When exposed to laminar shear stress, protein synthesis was modulated by shear stress (271).

Another effect of increased mechanical load is extracellular matrix synthesis and remodeling. *In vivo* studies using Wistar Kyoto rats with acute left ventricular pressure overload showed increased DNA synthesis and mRNA amounts of both collagen type I and III comparable to age-matched hypertensive rats. This suggests that valves adapt to a new mechanical environment by increasing DNA synthesis and collagen turnover (273). Collagen synthesis was shown to significantly increase at hypertensive and severe hypertensive pressure conditions as compared to leaflets exposed to a pressure of 100 mmHg, while no significant difference was seen in sulfated glycosaminoglycan or DNA synthesis (275). One of the earliest studies on the effects of pressure and shear stresses on

matrix metalloproteinase expression and activity was conducted by the Galis lab (32). Porcine carotid arteries were mounted in an *in vitro* organ culture system and exposed to a steady laminar shear stress of 15 dyn/cm^2 with a transmural pressure of 100 or 200 mmHg for 24 and 48 hrs. Results showed enhanced MMP-2 and MMP-9 activity in response to pressure, but not to shear stress.

Several studies have also demonstrated changes in aortic valve cell phenotype in response to mechanical forces. Changes to cell phenotype could potentially be crucial in a degenerative disease process, as we have outlined earlier the importance of the "activated" myofibroblast phenotype in initiating and propagating valve disease (140). *Ex vivo* studies of native porcine aortic valve leaflets exposed to independent effects of fluid forces, steady laminar shear stress and constant static and cyclic pressure at physiological levels exhibited a reduced level of α-SMA as compared to native levels (271, 275, 276). In contrast, a recent study from our laboratory showed that cyclic stretch is responsible for regulating the contractile phenotype of the cells, with elevated stretch resulting in increased α-SMA expression (7). These latter results could also be indication of the ability of the different mechanical forces to act in concert to modulate and maintain a healthy cellular phenotype.

The time that valves or valvular cells in culture take to respond to external stimuli is also of interest. We have seen in studies conducted by our laboratory that valves typically respond to mechanical forces in 48 hours (7, 8, 109, 124, 243, 275, 276). This has also been seen in studies by Gotlieb *et al* (59, 139, 164). In a study conducted by Walker *et al* (266), α-SMA expression was seen in porcine valvular interstitial cells cultured on a rigid plastic substrate in 48 hours. Addition of TGF-β1 was also seen to increase α-SMA expression of these interstial cells within the same timescale in a dose-dependent manner. Butcher *et al* (24) observed that porcine aortic valve endothelial cells cultured under steady shear stress of 20 dyn/cm^2 formed focal adhesion complexes in 48

hours. In another study by Durbin *et al* (58, 59), linear denuding wounds were made in confluent monolayers of porcine mitral valve interstitial cells plated on glass coverslips. From 6 to 24 h postwounding, iNOS localization was increased at the wound edge. At 48 h, iNOS was localized beyond the wound edge, into the monolayer, where the intensity of the signal gradually diminished until it was virtually imperceptible. Studies in our laboratory have shown that normal mechanical forces maintain native-valve phenotype (124). Elevated pressure, both steady and cyclic, caused enhanced extracellular matrix synthesis in porcine aortic valve leaflets (275, 276). Steady laminar shear stress also caused increased extracellular matrix protein synthesis. It is clear from these studies that mechanical factors such as pressure and shear stress are important in valve extracellular matrix remodeling; however, the molecular mechanisms remain largely unexplored. In addition, it is clear that an acute change in the mechanical environment can quickly result in changes in valve biology. Indeed, it is thought that the valve can acutely respond and adapt to changes in its mechanical environment to maintain its function (25).

More recently, studies have pointed to a concrete role for mechanical forces in the development and progression of degenerative aortic valve disease. Hypertension, which is a known risk factor for calcific aortic valve disease (193), results in a situation of elevated stress and stretch of the valve cusp. Cyclic stretch, which is the focus of this dissertation, has also been shown to modulate valve biosynthetic activity. Under physiologic conditions, the normal valve experiences approximately 10% stretch in the circumferential direction and 30% in the radial direction, which can change depending on changes in pressure load (250). Ku *et al* reported that cyclic stretch upregulated collagen synthesis in valve interstitial cells as well mesenchymal stem cells (126), which was also demonstrated recently by our laboratory on whole valve cusps (7). Increased cyclic stretch has been linked to elevated expression of matrix remodeling proteins (8) as well as pro-inflammatory markers (153). Warnock *et al* demonstrated that elevated cyclic

pressure is a potent stimulus for the up-regulation of VCAM-1 expression and the down-regulation of OPN expression (267). The same research group also demonstrated that pro-inflammatory protein expression was evident at cyclic strains of 5 and 20%, while a 10% strain did not elicit an inflammatory response. Merryman *et al* reported that valve interstitial cells respond to local tissue stresses by altering cellular stiffness via collagen biosynthesis (152). They also reported that the presence of cytokines such as TGF-β1 in a cyclic stretch environment could potentially result in altered matrix architecture and compromised valve function, underlining the importance of cyclic stretch in regulating valve structure and function (151).

Another important aspect of aortic valve cellular mechanobiology are the interactions between endothelial cells and interstitial cells. Such interactions have been demonstrated in vascular cells. Chiu *et al* (36-38) demonstrated that co-culture with smooth muscle cells under static condition induced endothelial cell gene expressions of ICAM-1, VCAM-1, E-selectin, as well as growth-related oncogene-alpha and monocyte chemotactic protein-1. Shear stress was found to abolish these smooth muscle cell-induced gene expressions. Studies by Vouyouka *et al* (264, 265) compared rat aortic smooth muscle cell proliferation and contractility in independent and endothelial cell co-culture under ambient and high pressure (130 mmHg). Results showed that factors released by endothelial cells suppressed smooth muscle cell proliferation in both atmospheric and high pressure conditions. There are relatively few co-culture studies performed on aortic valve cells or tissues. Studies on denuded tissue performed in our laboratory have demonstrated increased expression of disease markers such as matrix remodeling enzymes, BMP-4 and TGF-β1 in denuded cusps compared to intact cusps. Endothelial-interstitial cell communication will be examined in specific aim 2 of this dissertation.

The literature reviewed in this sub-section demonstrates a concrete association between altered mechanical loading, hypertension and aortic valve degenerative disease and calcification. Unfortunately, this field has not been accorded the attention it deserves. Elucidating the link between mechanical loading and various degenerative disease pathways would open the way for furthering research on treatments for these diseases. This thesis work will fill this gap in the field by elucidating the effects of normal and elevated cyclic stretch on aortic valve degenerative disease.

2.10 Rationale For Thesis Research

The literature review presented earlier points to a critical need for understanding aortic valve mechanobiology as part of the overall effort to achieve better treatment options for aortic valve diseases. There appears to be a delicate interplay between aortic valve mechanics, biology and its surrounding environment that either maintain a normal, healthy, functional aortic valve, or result in its progressive degeneration and eventual failure. Unfortunately, the cellular and molecular events leading to valve degeneration due to altered mechanical forces are poorly understood, and not well studied.

Most work to date has focused on understanding the effects of fluid shear stresses and pulsatile pressures on aortic valve cellular mechanobiology. Previous work in our laboratory has focused on understanding the effects of cyclic pulsatile pressure, and fluid shear stresses on aortic valve remodeling and disease, with considerable success. There are relatively few studies on the mechanobiology of cyclic stretch. This dissertation will therefore focus on elucidating the effects of normal and altered cyclic stretch on aortic valve remodeling and degenerative disease. An *ex vivo* approach using whole tissue was chosen since it retains both the cells and the native extracellular matrix, providing a better representation of native valves than cell culture models, an excellent three-dimensional model for tissue engineered heart valves, and the ability to accurately control the mechanical force applied on the tissue sample. Three specific aims will study three different aspects of degenerative aortic valve disease that are still not well understood. The first specific aim will elucidate the effect of cyclic stretch magnitude on aortic valve extracellular matrix synthesis and remodeling. The second specific aim seeks to understand the link between cyclic stretch and aortic valve calcification, and finally in specific aim three, the synergistic effects of cyclic stretch and serotonin (5-HT) administration will be studied. This information would allow for a better understanding of valve disease pathways and for the development of an optimal valve substitute.

CHAPTER 3

HYPOTHESIS AND SPECIFIC AIMS

Studies on the role of mechanical forces on aortic valve biology are crucial for understanding the normal function of the valve and elucidating failure and disease mechanisms and pathways that are implicated in aortic valve disease. At present, there is a lack of understanding of aortic valve mechanobiology. Establishing these mechanobiological pathways will help isolate key molecules that could be blocked through pharmacological or molecular therapies. In addition, these mechanobiological insights could be used to develop an optimal tissue-engineered valve substitute.

Cyclic stretch is one of the forces experienced by the aortic valve, primarily during diastole when the transvalvular pressure gradient causes the valve to snap shut. The three cusps extend to form a coaptive seal preventing backflow of blood into the left ventricle. Large membrane stresses are generated on the cusps, which are borne by the circumferentially-oriented collagen fibers and transmitted to the cells in the valve and the aorta via the extracellular matrix network. Under pathological conditions, changes in the mechanical environment can result in elevated stresses in valve cells. These elevated stresses result in abnormal cellular responses leading eventually to deterioration and degeneration of the valve (212).

Previous studies performed in our laboratory on the effects of shear stress and cyclic pressure (189, 275, 276) on aortic valve cusps have demonstrated that normal physiological forces maintain the native cellular phenotype, while altered forces result in increased expression of disease-related molecules such as matrix metalloproteinases (MMPs), cathepsins, and bone-morphogenic proteins (BMPs). Other researchers have demonstrated that cyclic stretch can modulate valve biosynthetic activity. Ku *et al*

reported that cyclic stretch upregulated collagen synthesis in aortic valve interstitial cells (126). Merryman *et al* reported that valve interstitial cells respond to local tissue stresses by altering cellular stiffness via collagen biosynthesis (152). They also reported that the presence of cytokines such as transforming growth factor- β1 (TGF-β1) in a cyclic stretch environment could potentially result in altered matrix architecture and compromised valve function (151). Intriguingly, calcified valves demonstrate increased expression of cytokines such as TGF-β1 (45, 113), BMPs (18), as well as alkaline phosphatase (178, 179). Additionally, active osteogenesis was reported in calcified human valve cusps (159). All these studies point to the potential role for stretch in the pathogenesis and progression of valvular degeneration and disease.

This dissertation will therefore focus on understanding the effects of isolated cyclic stretch on the biology, degeneration and pathology of aortic valve cusps. **The hypothesis of this dissertation is that elevated cyclic stretch induces aortic valve degeneration via expression of matrix remodeling enzymes and pro-calcific markers. Additionally, it is hypothesized that elevated cyclic stretch primes the valve to be more prone to valve disease as a result of secondary pharmacological and humoral insults.** The hypotheses will be tested via three specific aims, each with a focus on one aspect of degenerative aortic valve disease:

1) Effect of cyclic stretch on extracellular matrix remodeling.
2) Effect of cyclic stretch on aortic valve calcification.
3) Effect of cyclic stretch on serotonin-related valvular degeneration via stretch-sensitive receptors in the aortic valve.

The overall organization of the various specific aims is depicted in **Figure 3-1** below.

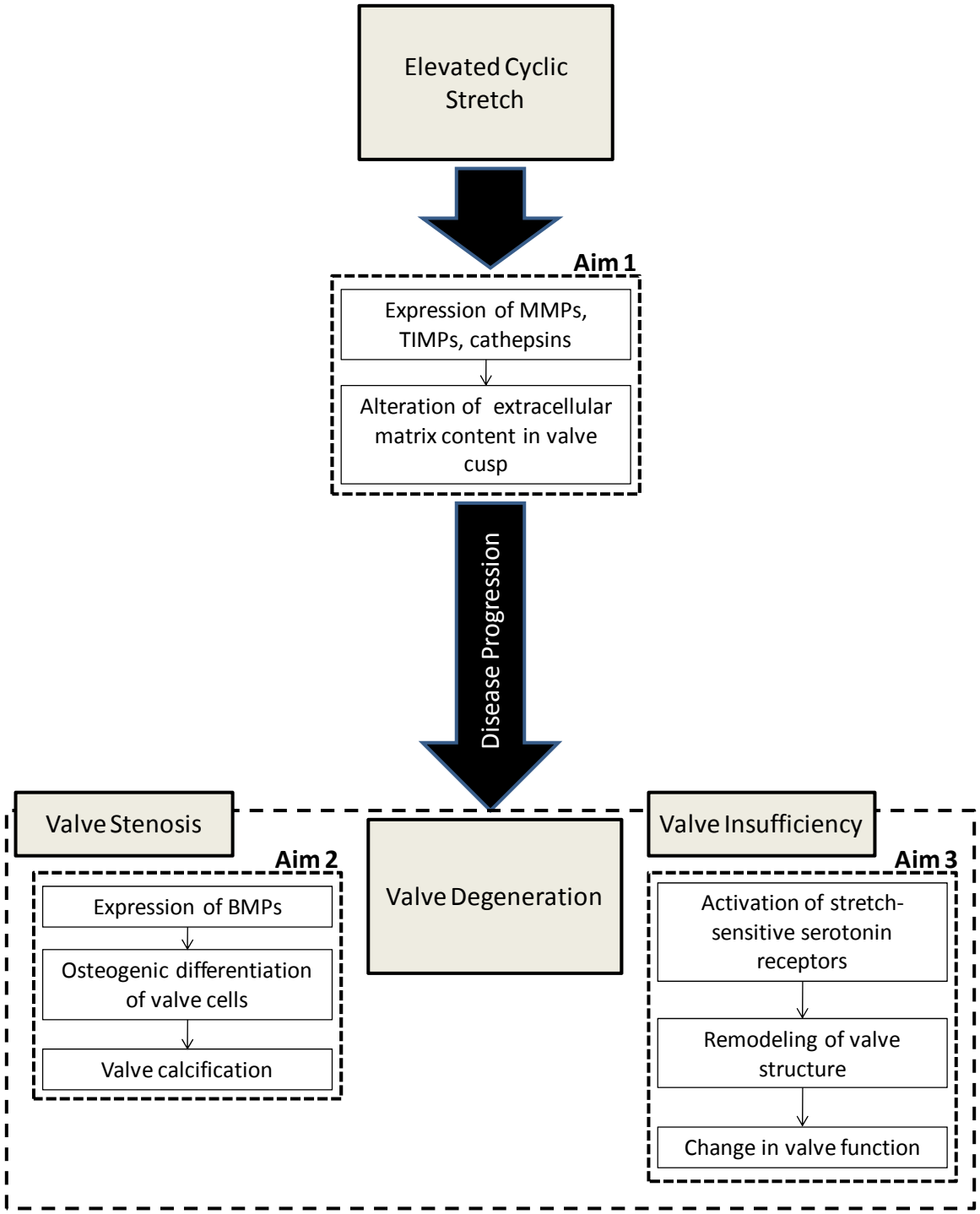

Figure 3-1: Overall schematic for the specific aims and hypothetical disease pathways in this dissertation. Each specific aim investigates one particular aspect of stretch-related aortic valve pathology.

These studies will be performed using an *ex vivo* cyclic stretch bioreactor and using porcine aortic valve cusps. The porcine model has been the animal model of choice for aortic valve studies in our laboratory due to its similar anatomy and structure to the human valve and the ease of availability of tissue. An *ex vivo* approach allows precise control of the mechanical environment, while preserving the valve cells in their native three-dimensional environment. The stretch bioreactor system will be described in detail in the following chapter. It will also be validated to ensure that valve samples are subject to uniform and reproducible levels of cyclic stretch, and that cyclic stretch is the sole significant mechanical force acting on the samples.

3.1 Specific Aim 1: Effect of cyclic stretch on extracellular matrix remodeling

Altered matrix remodeling is usually the first indicator of valve pathology. This specific aim will focus on understanding the effects of normal and pathologic stretch on aortic valve extracellular matrix content and remodeling. Under normal physiologic conditions, aortic valve cusps experience 10% cyclic stretch, and this value can go up to 15% and even 20% in patients with severe hypertension. The hypothesis of this aim is that elevated cyclic stretch will result in increased valve remodeling, enzyme expression and activity.

Aortic valve cusp samples will be subject to three levels of cyclic stretch (10% - normal; 15% - pathologic; 20% - severe pathologic) for 24 and 48 hours, with fresh and statically incubated valve cusps as controls. Tissue morphology, cellular proliferation and apoptosis, collagen, sulfated glycosaminoglycan, and elastin content will be analyzed. Also, expression and activity of matrix metalloproteinases (MMPs) -1, -2, and -9, tissue inhibitors of matrix metalloproteinases (TIMPs) -1 and -2, and cathepsins L, S, and K will be analyzed in response to these levels of stretch, using immunohistochemistry, gelatin zymography and immunoblotting.

3.2 Specific Aim 2: Effect of cyclic stretch on aortic valve calcification

This specific aim will focus on elucidating the effects of cyclic stretch on valve calcification, and more specifically on the role of bone morphogenic proteins (BMPs) on stretch-induced valve calcification. BMPs have recently been identified as potential mechanosensitive mediators/intermediates in calcific aortic stenosis and are hence important to investigate as they could be potential targets for the treatment of valve calcification. The hypothesis of this aim is that elevated cyclic stretch will result in increased expression of pro-inflammatory expression and accelerated valve calcification via a BMP-dependent pathway.

Aortic valve cusps will be subjected to cyclic stretch (10% - normal; 15% - pathologic) for 3, 7 and 14 days in an osteogenic medium. In addition, various concentrations of noggin (0, 1, 10, 100 ng/mL) will be added to the osteogenic medium, in order to understand the BMP-dependence of stretch-related valve calcification. BMP-4 will also be added to the osteogenic medium to verify the specificity of noggin and also to understand the effects of exogenously added BMP on valve calcification. Inflammation will be analyzed using immunohistochemistry for ICAM-1 and VCAM-1. Valve calcification will be studied via Alizarin Red staining, von Kossa staining, alkaline phosphatase activity assay and total calcium content. In addition, immunohistochemistry will be used to study BMP-2 and BMP-4 expression.

3.3 Specific Aim 3: Effect of cyclic stretch on serotonin-related valvular degeneration

Elevated circulating levels of serotonin or 5-hydroxytryptamine (5-HT) have been associated with increased incidence of valve fibrosis and degenerative pathology leading to valve insufficiency. Studies have shown that serotonin receptors on valve cusps may potentially be stretch-sensitive. This specific aim will focus on elucidating the synergistic effects of cyclic stretch and serotonin on valve collagen biosynthesis and function. The hypothesis of this aim is that aortic valve cusps respond to elevated levels of 5-HT via stretch-sensitive 5-HT receptors that result in increased extracellular matrix synthesis and altered mechanical properties.

Aortic valve cusps will be subject to cyclic stretch (10% - normal; 15% - pathologic) for 3 days in varying concentrations of serotonin (10^{-6}M, 10^{-5}M, 10^{-4}M). Pharmacological blockers of 5-HT_2 receptor sub-types will be added to the culture media. Cusps will be analyzed for collagen content, markers for collagen synthesis (lysyl oxidase and hsp47), cellular proliferation and apoptosis. In addition, mechanical properties of valve cusps cultured in the various treatment groups will be analyzed using a uniaxial mechanical testing device.

CHAPTER 4

MATERIALS AND METHODS

The objective of this dissertation was to understand the effects of cyclic stretch on three different aspects of degenerative aortic valve disease, organized into three specific aims (**Figure 3-1**). This chapter details the materials and methods employed in this dissertation. First, the design of the tensile stretch bioreactor system and methodology for its mechanical validation will be outlined. Mechanical drawings of the bioreactor and circuit diagrams for the control circuitry have been compiled in **Appendix A**. The next section will compile the protocols for the experimental setup of the stretch bioreactor for each specific aim. This will be followed by the methods employed for the biological analyses and uniaxial mechanical testing. Some of these biological protocols are common over the specific aims and hence have been consolidated in one section. This chapter will only provide the essential details for these biological and mechanical testing protocols. Detailed protocols have been compiled in **Appendix B** of this dissertation. All Matlab codes used in this dissertation are compiled in **Appendix D**. The final section will detail statistical methods to be employed for each of the specific aims. This section will also address issues relating to experimental repeatability as well as the randomization of the valve cusps.

4.1 Stretch Bioreactor System Development

4.1.1 Introduction to Stretch Bioreactor System

A tensile stretch bioreactor (**Figure 4-1**) was used in this dissertation to subject aortic valve cusp samples to different levels of cyclic stretch. The bioreactor was originally designed and developed in collaboration with the laboratory of Dr. Michael S. Sacks at the University of Pittsburgh, and adapted for this dissertation.

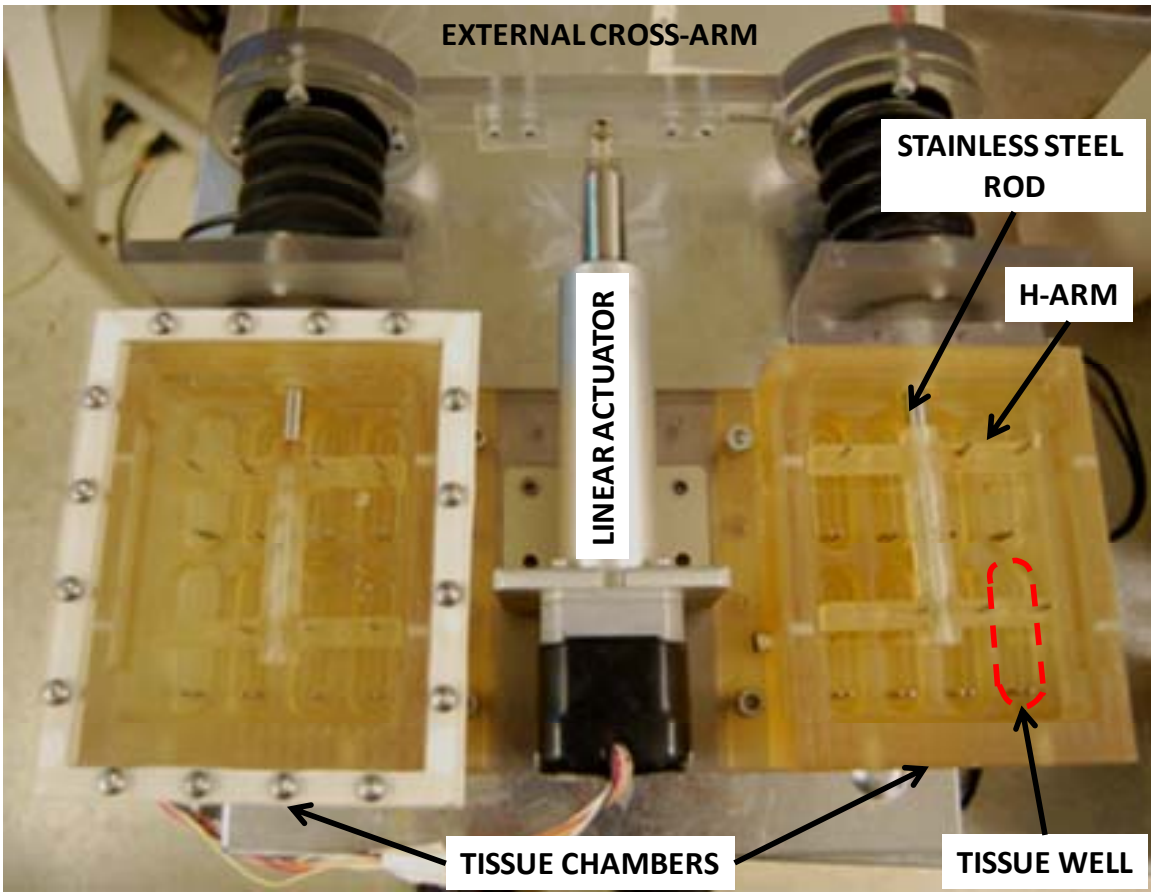

Figure 4-1: Photograph of tensile stretch bioreactor that was used in this dissertation. It was fabricated out of polysulfone (amber color) and polycarbonate (clear) and could be ethylene oxide sterilized. Detailed mechanical drawings are attached in **Appendix A**.

The bioreactor consists of two identical environmentally-sealed chambers, each containing 8 culture wells. Each well accommodates approximately 7 mL of culture medium and the device can hold 16 rectangular tissue sections. Each tissue well has a drain port that allowed media to be filled or removed without having to open the lid or stop the stretching motion of the tissue samples. Each tissue sample is coupled to posts on either side; a set of stationary posts located in the bottom of each tissue chamber, and a set of moving posts. The moving posts are located on an H-shaped arm that is coupled to a rigid, stainless steel rod. This rigid rod exits the tissue chamber and is further coupled to an external cross-arm and a linear microstepper actuator (#D-A.083-HT17-2-1-K-ES-BR/NRC4, Ultra Motion LLC, Cutchogue, NY). A photograph of tissue samples contained within the bioreactor is depicted in **Figure 4-2**. Detailed mechanical drawings for the bioreactor are compiled in **Appendix A**.

Figure 4-2: View of tissue chamber within stretch bioreactor depicting eight tissue samples coupled to H-shaped arm. Each tissue well is filled with tissue culture medium. Details on how the tissue samples are attached are compiled in **Section 4.3.1**.

The linear actuator was controlled by a stepper motor drive card (**Figure 4-3**A; #1240i, Applied Motion Products Inc., Watsonville, CA). This drive takes a 12VDC power supply (**Figure 4-3B**) and can be programmed to accept a trigger signal or output a binary trigger signal for the triggering and synchronization of external equipment. Triggering of the 1240i drive was not used for this dissertation. The circuit diagram for the power supply is compiled in **Appendix A**.

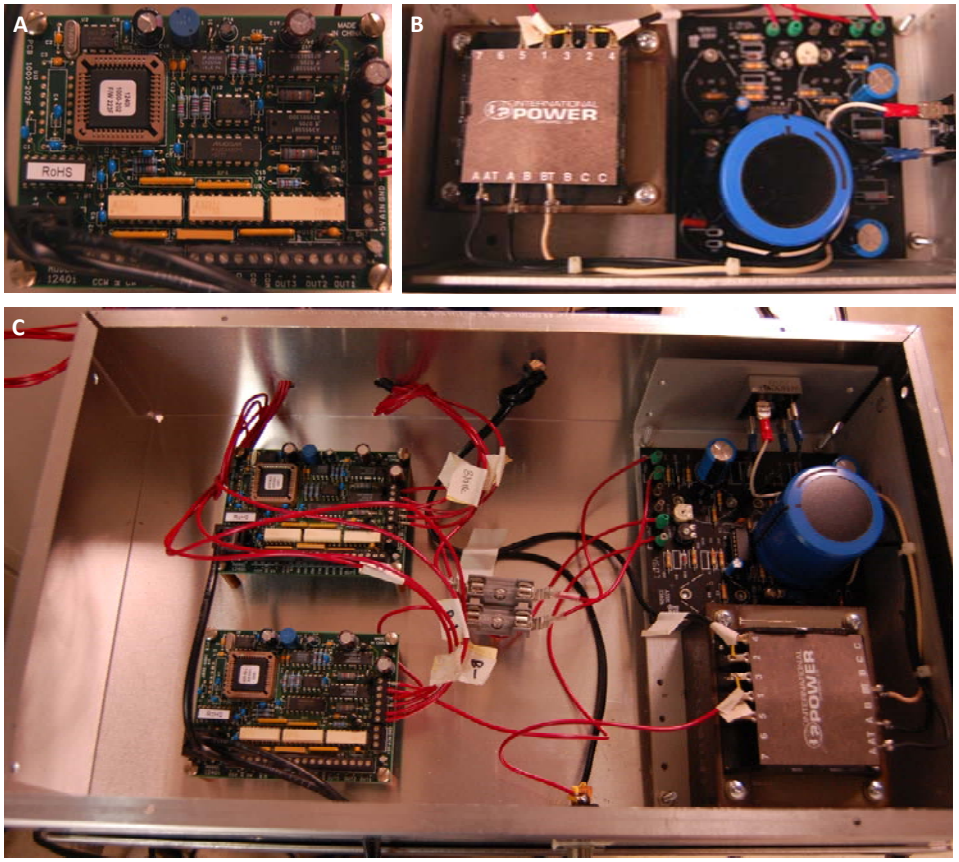

Figure 4-3: (A) 1240i microstepper motor drive controller card used to control the tensile stretch bioreactor. (B) Power supply designed for the 1240i microstepper drive. (C) Overall arrangement of two 1240i controller cards and power supply that was assembled to control two tensile stretch bioreactors. Detailed circuit diagrams are attached in **Appendix A**.

4.1.2 Derivation of Input Waveforms to Stretch Bioreactor

In order to efficiently study the effects of cyclic stretch on aortic valve biology and disease, it was necessary to derive a reasonably accurate stretch profile that can be imposed on the valve samples in the stretch bioreactor. The stretch waveforms were derived from *in vivo* experiments performed by Thubrikar *et al* (250), where the researchers quantified the one-dimensional changes in leaflet circumferential length over the cardiac cycle. These experiments were performed using a marker-fluoroscopy technique. They reported a change in leaflet length of approximately 10% under normal conditions (**Figure 4-4**). This deformation curve was then manually plotted out over a cardiac duration of 860 ms (corresponding to 70 beats per minute), and used as the normal (physiologic) waveform. Strain was then calculated and plotted (**Figure 4-5**).

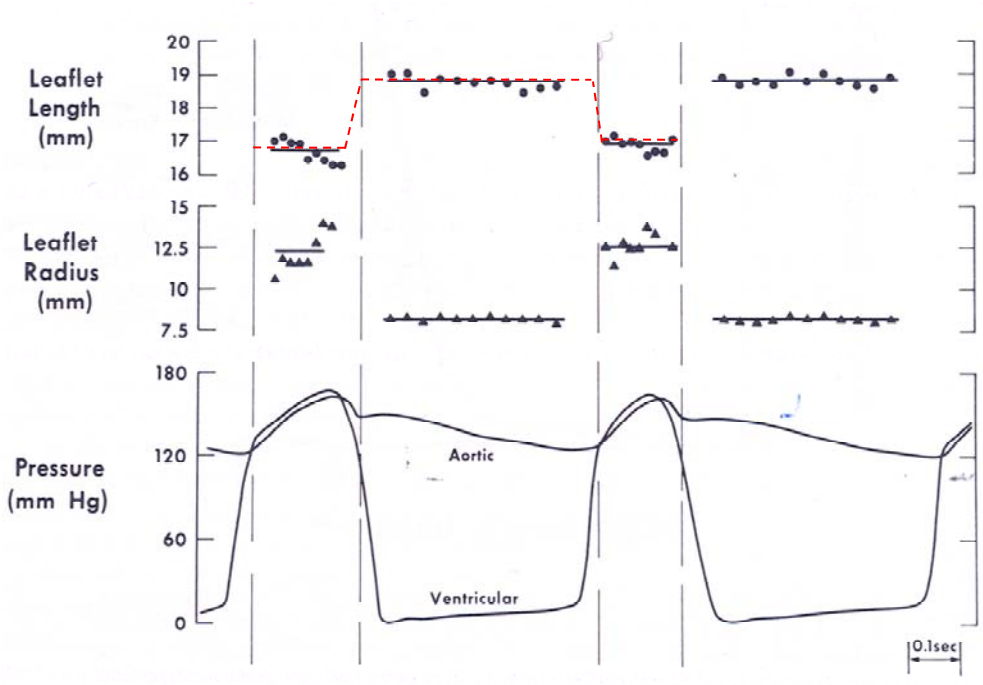

Figure 4-4: Plot of leaflet/cusp length in the circumferential direction, cusp radius and cardiac pressures over time from experiments conducted by Thubrikar *et al* (250). As the leaflet closes in diastole, its circumferential length increases. This corresponds to a peak strain magnitude of approximately 10%. The marker locations were plotted out (red dashed line) and tabulated in order to be input to the stretch bioreactor

In order to obtain pathologic and severe pathologic waveforms, the normal waveform was scaled to 15% and 20% peak strain respectively, maintaining the duration of systole and diastole. These levels of strain corresponded to an increase in mean transvalvular pressure of 40 mmHg and 80 mmHg respectively based on previous *in vitro* experiments performed in our laboratory (280). In these experiments, it was also validated that under normal physiological conditions (120/80 mmHg pressure, 5 L/min cardiac output, 70 beats per minute) the mean strain experienced by the aortic valve cusps was 10%.

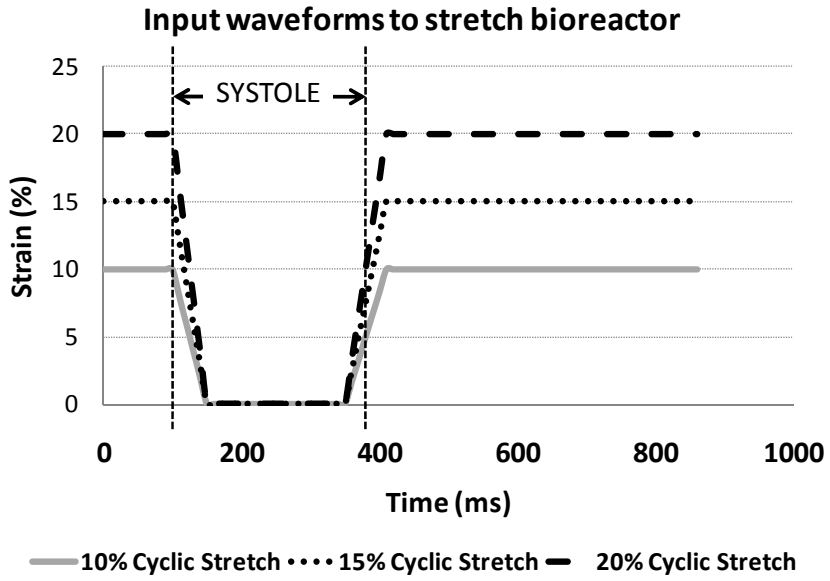

Figure 4-5: Input waveforms to the stretch bioreactor, representing normal (10%), pathologic (15%) and severe pathologic (20%) strain. A 5% increase in stretch/strain represents an increase of 40 mmHg in mean transvalvular pressure (280).

4.1.3 Control and Feedback of Stretch Bioreactor System

Frequency, amplitude, and displacement profiles for the stretch motion were programmed using the SI programmer software (Applied Motion Products Inc.) that was bundled with the 1240i stepper motor drive. The SI programmer software is a convenient bundled software where the user has the ability to program the motion of the linear actuator, via control over its position, velocity and duration of motion (**Figure 4-6**). The motion was discretized into four separate motions, based on the waveforms depicted in **Figure 4-5**, for a cardiac cycle duration of 860 ms:

(i) Extension – Corresponding to the coaptation and stretching of the valve cusps during valve closure (Duration = 75 ms),

(ii) Holding – Corresponding to diastole, where the valve cusps remain stretched and maintain a coaptive seal (Duration = 508 ms),

(iii) Retraction – Corresponding to the rapid opening phase of the valve cusps where stretch is relieved (Duration = 57 ms).

(iv) Holding – Corresponding to systole, where the valve cusps remain open (Duration = 220 ms).

These discrete motions of the linear actuator were programmed into the SI programmer software. The SI software programs used for each of the stretch waveforms are compiled in **Appendix A**. The next section describes the methods employed to validate the output of the linear actuator.

Figure 4-6: Screenshot from the SI programmer software. This picture depicts the main programming interface in the background with all the potential controls over the linear actuator in the foreground.

4.2 Mechanical Validation of Stretch Bioreactor

As this dissertation sought to understand the effects of stretch on aortic valve biology, it was of utmost importance to validate and quantify the stretch environment imposed on the valve samples. The applied stretch must be reasonably uniform across the analyzed valve specimen as well as between the different specimens in the tissue wells. At the same time, it must be validated that stretch is the dominant mechanical force acting on the valve leaflet samples.

4.2.1 Quantification of Stretch Environment in Stretch Bioreactor

A computer-vision based high-speed camera capture method was used to quantify the peak stretch experienced by the valve cusp samples as they are stretched in the tensile stretch bioreactor (**Figure 4-1**). The objectives of this particular study were to:

i) Validate that the mean peak stretch magnitude imposed is statistically similar for all 16 tissue wells of the stretch bioreactor

ii) Document local variations in stretch along the length of the tissue sample.

A row of five regularly spaced markers/dots (**Figure 4-7**) was placed on each valve sample using tissue marking dye (Black Tissue Marking Dye, Thermo-Scientific, Pittsburgh, PA). A high-speed camera (Basler A504K, Basler, Germany) together with an image grabbing system (EPIX CL3SD, Buffalo Grove, IL), was utilized to capture the dynamic motion of the cusp samples at 100 frames per second. All details and protocols pertaining to the image grabbing software are compiled in **Appendix E**.

A custom MATLAB code (compiled in **Appendix E**) was then used to track the motion of the markers and obtain marker coordinates as the samples were stretched in the bioreactor. The simple engineering strains and Greens strains for the four line segments between the five markers were then calculated from these marker coordinates. The Greens strain between the markers and the spring locations were not evaluated as these

sections would have been discarded anyway as part of the experimental protocol. This experiment was conducted for all 16 tissue wells of the stretch bioreactor and for the three different stretch levels used in this dissertation (10%, 15%, 20%).

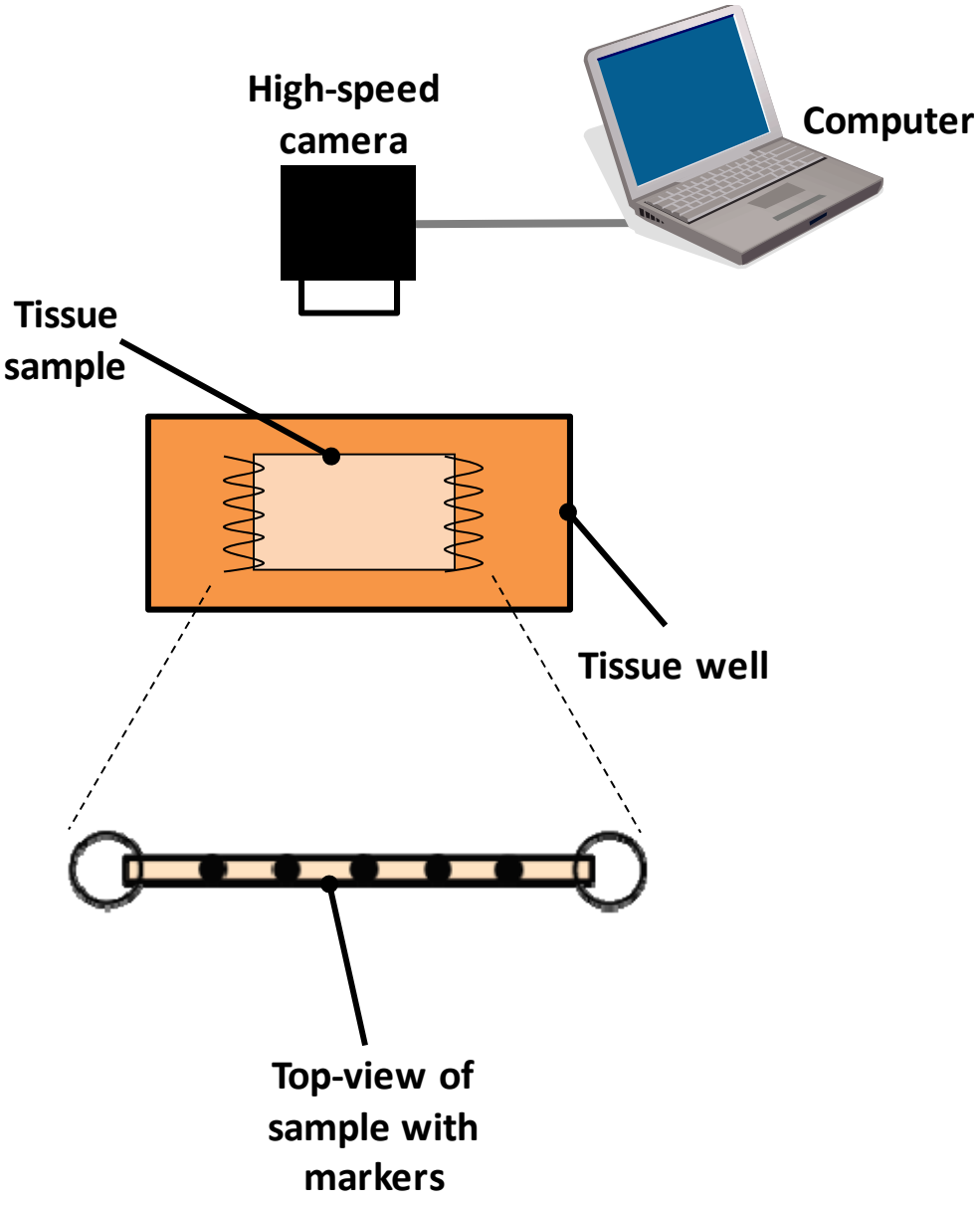

Figure 4-7: Schematic depicting high-speed camera experiments to determine strain on aortic valve leaflet tissue samples. Tissue marking die was used to place markers on the edge of the tissue sample, and these marker dots were tracked using a computer controlled high-speed camera system.

4.2.2 Quantification of Fluid Shear Stress Environment in Stretch Bioreactor

An initial concern with the experimental design was the fluid shear stresses induced on the cusp sample surface as it is undergoes cyclically motion in the tissue culture medium within the stretch bioreactor tissue well. High shear stresses on the aortic valve cusp can result in cellular responses that may potentially confound results obtained from stretch experiments. The objective of this analysis was therefore to determine the shear stresses experienced by samples in the stretch bioreactor analytically.

4.2.2.1 Analytical estimation of shear stress environment in stretch bioreactor

In order to estimate the shear stress analytically, it was first assumed that the shear stresses would be highest during the retraction phase of the stretch motion (i.e. when the leaflets are transitioning from a stretched configuration to the unstretched configuration). This corresponds to the opening phase of the aortic valve, and has the highest velocities and velocity gradients. The analysis in this section therefore focused on determining the shear stresses during this particular motion of the leaflet samples in the stretch bioreactor.

Focusing just on the retraction phase of the stretch motion, and by assuming that this motion is periodic, a Stokes' oscillating plate solution can be used to approximate the shear stresses on the surface of the leaflet (**Figure 4-8**). The spatial velocity profile and shear stress over time for a Stokes' oscillating plate is given by the following equations:

$$u(y,t) = Ue^{-y/\delta_s}\cos\left(\frac{y}{\delta_s} - \omega t\right) \tag{4-1}$$

$$\tau(y,t) = \mu\left(-\frac{U}{\delta_s}\right)\left(e^{-y/\delta_s}\right)\left[\sin\left(\frac{y}{\delta_s} - \omega t\right) + \cos\left(\frac{y}{\delta_s} - \omega t\right)\right] \tag{4-2}$$

Where is U is peak velocity, δ_s is a length scale factor defined as: $\delta_s = \sqrt{\frac{2\nu}{\omega}}$, where ν is the kinematic viscosity of the fluid, and ω the angular frequency of the motion of the plate. In addition, μ refers to the dynamic viscosity of the fluid.

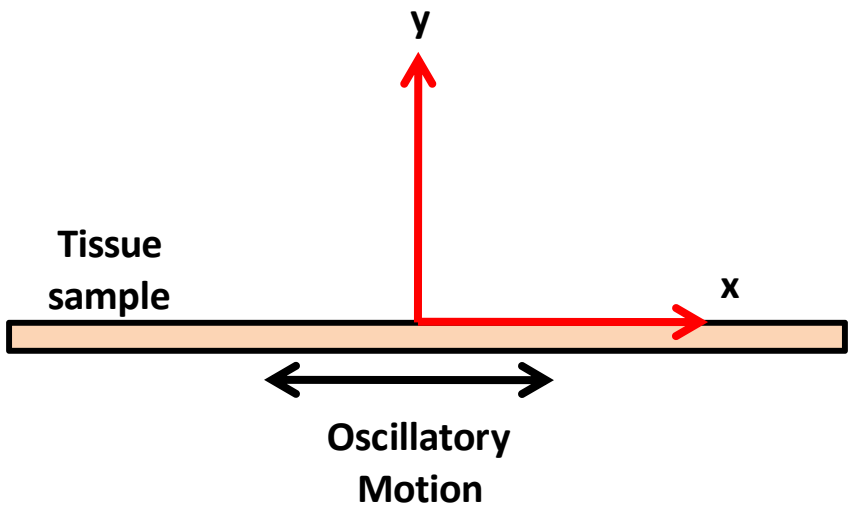

Figure 4-8: Schematic representing Stokes' oscillating plate assumption that was utilized to derive the shear stresses on the surface of the leaflet tissue sample.

A sinusoidal continuous velocity profile was fit to match the peak velocity of the leaflet sample. From this curve, the values for the parameters needed to solve for the shear stress on the surface of the sample can be obtained, and used to solve for the shear stresses on the surface of the leaflet surface, when $y = 0$.

4.3 Experimental Methods

Sterile and aseptic methods were employed for all experimental procedures dealing with porcine aortic valve tissue. All materials for the experiments (including surgical tools, bottles, bioreactors etc) were sterilized by one or more of the following methods:

i) Autoclaving at 120°C for 30 minutes

ii) Ethylene Oxide sterilization for 24 hours

iii) Sterile filtering using a 0.22 μm filter

Detailed protocols for experimental preparation and setup are compiled in **Appendix B**. All catalog numbers for the chemicals and reagents are compiled in **Appendix B** as well.

4.3.1 Tissue Procurement and Experimental Set-up

Fresh (within 10 minutes of slaughter) porcine hearts were obtained from a local slaughterhouse (Holifield Farms, Covington, GA) and the aortic valve root and a portion of the aorta was dissected using sterile surgical methods. The pigs were between the ages of 12 – 24 months. The valvular apparatus was then transported back to the laboratory in ice-cold sterile Dulbecco's Phosphate Buffered Saline (dPBS, Sigma, St Louis, MO). The aseptic techniques to follow were all performed in a laminar flow hood (Thermo-Scientific) at the Cardiovascular Fluid Mechanics Laboratory. In addition, handling and manipulation of the valve cusp itself was minimized to prevent damaging the fragile endothelial cell layer of these cusps.

The valve root was first cut between the left- and non-coronary cusps, along the commissures and spread open, in order to make the cusps more accessible for subsequent dissection (**Figure 4-9**A). The three cusps were dissected along the base, and a circumferentially-oriented 15 by 5-7 mm section was dissected from the central portion of each cusp (**Figure 4-9**B). These rectangular sections were then randomized and

allocated to the various treatment groups. It was therefore ensured that each sample in a particular treatment group originated from a different animal, and that there was a random mix of left, right and non-coronary cusps. Samples designated as fresh controls were processed immediately as outlined in the later sections. For all other samples, stainless steel springs were threaded along the short ends (**Figure 4-9**C), and samples were placed in sterile ice-cold dPBS, while the rest of the experiment is set-up.

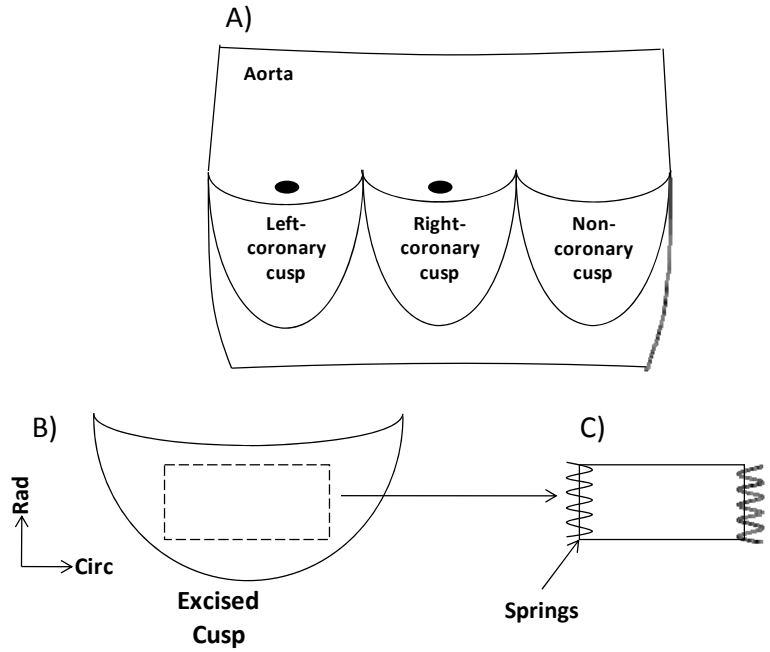

Figure 4-9: Schematic showing workflow for preparation of stretch specimens.

The linear actuator was coupled to the stretch bioreactor at this point, and the leaflet samples were mounted in the tissue wells. The wells were then filled with the appropriate formulation of culture medium, the lids placed on the tissue chambers, and the bioreactor placed in the incubator maintained at 37°C and 5% CO_2. The linear actuator was then adjusted to its zero position and the appropriate program started in the SI Programmer software.

4.3.2 Experimental Conditions For Tensile Stretch Bioreactor

4.3.2.1 Experimental Conditions for Specific Aim 1

The objective of specific aim 1 was to understand the acute effects of normal and abnormal levels of cyclic stretch on aortic valve extracellular matrix content and remodeling. Three levels of cyclic stretch were investigated:

i) 10% - Representing normal physiological stretch (250)

ii) 15% - Representing pathological stretch which may occur in the case of hypertension (280)

iii) 20% - Representing hyper-pathological stretch which may occur in the case of severe hypertension (280)

Leaflet samples were stretched for either 24 or 48 hours. These time points were chosen based on previous studies as necessary and sufficient to observe acute responses in valve cusps (7, 124, 140, 164, 276). Freshly excised valve cusps and statically incubated valve cusps served as controls for the experiments in this specific aim. Statically incubated cusp sections were prepared exactly in the same manner stretched cusps (with threading of springs), but were not stretched for the experimental duration. These samples were incubated in a 6-well plate for the entire experimental duration.

All samples were cultured in normal Dulbecco's Modified Eagle's Medium (DMEM; Sigma) supplemented with 10% fetal bovine serum (Fisher-Scientific, Pennsylvania, PA), 50 mg/L ascorbic acid, 3.7 g/L sodium bicarbonate, 1% (v/v) nonessential amino acid solution, and 1% (v/v) antimycotic-antibiotic solution (all Sigma). Upon completion of the culture (either stretch or static), samples were retrieved and immediately washed three times in ice-cold sterile dPBS before being processed and analyzed further.

4.3.2.2 Experimental Conditions for Specific Aim 2

As the objectives in specific aim 2 were to study the effects of inflammation and calcification, which are processes that take longer time, experiments were carried out for a longer duration. Experimental durations of 3, 7 and 14 days were studied in this specific aim. Three mechanical treatment regimes were explored in this study: (a) fresh tissue (acute control); (b) 10% stretch (physiologic); and (c) 15% stretch (hypertensive). Static controls were not used as they are not representative of a realistic mechanical environment for the aortic valve. This was based on insights obtained from specific aim 1.

Five different modifications of DMEM were initially used to understand their different pro-osteogenic and calcific potentials (Table 4-1). The high phosphate concentration (3.8 mM) and inclusion of TGF-β1 (1 ng/mL) in the osteogenic medium were based on pathophysiologically relevant conditions reported in hyperphosphatemia (143) and previous studies on cells in culture (45, 151).

Table 4-1: Different formulations of culture media used in order to develop a model for calcification in an ex vivo system.

No.	Culture Media	Composition
I	Normal medium	Normal DMEM supplemented with 10% FBS
II	Base osteogenic medium	Normal medium supplemented with: a) 1mM β-glycerophosphate b) 10 μM dexamethasone c) 0.9 mM PO_4^{3-}
III	Base osteogenic medium with high phosphates	Base osteogenic medium with: a) 3.8 mM PO_4^{3-}
IV	Base osteogenic medium with TGF-β1	Base osteogenic medium with: a) 1 ng/mL TGF-β1
V	Full osteogenic medium	Base osteogenic medium with: a) 3.8 mM PO_4^{3-} b) 1 ng/mL TGF-β1

To permit the characterization of the bone morphogenic protein (BMP)-dependent pathway of aortic valve calcification, four different concentrations of the BMP-antagonist noggin (R&D Systems) – 0, 1, 10, 100 ng/mL, were added to the DMEM formulation that elicited the strongest calcific response (i.e. DMEM formulation V as shown in the Results chapter). Noggin was selected as it is a well established BMP antagonist with a weak dissociation constant (K_d) of 20 pM (285). This would allow noggin to bind any expressed BMP and prevent its downstream action (i.e. binding to a receptor on the aortic valve cusp). Additionally, noggin has been previously shown to block the pro-inflammatory effects of BMP-4 expression on vascular endothelial cells (234). Therefore it is an ideal candidate to evaluate the BMP-dependence of aortic valve calcification. Upon completion of the experiments, samples were removed and immediately washed three times in ice-cold sterile dPBS in preparation for further analyses as outlined in **Section 4.4**.

4.3.2.3 Experimental Conditions for Specific Aim 3

The objectives in specific aim 3 were to study the effects of cyclic stretch on serotonin-related valvular degeneration. More specifically, the synergistic effects of serotonin and cyclic stretch on valve collagen biology were studied. As a result a time point of 3 days was used to culture the tissue samples. This time point was shown to result in the most stable expression of markers for collagen synthesis and content, by our laboratory (7, 124) and other researchers (126).

The first set of experiments sought to identify the concentration of serotonin that elicited the greatest response in terms of collagen content. Four different treatment groups, representing four different serotonin concentrations were used for this part of the study: 0, 1, 10, and 100 μM serotonin. These concentrations represent a physiologic range

of serotonin concentrations as demonstrated in recently published *in vitro* and *in vivo* studies (62, 91, 114).

For the latter portion of this specific aim, the objective was to identify the receptor subtypes that were most important in regulating serotonin and stretch-mediated collagen biosynthesis. Studies by other researchers have shown that the 5-HT_{2A} and 5-HT_{2B} receptors are likely to be important in regulating serotonin-related cardiac valvulopathies. These were the same receptor subtypes studied here. As in specific aim 2, pharmacological antagonists with strong affinity for the 5-HT receptor subtype were utilized. Concentrations and antagonists are outlined in **Table 4-2**, and were based on studies (*in vitro* and *in vivo*) conducted by other researchers (19, 123, 137). Upon completion of these experiments, samples were removed and immediately washed three times in ice-cold sterile dPBS in preparation for further analyses as outlined in **Section 4.4**. Samples for uniaxial mechanical testing were immediately preserved in dPBS at 37°C and tested immediately as outlined in **Section 4.6**.

Table 4-2: Different pharmacological antagonists for the 5-HT receptors used in specific aim 3.

5-HT Receptor	Antagonist and Concentration
5-HT_{2A}	50 mM ketanserin
5-HT_{2B}	10 μM SB240741

4.4 Biological Analyses Methods

A variety of quantitative and qualitative biological analyses methods were utilized to understand protein expression and cellular behavior of the aortic valve cusp samples under the different experimental conditions. The methodology for each of these techniques is provided here. Detailed protocols for all assays and stains have been compiled in **Appendix B**. Catalog numbers for all reagents, chemicals and antibodies are compiled in **Appendix B** as well.

4.4.1 Extracellular Matrix Assays

Commercial colorimetric assay kits were used to quantify the collagen, sulfated glycosaminoglycan (sGAG), and elastin content in tissue samples. These resulting samples were dehydrated for 48 hours at room temperature in a vacuum chamber (Yamato Scientific America, San Francisco, CA) and weighed. The tissue dry weight was then subsequently used as the normalizing factor when reporting extracellular matrix content. The tissues were then digested with enzymes dissolved in buffer solutions for a period of 24-48 hours, and the dissolved tissue was used for analysis.

The total amount of collagen, sGAG and elastin was determined using the Sircol Collagen assay kit, Blyscan sGAG assay kit, and Fastin Elastin assay kit (all Accurate Chemicals, Westbury, NY), respectively. These kits used quantitative dye-binding methods to determine the total quantity of the respective extracellular matrix component in the sample.

4.4.1.1 Sircol Collagen Assay

The collagen assay (Sircol collagen assay, Accurate Chemicals) is a quantitative dye-binding method designed for the analysis of soluble collagen. It was utilized here

specifically to quantify enzyme-soluble collagen. The tissue was first digested using pepsin, at a ratio of 1:3 of enzyme to tissue dry weight. The required amount of pepsin (Sigma) was dissolved in 0.5 mL of 0.5 M acetic acid (Sigma) and added to the tissue. The samples were then placed in a water bath at 37°C for 48 hours with occasional agitation. The collagen was converted to a soluble form, as pepsin cleaves part of the C-terminal non-helical region of the α-chains that make up the triple helix of tropocollagen. The samples were then assayed for pepsin-soluble collagen content, which will henceforth be referred to as total collagen content. The assay kit measures mammalian collagen, types I to IV. Collagen standards were prepared using acid soluble collagen, type I, supplied in the kit. Test samples and standard solutions in 0.5 M acetic acid were mixed in a Sircol dye reagent containing Sirius Red in 1.5 ml micro centrifuge tubes. The dye was mixed with the collagen with a vortex tube mixer (VWR, Suwanee, GA). Sirius Red is an anionic dye with a sulphonic acid side chain group that reacts with the side chain groups of the basic amino acids present in collagen thus forming a complex. After collagen-dye complex formation, the tubes were centrifuged to separate the complex pellet from the unbound dye. The supernatant from the tubes was then carefully removed, leaving the pellet at the bottom. A cotton tip was used to remove any remaining supernatant fluid from the tube. An alkali reagent was then added to these tubes and stirred to reconstitute collagen bound dye. The samples were placed in a 96-well plate reader, and the absorbance data was recorded at a wavelength of 540 nm. A standard curve was plotted using the data from the blank and standard samples. The slope of the curve was used as a conversion value to calculate the collagen content of the test samples based on the absorption values. A R^2 value of > 0.98 for the calibration equation was usually considered to give a good estimate, otherwise the assay was repeated.

4.4.1.2 Blyscan Sulfated Glycosaminoglycan Assay

Sulfated glycosaminoglycans (sGAG) in the leaflet tissue were analyzed using Blyscan assay (Accurate Chemicals) in a similar manner as the collagen assay. sGAG assay measures the total sulfated glycan content present in a soluble form. The tissue was digested with protease (Sigma, St.Louis, MO), at a ratio of 1:30 of enzyme to tissue dry weight. Protease dissolved in 0.5 mL of 0.1 M tris-acetate buffer with 10 mM calcium acetate was added to each sample and incubated in the same manner as the collagen samples. sGAG standards were prepared using chondroitin 4-sulfate supplied in the kit. The acetate buffer was used a reagent solution. Sample preparation was done the same way as described in the previous section. Blyscan dye reagent containing 1,9-dimethylmethylene blue in an inorganic buffer containing surfactants and stabilizers was added to all the tubes. Sufficient time was allowed for the dye to bind sGAG while agitating the samples on a vortex tube mixer (VWR, Suwanee, GA). Reaction between the dye and sGAG was carried out in the presence of excess unbound dye and an acidic pH thus producing an insoluble dye-sGAG complex. Tubes with samples containing sGAG turned purple/pink, and the complex precipitated, thus enabling separation from the unbound dye by centrifugation. The pellet was separated from the supernatant solution and dissolved in a dissociation agent to reconstitute the complex into a soluble form for measurement. Absorbance measurement was performed within 3 hours of preparation at a wavelength of 656 nm. The measurement and data analysis methodology were the same as that for the collagen.

4.4.1.3 Fastin Elastin Assay

The Fastin elastin assay (Accurate Chemicals) is also a quantitative dye-binding method for elastin analysis. The dry samples of tissue were digested with proteinase kinase (Fisher Scientific, Suwanee, GA) at an enzyme concentration of 0.5 mg in 1 mL of

buffer solution (5 mL of 50 mM tris-HCl, 3.72 g of 0.1 M EDTA, 1.168 g of 0.2 M NaCl (Sigma) and 95 mL of dH_2O) in each tube. Test and standard samples were prepared in the same manner as for the previous assays using bovine α-elastin standard. 1 mL of elastin precipitating agent was added to each of these samples and incubated in ice cold water overnight. The next morning the samples were transferred to ice and incubated for about 30 minutes to bring the sample temperature to 0°C. The samples were then centrifuged to separate elastin, which was mixed with dye reagent along with 200 µl of 90% saturated ammonium sulfate. The dye was then stirred for one hour to allow the dye to bind with the elastin. The Fastin dye reagent contains 5, 10, 15, 20- tetraphenyl-21, 23-porphrine in a water soluble form as the sulfonate (i.e tetra sulfonate). The dye binding to elastin followed a shape-and-fit phenomenon wherein the acidic dye was firmly retained by the basic amino acid side chain residues of elastin. After sufficient time was allowed for complex formation, the tubes were centrifuged and the pellet was separated from the supernatant. The pellet was then dissolved in the provided dissociation agent and absorption values were measured at 513 nm. The analysis was done using the method described in the previous sections.

4.4.2 Histology and Immunohistochemistry

After appropriate experimental treatment, cusps for histological staining were were fixed in 10% neutral buffered formalin (Fisher Scientific, Suwanee, GA) for 24 hours, saturated in 70% ethanol, processed in a tissue processor (Shandon Pathcenter enclosed Tissue Processor) in descending grades of ethanol, embedded in paraffin and cut into 5 µm sections using a microtome. Samples for immunohistochemistry were flash frozen in optimum cutting temperature (OCT) media (Electron Microscopy Sciences, Hatfield, PA) and cut into 5 µm sections using a cryostat.

Paraffin sections provide better preservation of morphology and tissue structures and are usually the method of choice for preparing tissue slides for histological examination. However, the temperature of processing for paraffin embedding (approximately 60°C) denatures some proteins and renders their antibody binding sites unavailable for immunohistochemical staining methods. As a result, we employed frozen sections for all immunostains.

Cells are essentially transparent, with little or no intrinsic pigmentation. Even red blood cells, packed with hemoglobin, appear nearly colorless when unstained, unless packed into thick masses. Stains are used to confer contrast, to make tissue components visibly conspicuous. Certain special stains, which bind selectively to particular components, may also be used to identify those structures. The essential function of staining is simply to make structures visible. The following sections will include a description of the histological staining procedures employed in this dissertation.

4.4.2.1 Hematoxylin and Eosin Staining

Hematoxylin and Eosin (H&E) staining is a commonly used staining method for tissue structure visualization. Hematoxylin is a basic dye that stains acid structures purple or blue. Structures like Chromatin (i.e., cell nuclei) and ribosomes that are stained by basic stains are described as basophilic. Eosin is an acidic dye that stains basic structures red. Structures such as collagen fibers, red blood cells, muscle filaments and mitochondria that are stained by acid stains are described as acidophilic. H and E staining was done automatically on a staining machine (Leica Autostainer, Vashaw Scientific, Norcross, GA). Paraffin sections were first run through a series of xylene substitutes (3 stations, 5 minutes each) and alcohols (100% x 2, 95% and 75%, each for 2 minutes), then washed in water for 2 minutes prior to immersing into hematoxylin for 30 seconds.

Afterwards, the slides went through water (2 minutes), acid alcohol (1 second), and water (1 minute), Scott's solution (30 seconds) and were then washed in water for 2 minutes. Following this, the slides were immersed in acid alcohol for 1 minute before being stained with Eosin for 30 seconds. Subsequently, the slides were run through a series of alcohols (95%: 30 seconds, 100%: 1 minute, 100%: 2 minutes x 2) and xylene substitute (twice, each for 2 minutes) and finished in xylene. A resinous mounting agent was applied and the slides were coverslipped and allowed to dry overnight before viewing.

4.4.2.2 Movat's Pentachrome Staining

Movat's staining protocol is a procedure that allows for the demonstration of a variety of tissue elements in a single section (163). For the unique structure like that of the aortic valve, it allows evaluation of the alteration of native structures under pathological conditions. The procedure utilized in this dissertation was based on Garvey's modification of Movat's staining (78), and was optimized to get the best possible results.

The procedure consists of the following major steps after deparaffinization. The slides were firstly incubated in alcian blue at 60°C for 10 minutes to stain the ground substance as well as glycoaminoglycans (GAG). Slides were subsequently washed in tap water and then immersed in a modified Verhoeff solution at room temperature for 6-7 min. It is a special stain for the elastic fibers and cell nuclei. The next step was a quick rinse in aqueous ferric chloride for 5-10 seconds to get rid of excessive Verhoeff stain. Then the slides were immersed in plasma stain allowing for visualization of fibrin, cytoplasm and muscle tissue. This was followed by a 15 minute immersion in polyacid to remove the excessive plasma stain. Subsequently, the slides were dehydrated in a graded

alcohol sequence and then stained in saffron (Saffron du Gatinais in absolute ethanol) for 15 minutes to 1 hour. Saffron binds to collagen and gives it a yellow color. Since saffron is soluble in water, the dehydration step was essential to prevent saffron loss. After saffron staining, the slides were dehydrated in a series of alcohol and cleared in xylene, and finally mounted with a resinous media and coverslipped. For this staining protocol, nuclei were stained blue-black, elastic fibers black, cytoplasm and fibrin red, collagen yellow and ground substances blue.

4.4.2.3 Picrosirius Red Staining

Picrosirius red staining was performed to examine collagen fiber structure and morphology. In bright-field microscopy collagen is red on a pale yellow background. Nuclei, if stained, are ideally black but may often be grey or brown. The long time in picrosirius red solution causes appreciable destaining of the nuclei. When examined through a circularly polarized filter the larger collagen fibers are bright yellow or orange, and the thinner ones, including reticular fibers, are green. According to Junqueira *et al* (118) the birefringence is highly specific for collagen. A few materials, including Type IV collagen in basement membranes, keratohyaline granules and some types of mucus, are stained red but are not birefringent. The protocol employed here was as follows. Deparaffinized slides were stained in picrosirius red solution for one hour. The slides were then washed in acidified water, three changes of 100% ethanol, and xylene before being mounted in a resinous medium and coverslipped.

4.4.2.4 Alizarin Red Staining

Alizarin red was used to stain for tissue calcification. Alizarin Red S, an anthraquinone derivative, may be used to identify calcium in tissue sections. The reaction is not strictly specific for calcium, since magnesium, manganese, barium, strontium, and iron may interfere, but these elements usually do not occur in sufficient concentration to interfere with the staining. Calcium forms an Alizarin Red S-calcium complex in a chelation process, and the end product is birefringent. Deparaffinized slides were hydrated and stained in Alizarin red solution (pH = 4.1 – 4.3) for 10 minutes while checking for staining microscopically. The slides were then dehydrated in acetone-xylene, cleared in xylene before being mounted in a resinous medium and coverslipped. Calcium deposits appeared orange-red when viewed under normal white light.

4.4.2.5 von Kossa Staining

Von Kossa staining was used as an additional method for demonstrating tissue mineralization. This technique is for demonstrating deposits of calcium or calcium salt so it is not specific for the calcium ion itself. In this method, tissue sections are treated with a silver nitrate solution and the silver is deposited by replacing the calcium reduced by the ultraviolet light, and thereby visualized as metallic silver. Briefly, deparaffinized sections were hydrated and incubated in 1% silver nitrate solution in a clear glass coplin jar placed under ultraviolet light for 30 minutes. After washing in several changes of distilled water, excess silver nitrate was removed by incubating in 5% sodium thiosulfate for 5 minutes. The slides were rinsed in distilled water, dehydrated through graded alcohol and cleared in xylene before being mounted in a resinous medium and coverslipped. Calcium deposits appeared black when viewed under normal white light.

4.4.2.6 General Protocol for Immunohistochemistry

The immunohistochemistry protocol was as follows. Slides were first thawed to room temperature, and permeabilized in acetone at -20°C. Sections were then blocked using either 10% animal serum in phosphate buffered saline (PBS, Sigma), or 1% Bovine Serum Albumin (BSA)/ PBS for 30 minutes. The choice of animal serum to use as the blocking agent depended on the species that the secondary antibody was raised in. This step is to ensure that there is no non-specific binding of the secondary antibody to the section. Following the blocking step, the slides were then incubated in primary antibody in 2 - 10% blocker for 2 hours. The sections were then saturated in biotinylated secondary antibody (Vector laboratories) in 2% blocker (Vector laboratories) for 1 hour. Subsequently, either Avidin-D Texas red or Avidin-D Fluorescein (both Vector Laboratories) fluorochrome was applied to the sections after the secondary antibody was washed off, for 30 minutes to 1 hour. The sections were then counterstained with 0.25 μgmL^{-1} 4',6-Diamidino-2-phenylindole (DAPI; Sigma), coverslipped and stored at $4^{o}C$. Slides were subsequently imaged under a mercury lamp using a TR/FITC/DAPI filter.

4.4.2.7 Cell Proliferation

Immunohistochemistry was utilized to study cellular proliferation. Labeling cells, which are active in the cell cycle, can assess the growth fraction of a tissue section. Cells in the synthesis phase will take up thymidine or analogs of thymidine such as 5-Bromodeoxyuridine (BrdU). Incorporated molecules can be identified by immunohistochemistry using an anti-BrdU antibody. Counting the number of labeled cells will give an estimate of the synthesis phase fraction.

Anti-BrdU (BrdU; Sigma) immunohistochemistry was therefore used to visualize proliferating cells. Experiments were run with 5 mgL^{-1} BrdU included in the DMEM for the last 24 hours of the experiment. BrdU can be toxic to tissues and was therefore only added to the culture media if cell proliferation assays were carried out. Deparaffinized sections were pretreated with proteinase K and subjected to 4N HCl (Sigma). The acid served to dissolve histones associated with DNA. This permitted uncoiling of the DNA and accessibility of reagents to all parts of the nucleic acids. The sections were then subjected to tris-buffered EDTA (Sigma, St.Louis, MO) which acts to neutralize the acid step previously performed. Blocking was performed once the pH was in the range of 7.0-7.5, which was determined using a pH indicator strip. The primary antibody, anti-BrdU (Dako, Carpinteria, CA) at a concentration of 1:20 in 1% crystalline grade bovine serum albumin (BSA, Sigma) in PBS, was applied to the sections and incubated for an hour at room temperature. The rest of the protocol was as outlined in the previous section.

4.4.2.8 Cell Apoptosis

Apoptosis or programmed cell death is a crucial process in development, normal cellular differentiation, and tissue homeostasis in all multicellular organisms. Apoptosis can be triggered by a variety of cellular death stimuli including tumor necrosis factor. A terminal deoxynucleotidyl transferase dUTP nick end labeling (TUNEL) assay kit (Roche Applied Science, Indianapolis, IN) was used to identify apoptotic cells. TUNEL is a common method for detecting DNA fragmentation that results from apoptotic signaling cascades. The assay relies on the presence of nicks in the DNA which can be identified

by terminal deoxynucleotidyl transferase, an enzyme that will catalyze the addition of dUTPs that are conjugated with a marker.

4.4.3 Immunoblotting

The use of immunohistochemistry allows determination of the spatial distribution of the protein of interest, and at most allows semi-quantitative analysis. Immunoblotting or western blotting as it more commonly known is performed to allow quantitative measurement of the proteins of interest. Immunoblotting employs antibody-antigen binding to identify the target protein of interest. Proteins are first separated by size, in a thin gel sandwiched between two glass plates. This technique is called SDS-PAGE (Sodium Dodecyl Sulfate Polyacrylamide Gel Electrophoresis). The proteins in the gel are then transferred to a PVDF, nitrocellulose, nylon or other support membrane. This membrane can then be probed with solutions of antibodies. Antibodies that specifically bind to the protein of interest can then be visualized by a variety of techniques, including chemoluminescence or radioactivity. All the Western blots in this study are visualized by chemoluminescence.

Briefly, after the appropriate experimental treatment, aortic valve cusp tissues were pulverized using a mortar and pestle in liquid nitrogen and homogenized in ice-cold RIPA buffer (Santa-Cruz, Santa Cruz, CA), and centrifuged at 15,000 rpm to pellet extracellular matrix debris. The supernatant was assayed for protein concentration using the BCA Protein Assay (Pierce, Rockford, IL). Equal amounts (30 μg) of tissue lysates were resolved by reducing SDS-PAGE. After transfer to a PVDF membrane (Millipore, Billerica, MA), the blots were blocked with 3% BSA, probed with primary antibody, and appropriate biotinylated secondary antibody. The membranes were finally incubated in horseradish peroxidase-conjugated streptavidin. Immunopositive bands were then detected using a luminol-based chemiluminescence reagent (Pierce, Rockford, IL) against

standard radiography film in a darkroom. The films were then analyzed by densitometry using the ImageJ program (4.5.3).

4.4.4 Gelatin Zymography and Reverse Zymography

Zymography is a technique that analyzes enzymatic activity of proteases, which cannot be achieved by either immunohistochemistry or immunoblotting, which detect both the active form and the latent form of the enzyme but allows no determination of the actual activity of this enzyme. Zymography techniques employ incorporation of an enzyme substrate (gelatin, casein, collagen etc) into the SDS-PAGE gel. This method is used to quantify the activities of gelatinases within the valve samples. After electrophoresis, the proteins are renatured and allowed to digest the substrate. The gels are then stained with a protein stain. Clear bands appear at the locations where the substrate was digested by the enzyme in the sample. The size and location of bands therefore correspond to the activity of a particular substrate enzyme within the sample.

More specifically, equal amounts (5 μg) of tissue lysate were resolved at 4°C by 10% non-reducing SDS-PAGE containing 1 mg/mL gelatin. After electrophoresis, the gels were cleared of SDS by incubating for 30 min with two changes of 2.5% (v/v) Triton X-100 (Sigma). Gels were then incubated in substrate buffer (50 mM Tris, pH 8.0, 50 mM NaCl, 10 mM $CaCl_2$ and 0.05% Brij-35) at 37°C for 8 – 10 h. The gels were then rinsed with deionized water and stained with 0.5% Coomassie Brilliant Blue and destained. Proteolytic activity was observed as clear bands against a blue background, and were analyzed using densitometry (4.5.3). Each zymography experiment was performed in duplicate.

Gelatin reverse zymography was used to analyze the activity of gelatinase inhibitors. In this technique, an enzyme is incorporated together with the substrate in the gel. Once the gel is placed in the renaturation buffer, the incorporated enzyme will also begin to degrade the substrate. This will be inhibited by specific gelatinase inhibitors within the sample, and the locations of these inhibitors will be characterized by darker bands against a lighter background (due to digestion of substrate).

Briefly, equal amounts (50 μg) of tissue lysate were resolved at 4°C by 12.5% non-reducing SDS-polyacrylamide gels containing 1 mg/mL gelatin and 150 ng/mL MMP-2/MMP-9 (Millipore). After electrophoresis, the gels were cleared of SDS by incubating for 30 min with two changes of 2.5% (v/v) Triton X-100 (Sigma). Gels were then incubated in substrate buffer (50 mM Tris, pH 8.0, 50 mM NaCl, 10 mM $CaCl_2$ and 0.05% Brij-35) at 37°C for 24 h. The gels were then rinsed with deionized water and stained with 0.5% Coomassie Brilliant Blue and destained. Inhibitory activity was observed as dark blue bands against a lighter blue background, and these bands were then analyzed using densitometry (4.5.3). Each reverse zymography experiment was performed in duplicate.

4.4.5 Alkaline Phosphatase Activity Assay

Alkaline phosphatase (ALP) is a hydrolase enzyme responsible for removing phosphate groups from many types of molecules, including nucleotides, proteins, and alkaloids. ALP is also secreted by osteoblasts and in this dissertation was used as a marker for osteogenic differentiation of valve cells. The protocol used was based on the

rate of formation of the yellow color of p-nitrophenol produced by hydrolysis of p-nitrophenylphosphate in alkaline solution is measured at 405nm and 37°C.

Samples were pulverized using a mortar and pestle in liquid nitrogen and homogenized in ice-cold RIPA buffer (Santa Cruz) before centrifuging at 15,000rpm to pellet extracellular matrix debris. The supernatant was assayed for protein concentration using the BCA Protein Assay (Pierce). ALP activity in the tissue lysate was assayed by adding 10mM p-nitrophenyl phosphate as a substrate in 0.1M glycine buffer (pH10.4) containing 1mM $ZnCl_2$ and 1mM $MgCl_2$. The quantity of p-nitrophenol formed was determined by spectrophotometry at 405nm and then monitored at 15, 30, 60, 120 and 180 minutes and after 24 hours. ALP activity was calculated from a standard and normalized with the protein concentration. The specific activity of ALP was reported as nmol per minute per mg protein.

4.4.6 Calcium Arsenazo Assay

Total calcium content in tissue samples was quantified using the calcium arzenazo assay. This was used as a marker to represent calcification of the tissue. At a neutral pH, the Ca^{2+} forms with arsenazo III a purple-colored complex, the color intensity of which is directly proportional to the concentration of calcium in the sample. Tissue samples were weighed and pulverized using a mortar and pestle in liquid nitrogen, incubated in 1M acetic acid for 24 hours at 4ºC to solubilize calcium, and centrifuged at 15,000rpm. The supernatant as well as calcium standards were assayed for calcium content using a calcium specific arsenazo dye reagent (Fisher Scientific). The quantity of reaction product formed was determined by spectrophotometry at 650nm. The calcium content was normalized with the weight of the sample and expressed as μg calcium per mg wet weight.

4.5 Image Analysis and Semi-Quantification Using ImageJ Software

Normally immunohistochemical techniques give a qualitative assessment of protein expression in a tissue sample. In this dissertation, all immunohistochemical stains were analyzed using ImageJ software (National Institutes of Health, Bethesda, MD) in order to obtain a semi-quantitative representation of the intensity and area coverage of immunopositive staining in a given tissue sample. This would allow one to more effectively compare the histochemical methods with results obtained from the quantitative methods. Standard image analysis was also performed for all immunoblotting films and zymograms using the same software.

4.5.1 Analysis of Picrosirius Red Images

In samples stained with picrosirius red, collagen fibers exhibit birefringence depending on their relative size. This principle can be used to quantify the relative proportion of the different maturity of the collagen fibers in the leaflet. A computational software was written for this purpose. Picrosirius red images were first imported into Matlab 7.01 (The Mathworks, Natick, MA) and converted into their hue, saturation and value components. Only the hue components were retained, and a histogram of hue frequency was obtained from the 8-bit hue images that contained 256 possible colors. The colors were defined as follows: red 2 to 9 and 230 to 256; orange 10 to 38; yellow 39 to 51; and green 52 to 128. These color ranges were determined, validated and published by Aikawa *et al* (3). All other hue values corresponded to interstitial space and were confirmed by visual inspection. The number of pixels within each hue range were determined and expressed as a percentage of the total number of collagen pixels (sum of all pixels) and plotted. This method has been employed by other researchers as well (3). The Matlab code has been compiled in **Appendix E**.

4.5.2 Semi-quantification of Immunohistochemistry Images

Image analysis of immunohistochemistry images allows semi-quantification of an otherwise qualitative image. The basic principle is to integrate the pixel-by-pixel intensity within an image field in order to obtain the total intensity of immunopositive staining per microscope image field. This is then normalized by the number of cells visible in the image fields to yield a quantity consistent to an expression of inflammatory marker per cell. Immunopositive staining appears either red (Texas Red) or green (Fluorescein), while cell nuclei are counterstained blue (DAPI), based on the fluorescently-conjugated antibodies that were used.

The number of cells was estimated by analyzing the image field captured using the DAPI filter of the mercury lamp, thresholding the blue channel image, and using the "analyze particles" function of ImageJ. The total expression of a given marker was assessed on microscope images captured by the camera using the Fluorescein (green) or TRITC (red) filter, depending on the marker of interest. Each image was split into its red, green and blue channels, and Image J was used to compute the integral of the red or green channel histogram. Finally, the cellular expression was calculated in each image as the ratio of the total expression of marker to the number of cells.

ImageJ was also used to quantify the results of the cell proliferation and apoptosis assays. Proliferating cells were detected using red fluorescence, while cells with apoptotic fragments were detected using the green fluorescence of the microscope. The DAPI filter was used to image cell nuclei present on the micrograph. The proliferation/apoptosis level was estimated as the ratio of the number of immunopositive cells to the total number of cells. Distinction was not made between endothelial and interstitial cells during the cell counting.

4.5.3 Densitometry of Immunoblots and Zymograms

In the case of immunoblot films and zymogram gels, the ImageJ software provides a dedicated macro to plot the histogram of individual lanes/bands in blots or gels. These histograms were then integrated to get the mean intensity of each immunopositive or zymogram band. These intensities for a particular protein or zymogen were then normalized by the intensity values for β-actin, which was used as a housekeeping protein.

4.6 Uniaxial Mechanical Testing

The first part of specific aim 3 of this thesis provides information on the biosynthetic and mitotic effects of serotonin. In order to extend these results to valve function, it would be necessary to understand changes in valve mechanical properties. Uniaxial mechanical testing was therefore conducted to understand the change in tissue mechanical properties under the various treatment groups with serotonin receptor antagonists. This will allow us to gain a good understanding of the effect of 5-HT on aortic valve biology, structure and function.

4.6.1 Tissue preparation and setup

The uniaxial tests were performed and completed no more than 2 hours after the stretch experiments using a Bose Enduratec® Elph testing machine (Bose Corporation) (**Figure 4-10**). A 5N load-cell was mounted along the axis of the motors (to the lower motor) to record real-time changes in load as the sample was tested. All control of the motors and load-cell were performed using the Wintest® Software bundled with the Bose tester. All data for the test (motor displacements and load) were recorded at a rate of 100 data points per second.

A high speed, high resolution camera (Basler A504k, Basler Vision Technologies, PA) and a halogen lamp were positioned on a tripod approximately 0.5m from the test sample (**Figure 4-10**). The light and lens (105mm f/2.8D AF Micro-Nikkor, Nikon, USA) were adjusted to achieve maximum contrast between the markers and background as seen in **Figure 4-11** below. The camera was connected to an EPIX high speed frame grabber card (PIXCI CL3SD Frame Grabber, EPIX Inc., USA) which were synchronized using the EPIX software. Images were recorded simultaneously at 100 frames per second with an 8 bit gray-scale and a resolution of 1280 × 1023 pixels.

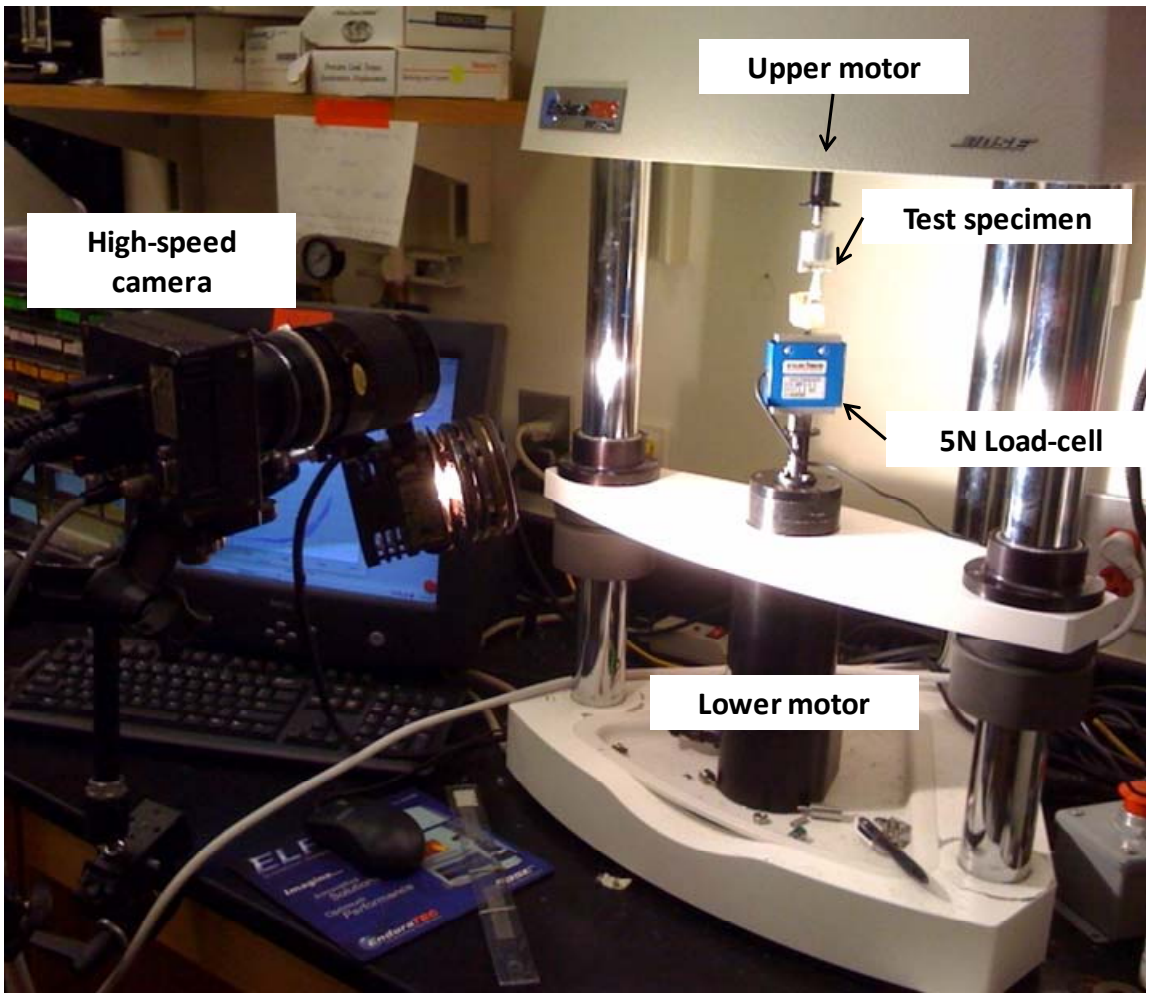

Figure 4-10: Photograph showing the setup for uniaxial mechanical testing. A 5N load cell was mounted in-line with the long axis of the sample. A high-speed camera was used to capture the deformation of the valve sample at 100 frames per second. The sample was topically hydrated with dPBS to ensure that it did not dry out during the experiment.

4.6.2 Experimental Protocol

After the stretch experiments, specimens were first quickly patted dry with soft tissue wipes (Kimberly-Clark Corporation, Neenah, WI) and a 4x3 marker grid (**Figure 4-11**) was placed in the central portion of the tissue using tissue marking dye (Thermo-Scientific). After the dye was allowed to dry, the sample was returned to dPBS to keep it hydrated.

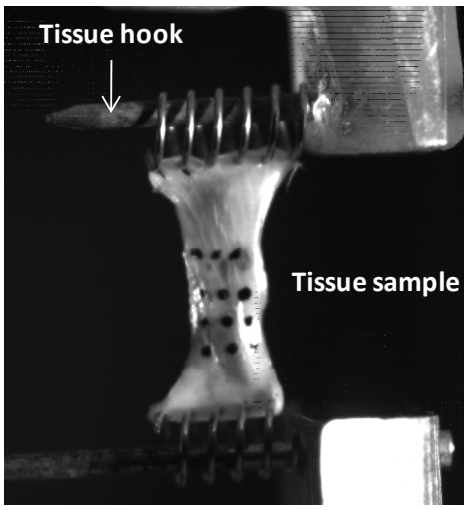

Figure 4-11: Picture showing tissue sample as viewed through the high-speed camera. The 4x3 marker array can be clearly imaged. Stainless steel springs were used to mount the sample to the tissue hooks.

The stainless steel springs (**Figure 4-9**) were used to couple the sample to the upper and lower arms of the uniaxial machine by custom tissue hooks (**Figure 4-11**). These hooks allowed secure placement of the tissue without slippage and would not result in stress-concentrations that would otherwise develop if the tissue had been clamped. These hooks also utilized the stainless steel springs that were in place for the stretch experiment. Further handling of the tissue was therefore minimized. Another advantage of using these springs is that the off-axis deformation of the tissue is minimized, and mechanical tests are done in a strip-biaxial configuration (239).

4.6.3 Maximum Physiological Load

Aortic valve maximum physiological load was estimated using Laplace's law ($T = \frac{\mathrm{Pr}}{2}$), assuming the valve was roughly spherical with a radius of 10mm.T is mean valve membrane tension (defined as the load per unit length over which it is applied), P is transvalvular pressure and r is radius. A transvalvular pressure of 80mmHg (~106.7kPa) was used, and substituting these values yielded a membrane tension of 53.35N/m. It was

decided to slightly overestimate the physiological condition because this would make it more likely that the physiologic condition would be included in the load range, so this estimate was rounded up by about 10% to 60N/m. This peak membrane tension level was converted to axial load by multiplying by the largest expected specimen dimension (15mm). This yielded a peak load value of 0.9 N.

4.6.4 Preconditioning of Samples

After the sample was mounted, the top motor was jogged until a load of 0.005N was read by the load-cell. This was designated as the tare load, and as the resting state of the valve specimen. Each sample was first preconditioned, where the specimen was stretched such that the membrane tension (T) (defined as the force per unit length of tissue over which it was applied) along each specimen edge was increased to 60N/m over a cycle period of 1 second (1Hz) for 20 cycles to allow the load-strain response of the valve to become repeatable. All loading was performed in the load control mode. It has been shown that the behavior of heart valve tissues are strain-rate independent (87, 88) and a frequency of 1Hz was chosen so that the experiments can be completed in a timely fashion, thereby minimizing exposure of the sample to the air. To increase test repeatability, all initial loading cycles were initiated at the tare load of 0.005N and all stretch data presented were referenced to the preconditioned tare configuration which was taken at the 0.005N tare load after the 20 preconditioning cycles.

4.6.5 Stretch Protocol

After the preconditioned tare reference of 0.005N was recorded, specimens underwent a stretch protocol to record their mechanical behavior. Each specimen was subject to 3 cycles of loading-unloading to 60N/m, and camera acquisition of the deformation was conducted simultaneously.

4.6.6 Analysis of Strain Data

Marker coordinates in the images were first automatically tracked over the image frames over the stretching motion using a protocol developed in our laboratory and utilized in several studies (280).

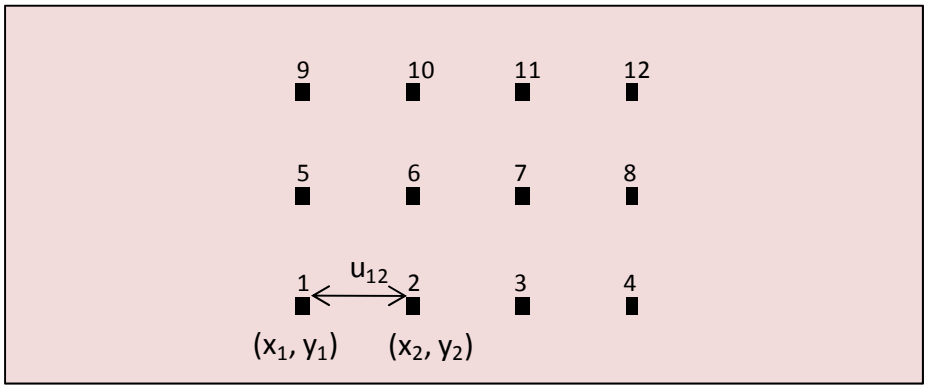

Figure 4-12: Schematic showing the labeling of the 12 markers on valve sample and the notation used for their coordinates and distance between two adjacent points. The nine different displacements were calculated based on the marker coordinates and the mean stretch ratio was calculated from this data.

These coordinates were then used to calculate the change in displacement (u) between adjacent points (**Figure 4-12**), where:

$$u_{12} = \sqrt{(y_2 - y_1)^2 + (x_2 - x_1)^2}$$

Only horizontally adjacent points were considered as we were interested in extracting strains in the direction of loading. This therefore yielded nine values of displacements for a particular image (u_{12}, u_{23}, u_{34}, u_{56}, u_{67}, u_{78}, u_{910}, u_{1011}, u_{1112}). In this fashion, displacements were obtained for the entire duration of the loading (i.e. over 100 frames of images). The stretch ratio (λ) between adjacent points was then calculated using the formula: $\lambda_{12,i} = \frac{u_{12,i}}{u_{12,0}}$, where subscript i refers to a particular image frame, while subscript 0 refers to the reference image frame. The mean stretch ratio for each

image frame was then obtained by taking the average of the nine stretch ratios (of each of the horizontal line segments between markers). The final step of this analysis was to calculate Green's strain (E) for each image frame from the stretch ratios using the formula:

$$E_i = \frac{1}{2}\left(\lambda_{mean,i}{}^2 - 1\right)$$

The membrane tensions (Force per unit length) were then plotted for each value of Green's strain. Since the data for load and strains were taken at the frame rate, there should be good correspondence between the load data and the strain data.

4.7 Statistical Methods

4.7.1 Power Analysis and Sample Size

A priori power analyses was performed using G*Power (ver. 3.0.10, Universität Kiel, Germany). The effect size and required sample size was calculated using data from the first set of experiments (**Section 5.2.1**). Ideally desired power (1 - β error probability) was 0.95, and α error probability was 0.05. Based on this data set, the calculated effect size was large at f = 0.829. The sample size per group for the required power was determined as n ≥ 7. The output from G*Power for this data set is captured in **Figure 4-13**.

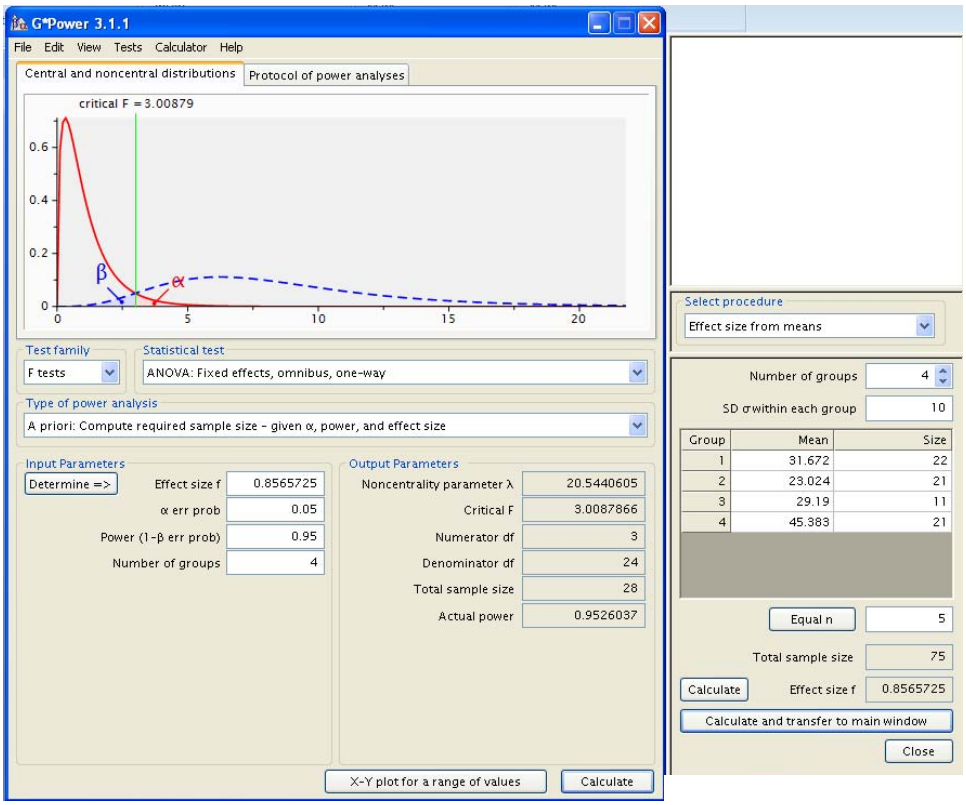

Figure 4-13: Output from G*Power demonstrating the required sample size (n=4) for the four groups in the data set to achieve a power of 0.95 with α error probability of 0.05. This translates to a sample size of at least n=7 for each treatment group.

The above power analyses was further verified with two more data sets from the first set of experiments, and it was determined that the minimum sample size for any experiment would be limited to n=7. Some of the experiments (especially in specific aim 2) were run with a smaller sample size of n=6 due to limited availability of tissue and loss of tissue to bacterial/fungal contamination. For those experiments, *post hoc* power analyses will be conducted to ensure that the minimum required power (1 - β error probability) of at least 0.7 could be achieved.

4.7.2 Experimental Variation and Repeatability

Biological tissues have high animal-to-animal variability and care was taken to minimize possible confounding effects. One method employed was to randomize the cusp samples before picking samples for the specific experimental treatment. By randomizing, variations due to anatomical location (i.e. left, right and non-coronary) as well as animal-to-animal variations will be averaged out.

Experimental repeatability is also of paramount importance. Although the stretch bioreactor can accommodate 16 different samples, samples for a particular treatment group would be obtained over at least 3 separate experimental runs. This would minimize any confounding influences from any particular batch of animals slaughtered at the abattoir.

It should be noted that each sample in a tissue well was designated as n=1. This is acceptable as each tissue sample within a treatment group originated from a different animal. No pooling of data was performed or required as there was enough material from each sample to perform all subsequent analyses.

4.7.3 Quantitative Data Statistical Analyses

Quantitative data from all experiments were first tested for normality via the Anderson-Darling method. Data was expressed as mean ± standard error. Minitab software (Minitab release 14, Minitab Inc. State College, PA), Excel (Microsoft Corp, Bellevue, WA) and R (Open Source**, http://www.r-project.org/**) will be used for the analyses. The difference between the samples will be considered significant if the p-value < 0.05.

Student t-tests will be used for testing the difference between sample groups when the data follow a normal distribution, and only two groups are being compared. A hypothesis test of the difference between population means and standard deviations will be used. ANOVA will be used for the analysis with Tukey's post-hoc test for comparisons between multiple groups. If the data are not normally distributed, Mann-Whitney and Friedman tests will be used in place of student t-tests and ANOVA, respectively. The Mann-Whitney test performs a hypothesis test of the equality of two population medians and calculates the corresponding point estimate and confidence intervals. In this analysis, the data from two populations that have the same distribution are assumed to be independent random samples.

CHAPTER 5

RESULTS

This chapter compiles all the results from this dissertation. The first section contains the results from the mechanical validation of the stretch bioreactor. The subsequent sections will report detailed results from each of the three specific aims. To recap, specific aim 1 sought to understand the effects of cyclic stretch on aortic valve extracellular matrix remodeling, which is generally an early indicator of degenerative aortic valve disease. The subsequent specific aims studied disease processes that were further downstream. Specific aim 2 studied the phenomena of inflammation and calcification, while specific aim 3 studied the effects of cyclic stretch on serotonin-related valvular degeneration.

To recall, three levels of cyclic stretch were imposed on porcine aortic valve cusp samples to simulate both physiological as well as pathological levels of stretch. 10% cyclic stretch is experienced by valve cusps under physiological conditions (250) and was used as the normal stretch magnitude. A magnitude of 15% cyclic stretch was used to simulate a pathological level of stretch; a magnitude of 20% stretch was used to simulate a severe or hyper-pathological level of stretch. The latter two levels of stretch were based on a paper published by our laboratory that reported a 5% increase in stretch/strain on the aortic valve cusp from an increase in mean peak pressure of 40 mmHg (280). A tensile stretch bioreactor was used to subject these levels of stretch on aortic valve tissue samples.

Only representative images of the immunohistochemistry and western blotting results have been printed in this chapter. The full set of micrographs and western blotting films are compiled on DVD. In addition, complete original numeric data for all the quantitative analyses are contained in **Appendix C**.

5.1 Mechanical Validation of Stretch Bioreactor

As outlined in the M chapter, it is crucially important to first validate and characterize the mechanical environment of the tensile stretch bioreactor before embarking on any experiments. In this dissertation, the stretch as well as the fluid shear stress environment of the cyclic stretch bioreactor was characterized and reported. The purpose of this validation was to verify that cyclic stretch was the dominant mechanical stimulation being imposed on the valve cusp samples.

5.1.1 Stretch Environment of the Bioreactor

High speed video camera capture was used to capture images of the samples as they deformed within the stretch chamber. These images were then tracked to quantify the strain experienced by four regions (**Figure 4-7**) on each sample in every single tissue well of the stretch bioreactor for three different input peak strain magnitudes (10%, 15%, 20%).

The mean peak strain magnitude (across all 16 tissue wells) experienced by a tissue sample in the stretch bioreactor was 9.81±0.47%, 14.91±0.75%, and 20.09±0.88% for 10%, 15%, and 20% input strain, respectively (**Figure 5-1**).

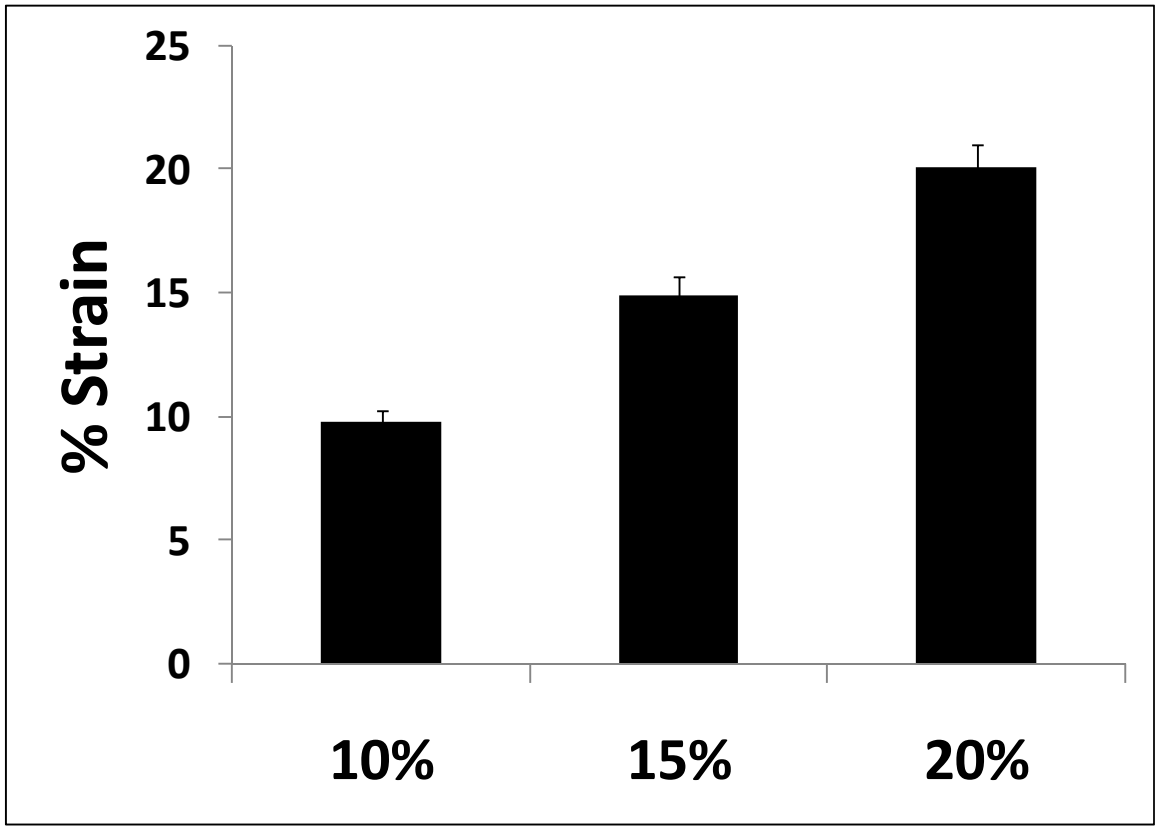

Figure 5-1: The actual peak strain magnitude experienced by a tissue sample in the tensile stretch bioreactor for 10%, 15%, and 20% input strain as determined by high speed camera capture. The standard deviation was less than 5% of the mean value for all three levels of strain.

The variation in strain across the four regions (**Figure 4-7**) of the leaflet sample for each tissue well was analyzed next. The results (**Figure 5-2**) demonstrate that the strains across the four regions of interest across the valve leaflet were relatively uniform with standard deviations that do not exceed 5% of the peak strain magnitude. Stress concentrations and high strains potentially exist along the edges of the sample where the springs are threaded. However, those regions are not used for biological analyses and they are cut and discarded after each experiment as outlined in the previous chapter.

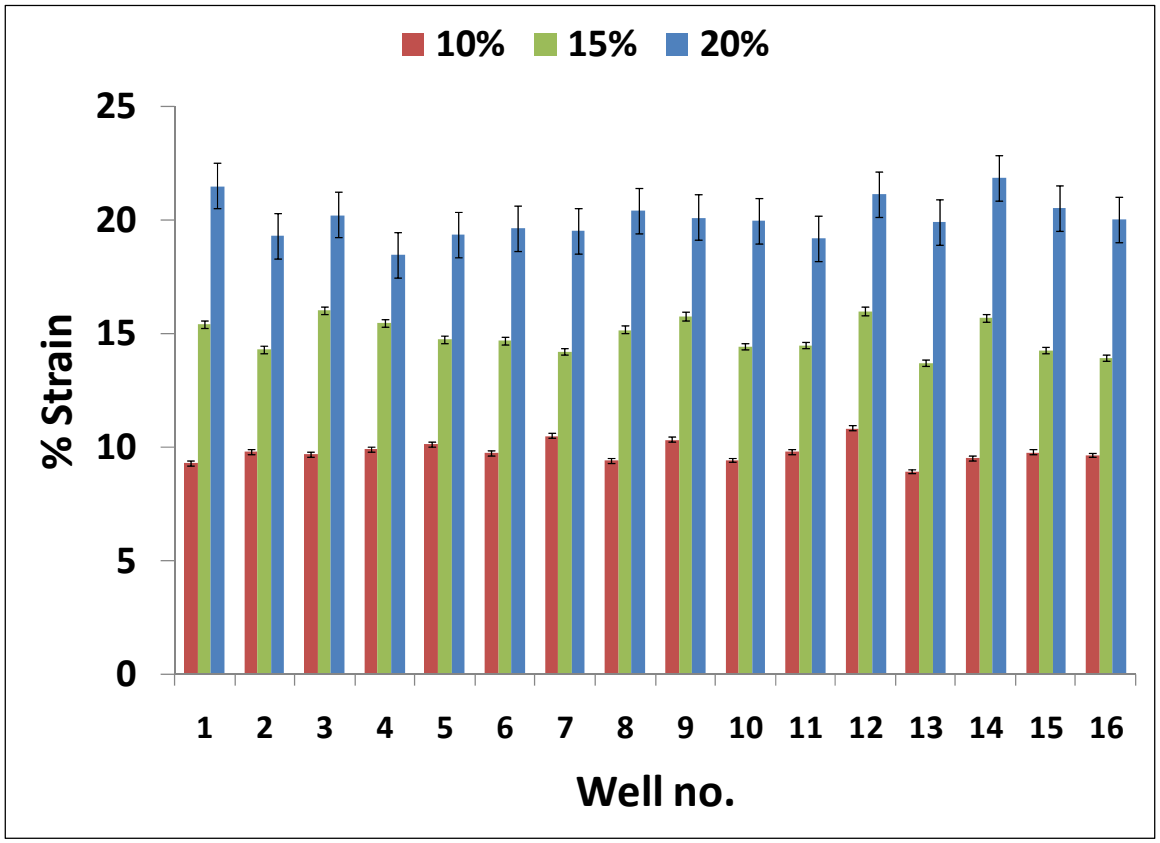

Figure 5-2: The mean strain (over the four regions) experienced by a sample in each of the tissue wells of the stretch bioreactor for the three peak input strain magnitudes (10%, 15%, 20%) of interest is depicted here in this graph. It can be noted by the standard error bars that the variation of strain within each sample was negligible.

5.1.2 Analytical Estimation of Shear Stress Environment in Bioreactor

Fluid shear stresses are experienced by a leaflet sample surface as it stretches and returns to its original configuration within the tissue culture medium in the tensile bioreactor. The maximum fluid shear stresses on the leaflet were estimated analytically by imposing an oscillating plate solution for when the sample returns to its undeformed configuration from the stretched configuration (i.e. during the simulated opening of the valve). The sample undergoes the highest stretch velocities during this portion of its deformation and it is therefore reasonable to assume that the fluid shear stresses will be highest.

To recall, the equations below represent the spatial velocity and fluid shear stress on the sample surface respectively. In particular, **Equation V-2** will provide information on the temporal variation of the fluid shear stresses experienced by a cusp sample in the tensile stretch bioreactor:

$$u(y,t) = Ue^{-y/\delta_s}\cos\left(\frac{y}{\delta_s} - \omega t\right) \tag{5-1}$$

$$\tau(y,t) = \mu\left(-\frac{U}{\delta_s}\right)\left(e^{-y/\delta_s}\right)\left[\sin\left(\frac{y}{\delta_s} - \omega t\right) + \cos\left(\frac{y}{\delta_s} - \omega t\right)\right] \tag{5-2}$$

Figure 5-3 shows the actual velocity waveform of the tissue (blue curve), and the fitted sinusoidal fit (pink curve) as it returns to the unstretched configuration from the stretched configuration. The sinusoidal curve (pink) was fit by matching the amplitude and period of the actual velocity waveform (blue). Based on this fit, the obtained parameters for **Equation V-1** are: $U = 5.029 cm \cdot s^{-1}$, $\omega = 55.12 rad \cdot s^{-1}$, and $\delta_s = 1.549 \times 10^{-4} m$. These parameters can then be used to evaluate and plot **Equation V-2**. The results (**Figure 5-4**) report that the maximum shear stress experienced by the sample is 0.3 Pa. Previous studies in our laboratory have shown that the change in

biosynthetic activity in the valve cusp is negligible at shear stresses below 1 Pa (274). It can therefore be concluded that the dominant force acting on the valve tissue in the bioreactor and causing a biosynthetic response is cyclic stretch.

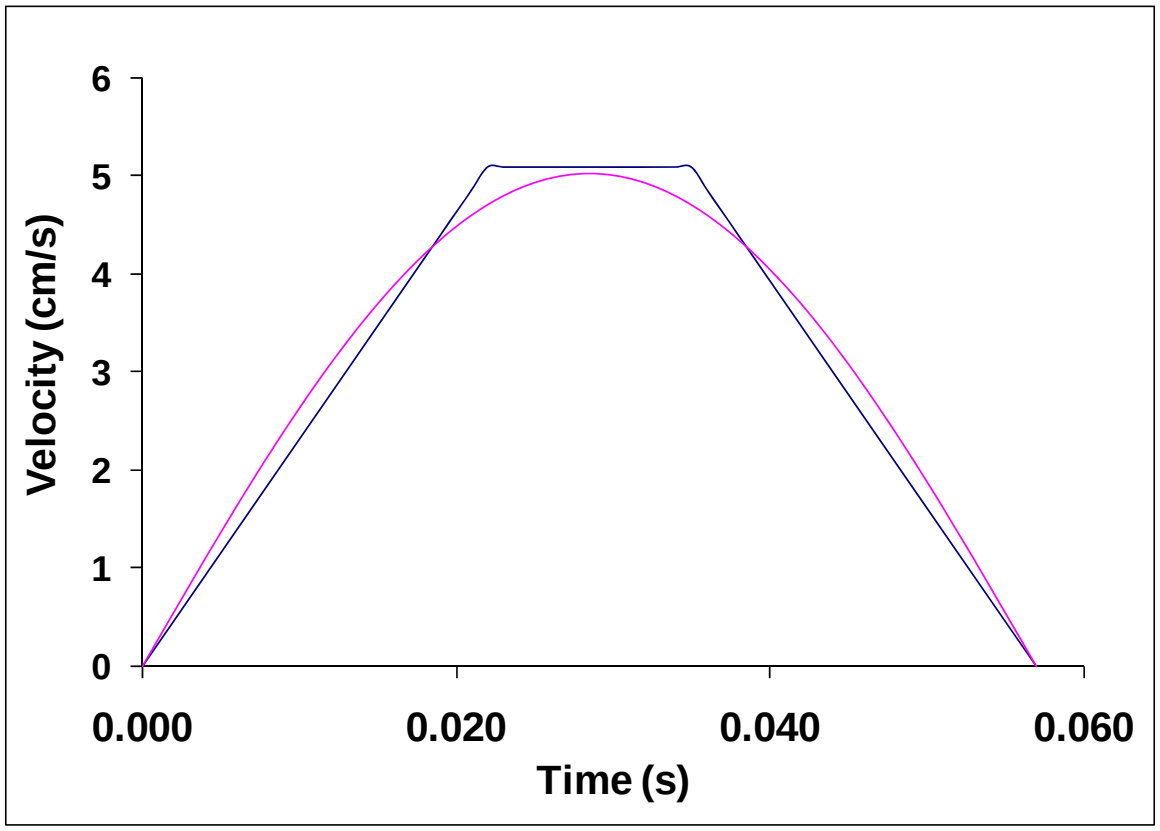

Figure 5-3: A sinusoidal curve (pink) was fit to match the peak velocity and frequency of the actual velocity of the tissue samples (blue). Numerical data for this curve is compiled in **Appendix C**.

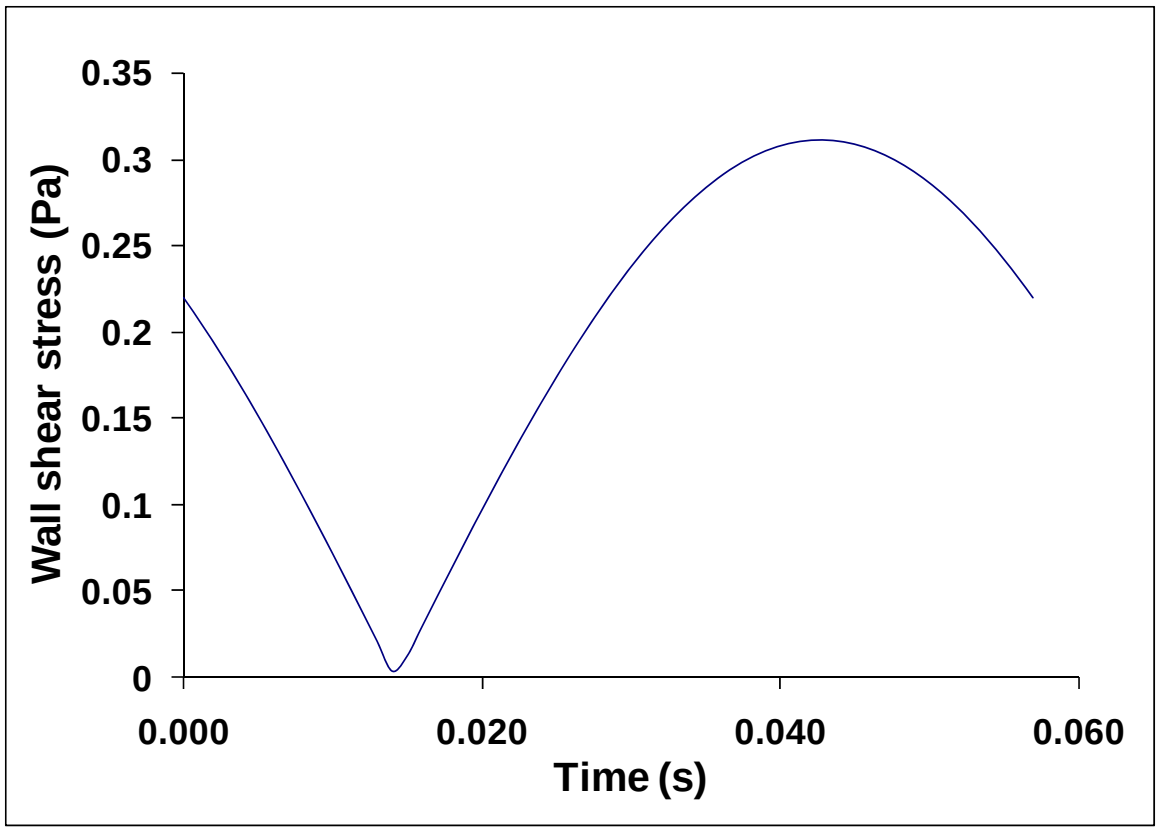

Figure 5-4: Absolute wall shear stress profile during the retraction motion of the tensile stretch bioreactor as calculated using **Equation V-2**. Peak fluid shear stress experienced by the valve leaflet was 0.3 Pa (3 dynes/cm^2).

5.2 Specific Aim 1: Effect of Cyclic Stretch on Aortic Valve Extracellular Matrix Content and Remodeling

The experiments in specific aim 1 sought to understand the effects of normal and pathological cyclic stretch on extracellular matrix content and remodeling. The first set of results summarizes the effect of cyclic stretch on collagen, sulfated glycosaminoglycan and elastin content. Following this, the effect of cyclic stretch on matrix metalloproteinases, tissue inhibitors of matrix metalloproteinases and cathepsins is reported. The final section reports the effect of cyclic stretch on cellular proliferation and apoptosis in the aortic valve.

All these experiments were conducted over durations of 24 and 48 hours with the objective of understanding the acute effects of cyclic stretch on aortic valve tissue. Previous studies from our laboratory have also demonstrated that culture durations of 24 to 48 hours are sufficient to observe biological changes in aortic valve cusps (243, 271, 274, 275).

5.2.1 Influence of Different Stretch Levels on Valve Extracellular Matrix and Structure

Collagen, sulfated glycosaminoglycan (sGAG) and elastin contents were measured using commercially available colorimetric assays from Biocolor (United Kingdom). The detailed protocols for these assays have been compiled in the M chapter and in **Appendix B**. These assays measure the total amount of extracellular matrix protein within the valve sample and once normalized by the weight of the tissue sample, are a robust measure of extracellular matrix content in the valve cusp. It should be noted here that these assays measure total matrix content and are not a measure of newly synthesized collagen. Routine Hematoxylin and Eosin and Movat's pentachrome staining was used to examine valve structure.

5.2.1.1 Collagen Content

Collagen is the primary structural protein in the valve cusp and its main stress-bearing component. Porcine aortic valve cusps cultured under normal 10% cyclic stretch had statistically similar ($p>0.05$) collagen content compared to fresh controls (**Figure 5-5**). When valve samples were cultured under pathological cyclic stretch (15%), collagen content significantly ($p<0.05$) increased (1.55-fold vs. 10% stretch; 1.43-fold vs. fresh) (**Figure 5-5**).

5.2.1.2 Sulfated Glycosaminoglycan Content

Sulfated glycosaminoglycan (sGAG) is located mostly within the spongiosa layer of the aortic valve cusp, and allows the collagen and elastin fibers to slip and slide over each other as the valve deforms, by providing lubrication. sGAG content was not significantly ($p>0.05$) altered between fresh and static controls (**Figure 5-6**). Cyclic stretch on the other hand significantly reduced ($p<0.05$) sGAG content (0.59-fold vs. 10% stretch; 0.45-fold vs. fresh) (**Figure 5-6**).

Analysis of the conditioned medium at the end of experimental duration revealed a statistically significant increase ($p<0.05$, $n = 6$) in sGAG secreted into the media (5.83±0.56 µg/mL of media) for stretched samples compared to fresh media (1.08±0.30). This latter result implies that sGAGs were leaching out of the valve cusp samples into the media due to the stretching motion imposed.

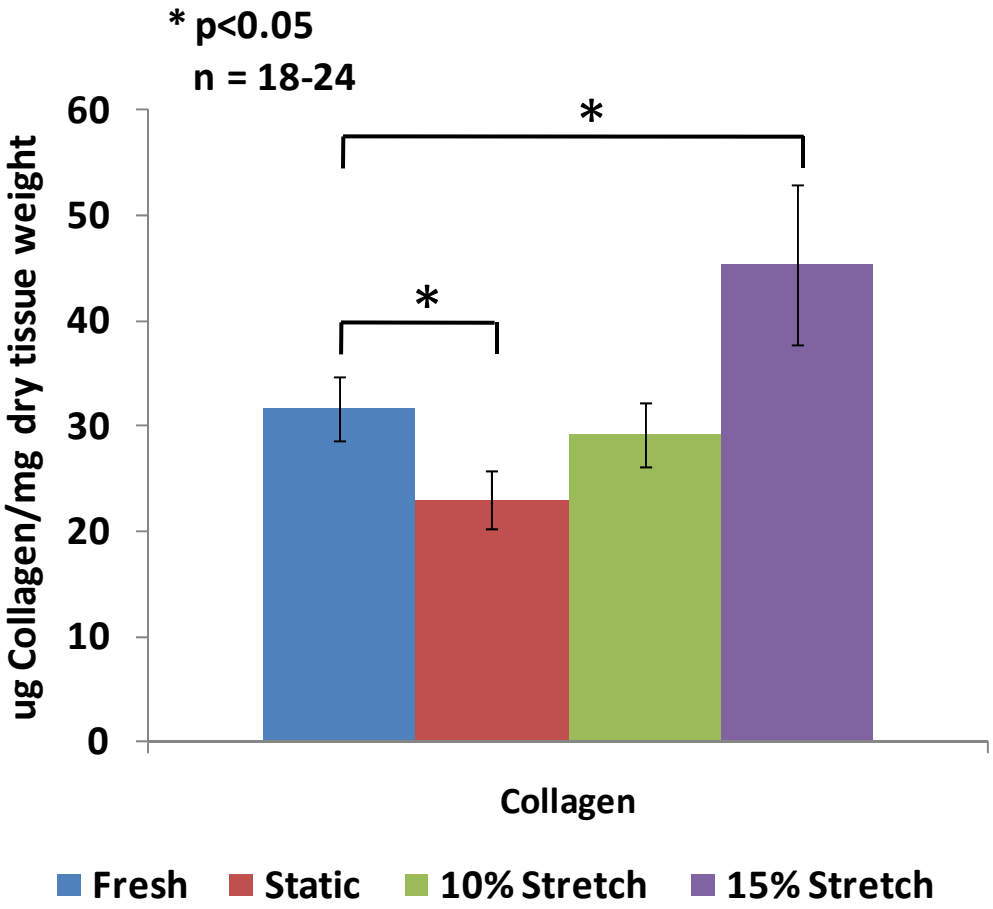

Figure 5-5: Change in content of collagen content of aortic valve cusps due to the following treatments: fresh control, static incubation, 10% cyclic stretch, 15% cyclic stretch after 48 hours.

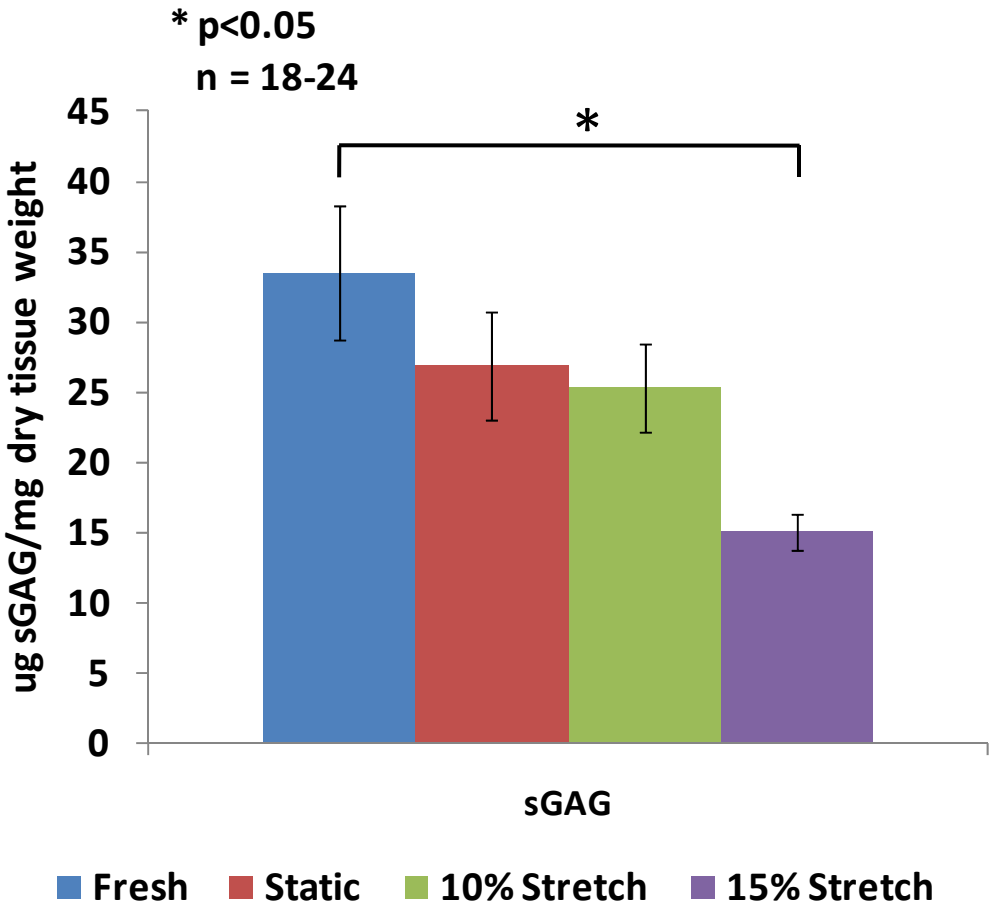

Figure 5-6: Change in content of sulfated glycosaminoglycan due to the following treatments: fresh control, static incubation, 10% cyclic stretch, 15% cyclic stretch after 48 hours.

5.2.1.3 Sulfated Glycosaminoglycan Content

Elastin is primarily located within the ventricularis aligned as radially-oriented fibers. As expected, there was no significant difference ($p>0.05$) in elastin content between the four treatment groups (**Figure 5-7**). Elastin turnover in the valve cusp occurs over a longer time scale than the 48 hour experimental time frame studied here.

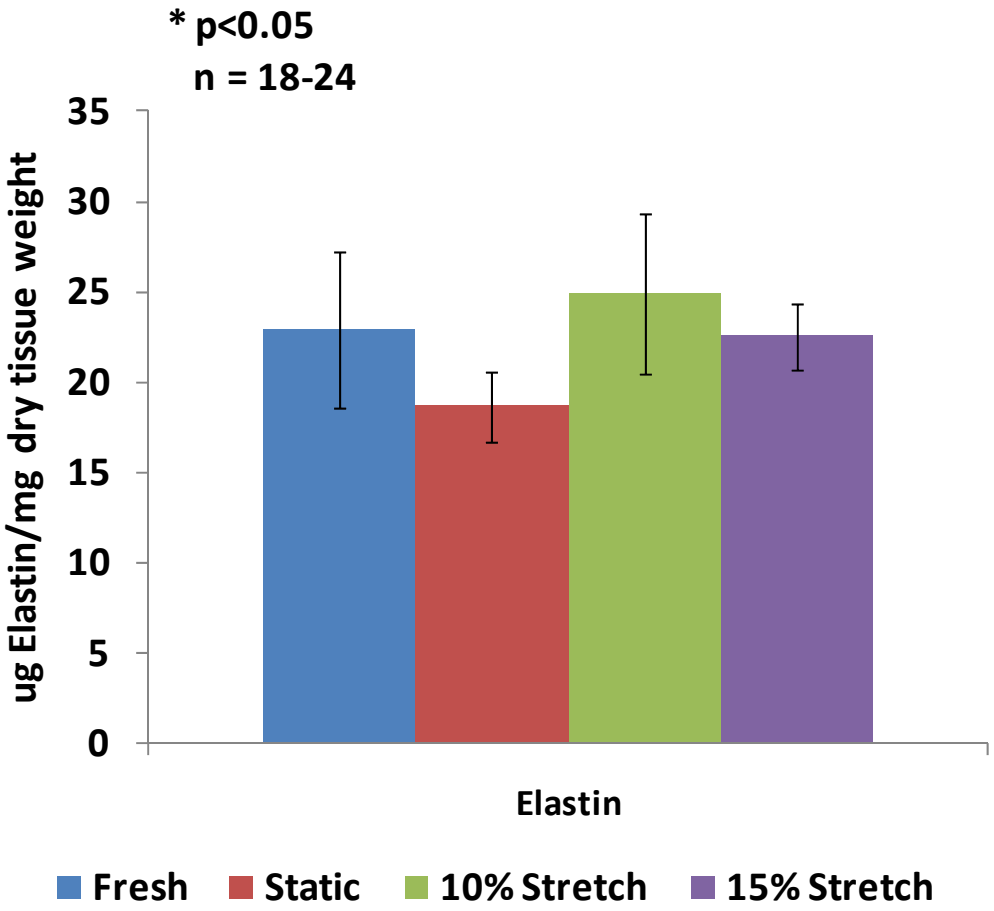

Figure 5-7: Change in elastin content of aortic valve cusps due to the following treatments: fresh control, static incubation, 10% cyclic stretch, 15% cyclic stretch after 48 hours.

5.2.1.4 Aortic Valve Tissue Structure

Hematoxylin and Eosin (H&E) staining and Movat's pentachrome was used to determine the effects of cyclic stretch on aortic valve tissue structure. These stains were also to ensure that cyclic stretching of the valve tissue in the stretch bioreactor did not result in physical tissue damage. H&E staining revealed loss of "ridged" fibrosa tissue architecture in samples stretched to 20%. This phenomenon is likely due to the high magnitude of stretch imposed on the tissue specimens. Normal (10%) and 15% stretch did not affect valve structure, and normal tri-layer tissue morphology was maintained (**Figure 5-8**).

Movat's pentachrome staining revealed loss of elastin architecture (black fibers) and glycosaminoglycan (blue) content at 20% stretch. 10% and 15% stretch groups were similar in tissue structure to fresh controls, with well defined and intact tri-layer morphology (**Figure 5-9**). This result is evidence that 20% stretch is acutely detrimental to the valve tissue. Subsequent results on cellular viability will provide further support for this conclusion.

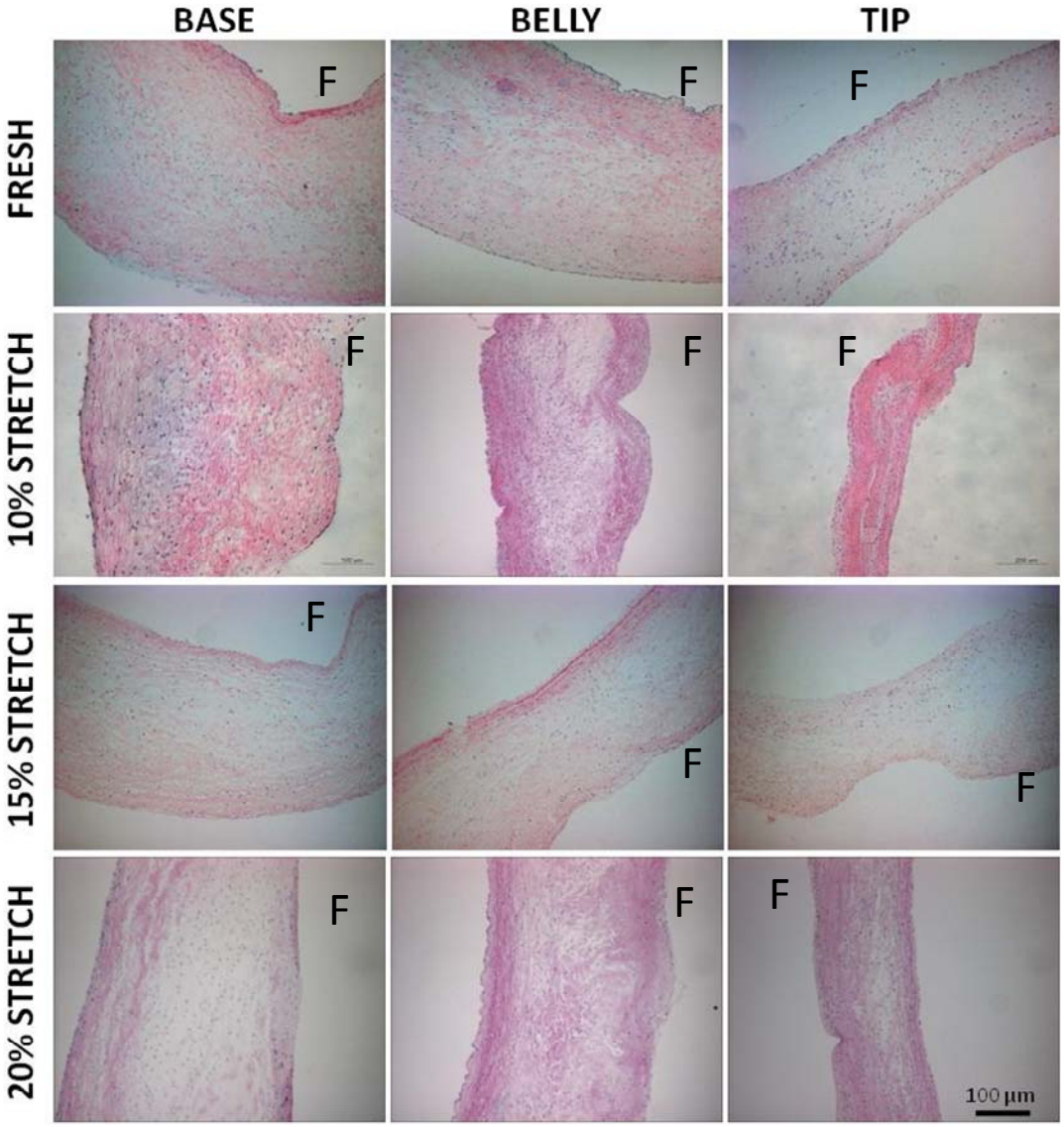

Figure 5-8: Hematoxylin and Eosin staining of samples stretched to 10%, 15% and 20% compared with fresh controls. Samples from the base, belly and tip sections of the aortic valve were stained

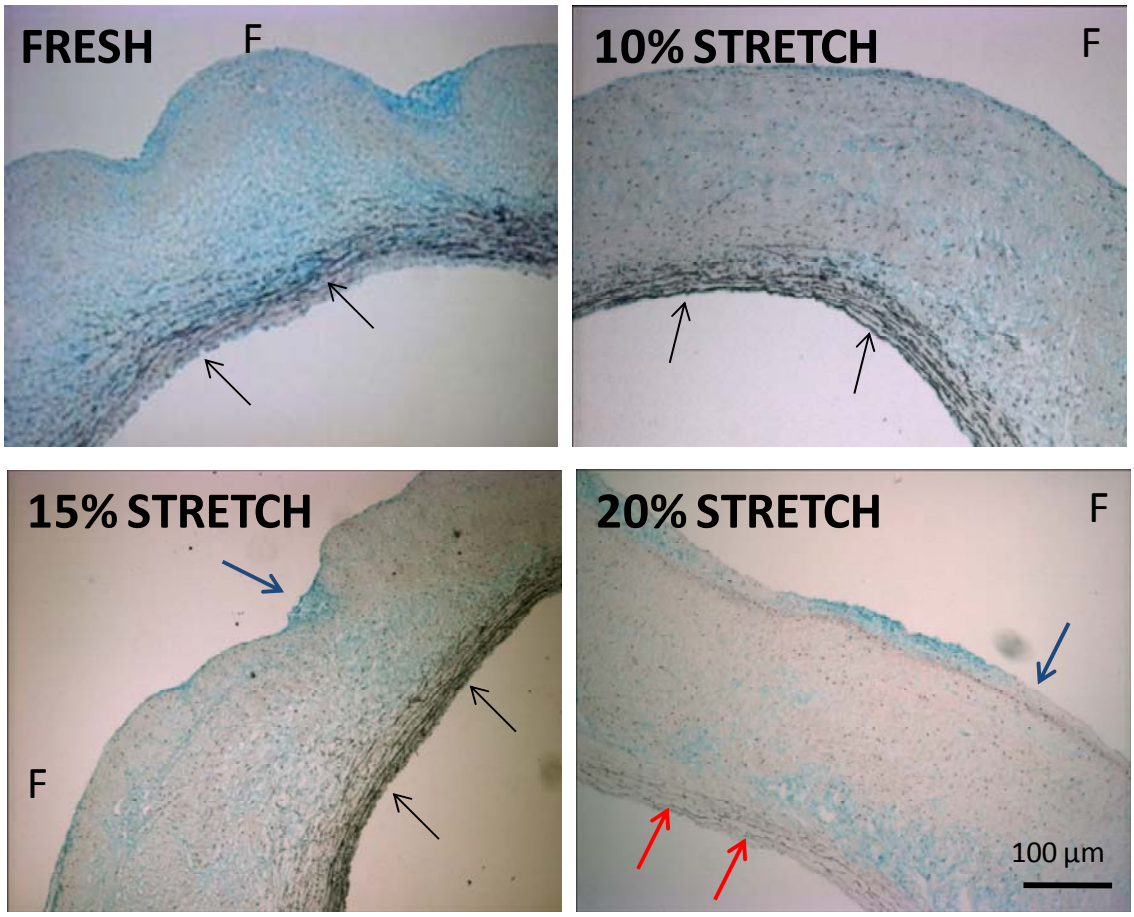

Figure 5-9: Movat's pentachrome staining of aortic valve cusps. Collagens are stained yellow, glycosaminoglycans blue and elastin fibers black. Loss of integrity of elastin architecture, indicated by red arrows can be observed under 20% stretch. One can also observe reduction in glycosaminoglycans in the 15% and 20% stretch results. This is consistent with previous data on sGAG content in the valve cusps.

5.2.2 Influence of Different Stretch Levels on Cathepsin L, S and K Expression

In this section, cathepsin L, S and K expressions were studied by immunohistochemistry and by semi-quantification of the immunohistochemistry images. Intracellularly, cathepsin L is a powerful protease involved in normal protein turnover (122). Extracellularly, cathepsin L has powerful collagenase and elastase activities, which necessitates its tight regulation by pH, reducing environment, and protein inhibitors. Cathepsins S and K have been shown to be associated with elastic lamina degradation during atherosclerosis plaque development (244, 245), as well as in myxomatous heart disease (191).

Immunohistochemical staining revealed that Cathepsin S and K expressions were upregulated by 15% cyclic stretch, while Cathepsin L expression was downregulated when compared with fresh controls (**Figure 5-10**). Expression of Cathepsin S was mainly localized to the fibrosa of the valve cusp, while Cathepsin K expression was broadly distributed throughout the entire cusp. Cathepsin L distribution in the fresh valve cusp depicted a broad homogeneous distribution throughout the cusp. Up until the 24 hour time point, there was no difference in cathepsin L expression compared to fresh control, but at 48 hours no cathepsin L expression was observed.

Semi-quantification of the 48 hour samples (**Figure 5-11**) revealed a significant decrease ($p<0.05$) of all cathepsins at 20% stretch, compared to 15% stretch (cathepsin L: 0.77-fold change; cathepsin S: 0.15-fold change; K: 0.40-fold change). Cathepsin L and K expression were comparable between fresh controls and 10% stretch, while cathepsin S expression was significantly reduced ($p<0.05$) at 10% stretch compared to fresh controls (0.37-fold change). As mentioned earlier, cathepsin L expression decreased significantly (0.14-fold change), while cathepsins S and K increased significantly (cathepsin S: 3.22-fold change; cathepsin K: 9.14-fold change) at 15% stretch compared to fresh controls.

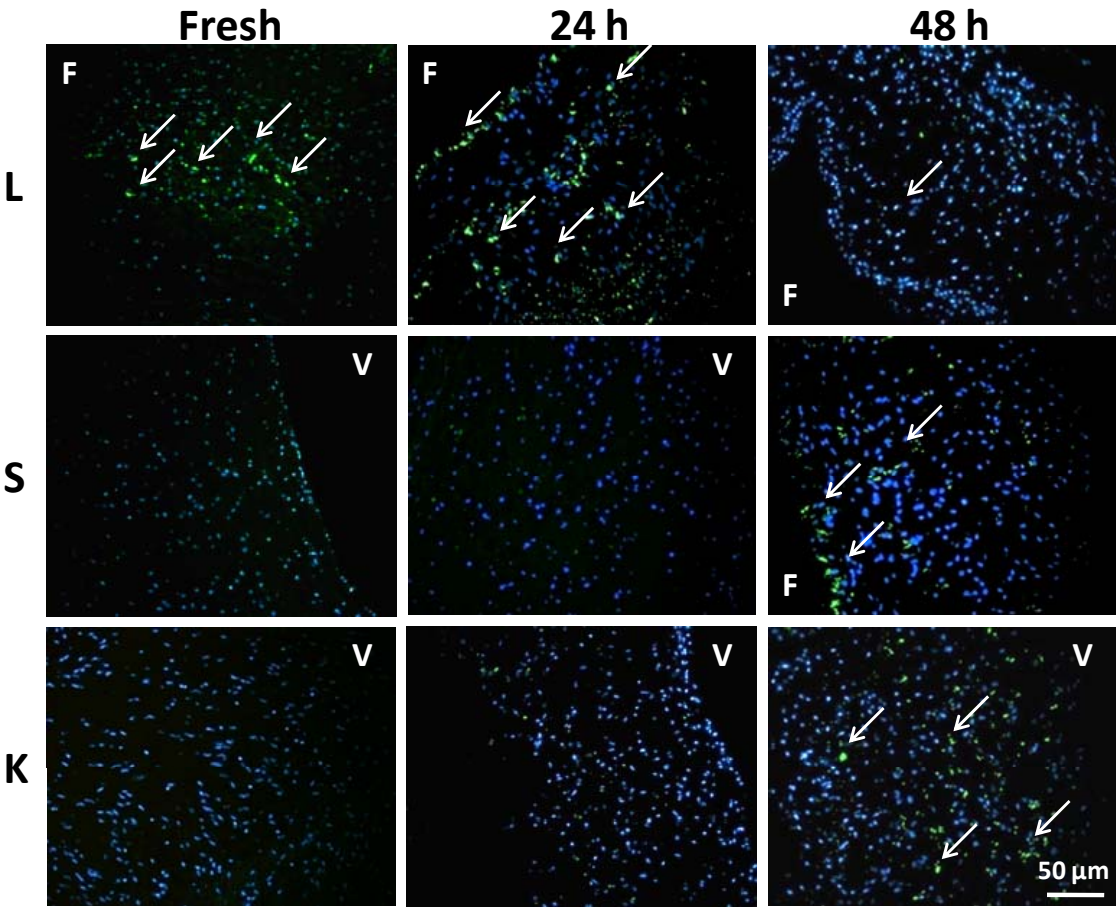

Figure 5-10: Immunohistochemical staining of cathepsins L, S and K at 15% stretch compared to fresh controls. Immunopositive cells are stained green. Arrows point to areas of strong staining. The images show that cathepsin L was expressed in the valve cusp in fresh controls, but not cathepsins S and K. In contrast, under pathological stretch conditions, cathepsin S and K were expressed across the cusp cross-section, while cathepsin L expression was reduced. (F-Fibrosa; V-Ventricularis)

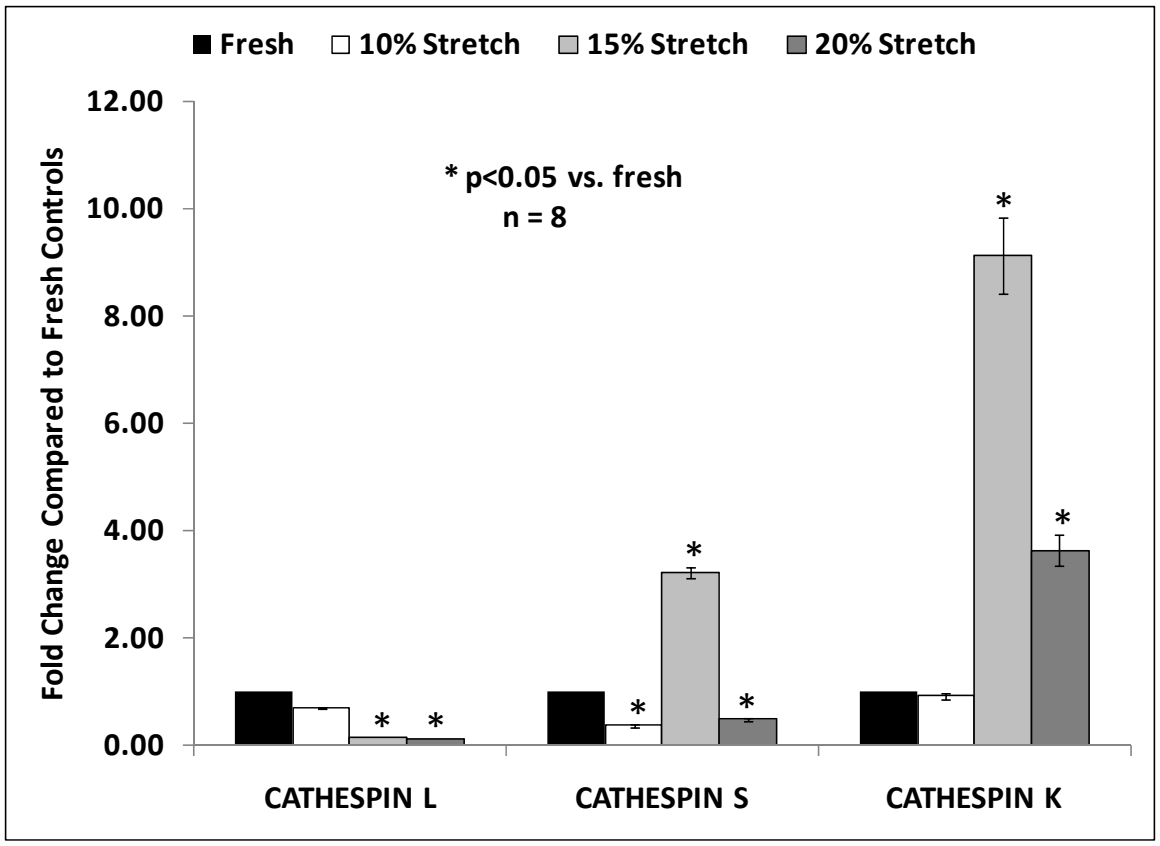

Figure 5-11: Semi-quantification of cathepsin immunohistochemical staining. There was a clear stretch magnitude-dependence in the regulation of cathepsins. Among the three cathepsins analyzed, cathepsin L was the dominant cathepsin in the fresh valve, while 15% stretch significantly increased expression of cathepsins S and K. Cathepsin S and K expression was significantly ($p<0.05$) lower at 20% stretch compared to 15% stretch.

5.2.3 Influence of Different Stretch Levels on Matrix Metalloproteinase and Tissue Inhibitor of Matrix Metalloproteinase Expression and Activity

Western blotting, zymography and activity assays were performed to understand the effect of different magnitudes of cyclic stretch on the expression and activity of matrix metalloproteinases and their tissue inhibitors. Most MMPs and TIMPs are secreted as inactive proproteins which are activated when they are cleaved by extracellular proteinases. As a result it is important to analyze both the expression and activity of these matrix remodeling enzymes. For coherence in presentation, the data in this section has been organized based on the particular molecule investigated. The first sub-section reports results from the collagenases (MMP-1) and their inhibitors (TIMP-1), while the second sub-section reports results from the gelatinases (MMP-2, MMP-9) and their inhibitor (TIMP-2). The final sub-section synthesizes all these data by understanding the relationship between: (i) enzyme expression and enzyme activity, and (ii) the enzyme and its inhibitor.

5.2.3.1 Matrix Metalloproteinase 1

Western blotting was used to study MMP-1 expression. MMP-1 expression was increased by static incubation as well as by cyclic stretch when compared with fresh controls (**Figure 5-12**). A biphasic relationship with stretch magnitude was observed, with MMP-1 expression significantly increasing between 10% and 15% stretch and subsequently decreasing at 20% stretch. There was no significant difference observed between the 24 and 48 hour experimental groups, and the biphasic relationship was observed at both time points.

A collagenase activity assay kit was used to quantify the activity of MMP-1 in valve cusp samples at the 48 hour time point. Collagenase activity (**Figure 5-13**) increased significantly ($p<0.05$) compared to fresh controls after 15% (4.21-fold increase) and 20% stretch (4.02-fold increase). There was no statistical difference ($p>0.05$) between fresh controls, static controls and samples stretched to 10%, or between 15% and 20% stretch. Intriguingly, the biphasic response observed in enzyme expression data was not seen here in the activity data.

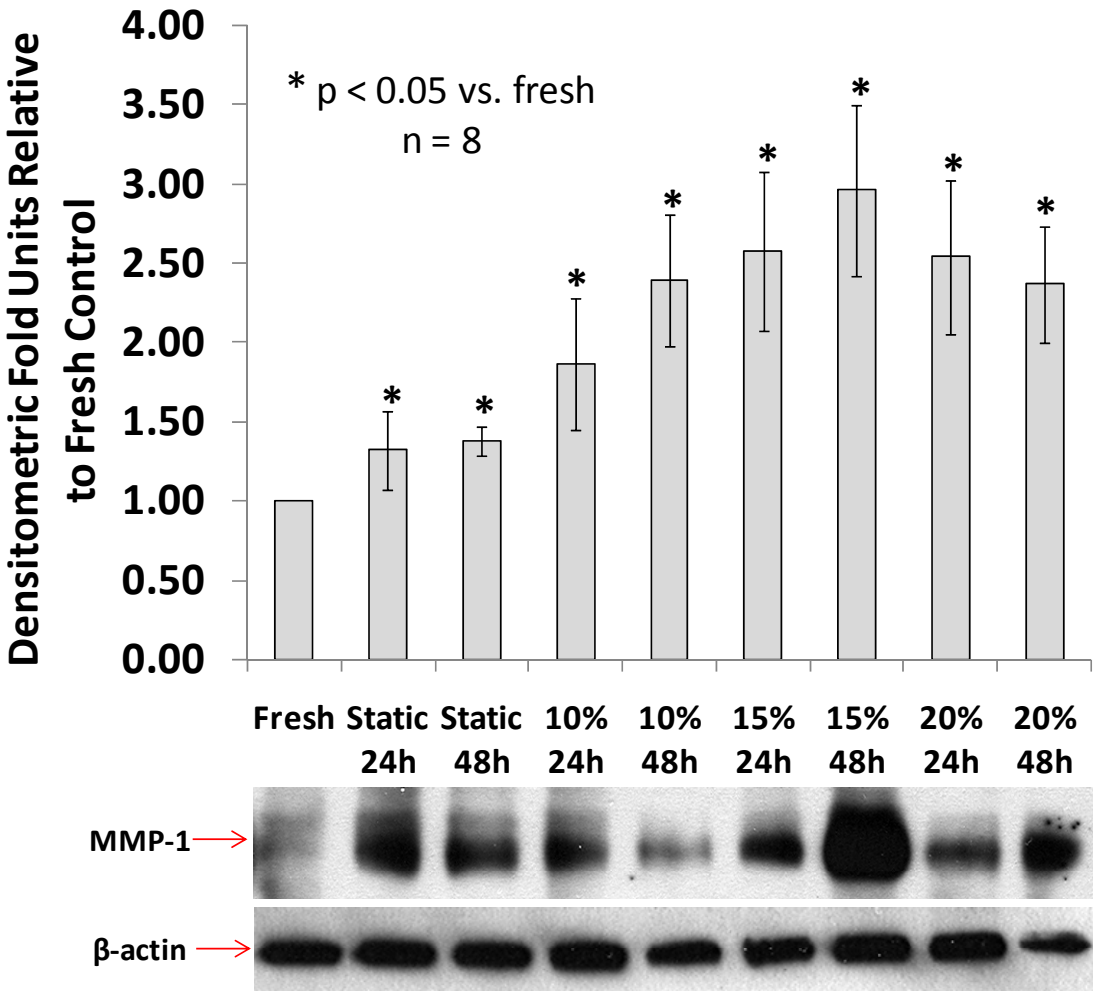

Figure 5-12: MMP-1 expression as determined by immunoblotting. A biphasic response can be observed here, with MMP-1 expression peaking at 15% stretch magnitude and dropping at 20% stretch. The responses of the valve samples were similar for both the 24 and 48 hour time groups.

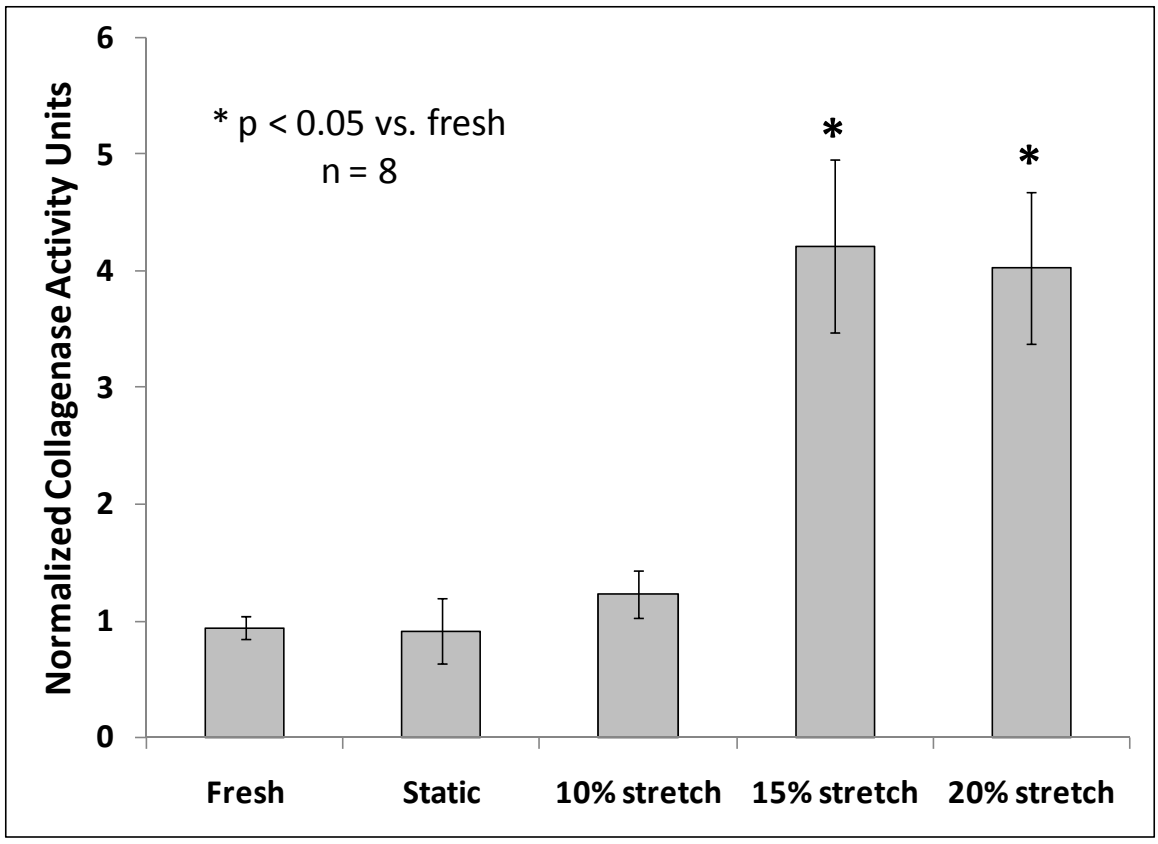

Figure 5-13: Collagenase activity progressively increased with increasing cyclic stretch. Activity was significantly higher at 15 and 20% cyclic stretch compared to fresh controls, static controls and 10% stretch. There was no significant difference in collagenase activity between fresh, static and 10% stretch groups.

5.2.3.2 Tissue Inhibitor of Metalloproteinase 1

TIMP-1 expression (**Figure 5-14**) and activity (**Figure 5-15**) were reduced significantly ($p<0.05$) at all levels of cyclic stretch when compared with fresh controls. When comparing within stretched valve cusps after 48 hours, TIMP inhibitory expression was minimum at 15% stretch (0.37-fold change compared to fresh), while TIMP inhibitory activity was lowest at 10% stretch (0.14-fold change compared to fresh). Inhibitory activity was significantly higher at 15% and 20% stretch ($p<0.05$) compared to 10% stretch (15%: 4.65-fold increase; 20%: 3.72-fold increase).

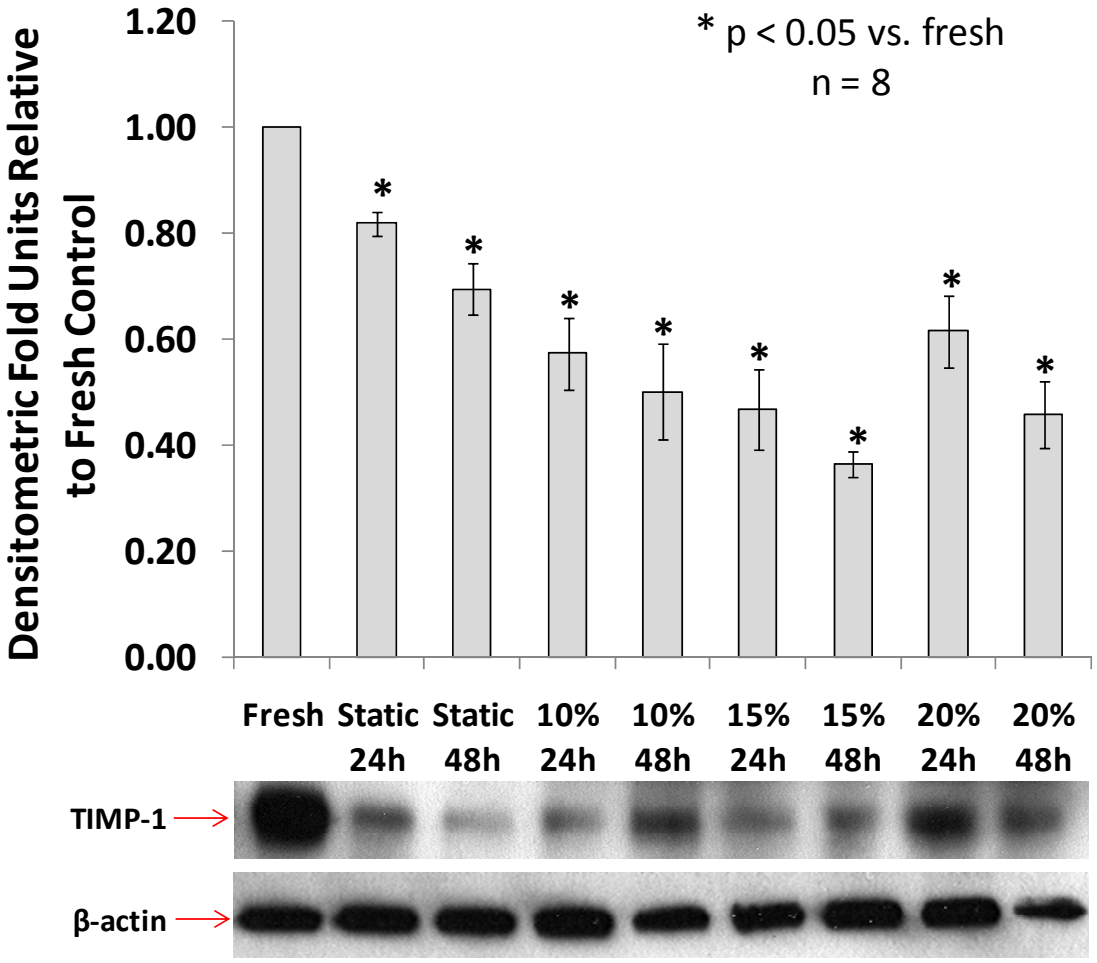

Figure 5-14: TIMP-1 expression as determined by immunoblotting. TIMP-1 expression decreased in stretched samples when compared to fresh controls and was minimum at 15% stretch.

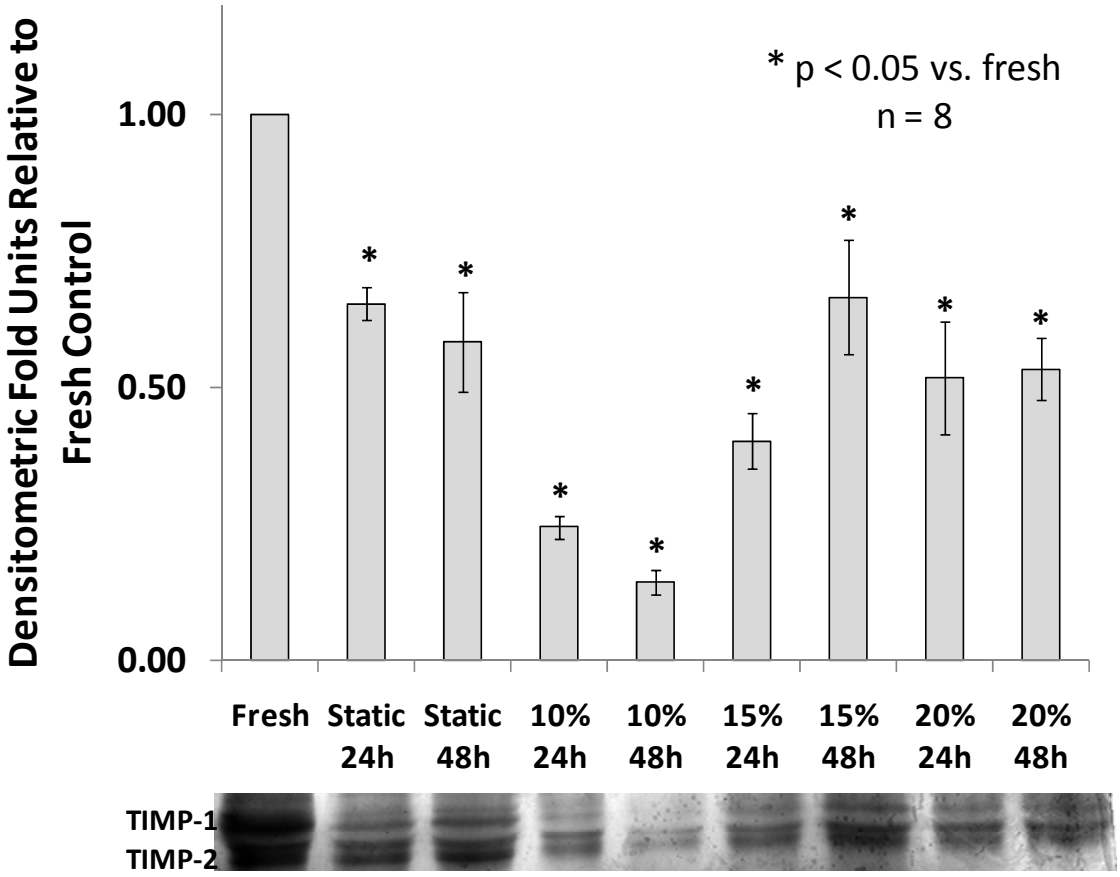

Figure 5-15: TIMP inhibitory activity as measured by reverse zymography was reduced by cyclic stretch. The smallest level of total TIMP activity was observed at 10% stretch. A biphasic response was observed here among the stretched groups, with total TIMP activity peaking at 15% stretch, before falling at 20% stretch.

5.2.3.3 Matrix Metalloproteinase 2 and 9

MMP-2 expression as determined by western blotting was significantly ($p<0.05$) upregulated at 15% stretch (1.97-fold) after 48 hours of culture, and significantly ($p<0.05$) downregulated at 20% stretch (0.84-fold) when compared with fresh controls (**Figure 5-16**). The biphasic response of the valve to cyclic stretch was observed again here in the results for MMP-2 expression.

Gelatin zymography (**Figure 5-17**) revealed modulation of MMP-2 and MMP-9 activity in a time- and magnitude-dependent manner. After 24h, there was no significant change ($p>0.05$) in total MMP activity for the 15% and 20% stretch groups compared to fresh controls. After 48h, MMP activity was increased significantly ($p<0.05$) at 15% (62% increase) and 20% cyclic stretch (62% increase) compared to fresh controls. The active form of MMP-2 was observed only in the static, 15%, and 20% stretch groups; MMP-9 activity was observed in the 15% stretch group only. There was no significant difference ($p>0.05$) in total MMP activity between 15% and 20% stretch groups. This last result is similar to that observed in the collagenase activity.

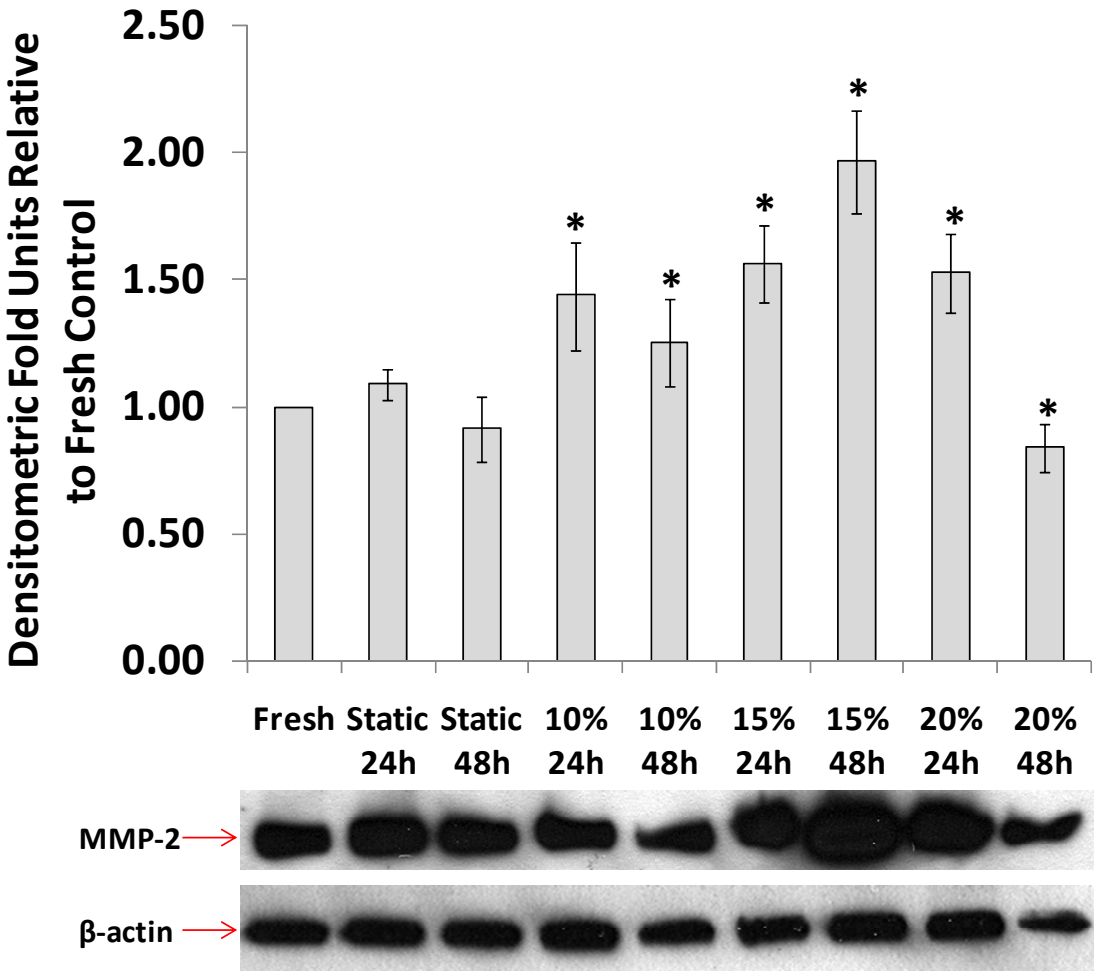

Figure 5-16: MMP-2 expression as determined by immunoblotting. MMP-2 expression was highest at 15% stretch, and minimum at 20% stretch. These changes in MMP-2 expression were significant compared to fresh controls.

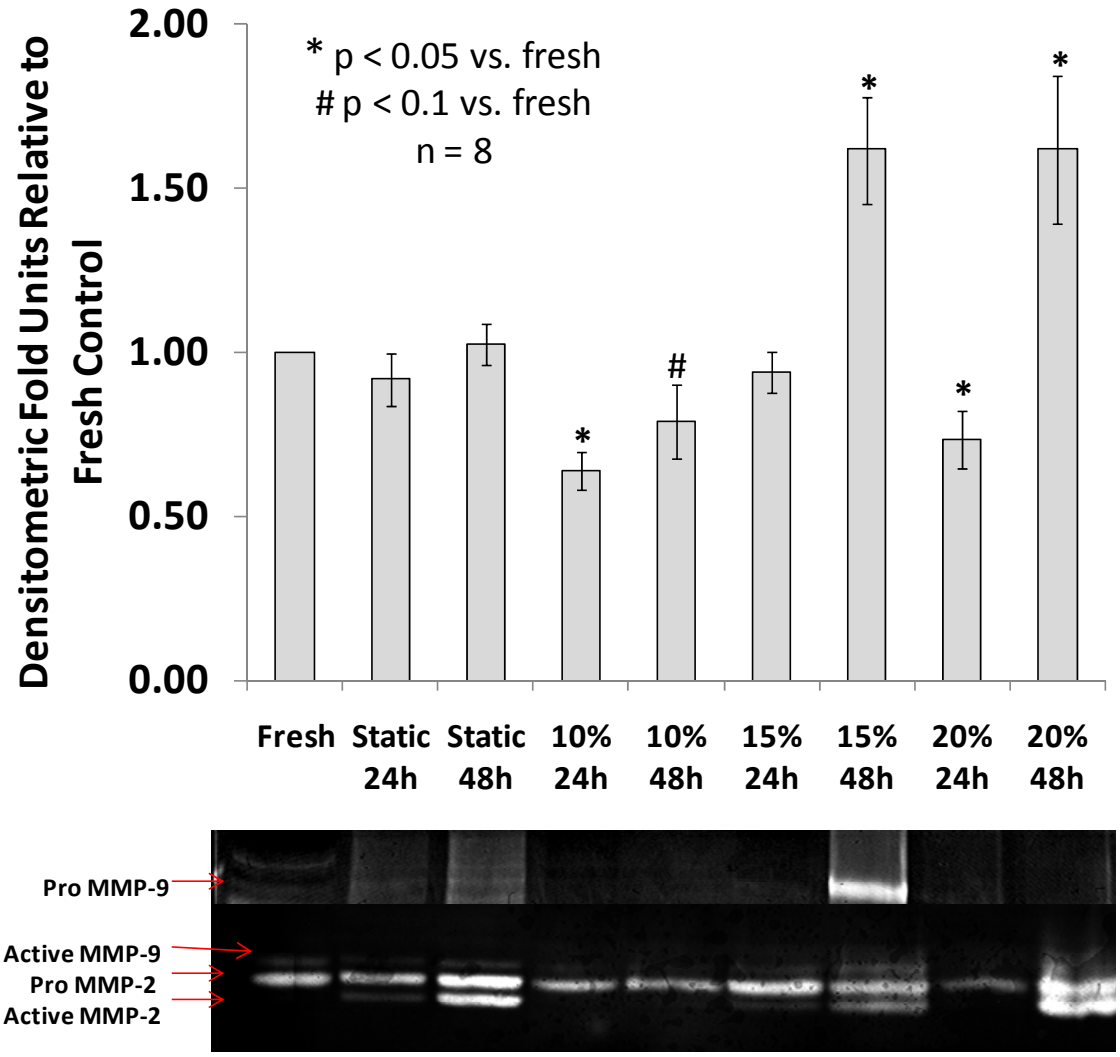

Figure 5-17: Gelatinase (MMP-2 and -9) activity was highest at 15% and 20% cyclic stretch after 48 h. Similar to MMP-1 activity, there was no significant difference between 15% and 20% stretch groups. A pro-MMP-9 band was clearly observed only for the 15% stretch (48 h only) groups.

5.2.3.4 Summary of Extracellular Matrix Remodeling Data

In **Section 5.2.3**, two general trends were observed in the stretch-behavior of the aortic valve cusps. The responses were either: (i) biphasic in stretch magnitude (MMP activity, TIMP expression), or (ii) reached a plateau, with no significant difference between 15% and 20% stretch groups (MMP expression, collagen content). A great strength of these studies was that the same sample/tissue lysate was used for all the different analyses. We therefore have several data points for a particular sample, and we could use this to examine trends or correlations in data. The objective of this section was therefore to understand if strong correlations existed between enzyme expression/activity and that of the corresponding inhibitor. In addition, another objective was to understand if enzyme activity and expression demonstrated a strong correlation.

The first task was to understand if enzyme expression and activity were correlated. Plotting these two metrics for each sample, it was observed in that enzyme activity correlated significantly (R^2=0.597, $p<0.05$) with enzyme expression (**Figure 5-18**), with a relatively reasonable coefficient of correlation (r=0.77). It can also be seen that normalized enzyme activity was about 96% that of normalized enzyme expression. The outliers could be attributed to the apparent differences between stretch-behavior for enzyme activity vis-à-vis enzyme expression, that is, the biphasic versus plateau behavior alluded to in the first paragraph of this sub-section.

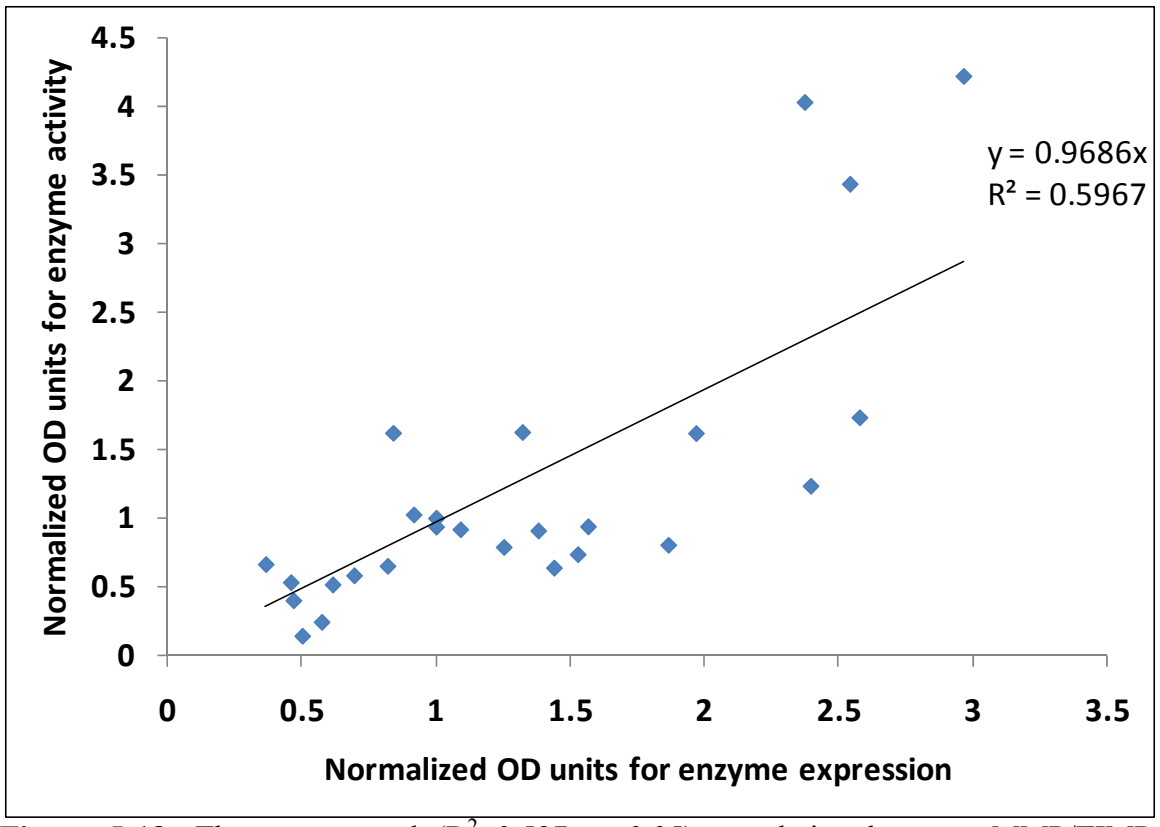

Figure 5-18: There was good (R^2=0.597, $p<0.05$) correlation between MMP/TIMP activity and expression for all the treatment groups (stretch level or time). Only samples with available paired data were used for this analysis.

In vivo, TIMPs regulate and control the expression and activity of MMPs. Therefore, an increase in TIMP levels would result in a general reduction in MMP levels in tissue samples. This agreed with the results from this study, where TIMP expression was strongly negatively correlated with MMP expression (**Figure 5-19**; R^2=0.755, $p<0.05$), when all the paired data were plotted on these two axes.

MMP-expression was normalized by the corresponding TIMP-expression for each sample to obtain a dimensionless parameter representing the overall matrix remodeling potential of the valve cusp in response to stretch. Plotting this MMP/TIMP ratio against stretch level (**Figure 5-20**) revealed that remodeling potential peaked at 15% stretch (at all time points) and was significantly different ($p<0.05$) compared to 10% and 20% stretch, and compared to unstretched valves. We can conclude from this particular result

that the "biphasic" behavior of the valve cusp to stretch dominates. The next section on cellular proliferation and apoptosis in some way offers some insight into why this may be the case.

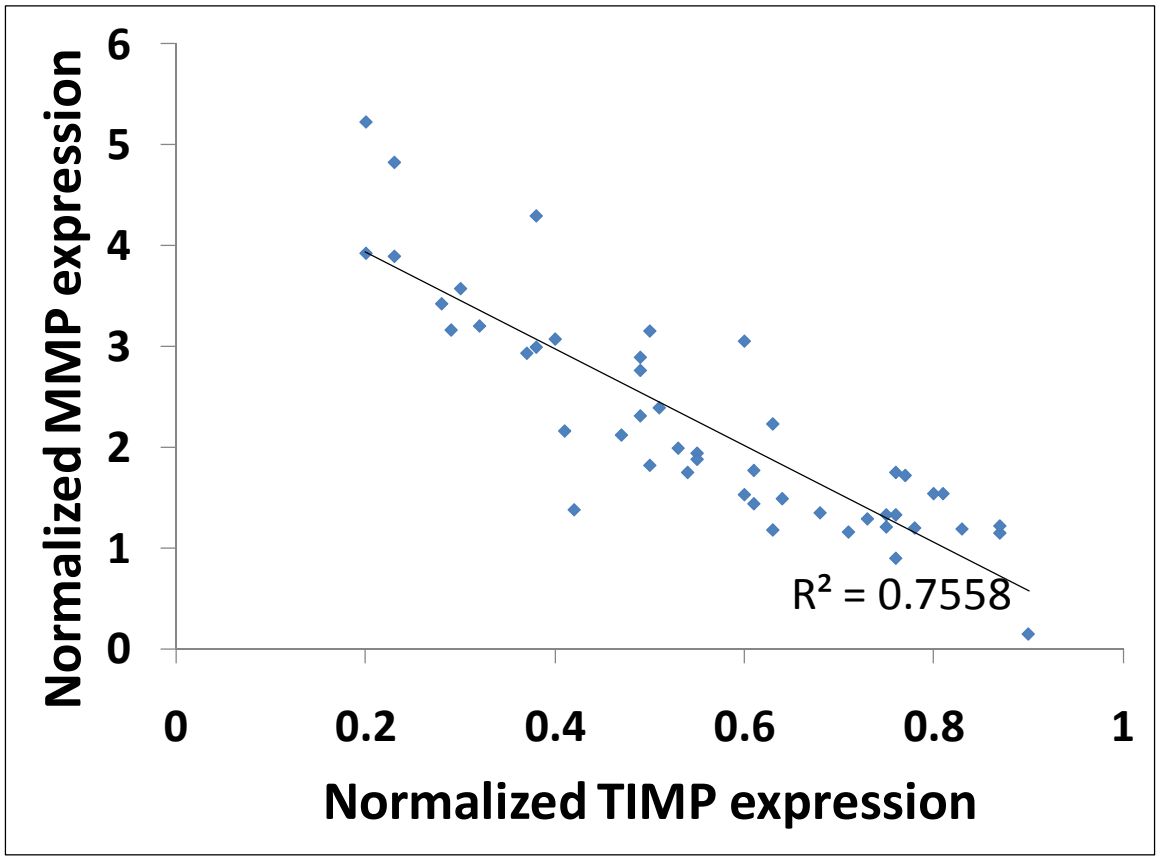

Figure 5-19: Correlation between MMP expression and TIMP expression. There was a strong and significant (R^2=0.755, $p<0.05$) negative correlation between TIMP and MMP expression. This is the normal relationship between these types of molecules as TIMPs generally regulate the expression and activity of MMPs, and a reduction in TIMP levels is expected to result in increased MMP levels.

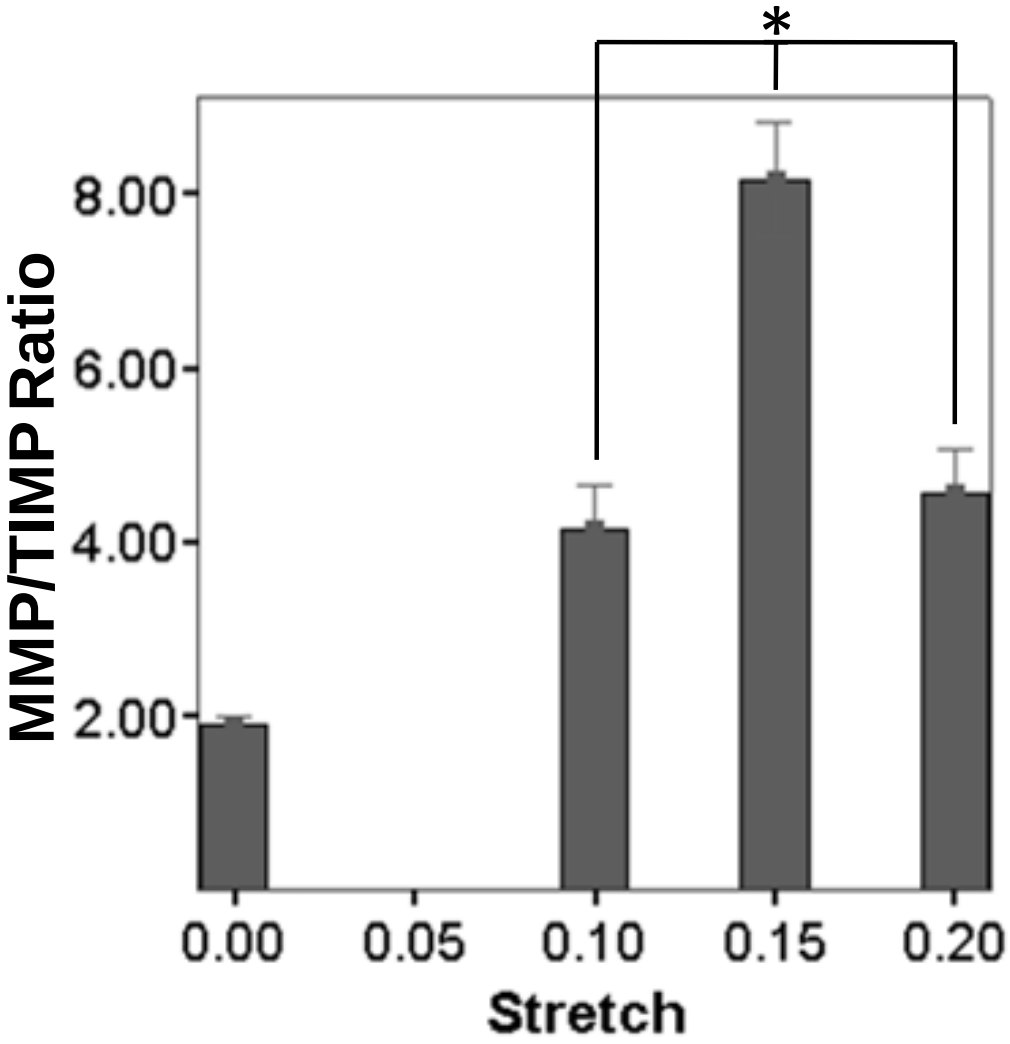

Figure 5-20: There was a significant increase in MMP/TIMP ratio under 15% stretch compared to 10% or 20% stretch. This parameter clearly demonstrated the effect of cyclic stretch on aortic valve remodeling.

5.2.4 Effect of different cyclic stretch levels on aortic valve cell proliferation and apoptosis

5.2.4.1 Cell Proliferation

Cell proliferation increased in a cyclic stretch magnitude-dependent manner. Via anti-bromodeoxyuridine (BrdU) immunostaining (**Figure 5-21**), the relationship between cyclic stretch magnitude and cell proliferation of aortic valve cusps was analyzed. The number of proliferating cells in the valve samples was dependent on the magnitude and duration of applied stretch (**Figure 5-22**). At 10% stretch, there were low numbers of proliferating cells even after 48h of culture. At 15%, proliferating cells were numerous and significantly ($p<0.05$) higher in number than 10% after 48h of culture, but not after 24h. In contrast, significantly ($p<0.05$) large numbers of proliferating cells were observed at 20% after just 24h, when compared to 10% stretch for the same time point. Statically incubated samples did not have a significant difference ($p>0.05$) in number of proliferating cells compared to 10% 24h stretch. Cell proliferation, where observed, was evenly distributed throughout the tissue and not localized to any surface.

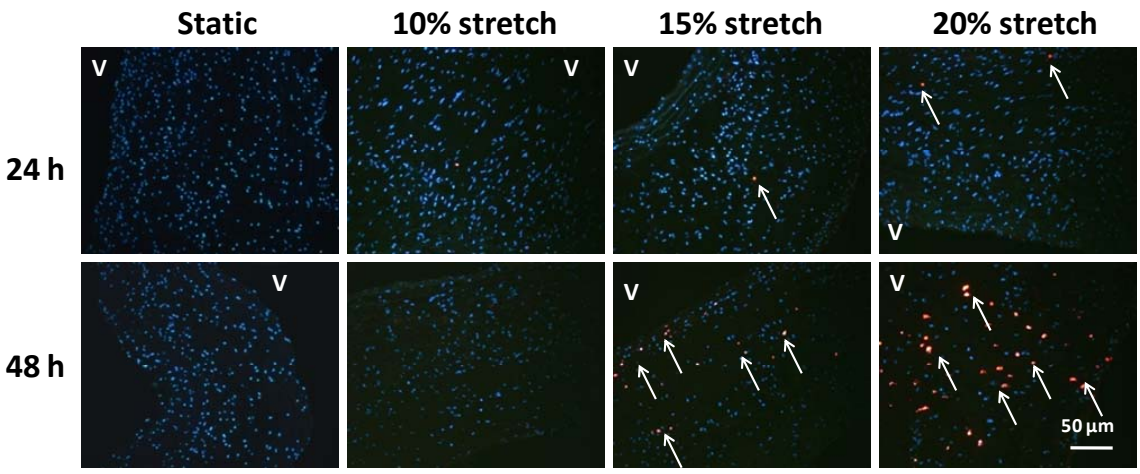

Figure 5-21: Cell proliferation was increased by cyclic stretch in a magnitude-dependent manner. Proliferation as measured by BrdU staining (arrows) is highest at 20% stretch after 48 hours showing numerous proliferating cells across the thickness of the cusp. Proliferating cells were not localized to either side of the valve cusp samples. (V-ventricularis)

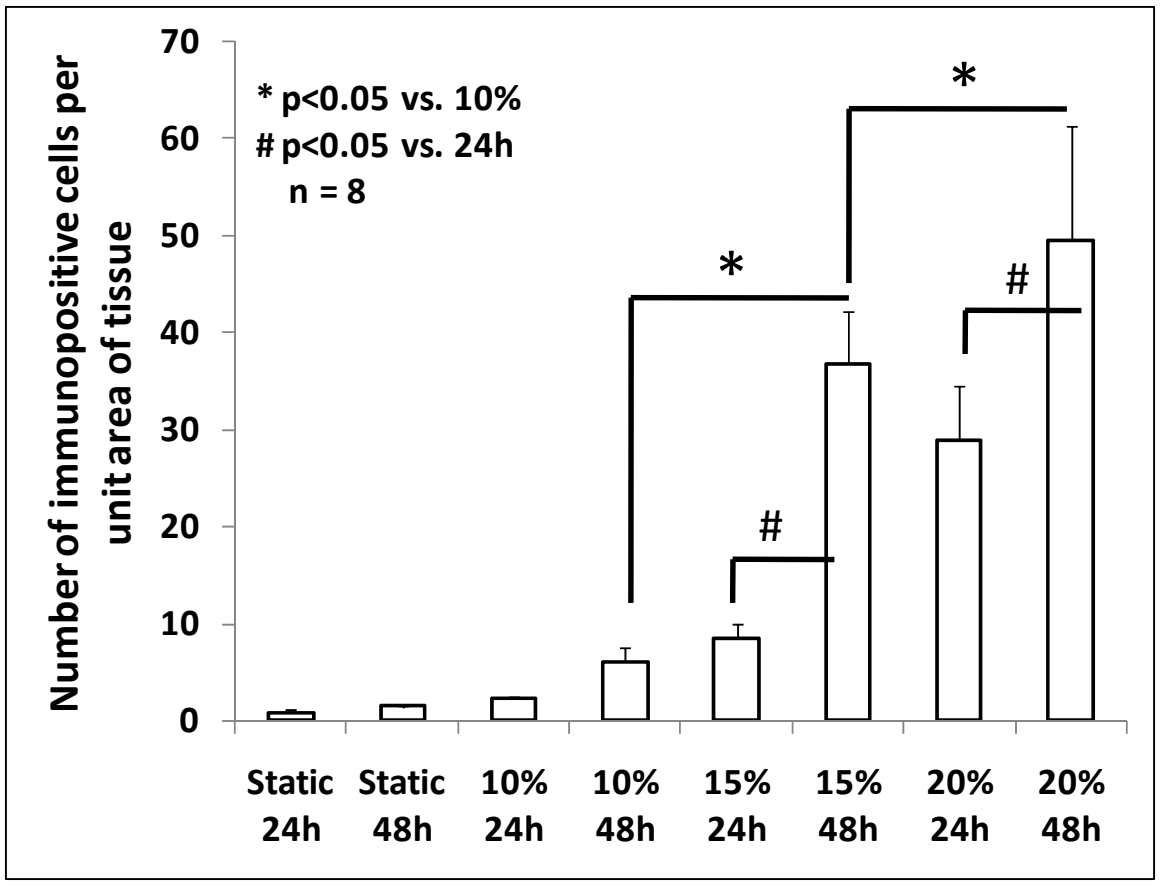

Figure 5-22: Proliferating cells were counted using ImageJ and normalized by the area of visible tissue in that image frame. These results demonstrate that cell proliferation increased significantly as the level of cyclic stretch increased. In addition, the longer the time of treatment (either static or stretch), the larger the number of proliferating cells.

5.2.4.2 Cell Apoptosis

Cell apoptosis increased in a cyclic stretch magnitude-dependent manner. Cell apoptosis (**Figure 5-23**), as determined by TUNEL immunostaining, was increased by cyclic stretch in a magnitude-dependent manner. The observed response was strongly exponential in stretch magnitude (R^2=0.997, $p<0.05$), with initially no significant difference ($p>0.05$) in TUNEL-positive apoptotic cell number from fresh to 10% stretch, and rapidly increasing in number beyond 15% (**Figure 5-24**).

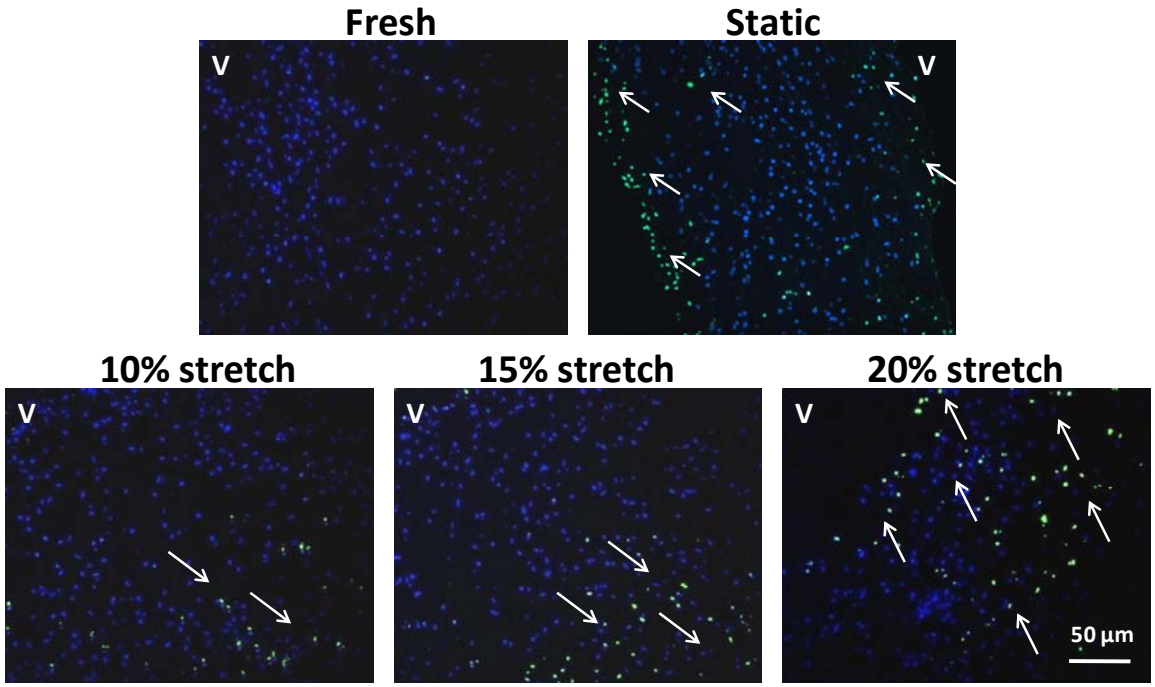

Figure 5-23: Apoptotic cells were determined by TUNEL staining (arrows). Apoptotic cells were more numerous in the static and 20% stretch groups. These TUNEL-positive cells at 20% were distributed throughout the thickness of the tissue. (V-ventricularis)

This indicates that elevation in stretch magnitude rapidly results in cell deterioration and death. The number of apoptotic cells was significant ($p<0.05$) at both 15% and 20% levels of stretch. Additionally, the number of apoptotic cells in the static controls was not significant ($p>0.05$) compared to 20% stretch samples and significant

($p<0.05$) compared to fresh controls, 10% stretch and 15% stretch. This demonstrates the important finding that mechanical stimulation (in the form of stretch for this dissertation) is a necessary condition to maintain cellular viability in a dynamic and mechanosensitive tissue such as the aortic valve cusp.

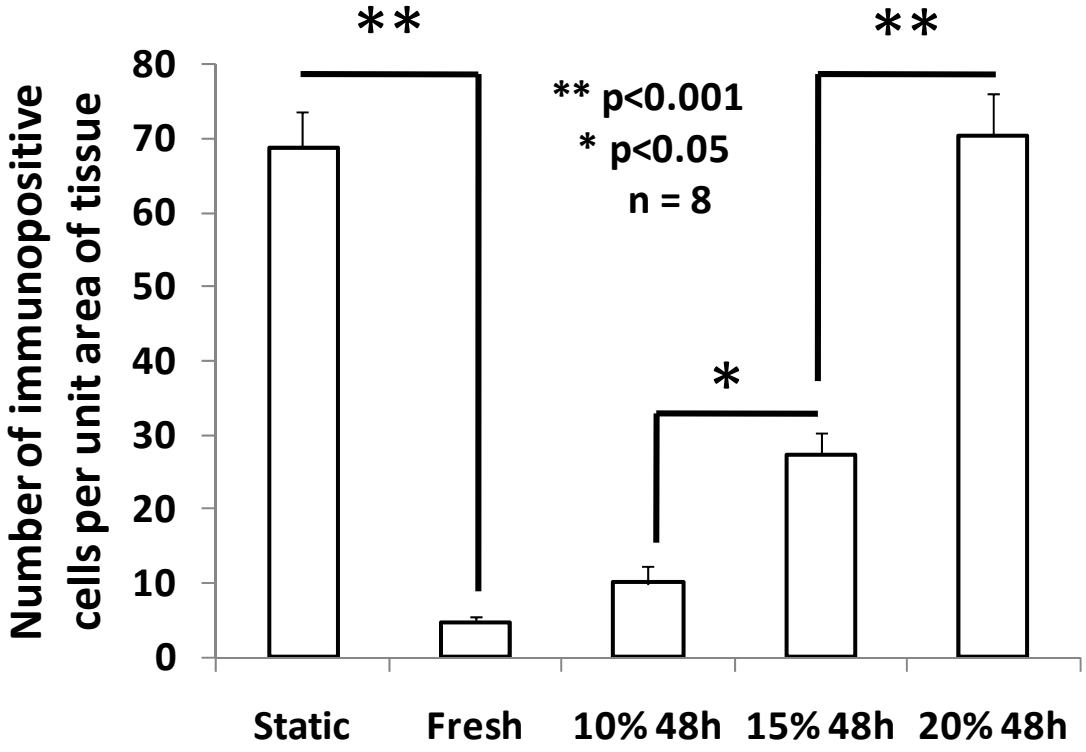

Figure 5-24: The number of apoptotic cells was significantly higher at 20% (70 immunopositive cells/unit area of tissue) compared to 10 and 15% stretch (10 and 27 immunopositive cells/unit area of tissue respectively) after 48 hours. The response was exponential in stretch magnitude. The numbers of apoptotic cells were statistically similar for the static and 20% stretch groups.

5.3 Specific Aim 2: Effect of Cyclic Stretch on Aortic Valve Inflammation and Calcification

The objective of this specific aim was to understand the effects of normal (10%) and pathological (15%) stretch on aortic valve inflammation and calcification. As outlined earlier, various formulations of osteogenic media (**Table 4-1**) were used to accelerate valve disease processes and thereby allowing study of valve calcification in an experimentally feasible timeframe. The effect of normal and pathological levels of cyclic stretch on valve calcification can then be teased out from the results.

The severe pathological level of stretch (20%) was not studied in this specific aim. As seen in the results from specific aim 1, there was severe cellular apoptosis at this level of stretch. In addition, imposition of 20% stretch on the valve cusp samples in the bioreactor often resulted in physical tissue damage which would be more of an issue in specific aim 2 as these experiments were conducted for longer time durations (7 and 14 days as opposed to 2 days). Structurally, this can be attributed to the fact that at 20% strain, the valve sample is in the linear portion of its stress-strain curve and that its collagen fibers are almost totally uncrimped (212).

5.3.1 Effect of Different Stretch Magnitudes on valve calcification

It has not been previously demonstrated whether aortic valve cusp tissue can be calcified *ex vivo* in an experimentally feasible timeframe. The hypothesis that porcine aortic valve cusps can be calcified by a combination of pathological levels of stretch (15%) and a pathophysiologically relevant humoral environment (high concentrations of phosphate and TGF-β1) was tested here. Fresh porcine valve samples and samples cultured for 7 days at 10% stretch (physiologic) or 15% stretch (pathologic) in normal DMEM (I – **Figure 5-25A** and **B**), osteogenic medium (II – **Figure 5-25C** and **D**), or osteogenic medium supplemented with high phosphate (III – **Figure 5-25E** and **F**) did not show positive alizarin red staining for calcification. Calcific nodule formation could be observed on the aortic surface in cusp samples exposed to both 10% and 15% stretch in osteogenic media with TGF-β1 (IV – **Figure 5-25G** and **H**).

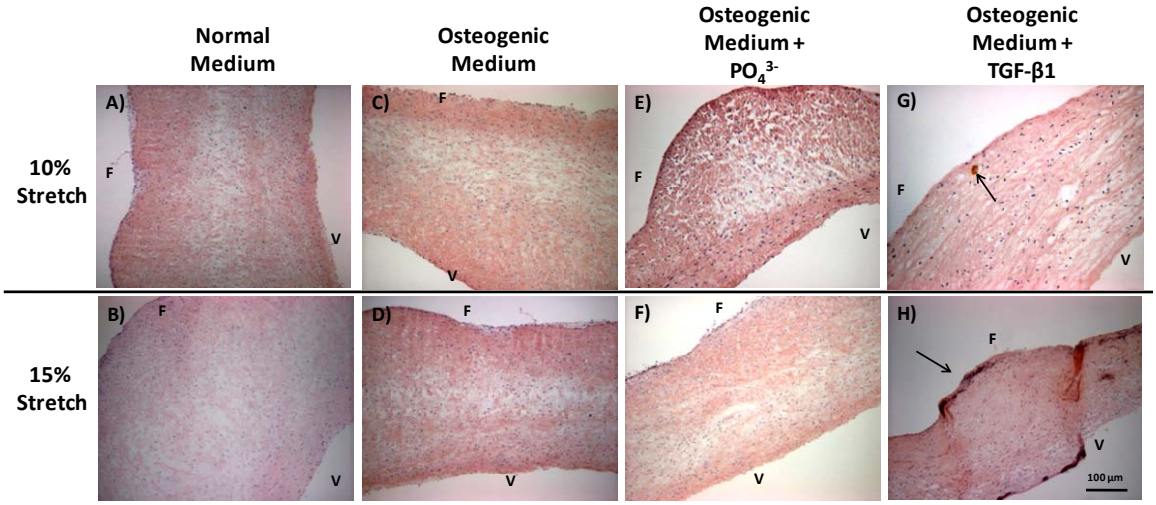

Figure 5-25: Alizarin red staining of porcine aortic valve cusps that were cultured for 7 days under 10% (A,C,E,G)) or 15% (B,D,F,H) stretch in normal DMEM, osteogenic DMEM, osteogenic DMEM with high phosphate (3.8mM), osteogenic DMEM with 1ng/mL TGF-β1 as indicated. Small calcific nodules were found only in G and H as marked with arrows. (F-Fibrosa; V-Ventricularis)

Treatment of valve cusps in fully osteogenic medium under 10% (physiologic) or 15% stretch (pathologic) for 7 days resulted in calcification in a stretch-dependent manner (Alizarin Red - **Figure 5-26A**, **C**; von Kossa – **Figure 5-26B**, **D**). The fibrosa side showed more intense staining than the ventricularis side of the cusp when exposed to 15% stretch. These results suggest that calcification of aortic valve cusps required both stretch and the fully osteogenic medium containing high phosphate and TGF-β1 levels, while neither stretch nor the fully osteogenic medium alone were sufficient. In addition, the fibrosa side appeared to be preferentially susceptible to calcification, which is consistent with previous observations in the clinic and on the bench (113, 227, 243).

The next set of experiments probed whether these calcification events were dependent on BMPs, by adding 100ng/mL of noggin to the fully osteogenic medium. As mentioned in the previous chapter, noggin has strong affinity for BMPs and TGF-β family ligands preventing them from binding with their receptor on the aortic valve cusp. There was no evidence of tissue mineralization in the 15% stretch with noggin groups (**Figure 5-26E, F**). This result points to the potential involvement of BMPs in regulating stretch-induced valve calcification, which will be further elucidated in the subsequent sections.

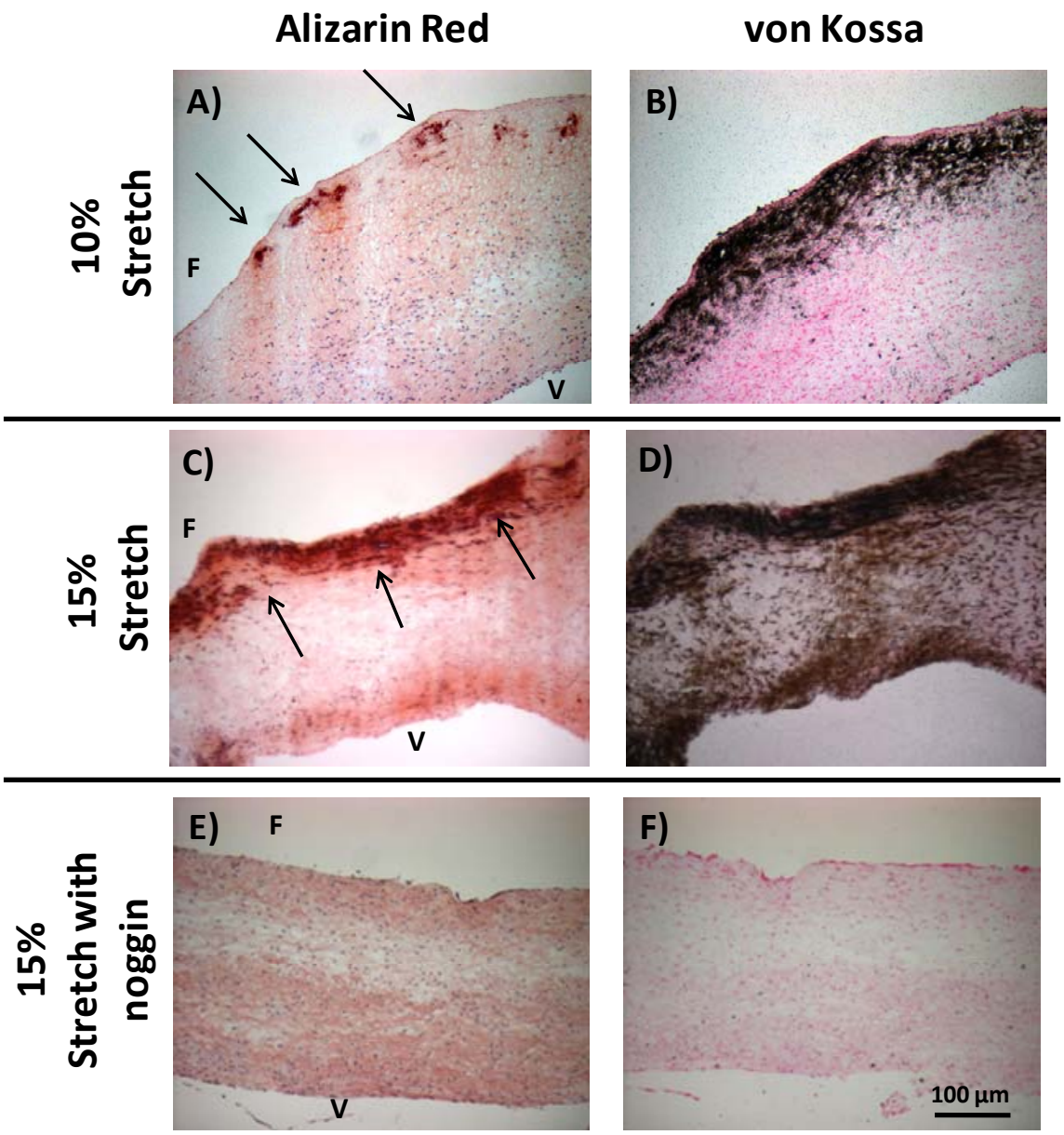

Figure 5-26: Cyclic stretch induced calcification of porcine aortic valve cusps, which was inhibited by noggin. Aortic valve cusps were exposed to 10% (A, B) or 15% (C, D) cyclic stretch for 7 days in fully osteogenic medium containing both high phosphate and TGF-β1. An additional treatment group contained fully osteogenic medium as well as 100ng/mL noggin with 15% stretch (E, F). Cusps were then stained with Alizarin Red (A, C, E) or Von Kossa (B, D, F). Calcific nodules are marked with arrows. (F-Fibrosa;V-Ventricularis)

5.3.2 Effect of Different Levels of Stretch on Cell Apoptosis

Previous studies have linked valve calcification to cellular apoptosis (45). In addition, it was also demonstrated in specific aim 1 that elevated cyclic stretch resulted in increased cellular apoptosis in a stretch-magnitude dependent manner. It was therefore tested here if exposing cells to physiologic (10%) or pathologic stretch (15%) for 7 days in the fully osteogenic medium induced apoptosis of aortic valve cusp cells.

TUNEL assay (**Figure 5-27** and **Figure 5-28**) showed significantly larger numbers of apoptotic cells when cusps were cultured with 15% stretch (180.6±49.5) in the fully osteogenic medium compared to 10% stretch (22.4±4.3) and fresh controls (4.2±0.9). In addition, cellular apoptosis was significantly reduced when samples were cultured with 100 ng/mL noggin (10% stretch: 3.2±0.9; 15% stretch: 12.7±1.9). For the 10% stretch with noggin group, the number of apoptotic cells was statistically similar to fresh controls.

The cellular apoptosis results appeared to match that of valve calcification (via Alizarin red and von Kossa staining). This indicates that stretch-induced aortic valve calcification may occur via a BMP-dependent pathway and that these processes are apoptosis-driven.

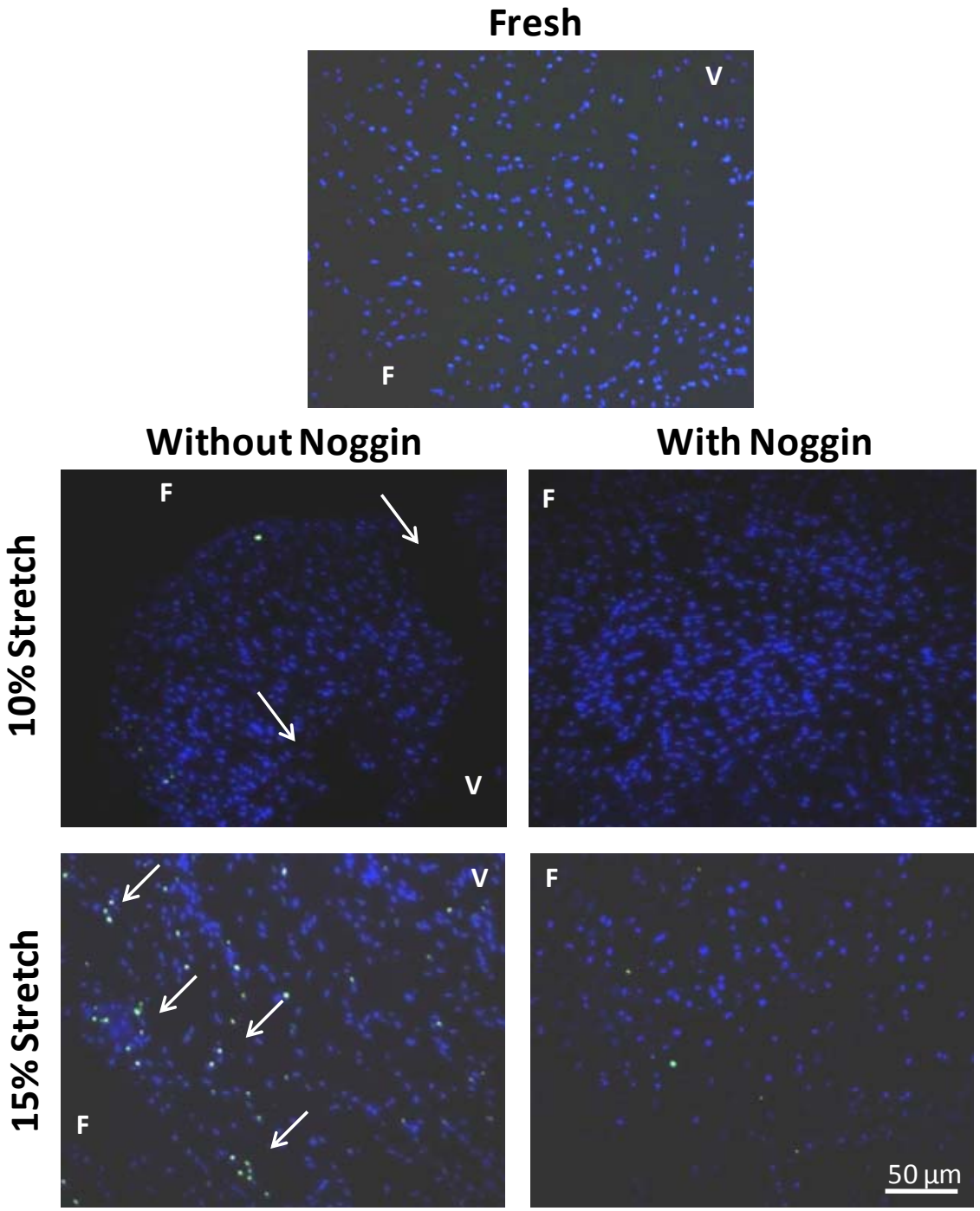

Figure 5-27: Representative micrographs of fresh valve cusps and cusps exposed to 10 or 15% cyclic stretch in fully osteogenic medium assayed for apoptosis by TUNEL staining (green) with DAPI nuclei counterstain (blue). Apoptotic cells detected marked with arrows

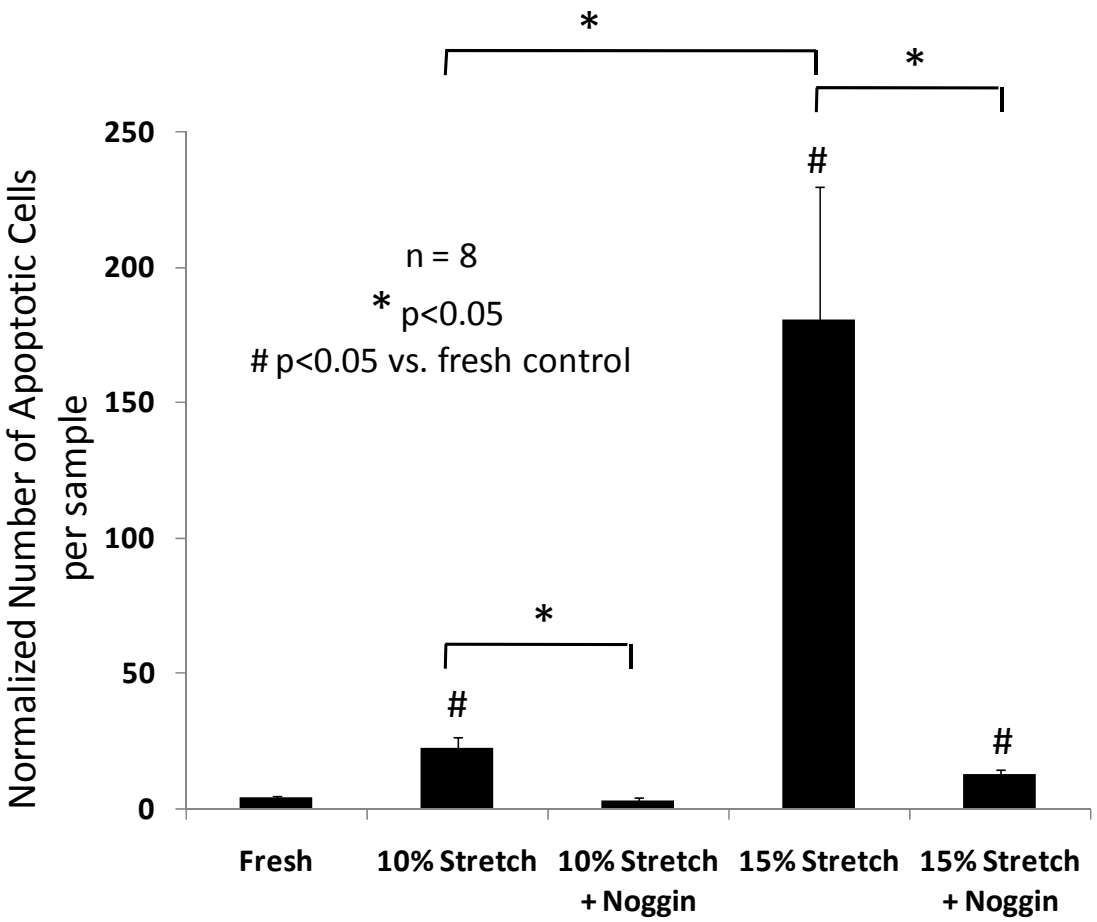

Figure 5-28: Apoptotic cells were counted for each treatment condition using ImageJ and normalized by the area of visible tissue in that image frame. Cell apoptosis was significantly higher under elevated (15%) stretch compared to normal (10%) stretch. Addition of noggin reduced cell apoptosis significantly for both stretch magnitudes. In addition, for the 10% groups, cell apoptosis with noggin was comparable to fresh controls.

5.3.3 Effect of Cyclic Stretch on Bone Morphogenic Protein Expression

The primary objective of this specific aim was to understand the BMP-dependence of aortic valve calcification. It was therefore important to first understand the effect of cyclic stretch on BMP expression. We used immunohistochemistry and semi-quantitative analyses to determine if BMP expression was increased by cyclic stretch in the fully osteogenic medium. The immunostaining was performed on aortic valve cusps that were stretched to 10 and 15% and in fresh controls. Colocalization studies could not be performed as commercially available primary antibodies were obtained from the same species (mouse).

Fresh samples did not show any discernable amount of BMP-2 or BMP-4 as detected by immunohistochemistry (**Figure 5-29**). Both 10% and 15% cyclic stretch significantly ($p<0.05$) increased BMP-2 (10% stretch: 4.46-fold; 15% stretch: 6.54-fold), and BMP-4 (10% stretch: 5.40-fold; 15% stretch: 13.37-fold) expression compared to fresh controls (**Figure 5-30**). In addition, BMP expression was also significantly ($p<0.05$) higher expression at 15% stretch compared to 10% stretch (**Figure 5-30**).

BMP-2 and BMP-4 expression was higher on the fibrosa side of the cusps compared to the ventricularis. This observation is consistent with other studies that reported the fibrosa surface to be more susceptible to valve disease (227, 243). In addition, BMP expression was primarily observed on the endothelial cell layer of the valve tissue, with some additional expression in the interstitial cells only for BMP-2. There appeared to be some colocalization of BMP-2-positive and BMP-4-positive cells particularly in the 15% stretch groups. Further evidence can be observed in the compiled immunohistochemistry images in **Appendix D**. It therefore appears that there are specific populations of endothelial cells within the valve cusp that express BMP-2 versus expressing BMP-4.

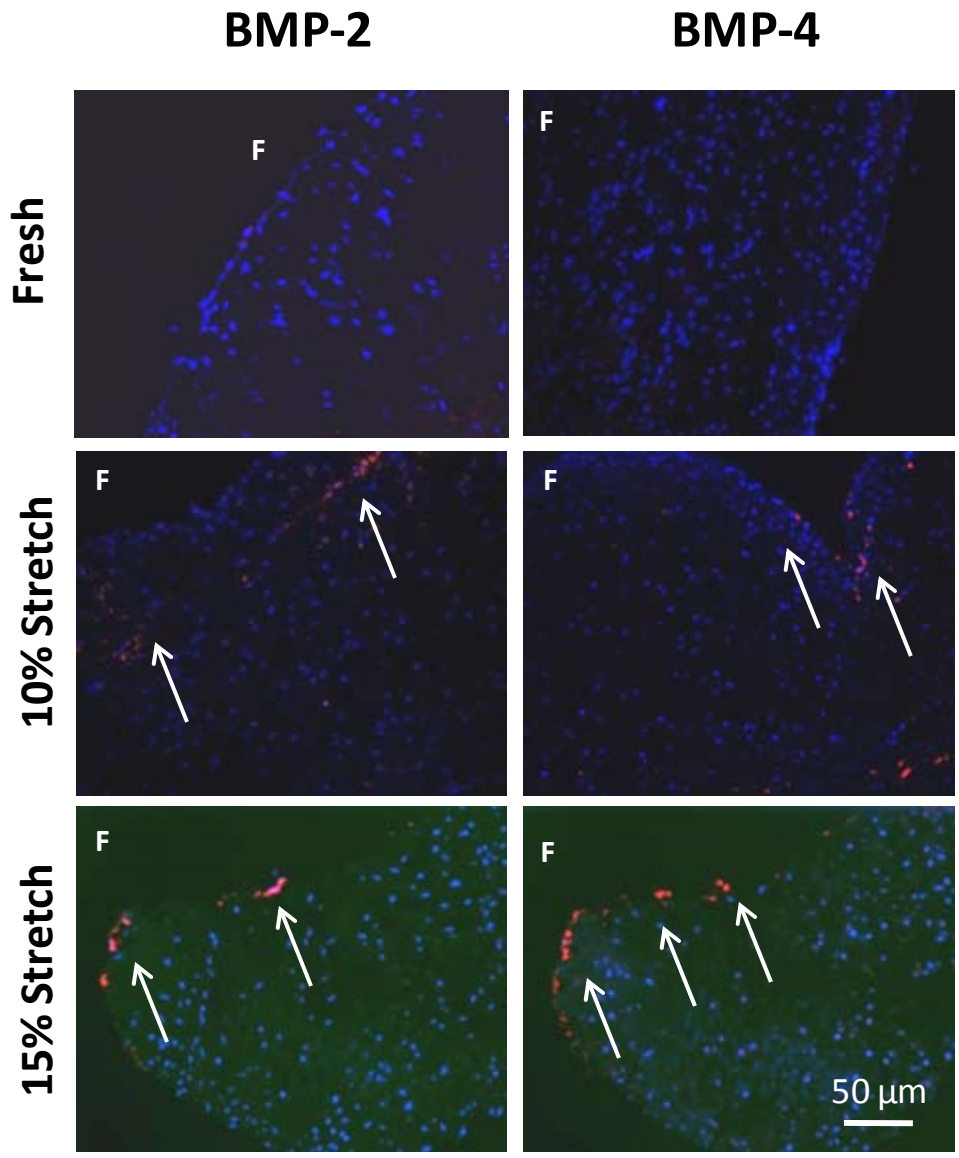

Figure 5-29: Representative micrographs of same tissue sections with BMP-2 and BMP-4 immunohistochemical staining after 3 days of culture (10% or 15% stretch) in fully osteogenic DMEM and in fresh controls. Expression of BMP was primarily observed on the fibrosa surface of the valve cusp. Some colocalization of BMP-2 and -4 was observed at the 15% stretch magnitude. (F-Fibrosa)

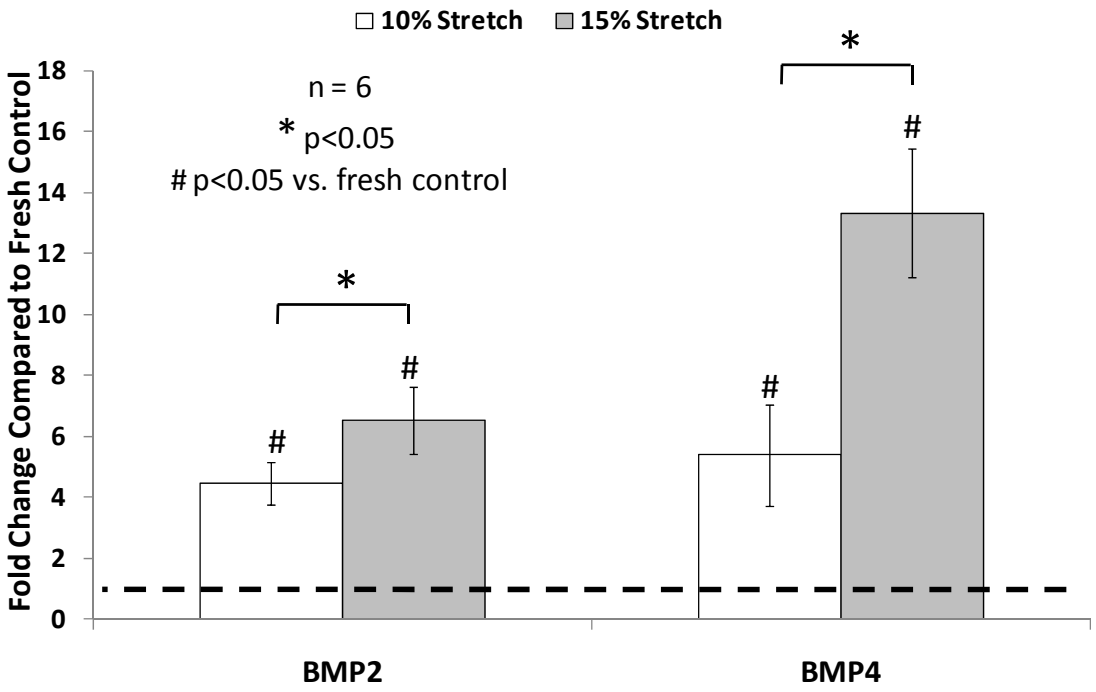

Figure 5-30: ImageJ was used to quantify the expression of BMP-2 and -4 in an image field normalized to the number of cells in that image field. Data was then expressed as a fold-change compared to fresh controls. BMP-2 and BMP-4 expression was significantly ($p<0.05$) increased by 15% stretch compared with 10% stretch. These samples were stretched for 3 days in fully osteogenic media.

5.3.4 Cyclic Stretch-Dependent Aortic Valve Calcification Occurs in a Bone Morphogenic Protein-Dependent Manner

Having established that cyclic stretch resulted in expression of BMP-2 and -4, the next step was to study if aortic valve calcification was dependent on this BMP-expression. That is, whether cusp calcification induced by pathological cyclic stretch was mediated in a BMP-dependent manner. As mentioned earlier, noggin, a pharmacological inhibitor of BMPs was used to bind with and block the downstream action of BMP. It was already reported in the previous section (**Section 5.3.1**) that incubation with noggin downregulated tissue mineralization and calcification as determined by histological staining. For this particular sub-section, several key markers characterizing the downstream molecular events in aortic valve calcification were analyzed. These were: (i) Runx2/Cbfa expression; (ii) Osteocalcin expression; (iii) Alkaline phosphatase (ALP) activity; and (iv) Total calcium content. The first three analyses will confirm that the valve interstitial cell has differentiated to an osteoblast phenotype, while total calcium content is a quantitative measure for valve calcification.

5.3.4.1 Runx2/Cbfa and Osteoblast Expression

Runx2 is a key transcription factor associated with osteoblast differentiation and is also a downstream transcription factor for BMP-2 and -4. Immunoblotting studies (**Figure 5-31**) demonstrated that Runx2 expression of aortic cusps was significantly ($p<0.05$) increased by 7 days of 15% stretch in the fully osteogenic medium, in comparison to fresh controls (2.24-fold) and 10% stretch (1.67-fold). 100ng/mL noggin treatment inhibited stretch-induced expression of Runx2 for both 10% (0.82-fold) and 15% stretch (0.64-fold). There was no significant ($p>0.05$) difference between fresh controls and normal (10%) stretch groups with noggin, and only a significant trend ($p<0.1$) between fresh controls and pathological (15%) stretch groups without noggin. This final result indicates that stretch-induced aortic valve osteoblast differentiation was dependent on bone morphogenic protein induced signaling pathways.

Identical trends were observed for osteocalcin expression (**Figure 5-32**). Osteocalcin expression was significantly increased by both 10% (2.67-fold) and 15% (8.25-fold) stretch when compared with fresh controls. These fold changes are greater than those observed for Runx2, which may be due to low basal levels of osteocalcin in a native aortic valve. In the presence of 100ng/mL noggin, there was significant reduction in osteocalcin expression for both 10% (0.50-fold) and 15% (0.23-fold) stretched groups.

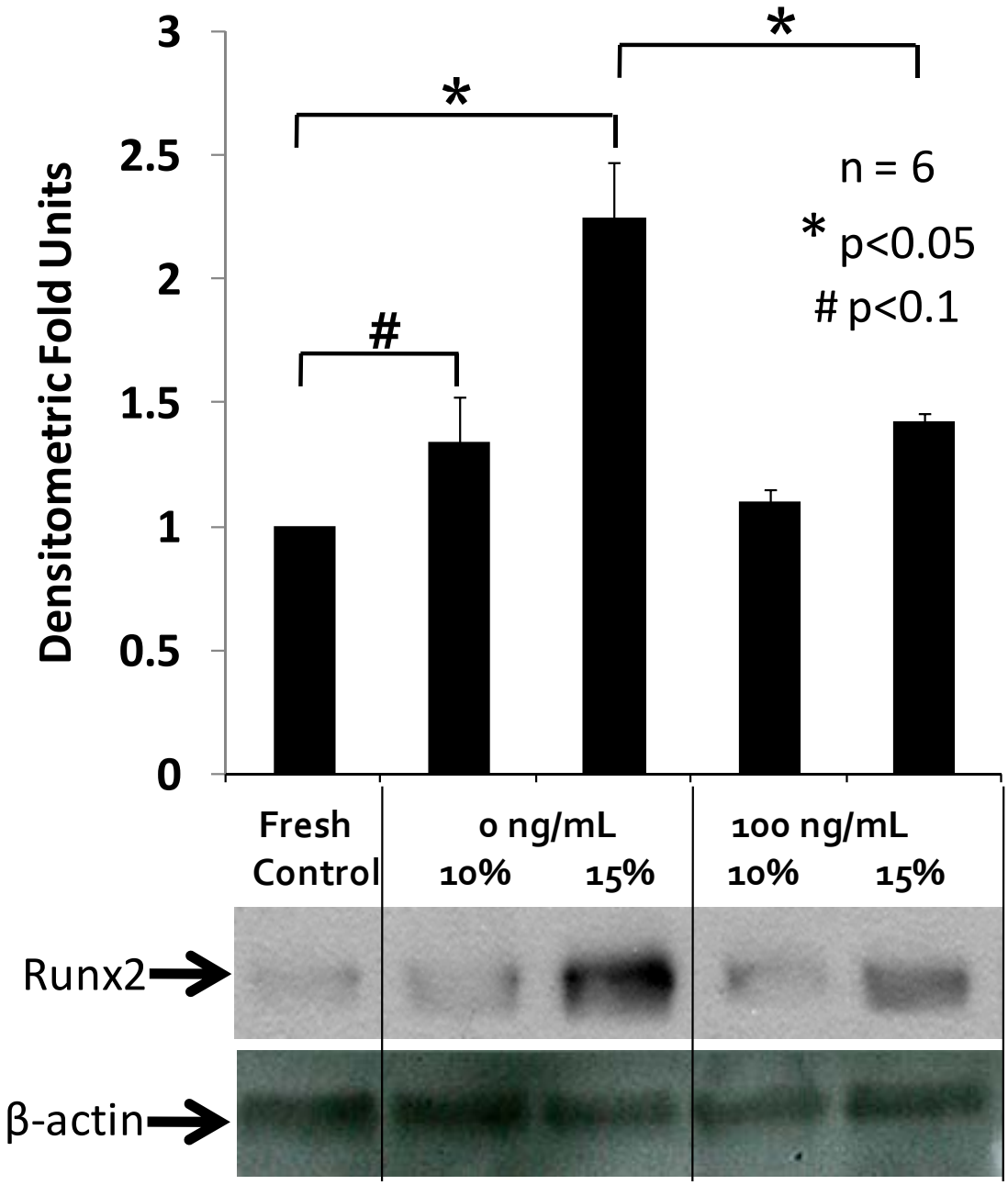

Figure 5-31: Runx2/Cbfa expression in stretched (10 and 15%) valves cultured in fully osteogenic DMEM in 0 and 100ng/mL noggin for 7 days. Runx2 expression significantly ($p<0.05$) increased with stretch magnitude, while addition of noggin significantly reduced Runx2 expression.

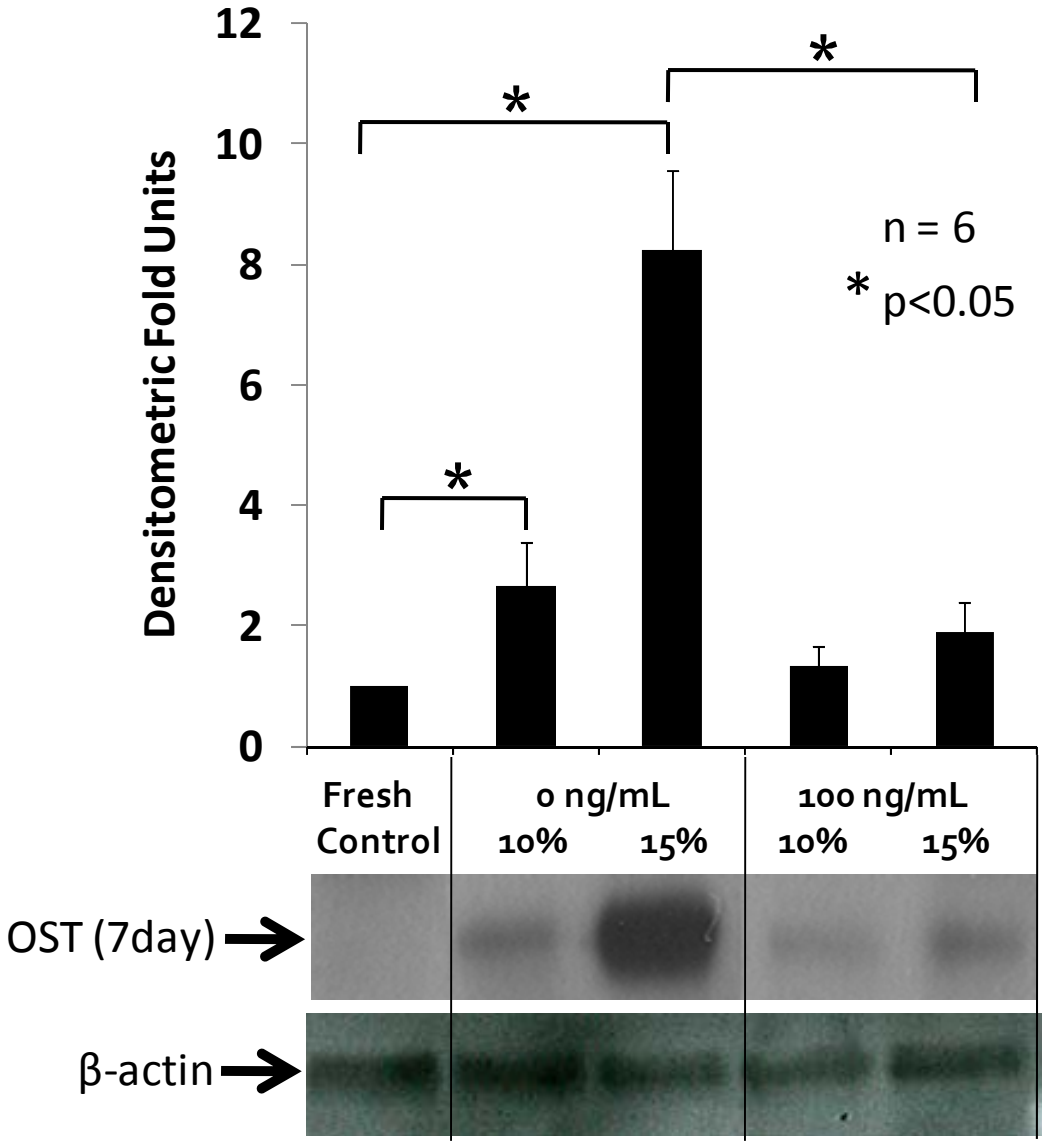

Figure 5-32: Osteocalcin expression in stretched (10 and 15%) valves cultured in fully osteogenic DMEM in 0 and 100ng/mL noggin for 7 days. Osteocalcin expression significantly ($p<0.05$) increased with stretch magnitude, while addition of noggin significantly reduced Osteocalcin expression.

5.3.4.2 Alkaline Phosphatase Activity

As mentioned earlier, ALP is an enzyme secreted by osteoblasts and was used as a marker for osteogenic differentiation of valve cells. ALP activity has been used in several studies as a specific marker for aortic valve osteoblast activity and calcification (45, 113, 177, 179). ALP activity was examined in cusps exposed to 10% or 15% cyclic stretch for 7 days in the fully osteogenic medium (**Figure 5-33**). The baseline ALP activity in fresh aortic valve cusp tissue was 1.7±0.8 nmol/min/mg protein, which agrees well with data published in literature (179). 15% stretch significantly ($p<0.05$) increased ALP activity above that of 10% stretch and fresh controls at all concentrations of noggin, indicating greater osteoblast cell activity at the elevated level of stretch. Intriguingly, noggin treatment inhibited stretch-induced ALP activity in a concentration-dependent manner. There was a successively significant ($p<0.05$) decrease in ALP activity for each increasing dose of noggin for both 10% and 15% stretch groups. For the 100ng/mL noggin concentration, there was no significant ($p>0.05$) difference in ALP activity between 10% and 15% stretch groups. It should also be noted that even at this highest noggin concentration, ALP activity was significantly higher than fresh controls, and this is due to the fully osteogenic media increasing the overall osteogenic potential of the valve samples. These results suggest strongly that calcification induced by a pathological level of stretch is mediated in a BMP-dependent manner. The dose-dependent response indicates that there may be promise in targeting the BMP signaling pathway to treat progression of aortic valve calcification.

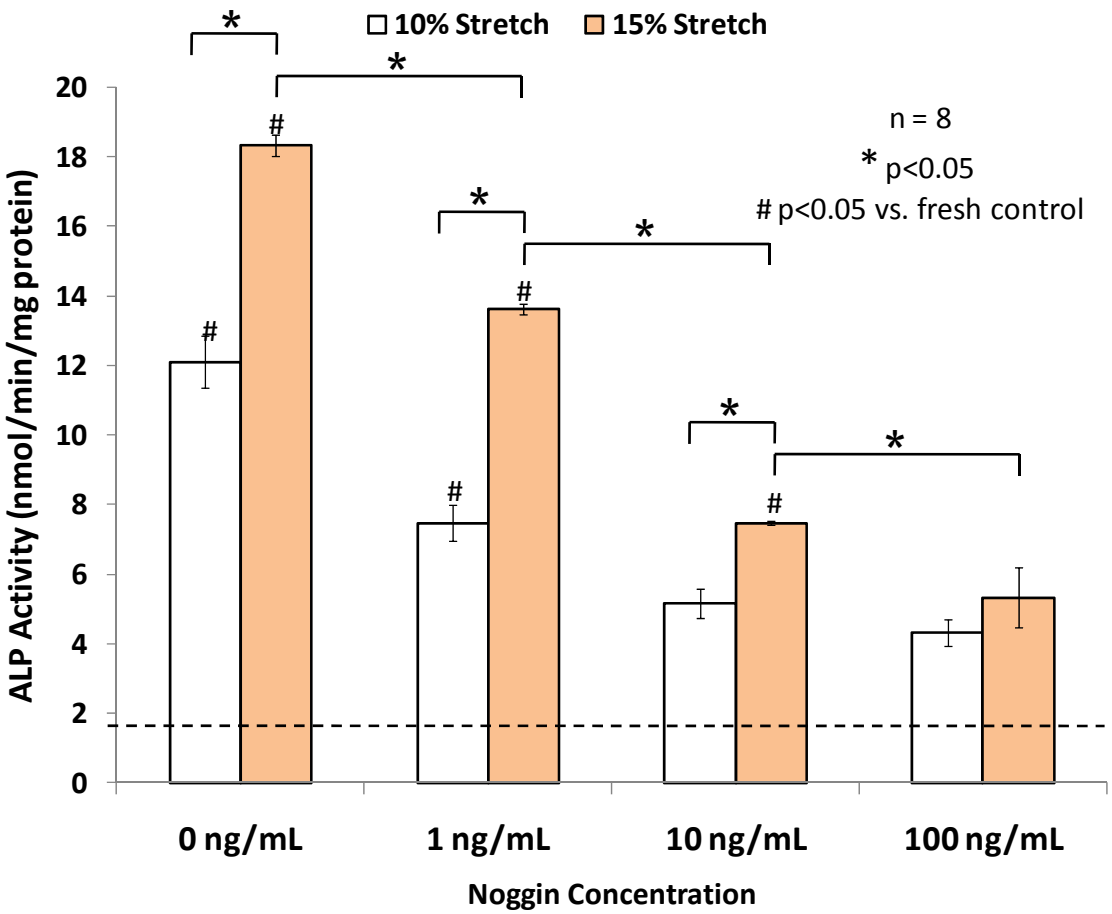

Figure 5-33: ALP activity in stretched (10 and 15%) valves cultured in fully osteogenic DMEM in 0, 1, 10, and 100ng/mL noggin after 7 days of stretch. Each successive increasing dose of noggin significantly decreased ALP activity for both 10% and 15% stretched sample groups.

5.3.4.3 Valve Total Calcium Content

Analyzing tissue total calcium content is a quantitative method for determining whether mineralization or calcification occurred within the tissue sample. Cusp samples were exposed to 10% or 15% cyclic stretch for 14 days in the fully osteogenic medium supplemented with or without the BMP inhibitor noggin (0, 1, 10, 100 ng/mL). Following this, total calcium content in each cusp was determined by the calcium arsenazo assay (**Figure 5-34**). Exposure of cusps to pathological stretch (15%) increased the calcium content by 5-fold compared to normal stretch (10%) in the fully osteogenic medium. Moreover, noggin blocked stretch-induced calcium increase in a concentration dependent manner with a similar dose-response curve as the ALP activity assay data (**Figure 5-33**). Doses as low as 1ng/ml of noggin showed a significant inhibition ($p<0.05$) compared to fresh controls, reaching a maximum inhibition level at 100ng/ml. Calcium content for the 15% stretch groups decreased significantly ($p<0.05$) for each successively increasing dose of noggin.

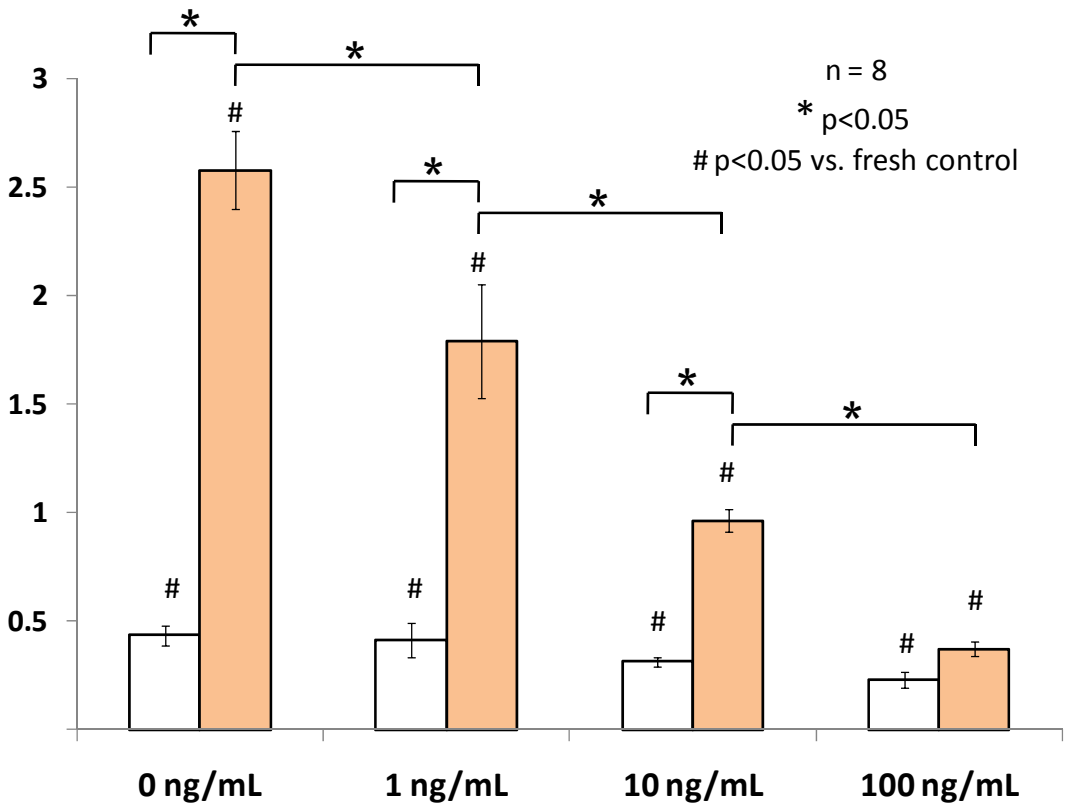

Figure 5-34: Calcium content in stretched (10 and 15%) valves cultured in fully osteogenic DMEM in 0, 1, 10, and 100ng/mL noggin for 14 days. Each successive increasing dose of noggin significantly decreased calcium content for both 10% and 15% stretched sample groups.

5.4 Specific Aim 3: Effect of Cyclic Stretch on Serotonin-Related Valvular Degeneration

Elevated circulating levels of serotonin or 5-hydroxytryptamine (5-HT), an endogenous vasoactive mediator have been reported to result in multiple cardiovascular pathologies such as cardiac valve fibrosis and systemic as well as pulmonary hypertension (75). The hallmarks of valve fibrotic lesions include excessive cellular proliferation, and increased extracellular matrix synthesis (33, 93) resulting in abnormal thickening of the valve cusp leading to change in valve mechanical properties. This can ultimately lead to geometrical changes in the valve and valvular insufficiency (46, 75). Additionally, other studies have also shown that some 5-HT receptor subtypes, such as the 5-HT_{2B} receptor, are mechanosensitive (137). It is also not known what role elevated stretch plays in 5-HT mediated valvulopathy. For these reasons, it is therefore important to characterize the response of aortic valves to 5-HT cultured under dynamic mechanical loading (i.e. cyclic stretch).

The objective of this specific aim was to understand the effects of normal (10%) and pathological (15%) stretch on serotonin-induced valve collagen content, collagen biosynthesis, cell proliferation and valvular mechanical properties. The effect of valve remodeling was studied in specific aim 1, and it was concluded that elevated stretch resulted in increased collagen content and turnover. The studies conducted in this specific aim would be used to understand if there was a further additive effect of serotonin overload on valve collagen turnover, which could lead to ultimate valve fibrosis and degeneration. In addition, two pharmacological antagonists (5-HT_{2A} antagonist: ketanserin; 5-HT_{2B} antagonist: SB240741) were used to understand if either of the 5-HT_{2A} or 5-HT_{2B} receptor-dependent pathways were stretch-sensitive.

5.4.1 Effect of Cyclic Stretch and Serotonin Concentration on Valve Collagen Concentration

As outlined earlier, the first set of experiments for this specific aim sought to identify the concentration of serotonin that elicited the greatest response in terms of collagen content. Four different treatment groups, representing four different serotonin concentrations were used for this part of the study: 0, 1, 10, and 100 μM serotonin. These concentrations represent a physiologic range of serotonin concentrations as demonstrated in recently published *in vitro* and *in vivo* studies (62, 91, 114). Once the serotonin concentration that causes the highest increase in collagen concentration is identified, the next step (subsequent sub-sections) would be to use that particular concentration exclusively to study the stretch sensitivity of the serotonin receptors.

Collagen content data as determined by the Sircol collagen assay (used previously for specific aim 1) reported a significant ($p<0.05$) increase with increasing 5-HT concentration up to 10μM (**Figure 5-35**). There was no significant ($p>0.05$) difference in collagen content between 0 and 1μM 5-HT for the 10% stretch groups, while collagen content significantly ($p<0.05$) increased for the 15% stretch groups (1.13-fold increase). Collagen content significantly ($p<0.05$) increased between 1 and 10μM 5-HT for both 10% (1.51-fold increase) and 15% stretch (1.13-fold increase) groups. Collagen content at 10μM 5-HT was also significantly ($p<0.05$) higher compared to fresh controls. At 100μM, collagen content is significantly ($p<0.05$) reduced compared to the 10μM 5-HT treatment groups for both 10% (0.33-fold change) and 15% stretch (0.54-fold change). In addition, the 10% stretch groups also had significantly ($p<0.05$) lower collagen content (0.66-fold change) compared to fresh controls.

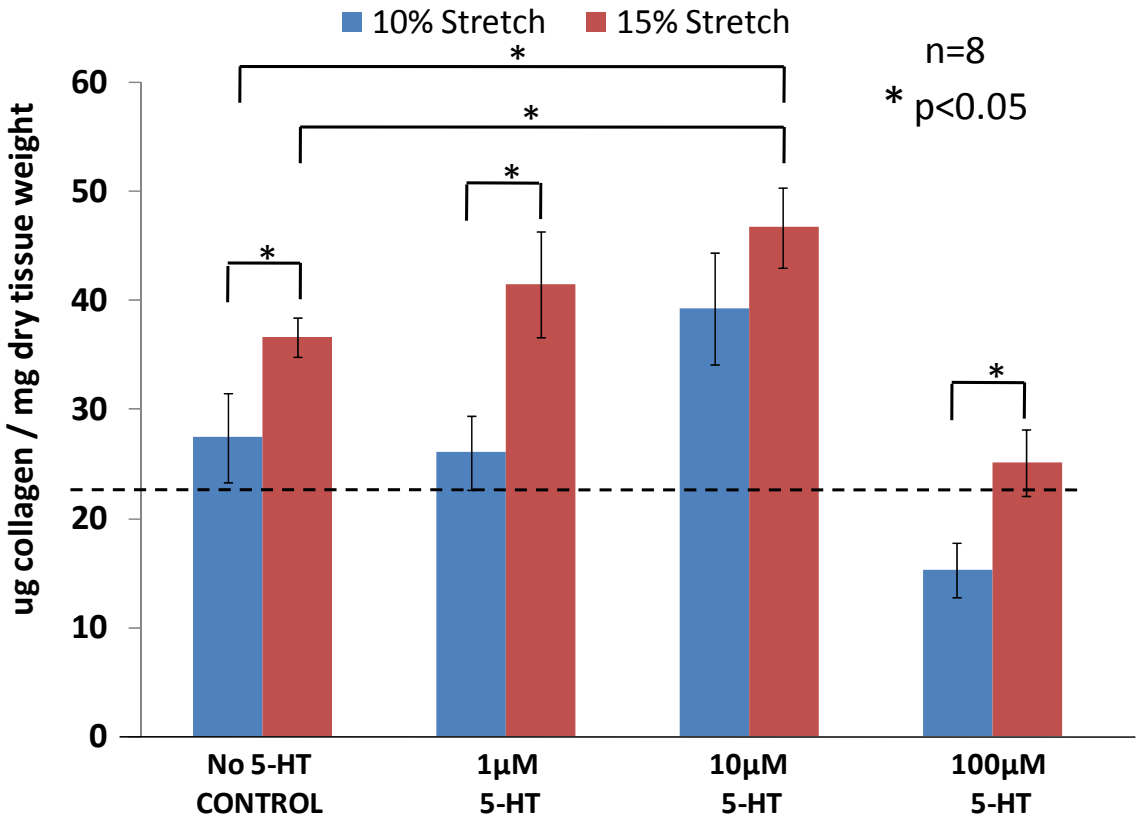

Figure 5-35: Collagen content in aortic valve cusps samples cultured under 10% and 15% stretch for four different concentrations of serotonin (0, 1, 10, 100µM). A biphasic response was observed, with collagen content increasing up until 10µM 5-HT, and decreasing significantly at 100µM 5-HT. Dashed line represents baseline collagen content in a normal fresh aortic valve cusp (22.22±1.51 µg collagen/mg dry tissue weight).

5.4.2 Effect of Serotonin Receptor Antagonists on Aortic Valve Collagen Content

This next experiment sought to understand whether the observed increases in collagen in the previous section occurred through stretch-sensitive 5-HT receptors. As outlined earlier, two additional treatment groups with different 5-HT receptor antagonists were studied here (50mM ketanserin: 5-HT_{2A} antagonist; and 10μM SB240741: 5-HT_{2B} antagonist). These pharmacological antagonists were added together with 10μM 5-HT as that was the concentration of serotonin that elicited the strongest response (**Figure 5-35**). These particular receptor subtypes were identified for study as they have been implicated before in valvular disease (19, 123, 137).

The results demonstrate that the 5-HT_{2A} receptor subtype is strongly stretch sensitive (**Figure 5-36**). There was a significant ($p<0.05$) decrease in collagen content compared to the no 5-HT control group (0.84-fold change) as well as the 10μM 5-HT group (0.66-fold change) for samples stretched to 15%. In addition, there was no significant ($p<0.05$) difference between the 10% (normal) and 15% (pathological) stretch groups when cultured with the 5-HT_{2A} antagonist, further strengthening the conclusion that this particular receptor subtype is stretch-sensitive. Contrary to these results, in samples cultured with the 5-HT_{2B} antagonist, there was a significantly ($p<0.05$) higher collagen content in the samples stretched to 15% compared to samples stretch under normal 10% conditions (2.00-fold increase). For samples stretched to 15%, there was no significant ($p<0.05$) difference between the 5-HT_{2B} antagonist group and the 5-HT only group (i.e. without the antagonist). This provides evidence that the 5-HT_{2B} receptor is not stretch sensitive.

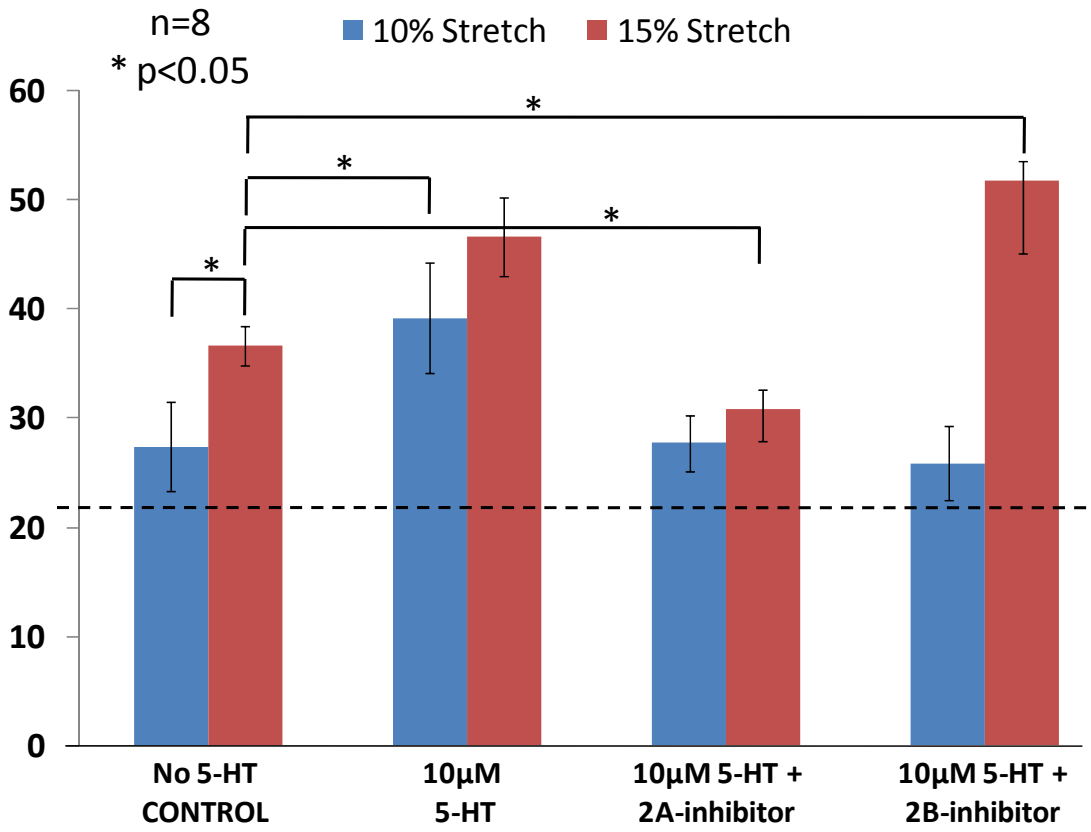

Figure 5-36: Collagen content of valves cultured with 5-HT_{2A} and 5-HT_{2B} receptor antagonists. With addition of the 5-HT_{2A} inhibitor, there was clear suppression of the stretch-5-HT-induced collagen increase. This phenomenon did not occur in the presence of the 5-HT_{2B} inhibitor. Dashed line represents baseline collagen content in a normal fresh aortic valve cusp (22.22±1.51 µg collagen/mg dry tissue weight).

5.4.3 Effect of Serotonin Receptor Antagonists on Aortic Valve Collagen Biosynthesis

Apart from analyzing total collagen content, it is important to understand the effect of stretch and serotonin on markers for collagen biosynthesis. Two common markers for collagen synthesis were chosen here: (i) heat shock protein 47 (hsp47), and (ii) lysyl oxidase (LOX). The same treatment groups as **Section 5.4.2** were studied here.

5.4.3.1 Heat Shock Protein 47 (Hsp47)

Hsp47 is an important chaperone protein for collagen synthesis as it is thought to be involved in the maturation of collagen molecules. There was no significant difference ($p>0.05$) in hsp47 expression between valves cultured at 10% stretch compared to fresh controls, while hsp47 expression was significantly higher ($p<0.05$) at 15% stretch. This result closely correlates with earlier observations about collagen content (**Section 5.4.2**). Valves stretched to elevated stretch (15%) with 5-HT demonstrated further increased expression of hsp47.

5.4.3.2 Lysyl Oxidase (LOX)

LOX is an enzyme that is responsible for the cross-linking of collagen and elastin. As such, LOX expression has implications for the structure as well as the function of the aortic valve cusp. For instance, increased collagen cross-linking might lead to stiffer cusp tissue, impacting proper closure of the valve. For valves cultured at 15% stretch, there was significantly higher ($p<0.05$) expression of LOX in the 5-HT groups as well as the samples cultured with the 5-HT_{2B} receptor antagonist. In contrast, samples cultured with the 5-HT_{2A} receptor antagonist had no expression of LOX . This set of results agrees well will **Section 5.4.2**, as we observe that once again, the 5-HT_{2A} receptor subtype appears to be stretch-sensitive in promoting collagen cross-linking.

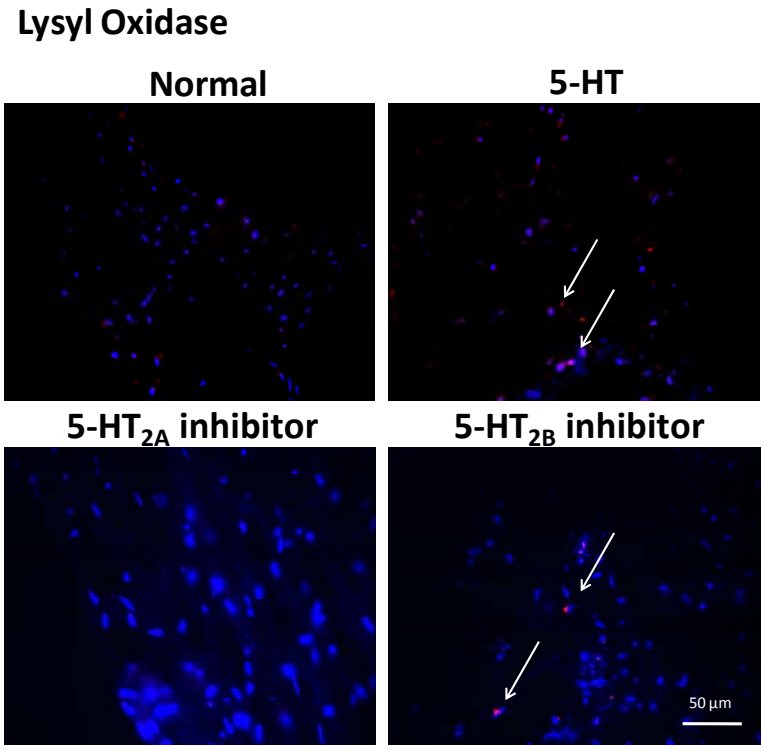

Figure 5-37: Representative micrographs showing lysyl oxidase staining of aortic valve cusps stretched to 15% (cells – blue; LOX – red).

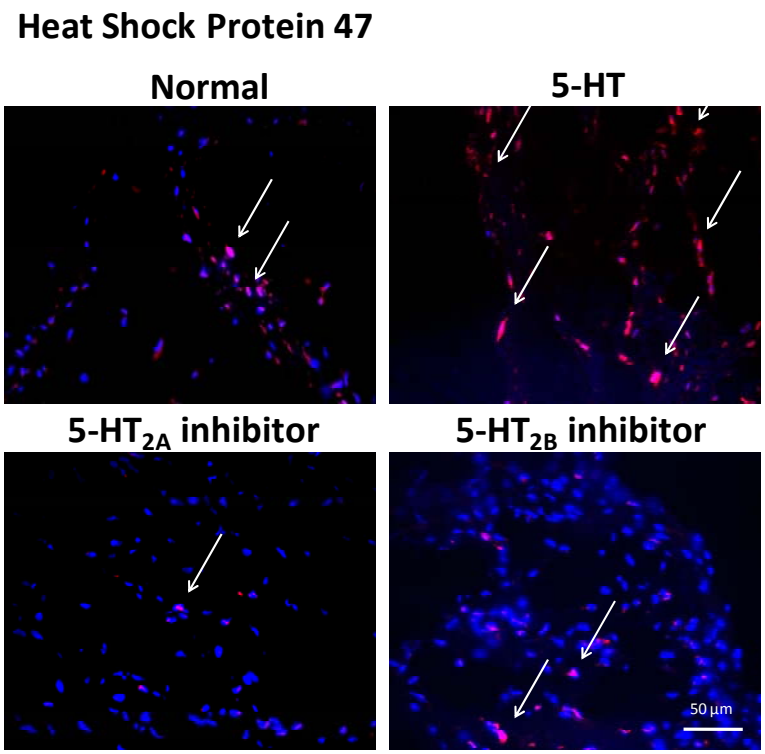

Figure 5-38: Representative micrographs showing hsp47 staining of aortic valve cusps stretched to 15% (cells – blue; hsp47 – red).

5.4.4 Effect of Serotonin Receptor Antagonists on Aortic Valve Mechanical Properties

Collagen is the primary structural protein of the aortic valve cusp. The results reported in the previous three sections demonstrate that 5-HT and cyclic stretch synergize to result in changes in aortic valve collagen synthesis, cross-linking and total collagen content. It was also demonstrated that these changes in collagen synthesis occur via a stretch-sensitive 5-HT_{2A} receptor-dependent pathway. This section sought to understand if these changes translated to a difference in the mechanical properties of the aortic valve cusp samples. Collagen is the primary stress-bearing fibers within the valve cusp and is the primary component that gives the valve its mechanical strength. Changes in collagen biochemistry reported in the earlier sections may translate to changes in valve mechanical properties. Valves samples were preconditioned to their physiological maximum loads and tested in a uniaxial mechanical testing apparatus, and membrane tension was plotted against Green Strain.

The results report some interesting observations (**Figure 5-39** and **Figure 5-40**). The fresh valve transitions from its toe region to the linear region on its tension-strain curve at approximately 20% strain. The curves for 10% stretch only, and for the 5-HT_{2A} and 5-HT_{2B} antagonists (10% stretch) overlap each other, transitioning to the linear regime at 15% strain (**Figure 5-39**). The samples stretched to 10% with 5-HT appear to be the stiffest group with a transition strain of about 12% (**Figure 5-39**).

For the samples stretched to the pathological level of stretch (15%), the 5-HT group was the stiffest with a transition strain of ~8%. Interestingly, the 5-HT_{2A} curve has deviated from the 5-HT_{2B} and no 5-HT control group (**Figure 5-40**) to transition at a higher strain of about 13%. This result strongly implies that 5-HT-induced valve stiffening occurs primarily via the stretch-sensitive 5-HT_{2A} receptor and to a lesser extent via the 5-HT_{2B} receptor, which does not appear to be stretch-sensitive.

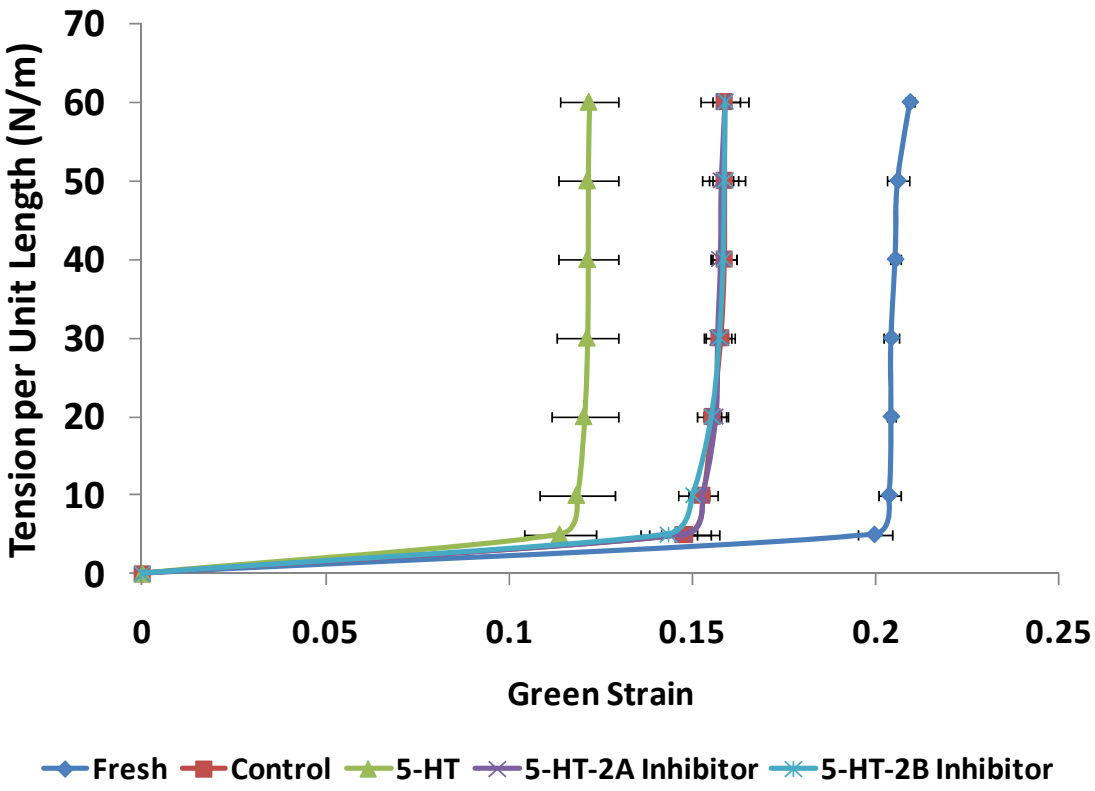

Figure 5-39: Tension per unit length vs. Green strain curves for samples cultured to 10% with fresh valves for comparison (green). Transition strain is at 20% for the fresh valve. As expected, the 5-HT group is the stiffest, with a transition strain of approximately 12%.

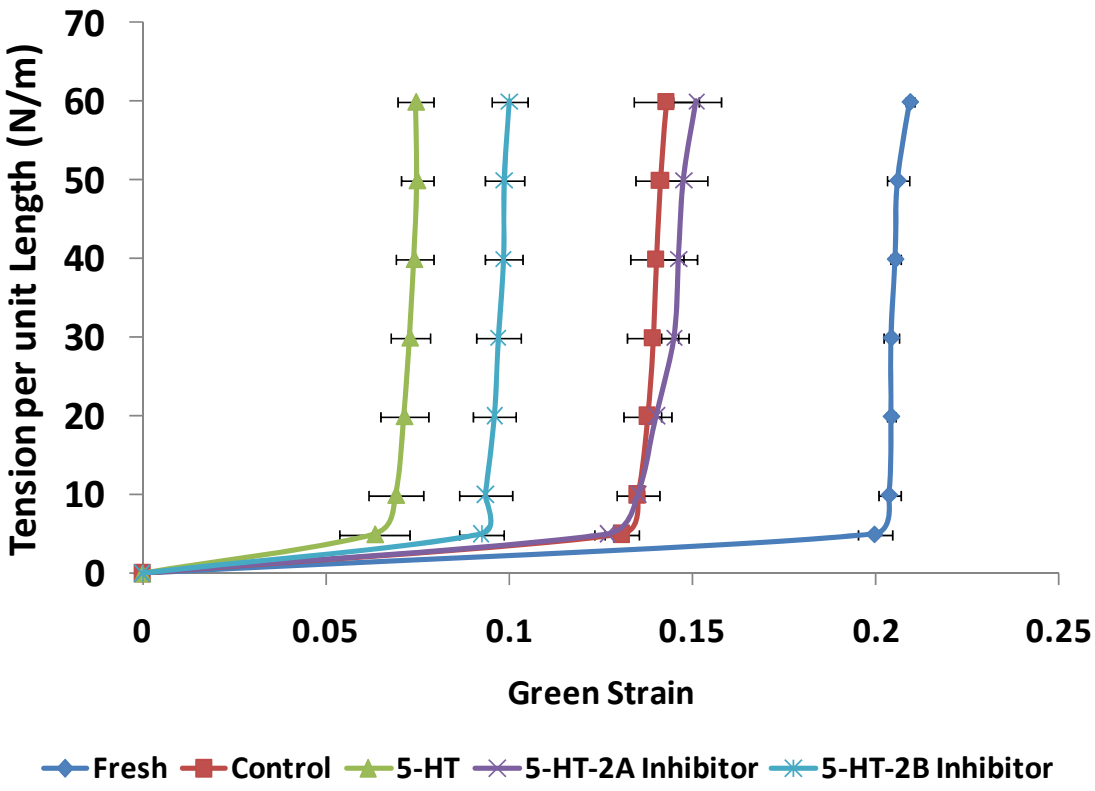

Figure 5-40: Tension per unit length vs. Green Strain curves for samples cultured to 15% with fresh valves for comparison (green). We observe deviation of the 5-HT_{2A} curve from the no 5-HT control and 5-HT_{2B} inhibitor groups. This demonstrates that addition of the 5-HT_{2A} receptor antagonist was able to suppress 5-HT and stretch induced changes to valve stiffness.

One also can note that the post-transition strain modulus is relatively consistent between all the sample groups for both the 10% and 15% stretch samples. This is consistent with the 3 day timeframe of these experiments, and the relative robustness of Type I collagen, which is the primary contributor of the post-transition stiffness of the aortic valve cusp. In fact, what has changed is the pre-transition or low-strain modulus. Indeed, one can observe how an increase in the pre-transition modulus can result in a decrease in the transition point of the valve sample. These low-strain moduli were computed and plotted (**Figure 5-41**). It can be observed that the modulus of stiffness increased significantly for the 5-HT groups for (10%) normal and elevated (15%) stretch. Stiffness significantly decreased in the 5-HT_{2A} inhibitor groups compared to the 5-HT

groups. These 5-HT_{2A} groups were not statistically different compared to the control groups. These results demonstrate that the 5-HT_{2A} receptor is stretch-sensitive. Stiffness in the 5-HT_{2B} groups was significantly lower compared to the 5-HT samples, but it was significantly higher than the controls, indicating that the 5-HT_{2B} group is not stretch-dependent.

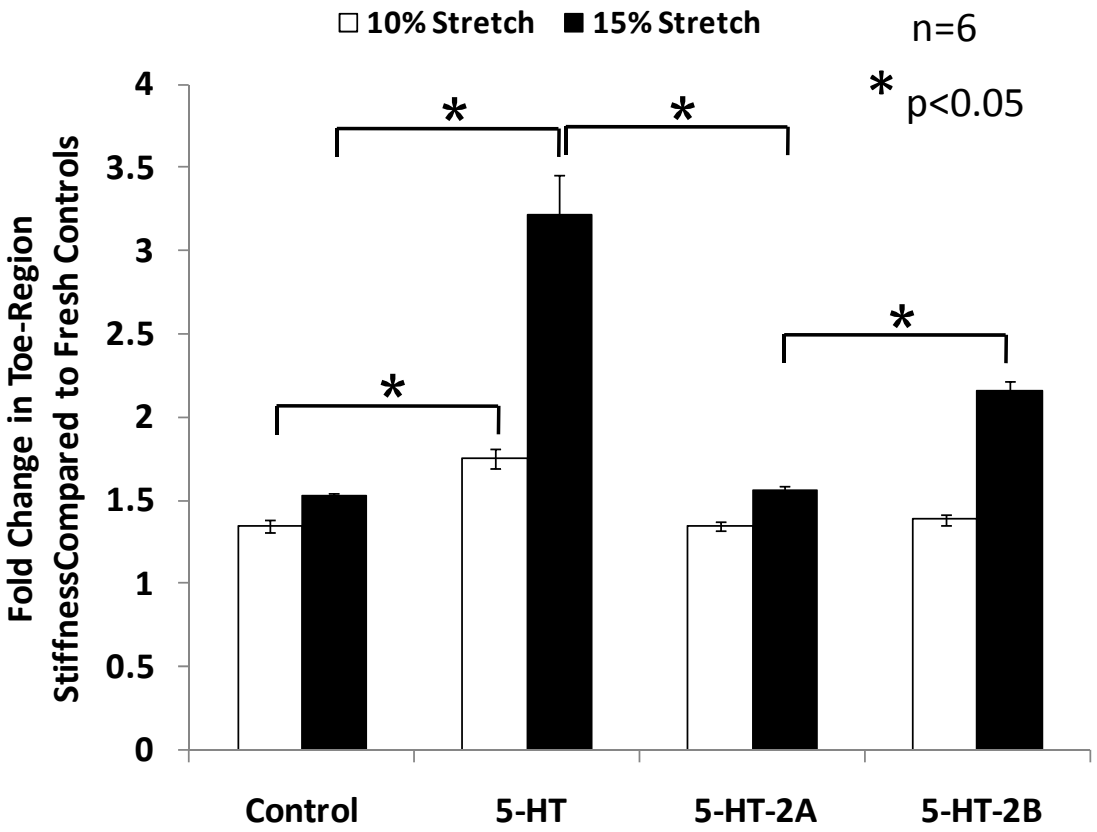

Figure 5-41: Fold-change in low strain modulus of samples compared to fresh controls. Modulus of stiffness increased significantly for the 5-HT groups for (10%) normal and elevated (15%) stretch. Stiffness significantly decreased in the 5-HT_{2A} inhibitor groups compared to the 5-HT groups. These 5-HT_{2A} groups were not statistically different compared to the control groups. These results demonstrate that the 5-HT_{2A} receptor is stretch-sensitive.

5.4.5 Effect of Serotonin Receptor Antagonists on Cellular Proliferation

The final result of this specific aim was to understand the effect of serotonin and cyclic stretch on cellular proliferation. Explanted valves from patients suffering carcinoid valve disease have demonstrated excessive cellular proliferation (114, 134, 194). In addition, we have observed in the previous specific aims that cellular proliferation was altered in response to cyclic stretch. Changes in cellular proliferation were therefore expected under the synergistic effects of stretch and 5-HT administration. As in the earlier sections of this chapter, these studies were performed using anti-BrdU immunohistochemistry.

It can be observed that cell proliferation appeared to be primarily regulated by the magnitude of stretch rather than the presence of 5-HT or 5-HT receptor antagonists (**Figure 5-42**). Among the 15% stretch groups, the 5-HT group and the 5-HT_{2B} antagonist group had significantly higher cellular proliferation than the no 5-HT control ($p<0.05$) and the 5-HT_{2A} ($p<0.05$) antagonist group. Once again, this result closely mirrors the collagen data (**Sections 5.4.2 and 5.4.3**) indicating that the 5-HT_{2A} receptor is stretch-sensitive. There was no significant difference ($p>0.05$) between 5-HT only groups and the 5-HT_{2B} groups at 15% stretch. However, there was a significant decrease ($p<0.05$) in cell proliferation for the 5-HT_{2B} group compared to 5-HT alone at 10% stretch. This result demonstrates the potential for 5-HT_{2B} antagonists to inhibit 5-HT mediated cellular responses, but this particular receptor antagonist does not appear to be particularly stretch-sensitive.

Proliferating cells appeared to appear on the fibrosa side of the valve cusp samples for the 10% stretch groups. For the 15% stretch groups, there was a relatively homogenous distribution of proliferating cells all throughout the thickness of the valve cusp. The spatial distribution of proliferating cells appeared to match the expression pattern observed in the collagen synthesis markers (**Section 5.4.3**).

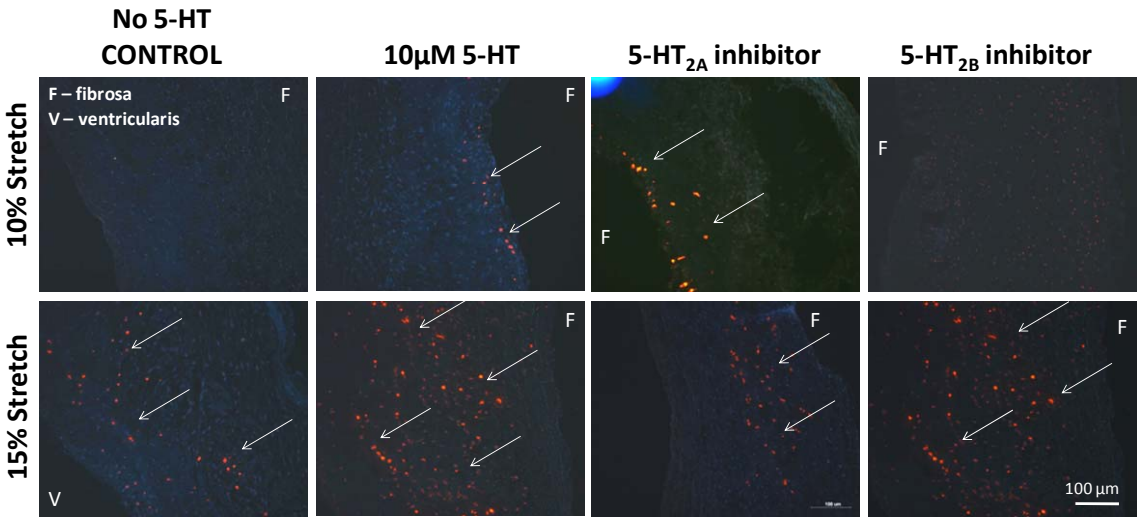

Figure 5-42: Cell proliferation (anti-BrdU) immunoassay demonstrates that cell proliferation increased in all treatment groups at the elevated level of stretch (15%), compared to their respective groups under normal physiological stretch (10%). The 5-HT_{2A} receptor was stretch-sensitive as that group had significantly lower ($p<0.05$) cell proliferation compared to 5-HT only groups under 15% stretch. The 5-HT only groups and 5-HT2B groups were statistically similar ($p>0.05$)

5.5 Summary of Results

In this chapter, results from three different specific aims were presented. Specific aim 1 studied acute changes to aortic valve extracellular matrix remodeling and turnover due to different magnitudes of cyclic stretch. Specific aims 2 and 3 studied phenomena occurring further downstream, focusing on the effects of cyclic stretch on two different aspects of degenerative valve disease: (i) Degenerative aortic valve calcification, and (ii) serotonin-mediated valve fibrosis (**Figure 3-1**).

In general, the results point to the fact that elevated stretch resulted in increased expression of disease-relevant markers. Normal physiological levels of stretch (10%) resulted in little change in biological or biosynthetic activity when compared with fresh controls. Expression of disease-related markers such as matrix remodeling enzymes, collagen oversynthesis and bone morphogenic proteins was increased significantly at 15% stretch. To recall, this level of stretch is representative of an increase in hemodynamic pressure of about 40 mmHg. As the magnitude of imposed stretch increased to 20%, there was severe cellular apoptosis. Expression of disease markers was not significantly different from 15% stretch, and this was thought to be due to the increased cellular apoptosis at 20% stretch. In summary, the response to stretch was primarily biphasic, with expression of markers related to valve disease demonstrating peak expression at a magnitude of 15% stretch.

The next chapter will focus on synthesizing these results in order to understand the various degenerative and pathological processes going on in the aortic valve cusp in response to cyclic stretch, and formulate potential disease pathways that link cyclic stretch to valve disease. Limitations of the current thesis work and potential future studies will also be highlighted.

CHAPTER 6

DISCUSSION

The results from three different but related aspects of degenerative valve disease were presented in CHAPTER 5. The objective of this dissertation was to investigate the effects of isolated cyclic stretch on aortic valve remodeling, calcification, and serotonin-related degenerative disease using a sterile *ex vivo* stretch bioreactor.

In this chapter, the results will be critically discussed in the context of the hypotheses and objectives of the specific aims of this research work. The next section will discuss the experimental model and approach utilized in this dissertation. It will also include a discussion on the validation of the stretch bioreactor system. The following section will present a high-level summary and synthesis of the effects of cyclic stretch on aortic valve remodeling and disease. This particular section will be split up into sections discussing aortic valve remodeling, structure, function, and aortic valve calcification. This chapter will conclude with sections on the significance of this dissertation work, and its limitations.

6.1 Experimental Model

6.1.1 Validation of Stretch Bioreactor System

Initial validation of the bioreactor showed that strains were uniform across the leaflet section. It was also validated that there was negligible fluid wall shear stress on the leaflet, and therefore cyclic stretch was the dominant force acting on the sample. The stretch bioreactor used in this study has been designed and validated in previous work by the Sacks laboratory (64, 151). It can be used to provide a controlled stretch environment to the valve cusps, and it has tremendous value as a benchtop model to study aortic valve disease. Indeed, as was demonstrated in specific aims 2 and 3, it could be used in the development and testing of potential pharmacological treatments for aortic valve disease. In addition, it is likely that this bioreactor model would be applicable for other tissue types not limited to heart valves (not tested in this dissertation).

6.1.2 In Vivo vs. In Vitro vs. Ex Vivo Experimental Approaches

An *ex vivo* experimental approach was adopted for this thesis work, and it was believed that such an approach had several advantages over *in vitro* and *in vivo* approaches. *Ex vivo* approaches seek to study the cells of any tissue within its own native matrix. None of the normal trypsinization, cell culture and passaging of cells are performed. This is especially advantageous as the response of the cell is modulated by cell-cell communication as well as cell-matrix communication. In the case of a mechanosensitive tissue like the valve cusp, the extracellular matrix serves to transmit mechanical cues via integrins to the cells, and this mechanotransduction component would be lost in an *in vitro* setting. Indeed, aortic valve interstitial cells in cell culture almost uniformly stain positive for α-SMA (**Figure 6-1A**), while native valve tissues are

only α-SMA positive in small cell bundles on the ventricularis side of the valve cusp (**Figure 6-1B**). It appears that the fibroblast and myofibroblast phenotypes of the valve cusp are lost in the process of cell culture. However, given appropriate cellular cues, the valve interstitial cell can change its phenotype *in vitro*. The significance of this phenomenon is therefore not clear, but it does point to *ex vivo* approaches as being more stable in maintaining an accurate phenotype of the valve cell.

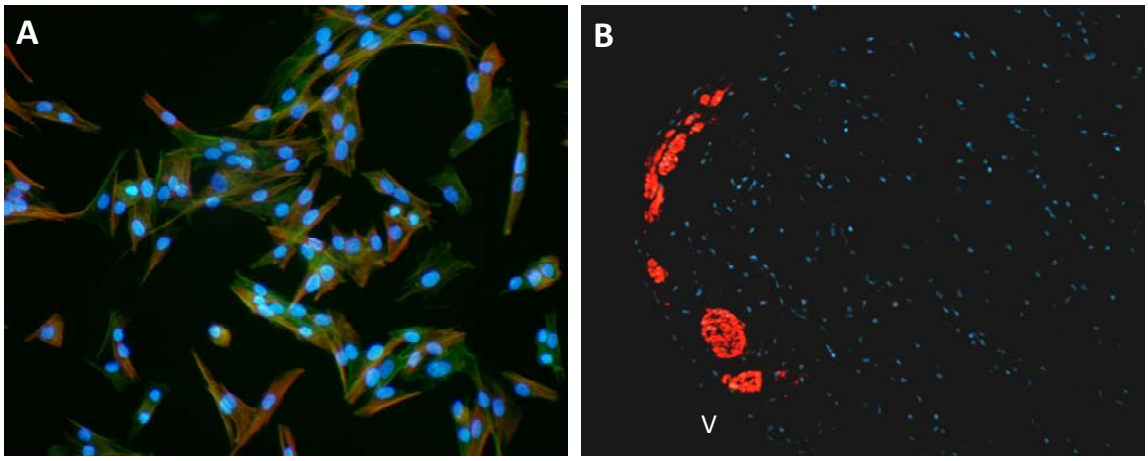

Figure 6-1: (A) Aortic valve interstitial cells in culture stain positive for α-SMA (red) and phalloidin (green). These cells have been stained after passage 3. (B) Native fresh porcine aortic valve cusps stain positive for α-SMA (red) near the ventricularis surface of the valve cusp. The cells for both panels are stained blue using DAPI. (V – ventricularis)

At the same time, when compared with an *in vivo* design, the approach adopted in this thesis allows imposition of very controlled stretch waveforms in a very controlled experimental setting. Increases in pressure or stretch would have to be achieved via aortic coarctation with little control over the exact value of the final pressure or stretch on the cusp surfaces. Experimental set up is as quick as *in vitro* methods. In addition, different drugs and media formulations can be evaluated in controlled doses. Finally, the costs associated with an *ex vivo* experimental approach are significantly lower than an *in vivo* approach.

However, that being said, one cannot ignore the value of *in vitro* and *in vivo* experimental approaches. Any developmental drug or surgical treatment needs to go through animal studies before it can be approved. However, development and initial testing can be greatly accelerated via *in vitro* or *ex vivo* testing. Additionally, development of treatments for aortic valve disease will require detailed molecular and pharmacological study of the disease pathways and this is best performed on cells in culture or co-culture. Further, one must also be aware of the inherent limitations of analyzing tissue samples histologically compared to immunocytochemical (ICC) staining of cells in culture. Embedding and sectioning tissue samples only sections a portion of the cells and the cellular cytoplasm, and one does not have access to the entire cytoplasm as in ICC. Therefore, it is possible to underestimate protein expression in a tissue section due to the "lost" cytoplasm.

Based on the above, it is therefore the opinion of this author that a multi-pronged approach is necessary for understanding valve disease and in particular, for developing a tissue engineered construct. One would need to utilize a combination of *in vitro*, *ex vivo*, and *in vivo* experimental approaches (**Figure 6-2**).

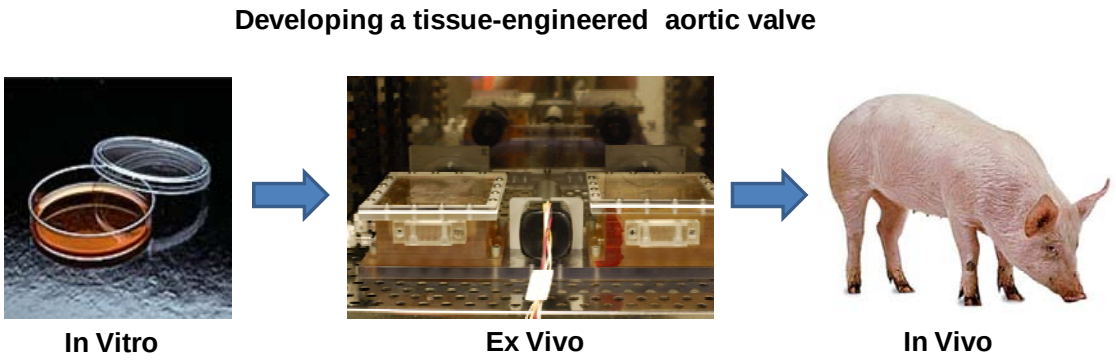

Figure 6-2: Combined approaches are needed for the efficient development of a tissue engineered valve construct.

6.1.3 Stainless Steel Coupling Method

Stainless steel springs were used in this study to couple the aortic valve samples to the stationary and moving posts of the tensile stretch bioreactor. This method has several advantages over other clamping methods. Firstly, the springs were threaded through the tissue at least five to six times and this allows for a more uniform force distribution across the width of the tissue. There was very little incidence of the tissue being ripped through the springs due to the cyclic motion of the linear actuator, with this mostly happening during application of the 20% stretch waveform. Ripping at 20% stretch was primarily due to the locking of the collagen fibers within the valve cusp sample. Secondly, due to the stiffness of the springs, the off-axis deformation (radial direction in this case) can be assumed to be negligible. Indeed, such a strip biaxial (239) deformation is more advantageous than uniaxial deformation for mechanobiological studies where any observed biological responses may be confounded due to influence from the off-axis component.

6.2 Effect of Cyclic Stretch on Aortic Valve Structure and Mechanics

6.2.1 Strains Experienced by Tissue vs. Strains Experienced by Cells

Before proceeding with a full discussion of the results, one must first consider if there are potential differences in the stretch experienced by the tissue (as imposed in this thesis), and the actual stretch experienced by the cells within the tissue matrix. Based on available literature, it is postulated that the cells are integrally connected to the extracellular matrix, and any stretching or deformation of the matrix is transferred directly to the cells. Indeed, Sacks *et al* showed that the cell nuclear aspect ratio doubles for a doubling in the stretch imposed on the tissue (209), indicating that there is a very close correlation between global stretch and local cell stretch.

6.2.2 Effect of Normal Stretch (10%) on Aortic Valve Biology

The results from this thesis demonstrated that normal magnitude of cyclic stretch (10% stretch) was able to maintain the normal cellular components of the valve cusp. It would be interesting to probe further into the meaning behind this observation. In a recent review paper by Sacks *et al* (209), the effects of stretch magnitude on cell and nuclear aspect ratio was reported. Via transmission electron microscopy, the paper demonstrated that the valve is at its most native morphology at 10% stretch when compared with 0% stretch or higher magnitudes of stretch. This particular result agrees very well with the results observed in this thesis. Indeed nuclear aspect ratio correlates very well with magnitude of imposed cyclic stretch and can be indicative of valve degeneration. For example, nuclear aspect ratio was doubled when the stretch was increased from 10% to 20% stretch, and this was the magnitude of stretch with the most cellular apoptosis.

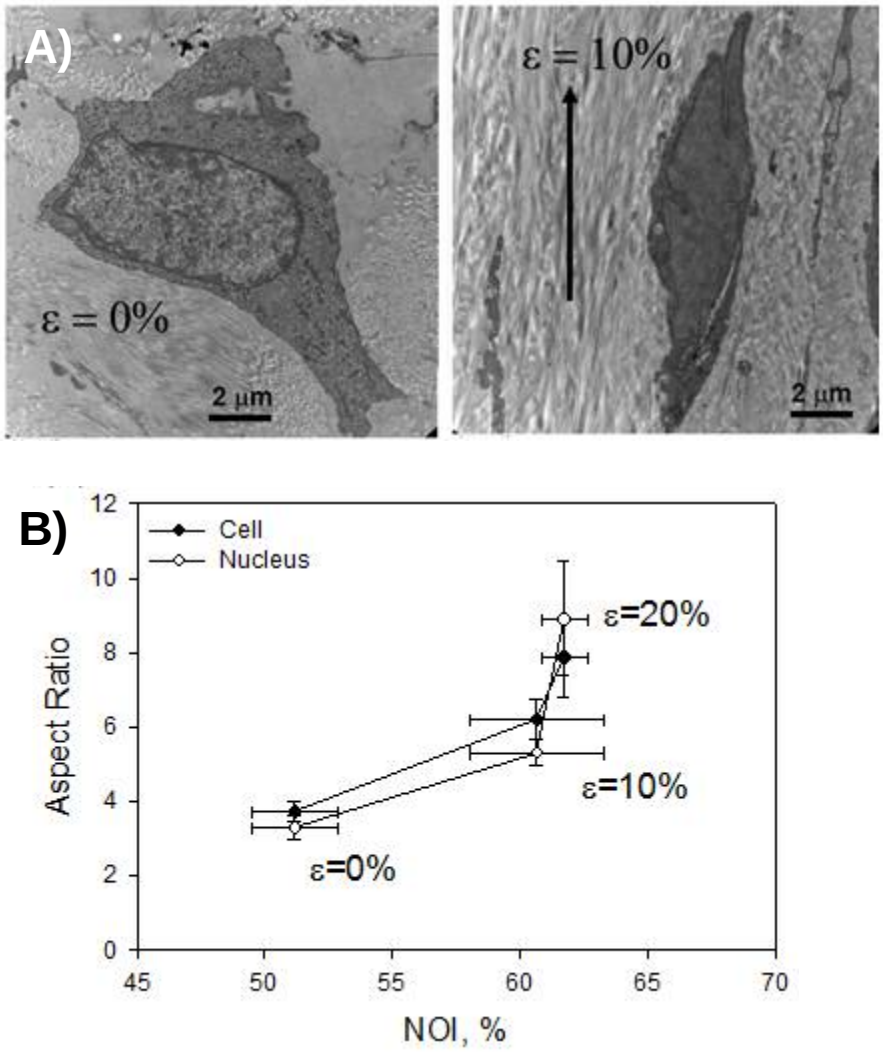

Figure 6-3: (A) Transmission Electron Micrography (TEM) of the aortic valve interstitial cells under 0 and 10% stretch with arrow showing direction of applied stretch. The cell at 10% has the normal elongated morphology of an interstitial cell. This may explain why cellular components can be maintained at 10% stretch. (B) Nuclear and cellular aspect ratio was changed similarly with stretch. There is almost a doubling of the aspect ratio between 10 and 20% stretch. Figure adapted from (209).

6.2.3 Extracellular Matrix Components

It was revealed that the collagen content of the aortic valve leaflets stretched to the pathological level of 15% was increased when compared to fresh and static control leaflets, while sGAG content was decreased in stretched leaflets compared to fresh leaflets. This magnitude of stretch corresponds approximately to a 40 mmHg increase in transvalvular pressure, as determined by Yap *et al* (280). Elastin content was comparable between the stretched and fresh leaflets. This suggests that exposure to isolated effects of circumferential cyclic stretch at altered levels has altered the extracellular matrix composition, consequently, altering the valve remodeling.

Collagen fibers, densely populated in parallel alignment along the circumferential direction of the leaflet, form the load bearing structure of the leaflet during each cardiac cycle (211, 250). The increase in collagen suggests that the leaflets adapt to altered mechanical loading due to the effects of isolated cyclic stretch, by either increasing synthesis, or decreasing degradation of collagen. The image analysis of the picrosirius red staining showed comparable proportions of newly synthesized fibers, and hence collagen synthesis in both fresh and stretched leaflets. The increased proportion of mature (red) fibers in stretched leaflets therefore leads us to believe that it is the reduced degradation of collagen that causes the overall total increase in collagen content. The preserved crimp in collagen fibers in the stretched leaflet, as evidenced by picrosirius red staining also implies that the native structure of collagen was not damaged by the stretching motion.

These data are in agreement with a study conducted by Ku *et al* (125) where porcine aortic valve interstitial cells were cultured on a collagen substrate and stretched for 48 hours. For cells subjected to 14% cyclic stretch, collagen incorporation in the cell layer was approximately 170% of unstretched cells. No significant changes were observed at time points less than 48 hours. This provides further evidence that 48 hours

of culture is a necessary and sufficient time point to observe changes in the valvular extracellular matrix. Indeed, the studies from this thesis on valve remodeling enzymes at 24 hours of stretch at times demonstrate unstable and very transient responses, which become more steady-state by the 48 hour time point. In addition, Hsp47 and LOX data (**Figure 5-37** and **Figure 5-38**) show that markers for collagen synthesis were increased with increasing magnitude of cyclic stretch, which is in line with the collagen assay data. The correlation between stretch magnitude and collagen synthesis has been corroborated via picrosirius red staining (7).

The semi-fluidic nature of the sGAGs in the spongiosa layer of the leaflet gives the leaflet considerable plasticity (250). It is therefore believed that the purpose of sGAG might be (i) to help reduce leaflet stresses by lubricating the relative motion of the other two layers as the leaflet deforms, and (ii) to dampen compressive forces during diastole (40). The absence of compressive stresses in this study, with the stretch being carried out at atmospheric pressure, might therefore explain the reduced levels of sGAG observed in the stretched leaflet compared to fresh leaflets.

Additionally, analysis of the culture medium at the end of experimental duration showed a statistically significant increase in sGAG content in the media (**Figure 6-4**). This suggests that cyclic stretching of the aortic valve leaflets resulted in secreting or leaching of the sGAG from the leaflets into the media, as the various layers of the leaflet rub against each other. This has been observed in fixed bioprosthetic valves before. A study conducted by Grande-Allen *et al* (85) also showed a loss of GAG from explanted porcine bioprosthetic valves due to leaching even under normal storage conditions. Although this study was conducted on fixed porcine tissue, there might be a potential for sGAGs to be forced out of the native porcine aortic valve either during static incubation or leaflet motion. In contrast, aortic valve leaflets when exposed to normal physiological forces undergo constant sGAG renewal by the interstitial cells (124).

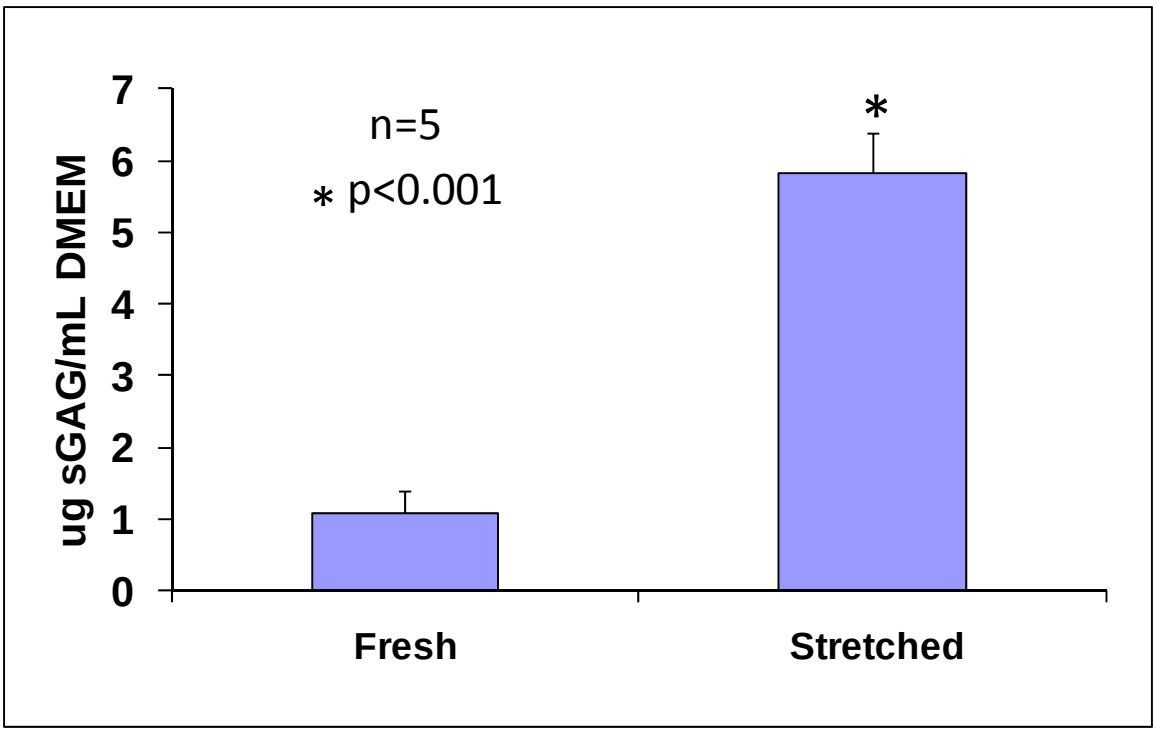

Figure 6-4: Measurement of sGAG content in the culture medium demonstrated significantly increased sGAG content in the tissue wells containing stretched tissue compared to fresh tissue culture medium.

Furthermore, the loss and leaching of GAGs may also be exacerbated by the fact that in the experimental protocol, we are surgically excising a rectangular section of tissue. This might cause a breach in the tissue "boundary" resulting in leaking of GAGs out from the tissue.

In the ventricularis layer of the leaflet, the major extracellular component is elastin in the form of fibers that are oriented primarily along the radial direction. The primary role of elastin fibers is to maintain a circumferential collagen fiber orientation and recoil the collagen fibers to their initial state after the external load has been released (260). Since the valve leaflets were cyclically stretched along the circumferential direction at physiological rates in the current study, it is possible that the elastin fibers were not "activated" beyond their normal levels and consequently additional synthesis of

elastin was not required, explaining why elastin content remained unchanged between fresh and stretched leaflets.

The above findings reinforce the fact that valve cells require mechanical stimulation to maintain a balance between synthesis and degradation of ECM components. This occurred without undue damage to the normal tri-layered structure of the aortic valve leaflet. Further analyses of the hematoxylin and eosin images demonstrated that the relative thicknesses of the fibrosa, spongiosa, and ventricularis were maintained between fresh valves and valves stretched to 10% and 15% stretch (**Figure 6-5**). However, as reported via Movat's pentachrome staining (**Figure 5-9**), 20% stretch resulted in severe deterioration of the normal tri-layered structure of the valve cusp, and is possible indication as to what may happen to a valve under acute elevated pressure loading.

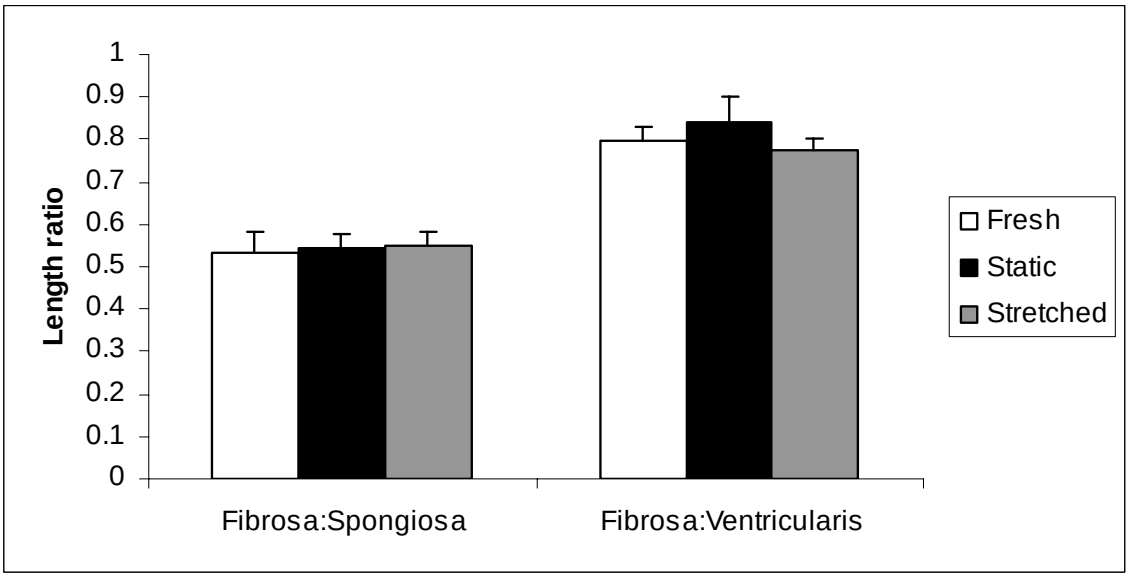

Figure 6-5: Fibrosa-to-spongiosa ratio and fibrosa-to-ventricularis ratio remained unchanged. There was no significant difference ($p>0.05$, $n=8$) in the relative thicknesses of the fibrosa, spongiosa and ventricularis layers between fresh, static and stretched leaflets (both 10% and 15% stretch).

6.2.4 Extracellular Matrix Remodeling Enzymes

The key findings of this thesis are: (i) normal cyclic stretch (10%) maintained the native levels of matrix remodeling activity; (ii) cathepsin L expression was reduced by elevated cyclic stretch, while cathepsin S and K expression was increased; (iii) elevated cyclic stretch (15% and 20%) results in acutely increased collagenase and gelatinase activity compared to controls. Our results therefore demonstrate the importance of cyclic stretch in regulating extracellular matrix remodeling. These findings suggest an important role for elevated cyclic stretch in the progression of degenerative aortic valve disease.

Understanding the mechanobiology of proteolytic enzymes such as MMPs and cathepsins is clinically important. Matrix proteolytic enzymes are expressed both early in valve disease progression and are also highly over-expressed in explanted diseased valves (119). Degenerative aortic valve disease involves progressive degradation of valve mechanical properties via changes in the extracellular matrix composition. Changes in valve mechanics can also result in changes in the hemodynamic environment in the valve via altered kinematics and leaflet curvatures. For example, progressive changes in stiffness of the valve can result in changes in the strain environment which might result in a feedback loop of accelerated valve degeneration (71, 171). It is also acknowledged that hypertension, a risk factor for valve disease (193), can increase the strain environment on the valve cusp (280). The effect of elevated levels of cyclic stretch observed in this study can therefore have important implications for hypertension-related valve degeneration.

Normal 10% stretch was able to maintain the expression and activity of the remodeling enzymes to native (fresh) levels, while elevated levels of cyclic stretch resulted in elevated levels of expression of matrix remodeling enzymes. The altered

levels of some of these enzymatic proteins suggest an acute disruption in the overall equilibrium between matrix synthesis and degradation under elevated levels of cyclic stretch. Interestingly, there was also significant upregulation of collagen content in cusps cultured to 15% and 20% stretch suggesting that there was a net synthesis of collagen under these experimental conditions. These findings underline the ability of the aortic valve cusp to continuously adapt and remodel its load-bearing components in order to function adequately in a changed mechanical environment. This observation is in agreement with the stress overload theory proposed by Robicsek *et al* (203). Additional studies are required to identify which specific collagen isoforms were synthesized in response to cyclic stretch.

We showed by immunohistochemistry that cathepsin S and K expression was upregulated by high levels of stretch. High levels of cathepsin L expression were observed in fresh valve cusps which was down-regulated by stretch. Cathepsin L may potentially be a key regulator of normal matrix turnover in the native valve, and if non-physiologic (15% and 20% stretch) stimuli are applied, a disease-remodeling pathway may be activated resulting in other cathepsins (S and K observed in this study) to be preferentially expressed. Indeed, in a recent study by Helske *et al*, it was revealed that cathepsin S, K and V expression and activity were the cathepsin sub-types that were upregulated in stenotic aortic valves (99). The associated increase in collagen content at 15% and 20% stretch led us to further speculate that cathepsin L is a key enzyme involved in normal collagen turnover in valve cusps, wherein its downregulation under 15% and 20% stretch resulted in increased collagen content. Previous studies in our laboratory showed that cathepsin L was downregulated by altered levels of cyclic

pressure (189) and laminar shear stress (187, 188). Therefore, consolidating all these findings, we can postulate the following pathway (**Figure 6-6**), where normal mechanical forces maintain the valve matrix via continued cathepsin L expression, while pathological loading regimes downregulate cathepsin L expression and lead to increased expression of disease-associated cathepsins S, K, and V. Further study could focus on the utility of these cathepsins as biomarkers for valve disease progression.

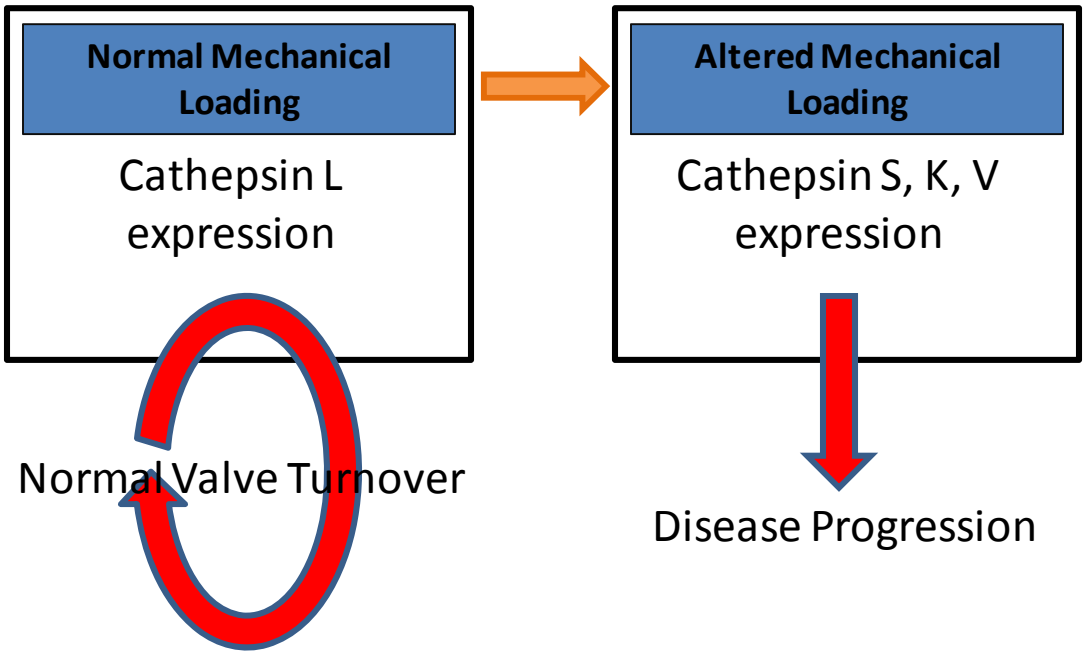

Figure 6-6: Schematic showing the importance of cathepsin L in normal valve turnover under normal mechanical forces, and the transition to cathepsin S, K and V expression in the case of altered mechanical forces.

Our study also showed that high stretch resulted in increased expression of MMP and reduced expression of the tissue inhibitors of MMPs. It is known that cytokines such as tumor necrosis factor-α (TNF-α) can contribute to increased expression of MMPs and cathepsins in diseased aortic valves (119). Indeed, the over-expression of MMPs that we

observed in response to 15 and 20% stretch was observed to be concurrent with cytokine expression such as cellular adhesion molecules (**Figure 6-8**) and BMPs (**Figure 5-29**). This hypothesis is further strengthened by the increased proliferation and apoptosis of valve interstitial cells that was observed at these levels of stretch. In addition, a parameter that can be used to represent this altered remodeling by normalizing proteolytic and inhibitory expressions (MMP/TIMP ratio) was presented (**Figure 5-20**). It is acknowledged that this is an idealized metric to assess tissue remodeling potential of the aortic valve under cyclic stretch, as there are numerous other MMPs and cathepsins involved in its remodeling *in vivo*. However, in the results reported in this dissertation, strong correlations were observed between the MMP/TIMP ratio and expression of other markers of compromised remodeling such as the cathepsins, cellular proliferation and cellular apoptosis. Another potential criticism of this metric could be that proteolytic activity, which is a subset of total expression of proteolytic enzymes, is more relevant to matrix remodeling. This is not expected to be of great concern here as we did observe reasonable correlation between enzyme expression and activity (R^2=0.597, $p<0.05$) for the studies performed in this dissertation. Indeed, the value of stretch where the highest remodeling was observed is also in good agreement with a similar study on valve interstitial cells reported by Ku *et al* (126). In this particular paper, the authors reported a significant increase in collagen synthesis (via [^{3}H]-proline incorporation) and mRNA expression at 14 and 20% stretch compared to lower magnitudes of stretch (7 and 10%).

6.2.5 *Implications for Valve Structure and Function*

Specific aim 1 reported the increase in valve collagen synthesis under elevated stretch conditions. The results presented in specific aim 3 demonstrate that there is increased collagen biosynthesis under combined stretch and serotonin administration, implying a synergy with the mechanical stimulation and serotonin-induced collagen oversynthesis. Mechanical testing also indicated increased tissue stiffness that correlated well with increases in collagen synthesis and content. Though not explicitly tested in this thesis, it is speculated that valve function could be compromised due to the increased stiffness of the valve samples.

6.2.6 *Implications for Serotonin-Induced Valve Disease*

As mentioned in the background chapter, elevated 5-HT levels have been associated with valvulopathy coinciding with fibrosis and increased cellular proliferation (14, 46, 47, 90, 194). *In vivo* these valves present with significant regurgitation (76, 90, 114), likely due to inability of the stiffer cusps to coapt effectively. It is speculated that this is primarily due to the increased collagen synthesis as demonstrated in this dissertation. It is intriguing why the primary mode of failure observed clinically for these valves is regurgitation, as stiffer cusps can also result in stenotic valves. Indeed, in a very recent paper by Peña-Silva *et al*, it was reported that elevated serotonin levels can result in increased oxidative stress in the valve cusp potentially leading to stenotic valve disease (186). It is speculated that 5-HT-induced valve stiffening occurs throughout the valve cusp resulting in reduced valve curvature, and ability of the valve to coapt effectively. Increased collagen cross-linking and collagen synthesis can result in leaflet thickening and possibly increased flexural modulus. This area is currently poorly understood and warrants further study.

Of even greater interest is the identification of the 5-HT_{2A} receptor as being mechanosensitive for collagen biosynthesis, and able to respond differentially to different magnitudes of cyclic stretch. Previous work by Levy *et al* has identified the 5-HT_2 receptor subtype as having potential roles in heart valve disease, with demonstrated ERK signaling (277). In addition, it was speculated that perhaps this receptor group is mechanosensitive by Liang *et al* that investigated the 5-HT_{2B} receptor subtype (70, 137). The results from Liang *et al* and this thesis indicate that different 5-HT receptor subtypes can regulate different biosynthetic pathways. This thesis identified the importance of the 5-HT_{2A} receptor in controlling collagen biosynthesis, while the 5-HT_{2B} receptor activates the nuclear factor-κB pathway (137). This thesis utilized pharmacological antagonists for 5-HT_{2A} and 5-HT_{2B} receptor subtypes to identify if any of these two receptor subtypes were mechanosensitive.

Initial results on the 5-HT dose curve demonstrated that 10^{-5}M 5-HT was the concentration that resulted in the greatest collagen synthesis and content. Further increases resulted in a drastic decrease in collagen content. It is speculated that this is due to two possible reasons. Firstly, it is possible that doses higher than 10^{-5}M might be toxic or at the very least non-ideal for the valve samples. Further studies investigating cell apoptosis and signaling molecules should offer better insight. That is, the valve cell might differentiate toward a more proliferative rather than a synthetic phenotype, which was also observed under a very high magnitude of cyclic stretch (20%). Secondly, it is also speculated that a competing pathway is activated at these higher doses of 5-HT. One such pathway could be the 5-HT transporter (5-HTT) mechanism. *In vivo*, excessive circulating levels of 5-HT are cleared by the 5-HTT reuptake mechanism (135). This is obviously not possible in our *ex vivo* system, but it may result in "blocking" of 5-HT receptors, thereby preventing 5-HT induced collagen synthesis.

As mentioned earlier, an exciting finding was that the 5-HT_{2A} receptor subtype was stretch-sensitive for collagen synthesis. These studies were performed with standard pharmacological competitive antagonists for the 5-HT_{2A} and 5-HT_{2B} receptor subtypes. Collagen content was reduced in the 5-HT_{2A} group under elevated stretch, but not in the 5-HT_{2B} group. This trend was also observed in the results for Hsp47, lysyl oxidase, as well as in tissue stiffness. Earlier studies have alluded to the possibility of stretch-sensitive 5-HT receptor subtypes, and this dissertation work has provided further convincing evidence for this phenomenon. Further cell culture studies are needed to elucidate the specific signaling molecules that are stretch-sensitive.

6.3 Effect of Cyclic Stretch on Aortic Valve Calcification

Specific aim 2 of this dissertation sought to understand if stretch-induced aortic valve calcification proceeded via a BMP-dependent pathway. This would be a key contribution to the field as subsequent research can focus on how best to target the BMP pathway (if shown to be important), in order to slow down or even reverse calcification. This was also a logical progression after specific aim 1, as several researchers have observed overexpression of matrix remodeling enzymes in diseased aortic valves, specifically in calcified valve cusps (160-162, 171). In fact, the experimental design for this dissertation was based on a hypothetical disease pathway proposed by O'Brien in a recent review paper (**Figure 6-7**).

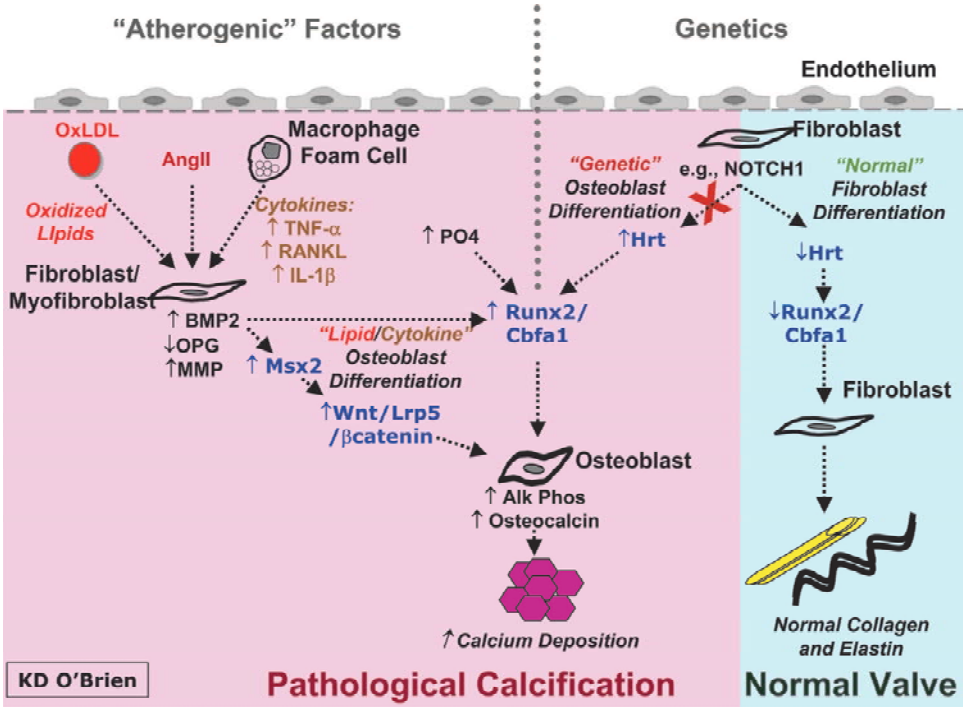

Figure 6-7: Potential interplay between genetic and atherogenic factors in the pathogenesis of valve calcification. Potential mechanisms include upregulation of MMPs and BMPs leading to activation of Wnt/Lrp5 or Runx2/Cbfa1 pathway leading to differentiation of the valve interstitial cell to an osteoblast-like phenotype.

To reiterate, the novel contributions of this thesis work in understanding aortic valve calcification mechanisms were: (i) it was demonstrated that the aortic valve can be calcified preferentially on the fibrosa side within a week in response to a pathologically relevant level of cyclic stretch and humoral conditions in *ex vivo* tissue culture; (ii) pathological stretch induced apoptosis and BMP expression preferentially on the fibrosa side; and (iii) the BMP antagonist noggin was able to block osteogenic and calcification events (ALP activity, Runx2 expression and calcium content in the valve cusps/tissue) that were induced by stretch. This study therefore points to the BMPs, particularly BMP-2 and/or -4 as key players in stretch-induced aortic valve calcification. These findings also suggest a potential importance of BMP antagonists in prevention or treatment of aortic valve calcification.

The *ex vivo* tissue culture system used in this study is an accelerated model for calcification, obtaining expression of BMPs and ALP after 3 and 7 days respectively and significant increases in tissue calcium content after 14 days. Therefore, an important contribution of this study is that this *ex vivo* system could be used to study valvular disease mechanisms on the bench-top before more detailed validation is done *in vivo*. BMP-blockers appear to be a potential route towards pharmacological treatment of aortic valve calcification, but the location and timing of drug delivery require much study. Prospective interventional trials will be especially important in establishing the benefits of any proposed pharmacological agent (74). However, most patients that present with clinical symptoms of valve calcification have usually progressed to an irreversible pathology that pharmacological treatments may not be maximally effective (198).

6.3.1 Effect of Cyclic Stretch Magnitude

One of the most important findings of this dissertation is that aortic valve cusps can be calcified within a week by treatment with a pathologically relevant level of stretch (15%) in fully osteogenic medium containing both high phosphate content (3.8mM) and TGF-β1 (1ng/ml). Neither the stretch nor the fully osteogenic medium alone could induce valve calcification within an experimental time frame of up to 14 days (data shown in **Appendix E**). These results suggest that stretch and the fully osteogenic medium act in an additive manner. While full mechanistic insights need additional studies, initial data suggest that increased BMP-4 expression, cellular apoptosis, and subsequent Runx2 expression and ALP activity as potential mechanisms. Reaching a threshold level of BMP by the additive actions of the mechanical (stretch) and atherogenic (TGF-β1 and phosphate concentration) factors may be a key event in determining if the aortic valve undergoes calcification. A recent review paper by O'Brien reported that the specific atherogenic factors studied in the present study, such as TGF-βs, BMPs and increased PO_4^{3-}, are especially important to the progression of valve calcification (171). Other factors such as the renin-angiotensin system, adhesion molecules, macrophages and oxidized lipids were also alluded to in this paper. These specific molecules were not studied in this thesis work, but the interplay between all these molecules is expected to be crucial in determining the overall "picture" of valve disease progression.

6.3.2 Side-Specificity of Observed Disease Responses

It has been observed clinically that calcific aortic stenosis is a side-specific disease, with calcium nodules occurring with greater frequency in the interstitium below the fibrosa surface of the valve cusp compared to that below the ventricularis surface (113, 160, 180, 195). In addition, gene profiling performed by Simmons *et al* has demonstrated the endothelial cells on the fibrosa surface to be more susceptible to valve calcification (227). In essence, the fibrosa surface appears to be more "primed" to calcify, whereas the ventricularis surface is more "protected". Recent studies from our laboratory have demonstrated that fibrosa side is also more susceptible to perturbations in its normal hemodynamic environment. Sucosky *et al* demonstrated that imposition of an altered shear stress waveform on the fibrosa surface resulted in increased expression of inflammatory proteins and cytokines such as BMP-4 and TGF-β1 (243). This was not observed when an altered waveform was imposed on the ventricularis surface. These findings indicate two important points: Firstly, it appears that the endothelial cells that are potentially acting as the mechanotransducer here. Although valve interstitial cells in culture have been demonstrated to respond to mechanical and chemical stimulation to result in BMP expression and calcification (45, 113, 179), *in vivo* these processes are likely to be much more regulated, involving signaling and initiation from the endothelial cells. Secondly, the differential propensity of the fibrosa and ventricularis layer of endothelial cells to progress down a disease pathology lends further evidence to the importance of endothelial cells in valve disease mechanobiology.

In light of these findings, it was of interest in this observation to understand if imposition of stretch resulted in side-specific responses. In particular, the imposed stretch was demonstrated to be uniform throughout the cusp section; it was therefore assumed that both sides of the valve cusp would receive the same mechanical stimulation. In the results chapter, it was reported that calcification and tissue expression of BMP was

preferentially expressed on the fibrosa side of the valve. Additionally, most of the expression of BMPs was observed on the endothelial layer of the valve cusps (**Figure 5-29**). This is in agreement with previous results on the effects of pathologic shear stresses on valve cusps published by Jo *et al* (243). Although other studies by Osman *et al* (179) and Clark-Gruel *et al* (45) have shown that interstitial cells can also be induced to express BMPs, this was not observed in the results from this thesis. It is speculated that the endothelial layer acts as the initial or early mechanosensor in the case of cyclic stretch, synthesizing key signaling molecules (such as BMP-2 and -4 in this case), which activate downstream events eventually leading to valve disease.

Ex vivo studies involving endothelial cell denudation could shed some additional light on this matter. In addition, isolated culture and profiling of the endothelial cells from the fibrosa and ventricularis surfaces of the cusp could aid in the elucidation of differences in gene expression profile of these two apparently heterogeneous endothelial cell populations. Further, one could perform culture valve interstitial cells using conditioned media from these endothelial cells to tease out side-specific signaling pathways and responses. However, it is well acknowledged that endothelial denudation is a motivating factor for disease initiation and progression (162, 180). Novel approaches therefore are needed to further understanding in this direction.

Further staining was performed to understand if this side-specificity extended to pro-inflammatory cell adhesion molecules as well (**Figure 6-8**). These molecules are also demonstrated to be intimately involved in valve calcification as demonstrated by Sucosky et al, Jo et al and others (115, 116, 234, 243). Immunopositive expression for e-selectin and VCAM-1 was observed in a stretch-sensitive manner on the endothelial cells lining the fibrosa surface of the valve cusp and not on the ventricularis side of the cusp. This is intriguing and needs to be investigated further. Studies could focus on the differential

mRNA and μRNA profiles (under mechanical loading) of these endothelial cells to understand if there are any clues as to the differential make-up of the cells from the two sides of the valve cusp.

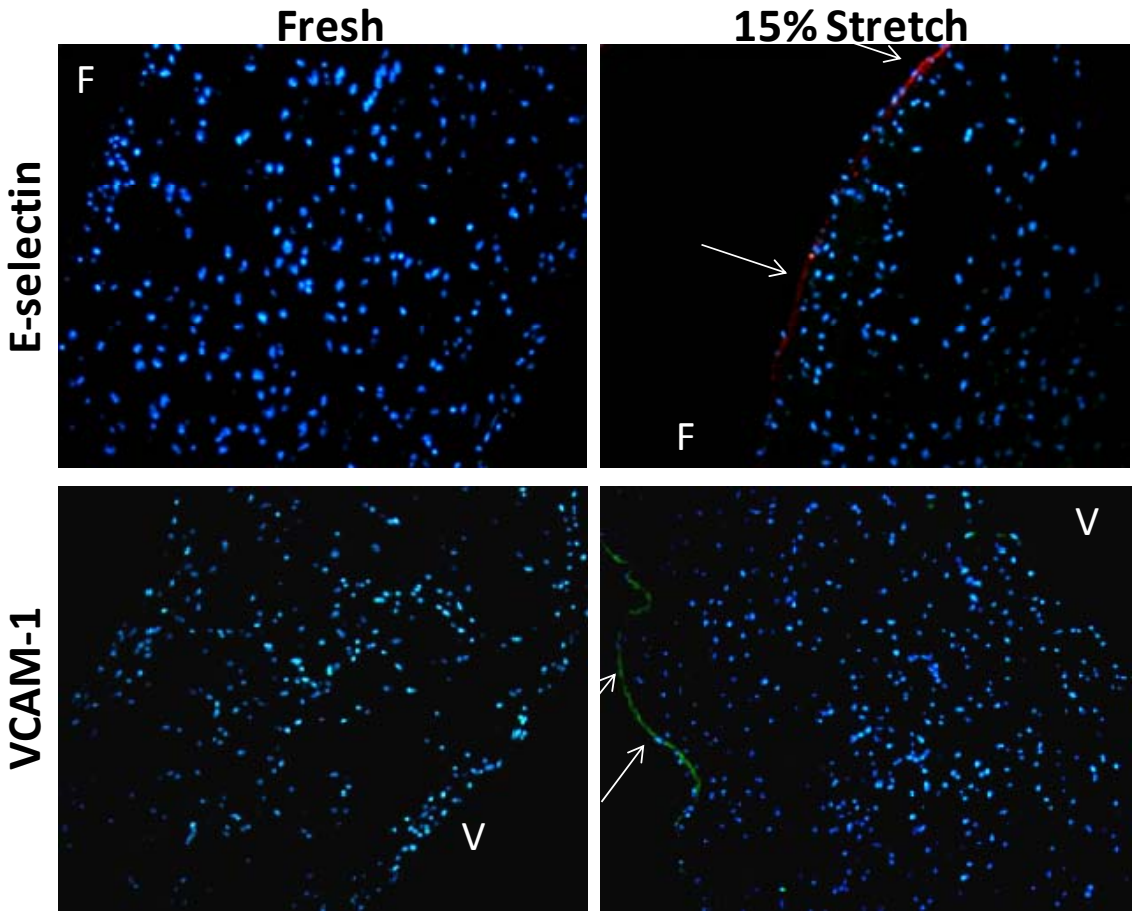

Figure 6-8: Samples stretched to 15% stretch demonstrate positive expression for e-selectin (red) and VCAM-1 (green) on the fibrosa surface of the valve cusp. In contrast, fresh samples are not immunopositive for these pro-inflammatory markers. In addition, positive expression was not observed on the ventricularis surface of the cusp samples. (V-ventricularis)

6.3.3 Calcification via Expression of Bone Morphogenic Proteins

Bone morphogenic proteins have always been mentioned in the same breath as vascular and valvular calcification, especially as a mechanosensitive signaling molecule. Work by Jo *et al*, Levy *et al* and Yacoub *et al* have demonstrated the importance of BMPs as markers that are expressed early in disease progression in cultured vascular and valvular cells (45, 154, 177, 234, 235). In these studies, BMPs were demonstrated to be expressed early on in disease initiation to promote inflammation and monocyte adhesion. These were also demonstrated in an *ex vivo* study on aortic valve cusps (243). Other studies have also demonstrated that addition of BMP and TGF-β1 can independently result in osteogenic differentiation of aortic valve cells cultured *in vitro* (45, 179). BMP-2 specifically can induce calcific nodule formation of aortic valve fibroblasts (160). As implied by the literature, BMPs are prominently expressed in diseased valves and are in fact expressed early on in the disease progression.

This thesis work demonstrated that BMPs and TGFs are more closely related than previously thought, with addition of exogenous TGF-β1 directly resulting in expression of BMP-2 and -4 after only 3 days. In the context of previously published work, this indicates a strong link, in the valve cusp, between altered mechanical forces, an "atherogenic" environment and BMP-influenced valve dysfunction. This study is also in agreement with *in vitro* studies on mesenchymal cells where BMP signaling activated the chondro-osteogenic Runx2/Cbfa pathway (171). Increased serum phosphate concentrations have also been linked to activation of the Runx2/Cbfa pathway (171) which was also observed in this study. Increased phosphate levels are observed in patients with renal disease, which is in fact a very strong risk factor for valve disease

(131, 143). This work also demonstrated stretch and BMP-influence in the expression of these key downstream transcription factors of BMP expression, leading to strong osteoblast behavior within the valve cusp. These events can be summarized in the schematic pathway as shown in **Figure 6-9**.

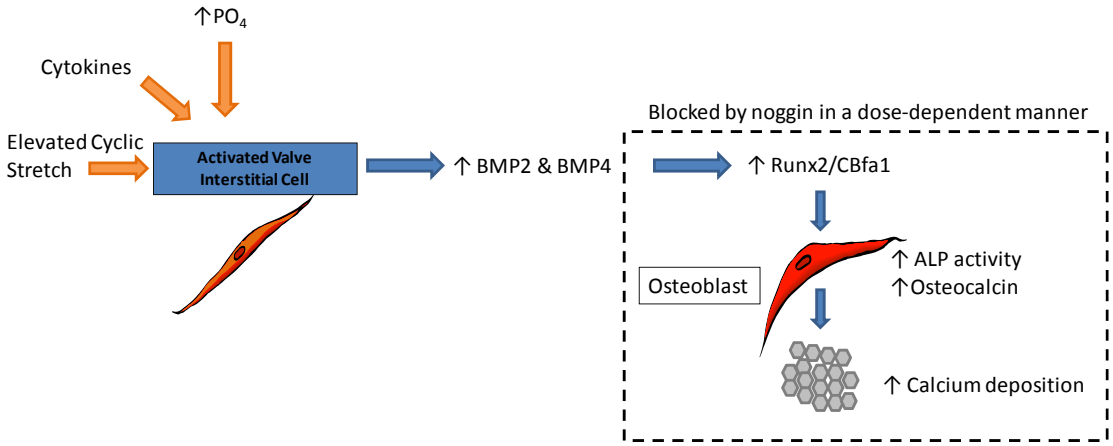

Figure 6-9: Schematic showing the pathologic pathway of elevated stretch-induced valve calcification. An atherogenic environment results in activation of the valve interstitial cell leading to initial expression of BMP-2 and BMP-4 leading to expression of the downstream transcription factor Runx2. This results in differentiation of the valve interstitial cell into an osteoblast-like phenotype associated with ALP activity, osteocalcin expression and calcium deposition. Incubation with noggin was able to inhibit events downstream of BMP expression in a noggin concentration-dependent manner.

Noggin was used in this study as an antagonist for BMPs drawing inspiration from studies by Jo *et al* (154, 234, 235). It was demonstrated that noggin can effectively inhibit BMP-induced aortic valve calcification (**Figure 6-9**). Other BMP antagonists include chordin and follistatin (31). Although these other molecules were not investigated, noggin is well established as a specific BMP antagonist with a weak dissociation constant (K_d) of 20pM (285), making it a good candidate for this study. Noggin has been shown to block the pro-inflammatory effects of BMP-4 expression on

vascular endothelial cells (234). Indeed, the value of noggin in this study is its ability to interfere with the action of BMPs while not affecting the expression of BMPs *per se*. Ultimately valve calcification could be a result of a breakdown of this delicate balance between agonists (BMPs) and antagonists (noggin) for calcific progression. Intriguingly, lending strength to this previous statement, it was demonstrated in this thesis that there was a strong dose response with noggin, with inhibitory effects increasing in a log-exponential manner with increasing noggin concentration (**Figure 6-10**). The exponential behavior leads us to speculate that a threshold level of effectiveness of noggin is reached, where further increasing doses result in diminishing effectiveness. Further study should focus on verifying these results with other pharmacological or molecular (siRNA or μRNA) antagonists for BMPs, before one can propose BMPs as potential targets for the treatment of valve calcification.

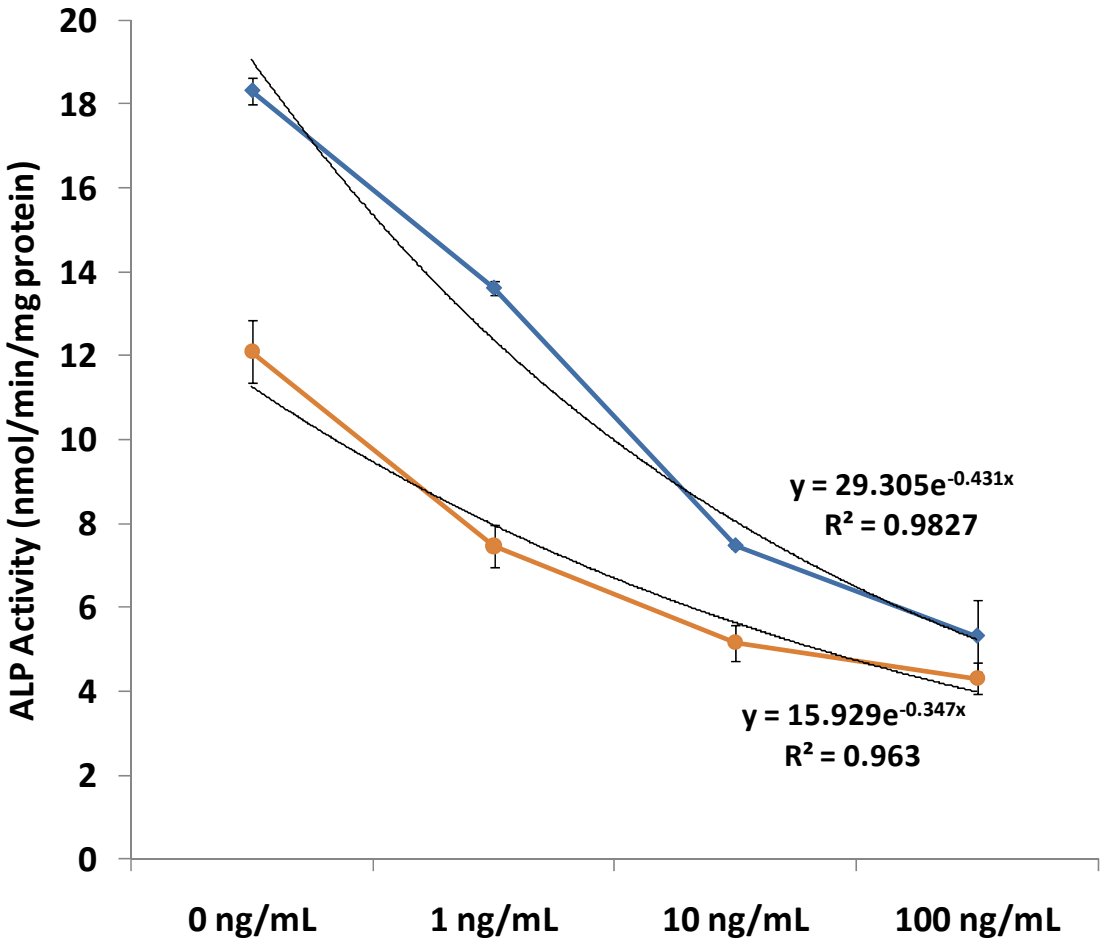

Figure 6-10: Strong log-exponential behavior is observed in the noggin dose response to ALP activity in the valve cusp. Correlations were good for both the 10% stretch group (orange curve), and the 15% stretch group (blue curve). Considering a typical exponential response of $y = Ae^{-bx}$, stretch magnitude appeared to affect both the magnitude (A) and phase (b) of the observed ALP response.

6.4 Cell Viability Under Cyclic Stretch Stimulation: Implications for Valve Disease and Tissue Engineering

Cellular viability is a key indicator of pathology in the valve. Excessive cell proliferation is observed in fibrotic valves such as those in patients suffering from carcinoid syndrome (46, 114, 277). At the same time, increased cellular apoptosis is a common indicator of inflammatory and calcific processes (196, 246, 281).

A clear dependence on stretch magnitude was reported for both cell proliferation and apoptosis in this thesis work. Our study demonstrated increases in both cell proliferation and apoptosis at 15% and 20% stretch, suggesting a disruption in normal homeostasis of the valve as the stretch on the valve increases. Physiologically, the valve experiences 10-12% stretch in the circumferential direction (251). Beyond 15-17%, the collagen fibers are fully stretched and "locked up" (141, 256). Therefore, at 20% there is a possibility of damage to collagen fibers and the attached interstitial cells (15, 16). It was speculated that the high levels of proliferation and apoptosis at 20% is an injury-response mechanism to counter the higher mechanical strains imposed on the valve, leading to increased cell apoptosis and compensatory proliferation in order to replace damaged cells. Additionally, cellular apoptosis is also known to be a hallmark of degenerative aortic valve disease (113). The above speculation is also consistent with the generally reduced level of remodeling observed at 20%, as the priority of the cell is thought to be proliferation. *In vivo*, the pressure load (and therefore the stretch) on the aortic valve cusp is not likely to increase in such an acute manner, and we can expect a constant adaptive remodeling of the valve in order to remain functional. However, hypertensive emergencies as a result of failure of normal autoregulation, and an abrupt rise in systemic

vascular resistance can occur (1), which may result in a situation of acute increase in stretch on the valve.

Another key finding was the increased apoptosis under static conditions. In addition, there was no cellular proliferation at all under these conditions. This result clearly demonstrates the mechanosensitive nature of the aortic valve cells, and the importance of mechanical stimulation to ensure continued valve cell viability. This result is not surprising considering that the valve is constantly under mechanical stimulation *in vivo*. It was for this very reason that subsequent studies did not involve statically incubated samples. It would have been difficult to tease out whether any observed tissue response was due to the lack of mechanical stimulation or the effect of other exogenously added factors.

As far as valve disease is concerned, it is believed that calcification could occur via either an apoptosis-driven pathway (196, 246, 281) or via an osteogenic and more matrix-dependent pathway (246, 281). Yip *et al* and others have demonstrated that depending on the mechanical and biochemical environment both processes can potentially occur (45, 281). These studies also demonstrated that TGF-β1 stimulates cellular apoptosis (45, 281). This thesis work demonstrated that cellular apoptosis was present for samples stretched to 15%, but to a lesser extent in 10% stretch. Apoptotic cells were predominantly expressed on the fibrosa, matching the observed pattern of preferential calcification on that same surface of the valve. This finding further lends strength to the speculation that valve calcification is side-specific. In addition, ALP activity, which is a marker for osteogenic differentiation was also higher at 15% stretch compared to 10% stretch. It is believed that both apoptosis- and osteogenic-driven

calcification could be occurring, but further study with apoptosis inhibitors is needed to confirm this.

These results also have relevance in the development and preconditioning of tissue engineered valve constructs. The magnitude of mechanical stimulation could be tailored to achieve the required rate of cell proliferation in the early preconditioning of a valve construct, before reducing the level of mechanical stimulation in order to maintain a quiescent construct that is capable of continuously maintaining its matrix.

6.5 Significance and Relevance of Study

This thesis work has reported several key, novel findings that will further research on: (i) elucidation of mechanisms of aortic valve disease, and (ii) the understanding of proper preconditioning regimes for tissue engineered cardiac valves.

6.5.1 Model pathway for Valve Calcification and Possible Treatment Targets

Results from the study show that elevated mechanical loading can transform the normally quiescent stable valve cell to an activated phenotype. Further work has demonstrated that this activated cell stains positive for α-SMA (7) and is a myofibroblast-like phenotype that can secrete cytokines and remodel the extracellular matrix of the valve (8). This activated phenotype appears to be especially sensitive to changes in its external environment. An atherogenic environment has been demonstrated to initiate a cascade of events, commencing with the differentiation of valve interstitial cells to an activate phenotype, and ultimately culminating in cytokine expression, osteoblast differentiation and eventual calcification. This atherogenic environment is clinically relevant in several ways. Elevated cytokine level (TGF-β1) is observed in patients with incidence of vascular and valvular pathologies, such as coronary artery disease (45, 113, 151). Elevated phosphate levels (hyperphosphatemia) are indicated in patients with renal disease (143). Synthesizing all the results from this thesis, a model pathway (**Figure 6-11**) can be drawn up, providing clues as to promising target molecules for molecular therapies.

This study has clearly identified bone morphogenic proteins as critical molecules in valve calcification. Further study therefore needs to focus on the various BMPs and their downstream signaling pathways in an effort to identify possible pharmacological treatments for valve disease. Possible candidates include the Runx2/Cbfa pathway and potentially the Wnt/lrp5 pathway. Perhaps BMPs can be used as biomarkers for the early

detection of valve disease progression. With the advancement of non-invasive imaging techniques, *in situ* examination of the valve cusp for these biomarkers may be a future possibility. Aikawa *et al* has developed such methods to detect cathepsins (2, 111). Development of a drug to treat valve calcification would be extremely valuable as it would allow patients to avoid valve surgery, and improve their quality of life.

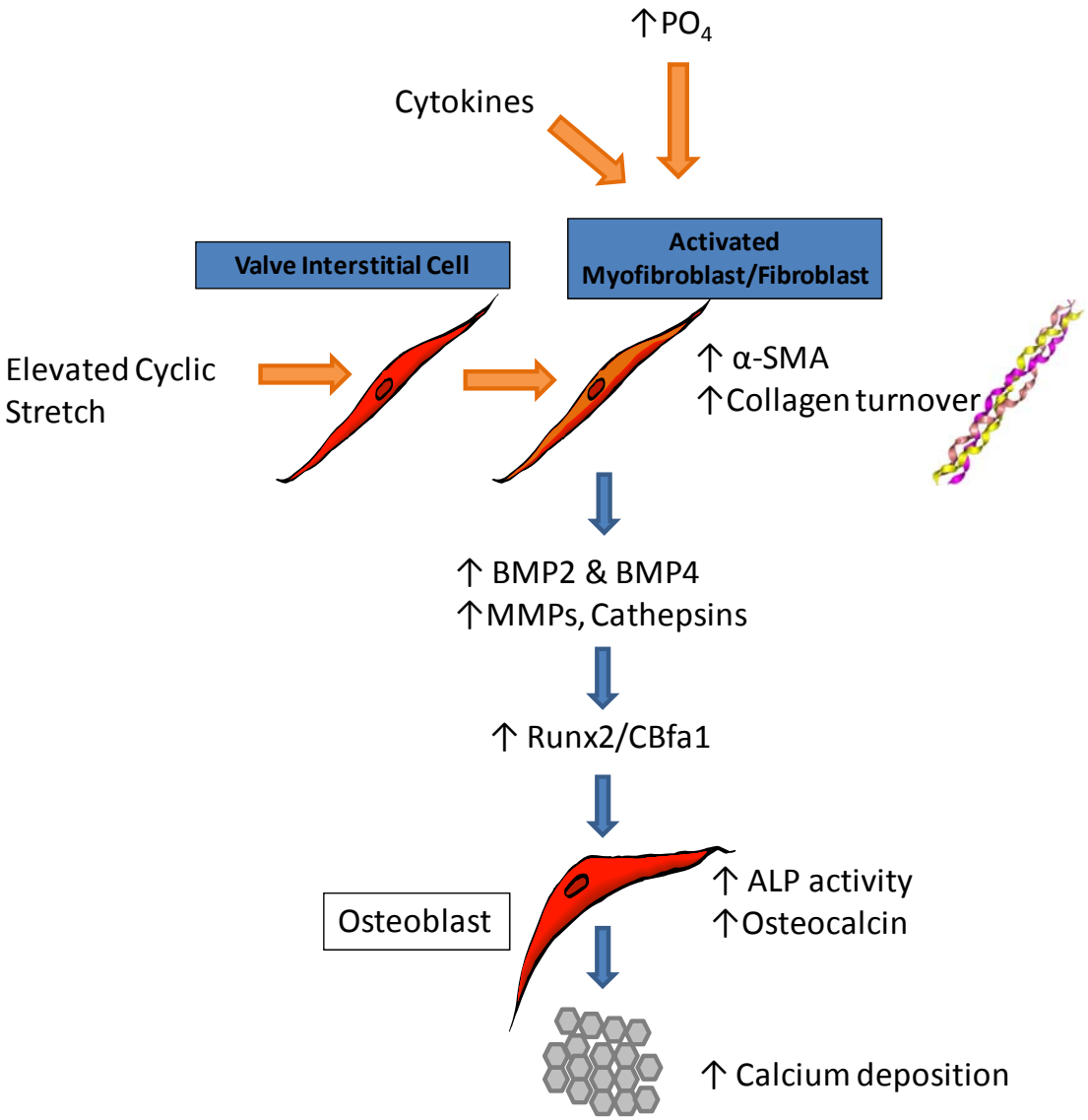

Figure 6-11: Model pathway for the activation of the valve interstitial cell via elevated stretch to an activated myofibroblast phenotype. Further activation via an atherogenic environment (TGF-β1 and elevated phosphates) resulted in BMP-induced valve calcification with expression of Runx2, osteocalcin and alkaline phosphatase activity.

6.5.2 Relevance to Hypertension and Renal Disease

Valvular calcification is common in chronic kidney disease, and is closely associated with findings of intimal arterial disease. The presence of inflammation and the duration of dialysis treatment contribute to this complication (131). Hypertension is a common disease especially in the western world, and is a significant risk factor for further cardiovascular (atherosclerosis, valve calcification), and renal disease. Prior to these end events, many times there is tissue fibrosis, and hypertrophy following the onset of hypertension. A direct consequence of elevated pressure is an increase in the stretch on the valve cusps. More specifically, there is an increase in strain of 5% for every 40 mmHg increase in pressure (280). Elucidation of the nature of cellular mechanisms activated by the presence of increased stretch therefore could advance our knowledge regarding the pathogenesis of hypertension. Indeed, studies have reported that patients suffering from heart valve who were also hypertensive demonstrated heavily fibrosed valve cusps with deposition of cellular waste and calcium (241). This is in agreement with the observations from this study, further pointing the relevance of this thesis work to understanding disease mechanisms under hypertension.

Elevated phosphate levels are encountered in patients with renal disease. The hyperphosphatemia simulated in specific aim 2 here is seen in end-stage renal disease (ESRD) patients (142, 143). Indeed, even arterial calcification is common in patients with advanced renal failure and ESRD and is thought to contribute to their increased cardiovascular mortality. Disease in this patient population is also related to expression of osteogenic factors such as matrix Gla protein, osteopontin, and alkaline phosphatase (142, 143). Some of these factors such as alkaline phosphatase were also key in valve disease as reported by this thesis. Therefore, although renal disease was not the main focus of this dissertation, our results points to a significant link between these patients and valve disease. The link between renal disease and valve disease is an understudied

field, and perhaps warrants further study. The *ex vivo* model developed in this thesis can be extremely valuable

6.5.3 Relevance to Serotonin Mechanisms in Heart Valve Disease

As mentioned earlier, elevated circulating levels of serotonin have been reported to result in multiple cardiovascular pathologies such as cardiac valve fibrosis and systemic as well as pulmonary hypertension (75). The hallmarks of valve fibrotic lesions include excessive cellular proliferation, and increased extracellular matrix synthesis (33, 93) resulting in abnormal thickening of the valve cusp leading to change in valve mechanical properties, all of which were observed in this study. This dissertation points to a link between elevated stretch loading and serotonin related valve disease. This has important implications for patients already suffering for cardiac disease. For example, it is speculated that stenotic patients with elevated transvalvular pressure gradients will be at increased risk for serotonin-related valvulopathy. It is also possible that hypertensive patients prescribed drugs such as the Fen-Phen cocktail, ergot derivatives or Prozac® that make use of serotonin biology are at increased risk of valvular disease. This field is understudied, and more research effort needs to be focused to examine this more carefully, and to identify if this group of patients are truly at risk.

6.5.4 Development of a Tissue Engineered Heart Valve

The results from this work could also be applied to the development of a preconditioning methodology for tissue engineered heart valves. Recent reports suggest that mechanical conditions during perfusion are important in guiding the development of tissue engineered constructs (6, 102, 167, 168, 192). In the present experiments, native porcine valve cusps were used as a model for a tissue engineered valve construct. Our results suggest that moderately elevated stretch can increase collagen deposition and cellular proliferation, in order to reach sufficient integrity for *in vivo* implantation. This

can be very useful since the current most extensively studied bioreactor for a tissue engineered valve, the pulse duplicator system developed by Hoerstrup *et al* (102), was not able to produce sufficient amount of collagen during in vitro conditioning. Based on our results, this could be attributed to the relatively low pressure ($30 < \text{Pressure} < 50$ mmHg) conditions in the pulse duplicator. In addition, our system can be used to provide an environment where growth factors can be supplied in a controlled manner to customize the growth of the construct.

6.6 Limitations of Study

Although this dissertation has addressed several unanswered questions relating to valve disease and valve mechanobiology, it has limitations and scope for improvement. These limitations are outlined in this sub-section.

6.6.1 Limitations of the Stretch Bioreactor System

In vivo, the valve cusp is under biaxial stimulation, with ~10% stretch in the circumferential direction and ~30% stretch in the radial direction. In the current work, only circumferential stretch was studied, but a more holistic approach would have been to study valve biology using a biaxial stretch bioreactor. By using springs and a "strip biaxial" configuration, we have attempted to minimize confounding influences of off-axis compression. In addition, since the ratio of actual *in vivo* stretch to maximum possible stretch of valve cusp was closer to unity in the circumferential direction, we chose to focus the initial studies on valve cusps oriented in the circumferential direction. In fact, initial experiments conducted in our laboratory on radially aligned strips did not demonstrate any significant difference in collagen content, when compared with fresh cusps. In these studies, radially aligned rectangular cusp sections were stretched to 30% stretch for 48 hours in the tensile stretch bioreactor. Collagen content and sGAG content were statistically similar between stretched and fresh groups. These results are compiled in **Appendix F** of this thesis.

Another limitation is the initial unstretched reference position of the valve cusps before starting the stretch experiment. As demonstrated in the results chapter, collagen content and tissue remodeling is altered after just 24 hours of stretch. As collagen content increases, it is therefore possible that the reference state of the valve cusp would change due to tissue remodeling. Changes were not observed in sample length, but we did notice thickening of the valve sample especially at the higher magnitudes of stretch. These

effects were minimized by resetting the initial position of the bioreactor whenever a media change was applied to the system. This occurred typically every 1-3 days.

6.6.2 Osteogenic Medium

For specific aim 2, a very strong osteogenic medium, with both TGF-β1 and increased phosphate concentration (from 0.9 mM to 3.8 mM) was used to induce valve calcification. Although this formulation was relevant to patients with end-stage renal disease, the main advantage was that it allowed calcific processes to occur within a reasonable experimental time frame of 14 days. It was a worry that further increases in culture time would make the system more susceptible to contamination, and this particular approach was accepted for this reason. Confounding influences from the fully osteogenic media were minimized by using appropriate controls. For this particular thesis, we used both fresh controls as well as valves stretched to normal magnitude of stretch (10%) with fully osteogenic media. For a cleaner study, further experiments should attempt to study valve calcification using normal phosphate levels with only added cytokines, but utilizing longer experimental durations. These experiments should first evaluate the ability of the stretch bioreactor to maintain tissue sterility for these extended experimental durations.

6.6.3 Biological Variability

Biological variability is a common concern when conducting experiments with cells or tissue. The variability comprises two types of variations: inter-animal and intra-animal variations. Valves from different animals may show a wide range of biological activity due to the age, size and health condition of the animal. Heart valves in this study came from slaughterhouse pigs, which were generally 1-2 years old and weigh about 350-450 lbs. The other potential source of variability arises from the differences between the three cusps, namely, the non-coronary, the right and left coronary leaflets. By

randomizing samples before allocating them to treatment groups, we could ensure that there was an equal mix of left, right and non-coronary cusps for each experimental result. In addition, all the presented results were based on 3 separate tissue isolations from the slaughterhouse. In this manner, biological variability between samples can be minimized.

An ideal experimental design would attempt to use samples from the same valve cusp (or at least the same valve) and allocate them to different treatment groups in order to get matches samples. This would no doubt increase the statistical power of the experiments enabling paired analyses to be performed. While this will be recommended for future research, adopting this approach will be limited by the physical size of tissue required for these stretch experiments. It was often not possible to obtain more than one decently sized rectangular tissue sample from the belly region of each cusp.

6.6.4 Interactions Between Endothelial and Interstitial Cells

In specific aim 2, expression of BMP-2 and -4 was observed on the endothelial cells of the aortic valve cusp samples. The downstream responses of ALP activity and tissue mineralization were observed in the interstitium. It is however still unclear how the signals are transduced to the interstitial cells from the endothelium. It would be valuable to understand the specific signaling molecules that are involved in these processes, as these molecules can serve as indicators of disease as well as potential targets for the blocking of such diseases. Such insights can only be obtained via studies on single cells and *in situ* monitoring of released signaling molecules.

CHAPTER 7

CONCLUSIONS

This thesis work demonstrated the effects of normal and elevated cyclic stretch on aortic valve remodeling and degenerative disease. These experiments were performed on porcine aortic valve cusps using an *ex vivo* tensile stretch bioreactor. The key findings from this thesis can be outlined as follows:

- The aortic valve endothelial cell appears to be a key mechanotransducer of cyclic stretch leading to degenerative valve disease.
- The aortic valve cell responds acutely to different magnitudes of cyclic stretch. It remains in a relatively quiescent phenotype under normal cyclic stretch (10%), differentiates to an activated synthetic phenotype under 15% stretch, and into a proliferative phenotype under 20% stretch.
- Elevated cyclic stretch was demonstrated to result in aortic valve calcification in a BMP-dependent manner. This particular mode of calcification was characterized by differentiation of the valve interstitial cell to an osteoblast-like phenotype with strong ALP activity, and could be inhibited by using a BMP-antagonist such as noggin.
- Elevated stretch was also shown to result in increased collagen biosynthesis in response to elevated 5-HT levels via the stretch-sensitive 5-HT2A receptor subtype.

Perhaps the most crucial finding of this thesis was the fact that stretch-induced valve calcification was dependent on early expression of bone morphogenic proteins (BMPs) primarily in the valve endothelial cells. Downstream transcription factors for BMP expression such as Runx2 and Osteocalcin were prominently expressed in response

to 15% stretch but not 10% stretch. Alkaline phosphatase activity was higher at 15% stretch compared to all other conditions indicative a phenotypic shift from a more quiescent phenotype to an activated osteoblast-like phenotype. BMP expression was focused on the endothelial cells, leading us to speculate that the endothelial cells are a key mechanotransducer in the valve cusp. All stretch responses could be inhibited by the BMP antagonist noggin in a dose-dependent manner, further demonstrating the importance of this cytokine in valve calcification. This knowledge could be potentially valuable in the development of drugs to treat and perhaps even prevent valve calcification.

Degenerative valve disease is often associated with proteolytic enzyme activity. Unsurprisingly, aortic valve remodeling responses to elevated cyclic stretch involved the classic proteolytic enzymes, namely, matrix metalloproteinases (MMPs), tissue inhibitor of metalloproteinases (TIMPs) and the lysosomal cathepsin proteases. A metric for valve remodeling was proposed and it was demonstrated that the value for this metric increased from 10% and 15% stretch, peaking at 15% stretch. This value for this metric was reduced level at 20% stretch, and this was attributed to the elevated level of cellular apoptosis at 20% stretch. More specifically, the valve interstitial cells appeared to adopt a more proliferative phenotype at 20% stretch with more rapid cell turnover, and were not in an activated synthetic cell phenotype (like at 15% stretch).

5-HT induced valve remodeling appeared to occur via a 5-HT_{2A} receptor-dependent mechanism. Increased collagen synthesis and crosslinking resulted due to 5-HT administration and these responses were more prominent at 15% stretch compared to 10% stretch. Mechanical tests revealed that these changes in collagen biochemistry resulted in transition to the stiff regime of the valve stress-strain curve at a lower level of strain. This can be mostly attributed to the increased collagen crosslinking. In addition, increases in collagen synthesis appeared to occur independent of the increased cellular

proliferation observed, which were primarily influenced by magnitude of stretch imposed, and not 5-HT administration. These results

In conclusion, the importance of cyclic stretch in altering valve remodeling, degenerative disease and calcification has been demonstrated in this thesis work. The information from this dissertation can be used to further probe deeper into the molecular signaling mechanisms of these responses in order to develop treatments that target degenerative valve disease. In addition, the correlation between cyclic stretch magnitude and collagen synthesis can be used as input for the preconditioning and testing of tissue engineered valve constructs.

CHAPTER 8

RECOMMENDATIONS AND FUTURE DIRECTIONS

The current study examined the effects of cyclic stretch on three different aspects of degenerative aortic valve disease: (i) valve remodeling; (ii) valve calcification; and (iii) serotonin-induced valve fibrosis. Based on the results, there are exciting possibilities for future work.

8.1.1 Understanding the Signaling Pathways of Aortic Valve Calcification

Current work was focused on understanding the "big picture" and identifying key molecules involved in stretch-induced valve calcification, such as MMPs, BMPs and Runx2. Further research now needs to focus on potential pathways that can be activated following BMP expression. Candidates include the classic Smad pathway associated with BMP expression (221), β2-adrenergic receptor activation (178), notch signaling (94) and the NFκB pathways (235). This by no means is an exhaustive list, and pharmacological and molecular approaches should be explored. In addition, these studies can adopt a "three-pronged" approach of *in vitro*, *ex vivo*, and *in vivo* studies. This would provide a complete understand of the cellular processes and allow for effective translation of that data to the more clinically-relevant animal model.

In addition, further work needs to be conducted on understanding the signaling molecules that are important in endothelial cell to interstitial cell mechanotransduction. It was speculated in this thesis that the endothelial cell is the primary mechanosensor, and it is still unclear how these mechanical signals are communicated to the interstitial cells to

cause them to become activated and diseased. These studies will be crucial for the complete understanding of aortic valve disease processes.

8.1.2 Effect of Combined Mechanical Forces

Past work in our laboratory has focused on understanding the effects of isolated mechanical stimulation on aortic valve disease with considerable success. The next step is to investigate the effects of combined loading on valve cusps using custom-built tissue bioreactors. The loading on the valve is dynamic and complex, and it is expected that tissue responses to two or more mechanical forces will not be a simple sum of the responses of each of the individual mechanical forces. Engelmayr *et al* has developed an elegant flex-stretch-shear bioreactor that can subject combined bending, stretch and fluid shear stresses on aortic valve cusp samples (66). We have developed an organ culture system (124) and a stretch-pressure bioreactor that can impose combined forces on valve samples.

In addition to studying the mechanobiology of the aortic valve cusp, future studies should also include analyses of the aortic root, annulus and sinus. All these components act in coherence *in vivo* to result in proper valve function. Indeed, in bicuspid aortic valve disease, very often there is concomitant sinus and root dilatation that contributes to the observed regurgitation (20, 21). Model systems therefore need to be built to study in a combined manner, the aortic valve and its surrounding structure under various normal and pathological mechanical loading. Possible approaches include organ culture as developed by our laboratory in the past (124).

8.1.3 Preconditioning of Tissue Engineered Constructs

Flexural and tensile strength remains the primary problem associated with tissue engineered valve constructs today. The current stretch bioreactor setup is therefore an exciting platform with which one can culture cells seeded on a scaffold in an attempt to achieve the required structural strength. Such initial cell-seeded construct should be tested under a variety of stretch magnitudes and growth factors with follow-up mechanical testing. The ultimate goal would be to implant these conditioned constructs into an animal and evaluate the efficacy of these constructs.

APPENDIX A MECHANICAL DRAWINGS

This appendix compiles the mechanical drawings for the tensile stretch bioreactor and the circuit diagram for the bioreactor power supply. All parts for the bioreactor except for the strut rod can be fabricated in either polycarbonate or polysulfone for biocompatibility. The strut rod is fabricated in stainless steel (Grade 316) for its rigidity and its non-corrosive properties. The bioreactor can be sterilized by ethylene oxide gas, hydrogen peroxide gas, or ultraviolet light. The bioreactor **cannot** be autoclaved.

List of parts is outlined here. The final page shows the assembly of the different parts:

1. Tissue chamber (2x pieces)
2. Base plate
3. Tissue chamber top (2x pieces)
4. H-bar
5. Strut rod (2x pieces)
6. Cross-arm
7. Cross-arm collar (2x pieces)

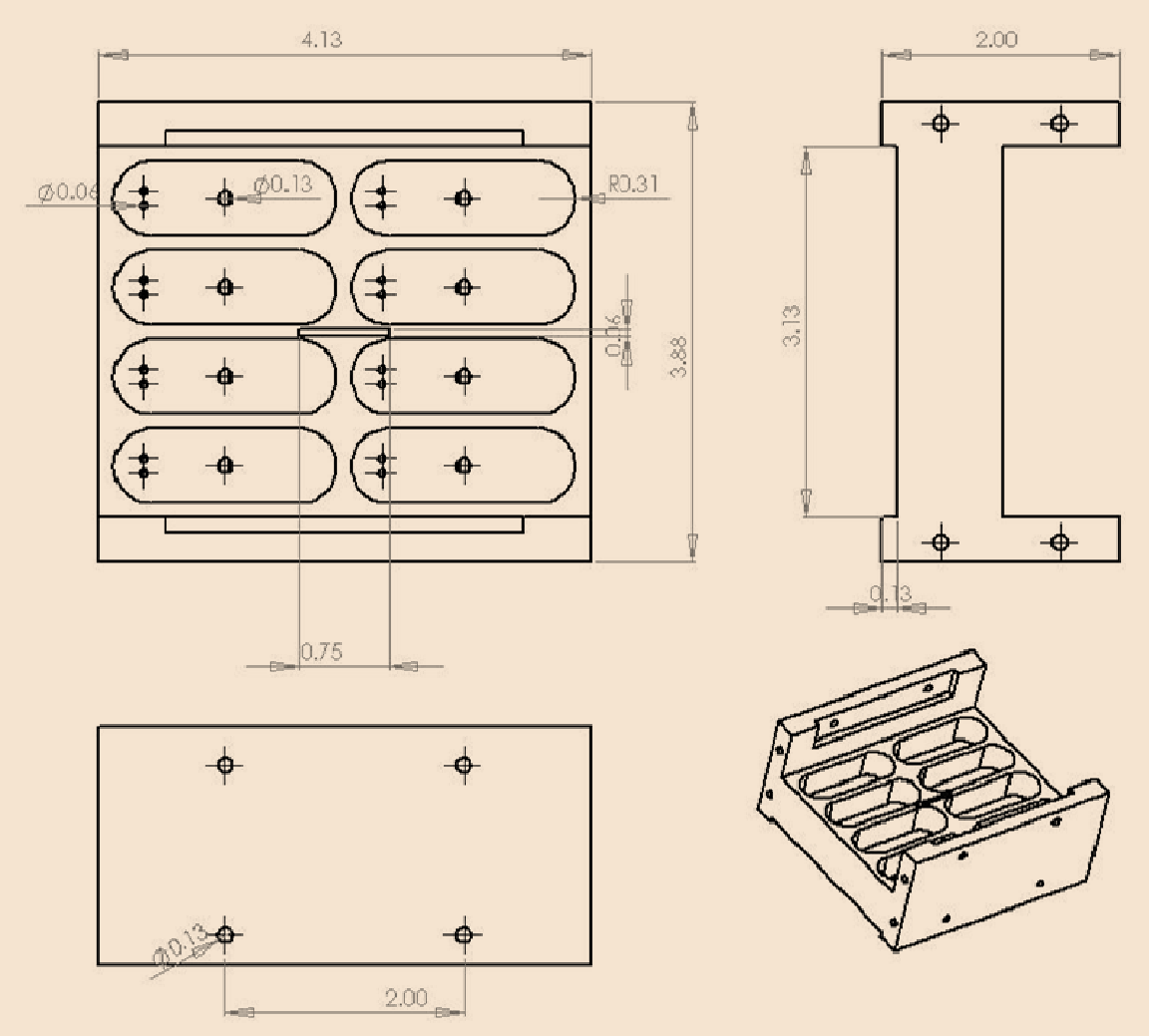

Figure A-1: Tissue chamber for the tensile stretch bioreactor. All dimensions in inches.

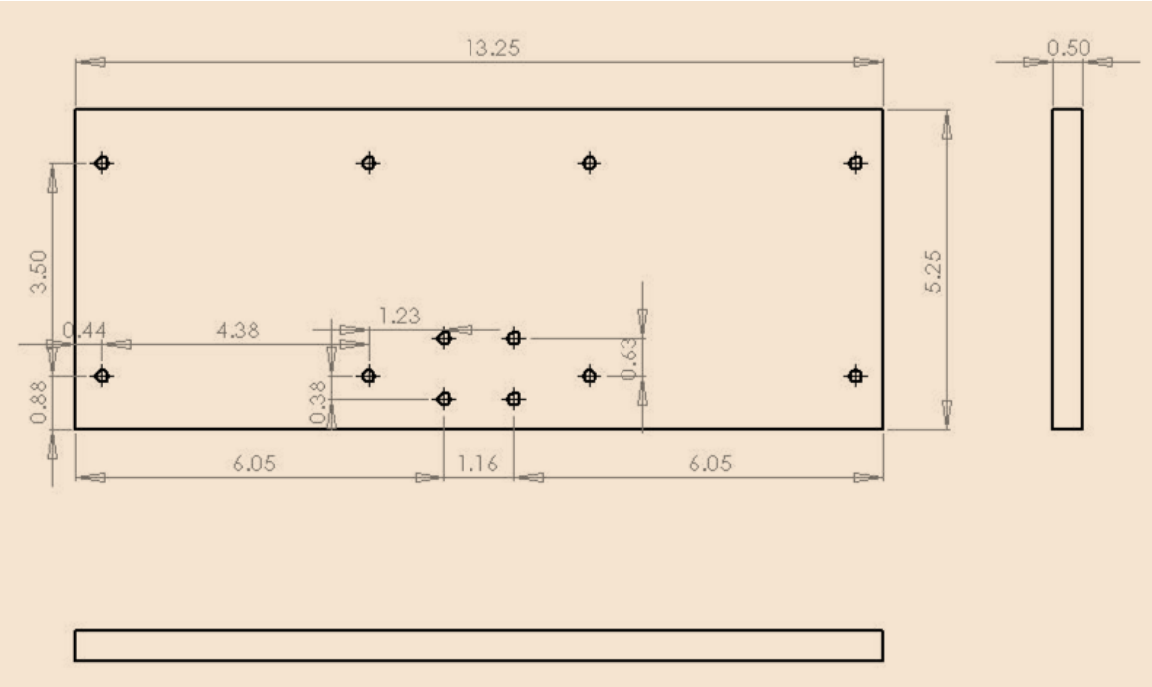

Figure A-2: Base plate that can accommodate two tissue chambers. All dimensions in inches.

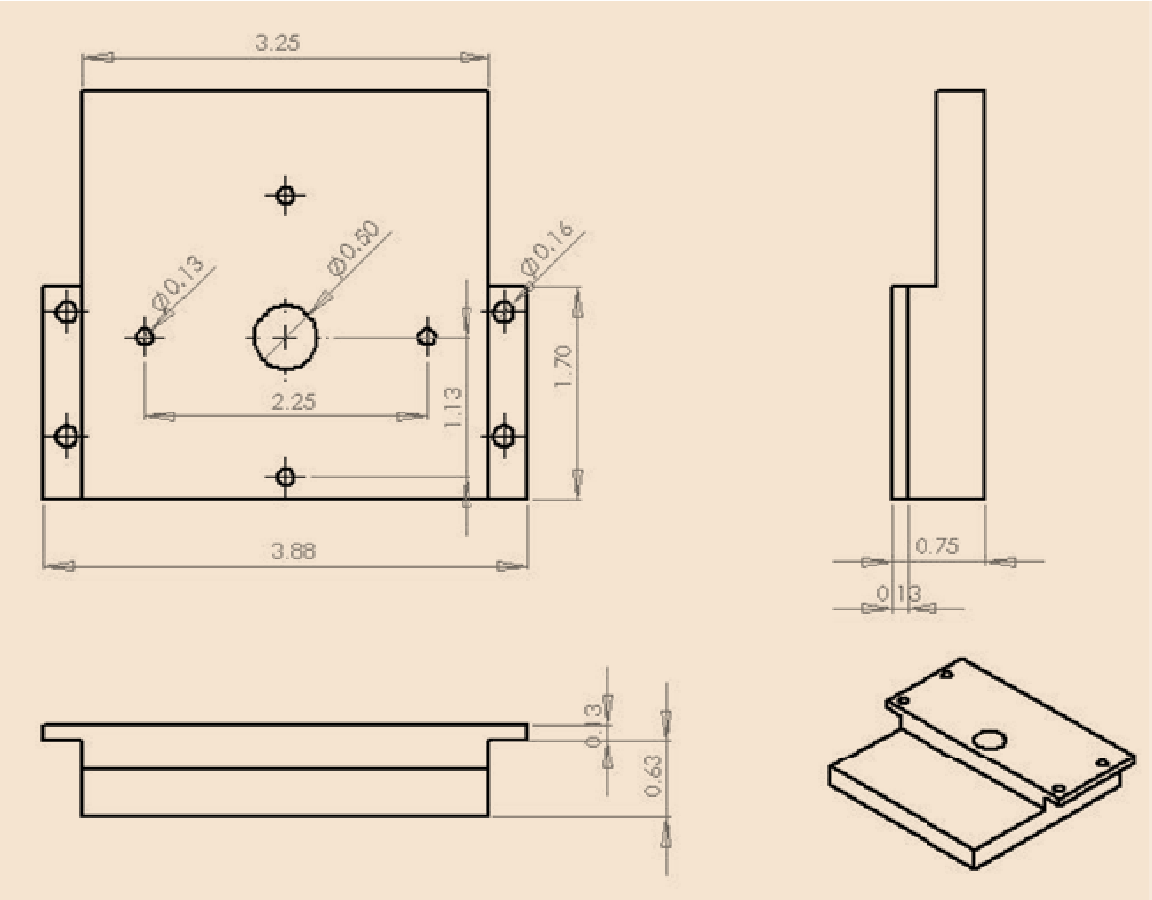

Figure A-3: Plate that couples the tissue chamber to the bellows and motor cross arm. All dimensions in inches.

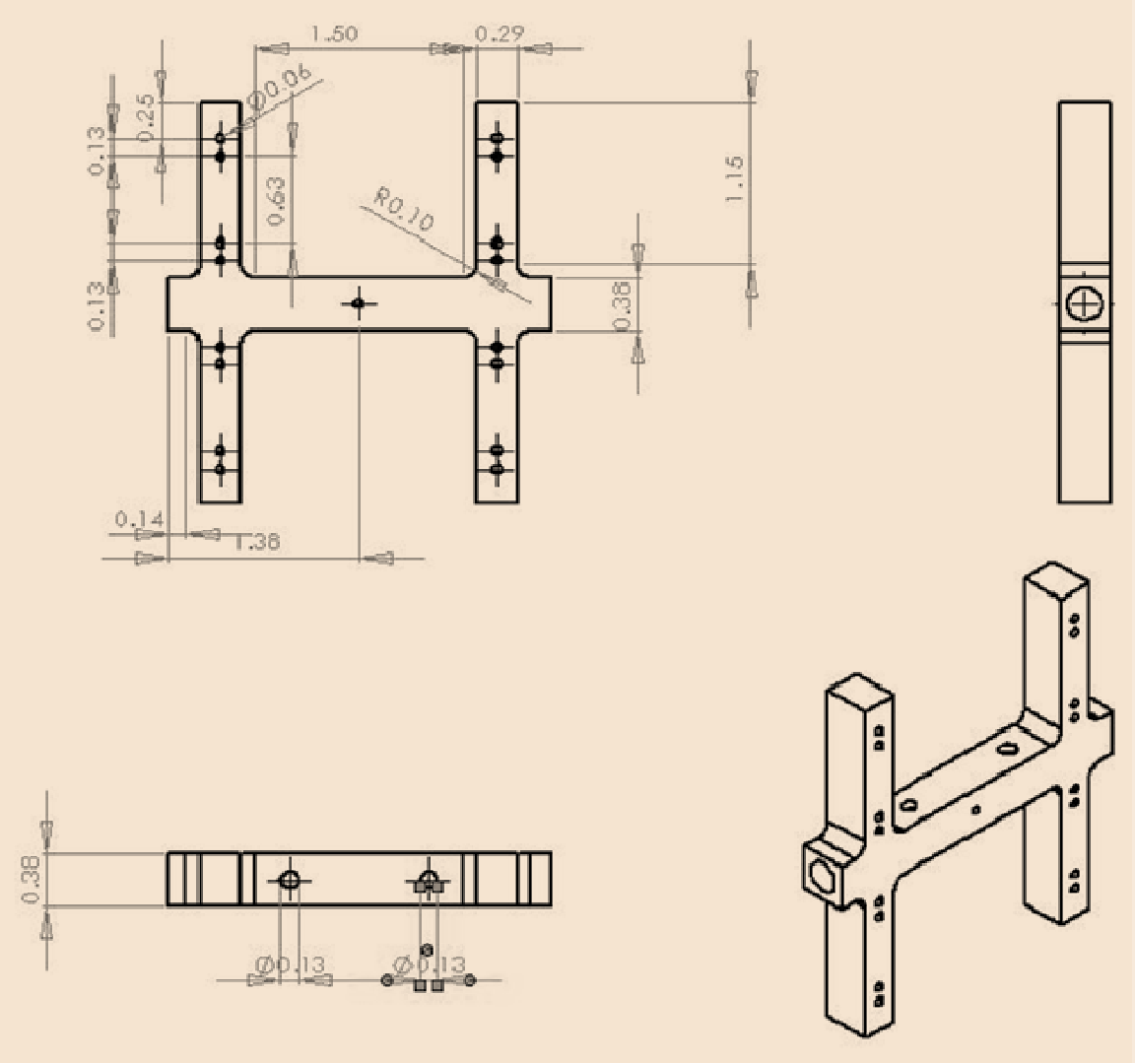

Figure A-4: H-arm that is used to couple to tissue in the tissue wells of the stretch bioreactor chamber. It is coupled to the motor cross arm by a stainless steel strut rod. All dimensions in inches.

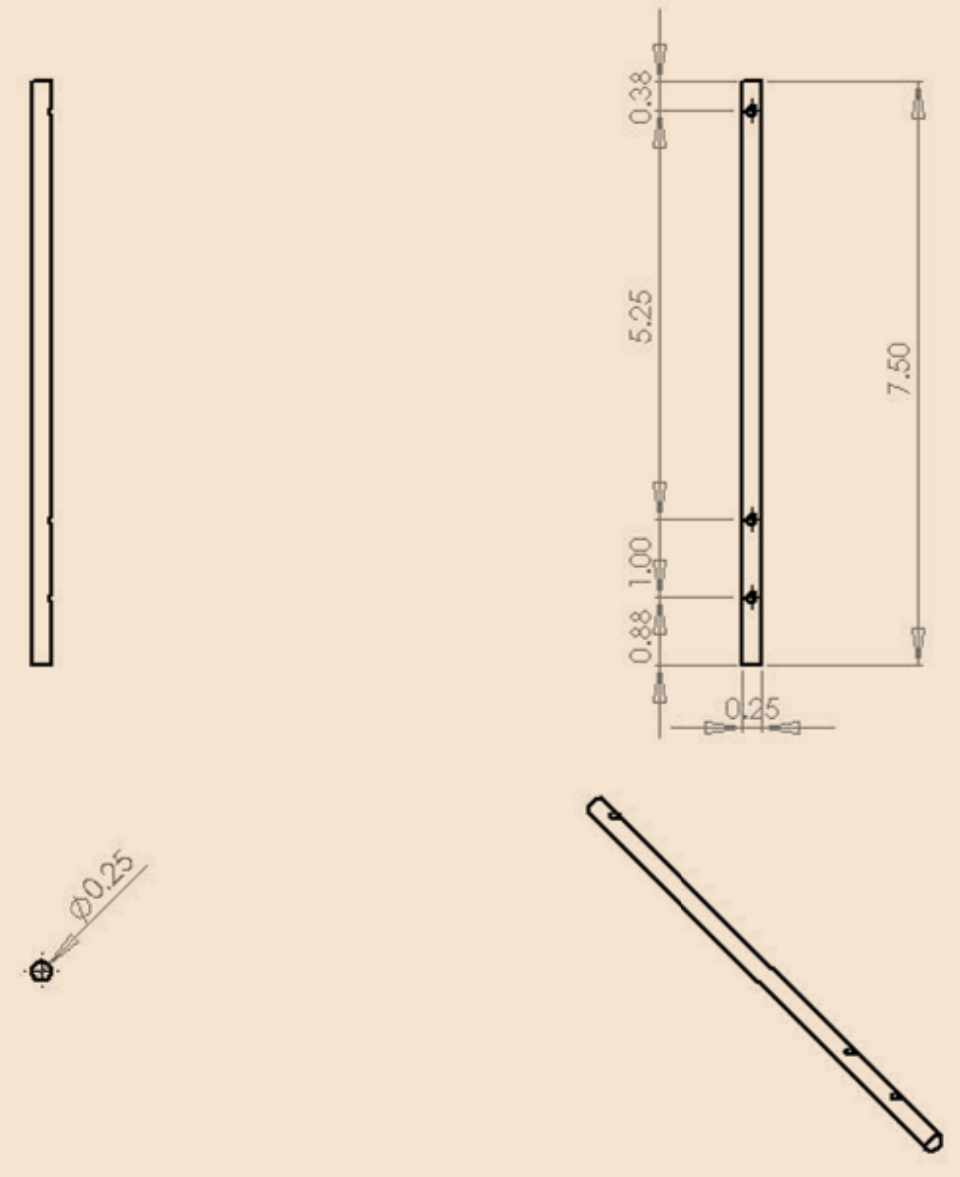

Figure A-5: Stainless steel strut rod that couples H-arm to motor cross arm. All dimensions in inches.

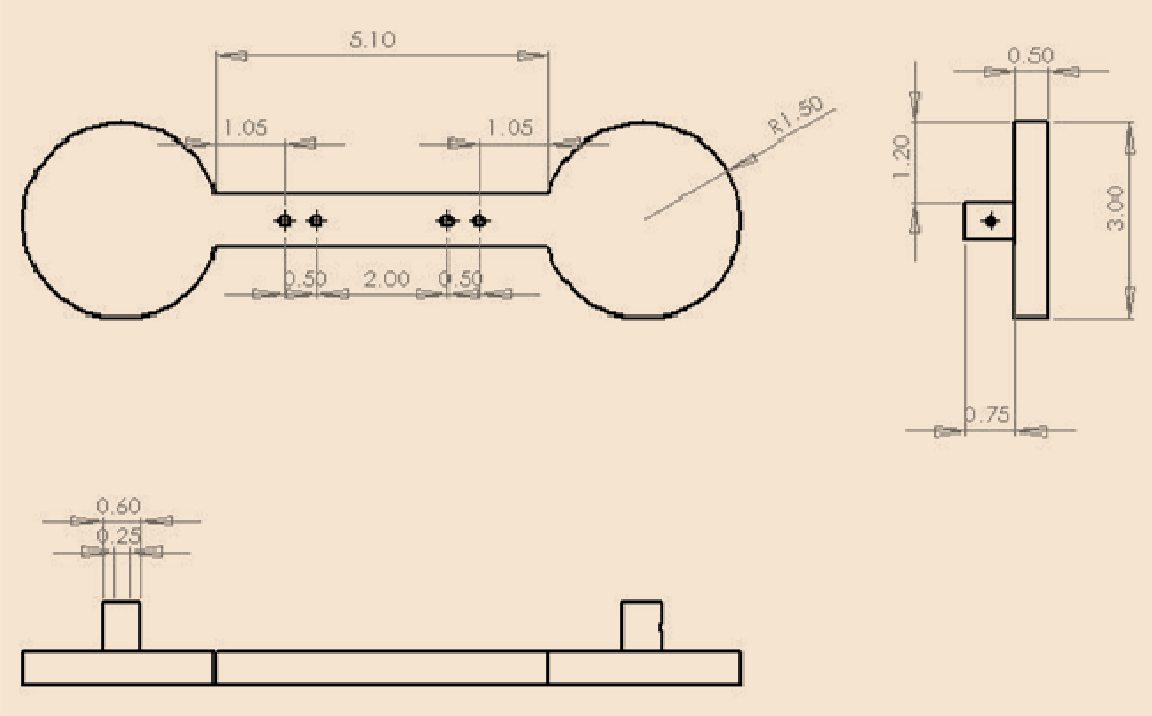

Figure A-6: Motor cross arm that is coupled in the center to the motor/linear actuator. At the two ends it is connected to stainless steel rods. All dimensions in inches.

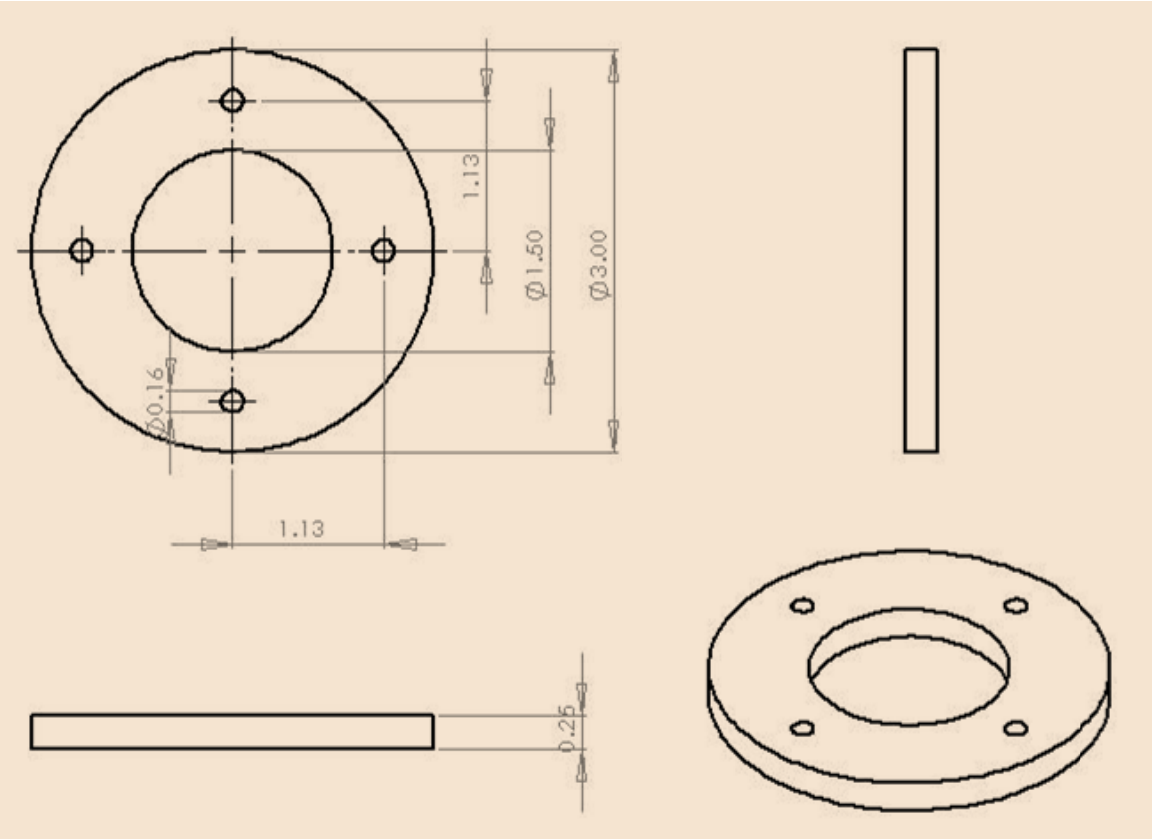

Figure A-7: Cross-arm collar that is used to sandwich the bellows in place. Bellows are used in order to environmentally seal the bioreactor and at the same time be deformable to accommodate the motion of the actuator. All dimensions in inches.

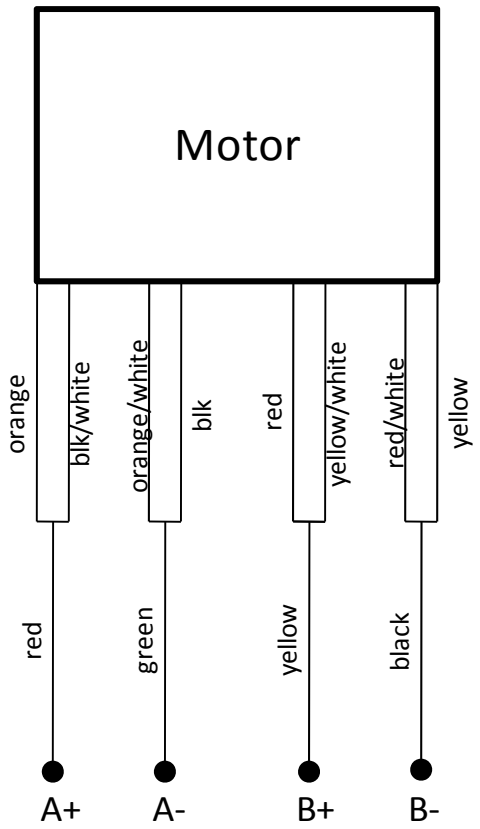

Figure A-8: Circuit diagram depicting connection between motor and Applied Motion 1240i controller card (A+, A-, B+, B-) connections. Sometimes the splicing between the pair of wires originating from the motor and its corresponding main connector to the 1240i board become frayed and the user is advised to take care accordingly. The 1240i takes standard 12-42 VDC power. Documentation is available at http://www.applied-motion.com/products/stepper/drives/1240i.php.

APPENDIX B PROTOCOLS

HARVEST AND CULTURE OF PORCINE AORTIC VALVES

Materials and Reagents:

For tissue harvesting:	
1x 6-well plate	Fisher #08-772-1B
1x surgical scissors	
1x curved forceps	
Dulbecco's phosphate buffered saline solution (dPBS) 500 mL	Sigma #D5773
Ethanol/Methanol spray bottle	
Stainless steel dissection tray (big)	Fisher/VWR
Cooler with ice	
Pipettor and sterile pipets	
Sterilization pouch	Fisher # 01-812-50

For stretch experiments:	
1x scalpel handle (no. 3)	Fisher #08-915-2
Sterile scalpel blades	EMS #72044-10
4x razor blades (0.009")	VWR #55411-050
Spacer rods	
Screws and nuts for spacers	
Stainless steel dissection tray	
Blue absorption pad	
1x 6-well plate	Fisher #08-772-1B
Stainless steel springs (cut-to-length)	McMaster #9663K14
1x straight forceps	
1x curved forceps	

Stretch Bioreactor and motor:	
Allen Key Set	Available at hardware store
5x 10/32 screws	
1x 10/32 nut	

For Dulbecco's Modified Eagles Medium (DMEM):	
DMEM Powder	Sigma #D5648
(formulation depends on experiment)	

Procedure:

Day before

1. Autoclave scissors and forceps in small sterilization pouch.
2. Autoclave tray and absorption pad in large sterilization pouch.
3. Autoclave all spacers, razor blades, surgical tools, screws, nuts and springs in a small sterilization pouch.
4. Pack and sterilize stretch bioreactor in ethylene oxide (EtO) sterilizer. Alternatively, fill wells of stretch bioreactor with ethanol/methanol, cover and place under UV overnight (not preferred).
5. Place all sterilization pouches under UV overnight.
6. Autoclave dPBS and put in fridge overnight.
7. On morning of slaughterhouse trip, fill cooler with ice and place dPBS bottle in it.

At slaughterhouse

1. Spray work area and tray thoroughly with alcohol.
2. Fill 6-well plate(s) with ice-cold dPBS.
3. Cut porcine heart between right and non-coronary leaflet and through the septum to reveal all three leaflets.
4. Excise each leaflet, wash in ice-cold dPBS and place in 6-well plate, keeping track of the anatomical position of each leaflet sample.
5. Repeat 3-4 for each heart.
6. After tissue collection, place 6-well plate(s) in ice and return to lab.

Experiment setup

1. Use sterile techniques and a laminar flow hood at all times.
2. Place DMEM from fridge into incubator/water bath at 37°C.
3. Using the spaced razor blades, cut out a rectangular section of valve tissue from the base/belly region of the leaflet.
4. Thread springs through each of the short ends of the leaflet section.
5. Couple linear motor to bioreactor.
6. Mount leaflets in the bioreactor and fill ~8 mL of DMEM in each well and place the bioreactor in the incubator.
7. Start the linear motor using appropriate code within Si Programmer.
8. Monitor bioreactor at least twice a day. Media should be changed every 1-3 days, or whenever it has turned yellow (due to generation of waste/metabolic by-products).

NOTES:

- Sterile techniques must be used at all times. Wearing face masks is not absolutely necessary for porcine tissue, but must be worn at all times for other tissue types (eg: human, ovine etc).
- An alternative to 6-well plates is to use autoclaved plastic containers and excise out the entire aortic valve with the root and a portion of the aorta and place it in ice-cold dPBS. The individual cusps will then be excised in a laminar flow hood in the laboratory.

TISSUE POST-PROCESSING

Materials and Reagents:

For tissue harvesting:	
1x 6-well plate	Fisher #08-772-1B
1x straight forceps	
1x curved forceps	
1x scalpel handle and sterile blade	
Sterile cold dPBS	

For frozen block preparation:	
Plastic molds	EMS #70180-70184
OCT compound	EMS #62550-01
Straight microdissection forceps	
Long hemostat	
Vacuum flask	EMS #61891-02
Liquid nitrogen	From IBB mechanical chase

For snap-freezing tissue (protein and RNA analysis):	
Cryovials	EMS #61800-1A
Cryovial holders (“canes”)	EMS #61080-10
Liquid nitrogen dewar	

Procedure:

Stopping of experiment

1. Autoclave surgical tools and dPBS well in advance. Refrigerate dPBS.
2. On day of experiment, bring dPBS to 37ºC in incubator or water bath. Fill 6-well plate with dPBS.
3. Return stretch bioreactor to laminar flow hood.
4. Use Si Programmer to stop linear motor.
5. Remove tissue from stretch bioreactor. If there are still samples in the bioreactor (eg: we are looking at different timepoints), immediately cover bioreactor and return to incubator and resume the linear motor.
6. Using scalpel, remove portion of leaflet that was attached to the spring.
7. Immerse leaflet in dPBS 3x to wash away DMEM. More washes may be necessary. Tissue should appear whitish and lose most of the pink color from the DMEM before proceeding to the next steps of the protocol. **dPBS should not be colder than room temperature as that might result in thermal shock to the tissue samples.**

Preparation of frozen blocks for histology/immunohistochemistry

1. Label plastic molds accordingly.
2. Arrange tissue samples at the base of plastic mold in appropriate orientation.
3. Fill mold with OCT compound.
4. Using microdissection forceps "stand" the tissue in the OCT compound. If *en face* sections are required, tissue should be placed face down in the mold.
5. Fill vacuum flask with liquid nitrogen.
6. Using long hemostat, dip OCT block in liquid nitrogen. Ensure that the block is not submerged (liquid nitrogen should NEVER contact the OCT directly). **Make sure liquid nitrogen does not fall on the OCT compound as it will cause bubbles and cracks to develop in the block.**
7. OCT blocks will start to solidify and turn opaque. Keep blocks in liquid nitrogen until just a small circle (approximately 5mm in diameter) of OCT on the top face of the block is left to be solidified. This will ensure that the block does not crack.
8. Place frozen blocks in -80°C freezer.

Snap-freezing of tissue for western blotting/gene analysis

1. Label cryovials accordingly.
2. Place one tissue sample per cyrovial and snap vials into cyrovial holder.
3. Place entire cryovials into liquid nitrogen (in the dewar).
4. Transfer cryovials to -80°C freezer. Alternatively, cryovials can be maintained in liquid nitrogen, but care should be taken to ensure that the liquid nitrogen level is always topped up.

ANALYSIS PROTOCOLS

PULVERIZATION OF CARDIAC TISSUE

Materials:

Mortar and pestle – the size of a Chinese tea cup
Liquid Nitrogen 2-3L
Thick Gloves
Tongs
Spatula
1-2 Styrofoam box(es) (big enough to hold 2 – 3 L of liquid N_2)
Funnel with a hole big enough to insert (slightly) into cryovials
Cryovials (At least 2.5" long so that boiling of N_2 will not cause tissue to escape from vial)
Tube rack to hold cryovials (preferable one that can float in the liquid N_2)

Procedure:

1. Place mortar and pestle, funnel, cryovials into Styrofoam box filled with ~ 2 L+ of liquid N_2.
    a. This is to ensure everything is at the same temp and that nothing will stick to the mortar and pestle (i.e. frozen grounded-up valve tissue).
2. Immerse tissue (you only need ~ 1 g for any biochemical study) into the liq. N_2 for at least 1 minute.
3. Using the tongs, bring the mortar out and leave it half filled with liquid N_2. Pull out the pestle and tissue and then in a twisting and pulsating downwards motion, push down on tissue, using one hand to hold the mortar down.
    a. Don't push too fast or too hard because some liq. N_2 and bits of tissue will spill out.
4. Continue grinding and pulverizing until the heart tissue is a very fine granular powder. This may take a few minutes.
    a. At times the grinding takes so long that more liq. N_2 will have to be added to the mortar.
    b. Use a small plastic cup and be careful when pouring it in (else tissue might spill out).
    c. Add enough liq. N_2 to make a nice tissue slurry as this will be important in later steps.

5. When done grinding heart tissue up, use tongs to get the cryovial and funnel. Set the cryovial onto the test tube rack and sit it upright. Insert the small hole of the funnel into the mouth of the cryovial.
6. Using your gloves, quickly pour the tissue slurry into the funnel-cryovial. If there is tissue left in the mortar, use the spatula (dip it into liq. N_2 first) and then scrape the remaining bits in. Finally, use the spatula and tap the side of the funnel so that the rest of the tissue funnels into the cryovial.

NOTES:

- For use in western blotting: Gently tap/scoop out 0.1 g of sample (more than 0.3 g is overkill); Add it to lysis buffer (make sure it contains protease inhibitors and a bit of citrate).
- Ground tissue should never be allowed to thaw. It should always be maintained in liquid nitrogen or in the -80°C freezer.

SAMPLE HOMOGENIZATION AND TISSUE LYSATE PREPARATION

Materials and Reagents:

Microcentrifuge tubes	Fisher #02-681-239
Styrofoam container with wet ice	
Rotor-stator homogenizer	In back lab
Sonicator	In back lab
RIPA Lysis Buffer	Santa Cruz # sc-24948

Procedure:

1. Prepare and label homogenization tubes and put powdered tissue samples into these tubes.
2. Prepare RIPA lysis buffer according to its instructions.
3. Add appropriate volume of ice-cold lysis buffer per sample tube. In general, the guideline is to use 3 mL lysis buffer per gram of tissue. (i.e. for a 5 x 5 mm aortic valve leaflet sample, use 200 µL lysis buffer)
4. Disrupt and homogenize tissue with electric homogenizer at lowest setting ("1") for about 30 – 60 s (make sure foam does not spill out of sample tube). Ramp up the homogenizer speed to "6" for about 15 s. Clean the homogenizer tip between samples.
5. Incubate on ice for ~20 minutes to let the foam subside. Repeat step 4 (at least 3 times) until tissue is completely homogenized.
6. Transfer to labeled microcentrifuge tubes and sonicate on ice for 30 seconds, three times. Take care that sonicator tip is completely submerged in the cell lysate in order to prevent splashing.
7. Centrifuge tubes at 5000 - 7000 g for 5 minutes at 4°C. Remove supernatant and centrifuge again if necessary. The supernatant fluid is the total cell lysate.
8. Conduct DC protein assay (if protein assay is not being conducted immediately, store tubes in -80ºC freezer. Store unused lysis buffer in fridge for up to a week).

<u>NOTES</u>:

- Sonicating the sample is recommended on top of the homogenization step #4. Alternatively freeze-thawing can be used.
- Make sure homogenizer blending bit is cleaned with Na-EDTA, acetone and then water before blendering the tissue lysate.
- Do not allow samples to thaw out at room temperature at any time. Preferably they should be kept at most at -20ºC.

IMMUNOHISTOCHEMISTRY

This protocol outlines the general double immunofluorescence protocol using fluorescent secondary antibodies. If only a single protein is to be stained for, directly go from step #9 to step #15 (counterstaining). All antibody concentrations used in this dissertation are provided in this appendix after the Western Blotting section.

Reagents:

Acetone	Fisher #A16P-4
Alcohol (Ethanol)	Fisher #A962-4
Phosphate buffered saline (PBS) buffer (1x)	Fisher #BP399-1
Bovine Serum Albumin (BSA)	EMD #2930
Fluorescent Mounting Gel	EMS #17985-10
Glass coverslips	From histology lab

Procedure:

Fixing/Antigen Retrieval:

1. Fixed paraffin embedded sections are deparaffinized[1], and rehydrated in descending grades of alcohol. Sections are washed 1x 5min in PBS. (Use autostainer in histology lab. Instructions are indicated on autostainer itself.).
2. Frozen sections are thawed immediately before use at room temp, ~ 10-30 min prior to start of procedure. The frozen sections are fixed in ice-cold acetone for 5 min in the freezer and air dried for 10-15 min. Sections are rehydrated in PBS for 5 min.
3. Fixed frozen and paraffin embedded sections may require some form of antigen retrieval. The tissue can be treated with proteases, detergents or heat. Examples of some commonly used proteases are:
   a) 1μg/mL proteinase K for 10 min at room temp. (Dilute 7.5 μL of 20 mg/mL stock prot. K in 150 mL of PBS).
   b) 100ug/mL pronase A pretreatment of the tissue for 10 min at RT, including anti-vWF (Dilute 150 μL of 100 mg/mL stock pronase A in 150 mL of 1x PBS).

   Also try trypsin or triton-X100. Antigen retrieval may be applied using citrate buffer and microwave heating. (Refer to the antibody data sheet for possible starting points).
4. Wash slides in 1x 5min in PBS at RT.

[1] Paraffinization is carried out in Histology Lab. Refer to Histology Lab Tech for details.

Protein of interest #1:

5. Block tissue using serum solution from the secondary source of the first primary antibody applied for 30 minutes at RT. *(eg: if using mouse anti-smooth muscle actin, use mouse serum).*
6. Prepare the working dilution[2] of the primary antibody in 1% BSA in PBS (BSA/PBS). Blot off serum and apply primary antibody. Incubate sections in a humid chamber for 1h at RT.[3]
7. Blot off excess antibody and wash slides in PBS for 2x 5min at RT.
8. **This step onwards to be performed in the dark:** Prepare working dilution of the fluorochrome-conjugated secondary antibody in BSA/PBS, and add 2% of normal serum from the source animal of the secondary antibody. Apply antibody and incubate 30 min at RT in a humid chamber.
9. Blot off excess antibody and wash slides in PBS for 2x 5min at RT.

Protein of interest #2:

10. Block tissue using serum solution from the secondary source of the second primary antibody applied for 30 minutes at RT.
11. Prepare the working dilution of the second primary antibody in grade BSA/PBS. Blot off serum, apply primary, and incubate sections in a humid chamber for 1h at RT.
12. Blot off excess antibody and wash slides in 1x PBS twice for 5 min each at RT.
13. Prepare working dilution of the fluorochrome-conjugated secondary antibody in BSA/PBS, and add 2% of normal serum from the source animal of the secondary antibody. Apply antibody and incubate 30 min, rt in a humid chamber.
14. Blot off excess solution and wash slides in 1x PBS twice for 5 min each at RT.

Counterstain:

15. Incubate cells with 0.2 μg/mL DAPI (50 μL in 250 mL 1x PBS) for 5 min.
16. Wash slides in 1x PBS twice for 5 min each at RT.
17. Coverslip using fluorescent mounting medium and store at 4°C protected from light.

NOTES:

- For extended storage of samples, protect stained sections from light and keep refrigerated at 4°C.

[2] Refer to previous work done with the antibody to determine working dilution or refer to data sheet of antibody for starting dilution. If using Ab for the first time you will need to run a series of dilutions to determine optimal working concentration.

[3] All incubation times in this protocol are provided here as a reference point. You will have to determine the particular incubation time for that particular Ab.

GEL ELECTROPHORESIS AND WESTERN BLOTTING

Materials:

Gel casting stand	Biorad #165-8003
Gel casting holder	Biorad #165-8003
Glass plates	Biorad #165-3308
Glass spacer plate	Biorad #165-3312
Gray casting pads	Biorad #165-8003
Green lane 1.5 mm combs (10 or 15-well)	Biorad #165-3365
Gel loading guide	Biorad #165-8003
Buffer tanks with lids	Biorad #165-8004
Electrophoresis chamber	Biorad #165-8004
Transfer chamber	Biorad #165-8004
Black and white transfer case	Biorad #170-3930
Transfer sponge	Biorad #170-3930
Transfer filter paper	Biorad #1703932

Reagents:

For Gel:	
3x bis-tris buffer	
OR	
5x separating buffer 5x stacking buffer	
Protogel (30%)	Nat'l Diag #EC-890
10% sodium dodecyl sulfate (SDS)	Sigma #L4390
1.5% ammonium persulfate (APS)	Sigma #A3678
TEMED	Sigma #T9281
1-butanol	Sigma #B85919

For electrophoresis:	
MOPS (high Mw) running buffer	Sigma #M1254
MES (low Mw) running buffer	Sigma #M3671
OR	
Tris-glycine-SDS (Running) buffer	
Molecular weight marker	Bio-rad #161-0324EDU
1x sample buffer	

For transfer:	
PVDF membrane	Millipore # IPVH00010
TG transfer buffer	
TBS-tween (TBST) buffer	

Procedure:

SDS-PAGE:

1. Get clean gel casting stand (each stand allows for two gels), one green gel casting holder for each gel, two glass plates, and two 1.5 mm spacer platses.
2. Clean all plates with alcohol and dry with Kimwipes.
3. Assemble flat plate and spacer plate in casting holder and secure tightly onto casting pads; check for leaks with dH2O.
4. Prepare stacking and resolving gel according to the following recipes. The bis-tris system is a more reducing gel and has better band separation (like a gradient gel). This makes 19 mL of resolving gel and 7.5 mL of stacking gel. This is enough for 2 gels:

Bis-tris system:

	10% resolving gel	12.5% resolving gel	Stacking gel (4%)
dH_2O	6.13 mL	4.54 mL	2.2 mL
Protogel	6.41 mL	8 mL	1.5 mL
Bis-tris buffer	5.48 mL	5.48 mL	2.13 mL
1.5% APS	960 µL	960 µL	1.5 mL
10% SDS	196 µL	196 µL	75 µL
TEMED	25 µL	25 µL	10 µL

Tris-glycine system:

	10% resolving gel	12.5% resolving gel	Stacking gel (4%)
dH_2O	7.78 mL	6.18 mL	3.8 mL
Protogel	5.33 mL	8 mL	2 mL
Buffer	separating buffer 3.84 mL	separating buffer 3.84 mL	stacking buffer 2 mL
1.5% APS	960 µL	960 µL	2 mL
10% SDS	192 µL	192 µL	100 µL
TEMED	25 µL	25 µL	10 µL

5. Add TEMED last and swirl contents to mix thoroughly and add ~7.8 mL in each side of the gel setup; add 0.2 mL of 1-butanol to take away bubble and even gel surface; allow to polymerize for 10 min.
6. Wash out 1-butanol with dH2O and dry gently using paper towel.
7. Insert lane combs between glass plates, and similarly add ~2 mL stacking gel and push down combs (clean first with dH2O) ensuring that there are no bubbles; allow to polymerize for 10 min.

8. Gently pull out combs, and rinse away bubbles with running buffer.
9. Put each gel in beige holder and secure. Make sure that shorter glass plate is on the inside of the holder. Each holder holds two gels. If only one gel is run, place "dummy" gel on other side. Insert holder into buffer tank.
10. Pour running buffer into middle of gel assembly so that it overflows to the outside area until the level reaches that of the inside.
11. Using gel loading guide, add samples into each lane (max. 60 µL for 10-lane, and 35 µL for 15-lane). Add 5 µL molecular weight marker to left-most lane. If lanes are empty, fill with equal amount (as adjacent lanes) of 1x sample buffer. This will ensure horizontal running of the protein front (i.e. no skewing).
12. Run at the following recommended voltages:
    a. Bis-tris: 150 V constant (~1 h)
    b. TGS: 80 V constant (~2.5 h)

Western Blot:

13. After electrophoresis, we need to transfer proteins from gel to a membrane that is suitable for antibody probing.
14. For each gel to transfer to a membrane:
    a. Get rectangular tub, transfer buffer from cold room, one black and white transfer case per gel, two pieces of filter paper, two sponges, container of ice.
    b. Cut out rectangular piece of PVDF membrane and notch top right hand corner in order to distinguish between different membranes.
    c. Soak membrane in methanol.
    d. Soak membrane in cold transfer buffer for at least 30 min. **VERY IMPORTANT!!!** This will ensure that there is no shrinkage of the membrane during the actual transfer.
    e. Pour transfer buffer into rectangular tub. Open black/white transfer case into blue tub so that the white side is on the right and black is on the left.
    f. Put one sponge on the black surface and one filter paper on top of it.
    g. Put membrane on top of filter paper on white side with the trimmed corner on the top-right. **It is very important also to keep track which side of the membrane was in contact with gel as this is the side that will have the higher concentration of protein.**
    h. Remove gel from electrophoresis container, and use a razor blade to gently pry glass plate. Cut away stacking gel and gently loosen resolving gel from glass plate. Place gel on top of membrane with molecular weight marker on the same edge of membrane as the trimmed corner.
    i. Put filter paper and sponge on top of gel and close black and white container and engage locking mechanism. Make sure there are no bubbles and that all components are aligned.
15. Insert into transfer tank according to appropriate polarity; pour buffer from tub into transfer tank.
16. Put transfer tank into tub and fill tub with ice and take to cold rom.

17. Run transfer in cold room at the following recommended voltages:
    a. 70 V: for 3 h (preferred)
    b. 30 V: overnight

Immunoprobing:

18. After transfer ends, remove membrane and wash with dH2O or TBST for 5 min.
19. Next soak in Ponceau Red solution for 5 min. Then rinse with dH2O until red bands of protein show up. This step is to verify that proteins have indeed transferred from gel to membrane and that there was equal protein loading in each lane.
20. At this point, the membrane can be cut with a razor blade horizontally so that more than one antibody can be probed for. **This should only be done if a protocol for that particular antibody has been established and it is known at what molecular weight it will appear.**
21. Wash membrane 2 – 3x in TBST to remove Ponceau stain.
22. Block membrane in blocker (either 5% nonfat dry milk or 3% BSA in TBST) for 1 hour at RT
23. Wash membrane for 5 min 1 – 2x in fresh blocker at RT.
24. Incubate in appropriate concentration of primary antibody diluted in blocker overnight at 4ºC.
25. Wash membrane for 5 min 3x in fresh blocker at RT.
26. Incubate in appropriate concentration of HRP-conjugated secondary antibody for 1 – 2 hours at RT.
27. Use Pierce Western Blotting substrate to visualize bands in the dark room.

NOTES:

- All reagents and buffers must be absolutely clean and filtered without any particulate matter, as that would result in background signal on the PVDF membrane.
- All new antibody dilutions should be tested using a concentration dilution curve.

ANTIBODY DILUTIONS

The antibodies, catalog numbers and their respective dilutions used in this dissertation for both immunohistochemistry and western blotting are compiled here. As mentioned earlier, any new antibodies for future studies need to be titrated using a series of dilutions/concentrations to identify the dilution that yields the best signal to noise ratio.

Antibody against	Dilution		Catalog Number
	For IHC	For Western	
α-SMA	1:200	1:100	Dako #M0851
β-Actin	-	1:1000	Sigma #A1978
MMP-1	-	1:50	Santa Cruz #sc-6837
MMP-2	-	1:75	Calbiochem #IM33L
MMP-9	-	1:50	Calbiochem #IM37
TIMP-1	-	1:20	Millipore #AB770
Cathepsin L	1:25	-	Santa Cruz #sc-6501
Cathepsin S	1:20	-	Santa Cruz #sc-6503
Cathepsin K	1:20	-	Santa Cruz #sc-6506
brDU	1:200	-	Dako #M0744
BMP-2	1:25	-	Santa Cruz #sc-6895
BMP-4	1:50	-	Santa Cruz #sc-12721
Runx2	-	1:100	Santa Cruz #sc-10758
Osteocalcin	-	1:50	Millipore #AB10911
Hsp47	1:200	-	Santa Cruz #sc-8352
Lysyl Oxidase	1:100	-	Santa Cruz #sc-32410

MMP GELATIN ZYMOGRAPHY

Materials and Reagents:

For Gel:	
0.75 mm glass spacer plates	Biorad #165-3312
Gel casting apparatus as per western blotting protocol	
Stock gelatin 4.66 mg/mL	Sigma #G-9382
Other gel reagents as per western blotting protocol	

For zymography assay:	
2.5% Triton-X 100	Sigma #T8532
1x Zymogram development buffer	Biorad #161-0766
Stain solution (2.5% Coomassie Blue R250)	Sigma #B6529
Destain solution	

Procedure:

1. Make gels according to the following recipe at 4°C in 0.75 mm glass plates (16 mL total volume – makes 4 gels):

	10% resolving gel	**12.5% resolving gel**	**Stacking gel (4%)**
Gelatin stock	3.43 mL	3.43 mL	
dH_2O	3.06 mL	1.72 mL	3.8 mL
Protogel	5.33 mL	6.67 mL	2 mL
Buffer	separating buffer 3.2 mL	separating buffer 3.2 mL	stacking buffer 2 mL
1.5% APS	800 µL	800 µL	2 mL
10% SDS	160 µL	160 µL	100 µL
TEMED	20 µL	20 µL	10 µL

2. Use 3.8 mL of resolving gel per plate; load gels with 8 – 10 µg of protein.
3. Run gels at 80V at **4°C** (Should take 3 – 4 h).
4. Gels washed 2x 15 min in 2.5% Triton-X 100 at RT.
5. Wash to equilibrate with development buffer for at least 30 min.
6. Incubate for 12 hours at 37°C in development buffer.
7. Stain for 1 h at RT on belly dancer and destain until bands are resolved.

REVERSE ZYMOGRAPHY

Materials and Reagents:

For Gel:	
1.5 mm glass plates	Bio-rad #165-3312
6.86 mg/mL stock gelatin	Sigma #G-9382
20 µL of 0.1 mg/mL pro-MMP-2/-9 standard	Millipore #CC073
Rest as per gelatin zymography	

For zymography assay:
As per gelatin zymography

Procedure:

1. Dissolve MMP standard in 80 µL SDS to make 100 µL total volume.
2. Make gels according to the following recipe at 4°C in 0.75 mm glass plates (16 mL total volume – makes 4 gels):

	10% resolving gel	12.5% resolving gel	Stacking gel (4%)
Gelatin stock	3.43 mL	3.43 mL	
MMP-2/-9 std	100 µL	100 µL	
dH2O	3.06 mL	1.72 mL	3.8 mL
Protogel	5.33 mL	6.67 mL	2 mL
Buffer	3.2 mL separating buffer	3.2 mL separating buffer	2 mL stacking buffer
1.5% APS	800 µL	800 µL	2 mL
10% SDS	80 µL	160 µL	100 µL
TEMED	20 µL	20 µL	10 µL

3. Use 3.8 mL of resolving gel per plate; load gels with ~40 µg of protein (it may require more in some cases as there is very small amounts of endogenous TIMPs).
4. Gels washed 2x 15 min in 2.5% Triton-X 100 at RT.
5. Wash to equilibrate with development buffer for at least 30 min.
6. Incubate for 12 hours at 37°C in development buffer.
7. Stain for 1 h at RT on belly dancer and destain until bands are resolved.

MOVAT'S PENTACHROME PROTOCOL

Reagents:

For 1% Alcian Blue Solution (Stable for 2 months)	
Alcian blue, 8 GS 1g	Sigma #A5268
Glacial acetic acid 1 mL	Sigma #242843
dH_2O 100 mL	

For Hematoxylin Solution (Verheoff's) (Stable for several months)	
10% Absolute alcoholic hematoxylin, 25 mL	Sigma #HT25A (whole kit)
Absolute alcohol 25 mL	
10% aqueous Ferric chloride (Make fresh) 25 mL	
Iodine solution 25 mL	
Iodine 2 g	
Potassium iodide 4 g	
dH_2O 100 mL	

Dissolve 4 g Potassium iodide in 4-8 mL dH_2O, and then add 2 g Iodine. After Iodine is dissolved dilute to 100 mL.

For Sodium Thiosulfate (Make fresh)	
Sodium Thiosulfate 5 g	Sigma #S7026
dH_2O 100 mL	

For Crocein Scarlett – Acid Fuchsin Solution	
Stock A	
Crocein Scarlet MOO 7B 0.1 g	Sigma #27970
Glacial acetic acid 0.5 mL	Sigma #242843
dH_2O 99.5 mL	
Stock B	
Acid fuchsin 0.1 g	Sigma #F8129
dH_2O 99.5 mL	
Glacial acetic acid 0.5 mL	Sigma #242843

Working Solution:
Stock A 8 parts + Stock B 2 parts

For Alkaline Alcohol (pH 8 or above)	
Ammonium hydroxide 10 mL	Sigma #320145
Alcohol 95% 90 mL	Sigma #AC61509-0020

For 5% Sodium Thiosulfate	
Sodium Thiosulfate 5 g	Sigma #S7026
dH_2O 100 mL	

For 0.5% Acetic Acid	
20% acetic acid 25 mL	Sigma #242843
DH2O 100 mL	

For 5% aqueous phosphotungstic acid	
Phosphotungstic acid 10g	Sigma #P4006
dH_2O 200 mL	

(To remove the Crocein Scarlet-acid fusin stain from the extra cellular connective tissue and ground substance. When the solution is removed the staining with insoluble monastral fast blue is again shown.)

For Alcoholic Saffron Solution	
Saffron (Safran du Gatinais) 6 g	Sigma #199613
Absolute alcohol 100 mL	Sigma #AC61509-0020

(Keep tightly closed to prevent hydration. Incubate at 56-58°C for 48 hours.)

Procedure:

1. Deparaffinize and hydrate to dH_2O.
2. Stain in alcian blue for 20 min. (*Stains for ground substance and mucin blue*).
3. Wash in running water for 10 min.
4. Place slides in alkaline alcohol for 1-2 hour. (*Converts the alcian blue into insoluble monastral fast blue*).
5. Wash in running water for 10 min. **Complete removal of alkaline alcohol with running water is important. Failure to remove all alkaline alcohol will inhibit the stain that follows.**
6. Rinse in dH_2O.
7. Stain in Verheoff's hematoxylin solution for 15 min. (*Stain for nuclei & elastin fiber-black*).
8. Rinse several changes of dH_2O.
9. Differentiate in 2% aqueous ferric chloride and agitate slides gently. (Stop differentiation with several changes of tap water and check microscopically for black elastic fiber staining and gray background. Repeat 2% ferric chloride treatment and tap water rinses as necessary. If elastic fiber staining is too pale, restain in the saved Verhoeff's solution.)
10. Place slides in sodium thiosulfate for one min.(Discard solution)
11. Wash in running tap water for 5 min; rinse in dH_2O.
12. Stain in crocein scarlet-acid fuchsin (8:2) for 1½ min. (Stain for fibrinoid, fibrin-intense red, muscle-red).

13. Rinse in several changes of dH_2O
14. Rinse in 0.5% acetic acid water.
15. Differentiate slides in 5% aqueous phosphotungstic acid, 5-10 min. (Check microscopically. Continue differentiation until collagen is pale pink in color and the ground substance, initially colored red, becomes bluish in color.)
16. Rinse in 0.5% acetic acid water. (To remove phosphotungstic acid).
17. Rinse in 100% alcohol X3.
18. Stain in Saffron for 15 -20 min. Use a screw capped coplin jar for this step, and keep the jar sealed during the staining procedure. If collagen is not sufficiently yellow, stain for a longer period (Stain for collagen & reticular fiber-yellow).
19. Rinse in 100% alcohol X3 and xylene X2 and mount in mounting mediums.

ALIZARIN RED STAIN

Reagents:

For Alizarin Red Solution	
Alizarin Red S 2g	Sigma #05600
dH_2O 100 mL	
0.5% Ammonium Hydroxide	Sigma #320145

Mix the solution, adjust the pH to 4.1 – 4.3 using 0.5% Ammonium Hydroxide. **The pH is critical. Make fresh.**

Procedure:

1. Deparaffinize slides and rehydrate to 70% alcohol.
2. Rinse in dH_2O at RT.
3. Incubate in Alizarin Red S Solution, for 30 seconds to 5 minutes. Check microscopically for an orange-red color.
4. Shake off excess dye and blot sections using Kimwipes.
5. Use autostainer in histology lab for Hematoxylin counterstain. (optional)
6. Dehydrate and clear.
7. Coverslip and store at RT.

VON KOSSA STAIN

Reagents:

For 5% Silver Nitrate Solution *(Stable for 1 year)*	
Silver nitrate 25 g	Sigma #S8157
dH_2O 500 mL	

Mix well and pour into clean brown bottle and store in refrigerator at 4°C.

For 5% Sodium Thiosulfate *(Make fresh)*	
Sodium Thiosulfate 5 g	Sigma #S7026
dH_2O 100 mL	

For Nuclear Fast Red (Kemechtrot) Solution	
Nuclear fast red 0.1 g	Sigma #229113
Aluminum sulfate 5 g	Sigma #368458
dH_2O 100 mL	
Thymol 1 grain	Sigam #T0501

Dissolve aluminum sulfate in water. Add nuclear fast red and slowly heat to boil and cool. Filter and add a grain of thymol as a preservative.

Procedure:

1. Deparaffinize slides and rehydrate to dH_2O at RT.
2. Incubate slides in 5% silver nitrate solution placed under bright sunlight or under a 60W lamp. Place foil or mirror behind the jar/tray to reflect the light. Leave for 1 hour or until calcium turns black. (For best results use UV lamp)
3. Wash 3x dH2O for 5 min at RT.
4. Wash 1x in 5% sodium thiosulfate for 5 min at RT.
5. Wash 1x in tap water, 1x in dH_2O.
6. Incubate slides in Nuclear Fast Red for 5 min at RT.
7. Wash briefly in dH_2O.
8. Dehydrate and clear.
9. Coverslip and store at RT.

DEHYDRATION PROTOCOL FOR SLIDES (FROM WATER)

Reagents:

Ethanol or Methanol	Fisher #A962-4
Xylene	Fisher #O5082-4
Cytoseal mounting medium	EMS #18006

Procedure:

1. Hydrate slides in dH2O.
2. Incubate slides for 20 – 30 seconds at RT in the following reagent sequence:
    a. 70% alcohol
    b. 90% alcohol
    c. 100% alcohol
    d. 100% alcohol
    e. 100% xylene
    f. 100% xylene
3. Coverslip using cytoseal mounting medium.

ALKALINE PHOSPHATASE ACTIVITY ASSAY

Reagents:

Lysis buffer	Santa Cruz #sc-24948
Substrate buffer: glycerine 0.1M	NE Biolabs #B7011S
$ZnCl_2$ 1mM	
$MgCl_2$ (pH = 10.4) 1mM	
Substrate solution: p-nitrophenyl phosphate 10 mM	Sigma #N4645
Standard: p-nitrophenol 10 mM	Sigma #241326
Experimental Sample lysates	

Procedure:

1. Prepare substrate solution **FRESH**: (37.11 mg substrate in 10 mL substrate buffer).
2. Prepare the following standard dilutions in microcentrifuge tubes: (in mM) 500, 250, 125, 62.5, 31.25, 15.63, 7.81, 3.91, 1.95, 0.98, 0.49, 0.25, 0.

500mM standard tube		*Rest of standard tubes (serial dilution)*	
Substrate buffer	800 µL	Substrate buffer	450 µL
Lysis buffer	100 µL	Lysis buffer	50 µL
10mM standard	50 µL	From previous std	500 µL

3. Add 200µL of standard to a 96-well plate in duplicate.
4. Add 20µL of sample lysate in duplicate.
5. Add 180µL of substrate solution to each sample.
6. Read samples on a plate reader 405 nM at 0, 15, 30, 60, 120 and 180 minutes and after 24 hours.
    a. Cover plate with saran wrap and incubate at 37°C in between readings.
7. Plot normalized rate of increase in absorbance for each sample

CALCIUM ARSENAZO ASSAY

Reagents:

PBS	Sigma #P5368
Acetic acid 1N	Sigma #242843
Calcium reagent (Arsenazo III)	DCL#140-24(1L)
Calcium standard 1 mg/mL	Sigma #05-1050

Procedure:

1. Wash samples 3X with **calcium-free** PBS. This can be purchased.
2. Remove samples from wells/plates and place in microcentrifuge tube with 500 µL of 1N acetic acid.
3. Vortex samples overnight in refrigerator.
4. If needed, spin samples down in small centrifuge on maximum speed for 8-10 minutes, and remove supernatant into fresh tubes.
5. Prepare standards (maximum 100 µg/mL, and 6 serial dilutions; in 1N acetic acid).
6. Pipette 25 µL of standards and samples in triplicate to a **clear** Costar 96-well plate.
7. Add 300 µL of reagent to each well (dilute samples if color change is more than maximum standard).
8. Incubate for 30 seconds at room temperature.
9. Read samples on plate reader at 650 nM (color is stable for 30 minutes).

NOTES:

- For cells in plates, put acid in plate overnight at 4C. Next day use cell scraper to scrape off the cells, and transfer cells and acid to microcentrifuge tubes. Vortex samples overnight in refrigerator.
- Store samples at -20C.
- According to the reagent manual, when using 20µL of sample and 2 mL of reagent (1/100 ratio), the assay is linear up to 200µg/mL. The linearity will depend on the ratio of sample/reagent used. When using the ratio above, the relationship is linear for < 20 µg/mL, but a quadratic equation fits the standards very well. A fourth order polynomial equation fits the standards almost perfectly.
- In the case of the ratio above, the saturation limit of the assay is ~175 µg/mL.
- To figure out the dilutions required for each group, you can compare color change in 1-2 samples from each group with the standards using n=1.

SIRCOL COLLAGEN ASSAY

Reagents:

Pepsin	Sigma #P7000
Acetic acid 0.5 M	Sigma #242843
Sircol collagen assay kit	Accurate Chem #CLRS1000

Procedure:

1. Digest tissue in pepsin dissolved in 0.5M acetic acid (buffer) for 48 h at 37°C. Stir vigorously during this period. Pepsin: tissue (dry weight) ratio of 1:3.
2. Prepare reagent blanks (100 µL buffer), collagen standard (double aliquots containing 5, 10, 25, 50 µg) and test samples (10-100 µL); adjust the contents of all tubes to 100 µL with 0.5 M buffer.
3. Add 1 mL Sircol Dye reagent and cap all tubes, mix.
4. Place tubes on a mechanical shaker for 30 min.
5. Transfer tubes to a micro centrifuge and spin at > 10,000 xg for 10 min.
6. Invert the tubes to drain the unbound dye.
7. Add 1 mL alkali reagent and mix.
8. Transfer 200 µL aliquots of samples from tubes to a 96-well multi-well plate.
9. Place the plate in a microplate reader, read the absorbance at 540 nm.

BLYSCAN SULFATED GLYCOSAMINOGLYCAN ASSAY

Reagents:

Protease	Sigma #P7431
Tris-acetate 0.1M	Sigma #93296
Calcium acetate (buffer) 10mM	Sigma #402850
Blyscan glycosaminoglycan assay kit	Accurate Chem #CLRB1000

Procedure:

1. Digest tissue in protease dissolved in 0.1M tris-acetate with 10mM calcium acetate (buffer) for 48 h at 37°C or 24 h at 60°C. Stir vigorously during this period. Protease: tissue (dry weight) ratio of 1:30.
2. Prepare reagent blanks (100 µL buffer), GAG standard (aliquots containing 1.0, 2.0, 3.0, 4.0, 5.0 µg) and test samples (10-100 µL); adjust the contents of all tubes to 100 µL with buffer.
3. Add 1mL Blyscan Dye reagent and cap all tubes, mix.
4. Place tubes on a mechanical shaker for 30 min.
5. Transfer tubes to a micro centrifuge and spin at > 10,000 xg for 10 min.
6. Invert the tubes to drain the unbound dye.
7. Add 1 mL dissociation reagent and mix.
8. Transfer 200 µL aliquots of samples from tubes to a 96-well multi-well plate.
9. Place the plate in a microplate reader, read the absorbance at 656 nm.

FASTIN ELASTIN ASSAY

Reagents:

Proteinase K	Sigma #P2308
Tris-HCl 50mM	Sigma #T3253
EDTA 0.1M	Sigma #E6758
NaCl (buffer) 0.2M	Sigma #S7653
SDS 0.1 mg/mL	Sigma #L4390
Fastin elastin assay kit	Accurate Chem # CLRF4000

Procedure:

1. Determine dry weight of the tissue sample and digest the tissue with proteinase K dissolved in 50mM tris-HCl, 0.1M EDTA and 0.2M NaCl (buffer) for 48 h at 37°C or 24 h at 60°C. To each sample add 0.5 mg/mL of enzyme an 0.1 mg/mL of SDS.
2. Precool elastin precipitate at 4°C before use.
3. Prepare reagent blanks (100 µL buffer), elastin standard (aliquots containing 12.5, 25, 50, 75 µg) and test samples (10-100 µL); adjust the contents of all tubes to 100 µL with buffer.
4. Add 1mL Fastin Dye reagent and cap all tubes, mix.
5. Place tubes on a mechanical shaker for 30 min.
6. Transfer tubes to a micro centrifuge and spin at > 10,000 xg for 10 min.
7. Invert the tubes to drain the unbound dye.
8. Add 1 mL dissociation reagent and mix.
9. Transfer 200 µL aliquots of samples from tubes to a 96-well multi-well plate.
10. Place the plate in a microplate reader, read the absorbance at 513 nm.

PICROSIRIUS RED STAIN

Reagents:

For Picro-sirius Red Solution *(Keeps for 3 years and can be used many times)*	
Sirius red F3B (C.I. 35782) (Direct Red 80) 0.5 g	Sigma #365548 or #43665
Saturated aqueous solution of picric acid 500 mL	Fisher #88-89-1

Add a little solid picric acid to ensure saturation (This is important).

For Acidified Water	
Acetic acid (glacial) 5 mL	Sigma #EMD AX-0079-2
dH_2O 995 mL	

For Weigert's Iron Hematoxylin Solution *(Stable for 3 months)*

Stock Solution A:	
Hematoxylin 1 g	Fisher #AC22975-0250
95% Alcohol 100 mL	Fisher #A962-4
Stock Solution B:	
29% Ferric chloride in water 4 mL	Fisher #I86-10
dH_2O 95 mL	
Hydrochloric acid, concentrated 1 mL	Sigma #320331

Working Solution:
Mix equal parts of stock solution A and B. This working solution is no good after 4 months.

Procedure:

1. Deparaffinize and hydrate in dH_2O.
2. Stain nuclei with Weigert's haematoxylin for 8 minutes, and then wash the slides for 10 minutes in running tap water).
3. Stain in picro-sirius red for one hour (This gives near-equilibrium staining, which does not increase with longer times. Shorter times should not be used, even if the colours look OK.)
4. Wash in two changes of acidified water.
5. Physically remove most of the water from the slides by vigorous shaking.
6. Dehydrate and clear.
7. Coverslip and store at RT.

APPENDIX C RAW DATA

This appendix contains all the raw quantitative date of this dissertation. The associated figure for each table of raw data is referenced for the convenience of the reader.

Specific Aim 1: Collagen Assay (Figure 5-5)

Collagen Content			
Fresh	**Static**	**10% Stretch**	**15% Stretch**
24.83766	17.89773	14.13091	26.55502
13.56534	16.71651	37.27364	49.0846
39.77273	11.22995	36.21826	18.97727
20.625	38.54167	20.19441	19.00826
51.27005	22.86932	24.1575	99.02597
23.50852	20.71678	30.19998	15.00947
14.18269	32.6049	39.00519	42.92929
31.72348	9.232955	14.66478	64.7096
16.58058	24.43182	17.58096	12.62175
24.31818	9.309441	39.03954	44.09091
51.62338	45.86039	36.69639	164.7254
30.19481	25.51653	41.1165	20.07576
61.72727	17.66529	29.1329	43.27652
32.67045	54.9513	30.2131	20.24148
21.16477	22.85354	28.1231	96.59091
15.34091	8.901515		41.73769
51.84659	11.59091		26.13636
46.37784	12.08965		34.96901
16.0564	17.37013		24.89669
26.10646	44.80114		56.64773
40.17857	26.13636		46.76573
29.0855	15.22989		30.34091
45.68966			

Specific Aim 1: Sulfated Glycosaminoglycan Assay (Figure 5-6)

sGAG Content			
Fresh	**Static**	**10%**	**15%**
28.95641	23.87415	73.59524	13.7532
28.82981	11.49461	21.34014	1.935776
15.42665	26.03056	23.86667	15.64598
113.7852	14.71882	20.96599	20.33948
23.28291	25.25815	16.74471	23.04762
19.53175	22.38095	16.55265	12.91209
29.58036	17.50916	20.82149	8.315476
34.53571	32.46269	16.50083	23.31293
32.97402	32.51599	22.80272	12.85833
25.58681	32.42952	21.86081	14.8747
17.23978	9.439362	23.15238	15.93171
51.45108	21.35556	26.88571	14.21569
20.40852	18.09722	12.49132	17.4007
33.5102	16.67937	16.21932	11.11035
22.21795	22.08333	24.99603	12.73276
22.49524	94.61028	36.49507	22.36143
90.60254	42.06744	32.24404	18.20989
24.09075	23.22761	28.72321	11.15121
28.39506	25.90909		
24.31429	33.50794		
21.55337	19.41991		
30.08571			
31.90476			

Specific Aim 1: Elastin Assay (Figure 5-7)

Elastin Content			
Fresh	**Static**	**10%**	**15%**
17.68973	8.62312	31.33451	13.63636
28.22421	16.71627	33.01235	19.05788
30.8618	7.270408	28.61552	18.68622
18.06723	21.75	31.33451	13.97516
9.982436	15.05838	33.01235	22.75346
26.9032	23.50618	28.61552	29.68074
17.9778	30.46218	14.76475	14.31197
24.57143	12.14827	17.41573	19.04762
12.17992	21.64575	4.240235	28.52925
14.76475	23.52302	11.16268	19.32737
17.41573	7.649092	8.535004	35.44974
4.240235	22.01545	18.12408	24.72385
11.16268	35.50562	19.39681	16.08368
18.12408	19.99489	15.75281	24.64727
19.39681	17.06795	23.86419	27.36626
15.75281	15.51966	95.88015	39.00463
23.86419	34.76904	28.19021	17.14249
95.88015	10.08682	17.7662	
28.19021	11.40449	11.22334	

Specific Aim 1: Zymography Data

Gelatin Zymography Data (Figure 5-17)								
	Valve 1	**Valve 2**	**Valve 3**	**Valve 4**	**Valve 5**	**Valve 6**	**Valve 7**	**Valve 8**
Fresh	1.00	1.00	1.00	1.00	1.00	1.00	1.00	1.00
Static 24h	1.18	0.81	0.91	1.32	0.88	0.88	0.59	0.78
Static 48h	1.32	1.03	1.19	0.97	0.88	0.88	0.83	1.11
10% 24h	0.81	0.50	0.70	0.58	0.43	0.61	0.54	0.93
10% 48h	0.76	0.45	0.74	0.55	0.59	1.47	0.81	0.96
15% 24h	0.89	0.60	1.10	1.01	1.07	1.02	0.76	1.07
15% 48h	1.59	1.27	1.57	1.11	2.51	1.95	1.74	1.21
20% 24h	0.82	0.53	0.79	0.64	0.86	1.17	0.32	0.76
20% 48h	1.24	1.18	1.23	2.23	2.35	2.46	0.80	1.45

Reverse Zymography Data (Figure 5-15)								
	Valve 1	**Valve 2**	**Valve 3**	**Valve 4**	**Valve 5**	**Valve 6**	**Valve 7**	**Valve 8**
Fresh	1.00	1.00	1.00	1.00	1.00	1.00	1.00	1.00
Static 24h	0.73	0.71	0.69	0.66	0.55	0.58	0.56	0.61
Static 48h	0.74	0.64	0.78	0.71	0.43	0.20	0.31	0.43
10% 24h	0.24	0.31	0.29	0.23	0.17	0.23	0.19	0.23
10% 48h	0.15	0.25	0.13	0.12	0.12	0.09	0.11	0.24
15% 24h	0.51	0.41	0.49	0.49	0.19	0.33	0.43	0.45
15% 48h	0.84	0.85	0.84	0.76	0.45	0.24	0.88	0.71
20% 24h	0.42	1.01	0.47	0.40	0.50	0.30	0.53	0.65
20% 48h	0.37	0.78	0.53	0.43	0.57	0.51	0.43	0.75

Collagenase Activity Data (Figure 5-13)								
	Valve 1	**Valve 2**	**Valve 3**	**Valve 4**	**Valve 5**	**Valve 6**	**Valve 7**	**Valve 8**
Fresh	1.19068	0.65415	0.77089	1.03705	1.03076	1.1235	1.3245	0.6541
Static 24h	0.90137	0.41481	0.70921	0.47513	0.8731	0.6843	0.54321	0.4327
Static 48h	1.62326	1.09651	0.48501	0.43181	0.45641	0.548	0.4987	0.98742
10% 24h	0.26388	1.46832	0.92017	0.41011	0.9616	1.05789	1.3242	1.13257
10% 48h	0.59785	1.59768	1.64689	0.66498	1.70706	1.19067	1.68741	1.35741
15% 24h	0.28264	0.74652	0.47593	6.80943	0.34671	0.46513	3.3274	1.8674
15% 48h	2.06443	4.89658	4.39279	3.6942	6.02904	5.3654	5.6874	4.68741
20% 24h	6.01332	2.63224	1.46097	2.49807	5.33676	2.64233	3.2164	5.48712
20% 48h	2.97323	2.74518	5.35442	5.86037	3.19685	4.6543	4.3579	5.35468

Specific Aim 1: Western Blotting Data

MMP-1 Western Data (Figure 5-12)								
	Valve 1	**Valve 2**	**Valve 3**	**Valve 4**	**Valve 5**	**Valve 6**	**Valve 7**	**Valve 8**
Fresh	1.00	1.00	1.00	1.00	1.00	1.00	1.00	1.00
Static 24h	1.54	0.15	1.75	1.54	1.22	1.72	1.65	1.36
Static 48h	1.35	1.29	1.53	1.15	1.21	1.75	1.23	1.13
10% 24h	2.39	3.57	1.99	1.18	1.16	0.90	2.57	3.27
10% 48h	2.89	3.89	2.99	1.77	1.33	1.49	2.64	1.98
15% 24h	2.31	4.82	2.76	1.82	1.20	2.56	3.99	2.87
15% 48h	3.07	5.22	3.42	2.16	1.38	2.53	6.13	4.45
20% 24h	3.15	4.29	3.05	1.33	1.19	2.23	3.42	2.98
20% 48h	2.93	3.92	1.88	2.12	1.44	1.94	1.64	3.54

MMP-2 Western Data (Figure 5-16)								
	Valve 1	**Valve 2**	**Valve 3**	**Valve 4**	**Valve 5**	**Valve 6**	**Valve 7**	**Valve 8**
Fresh	1.00	1.00	1.00	1.00	1.00	1.00	1.00	1.00
Static 24h	1.22	1.14	1.10	1.09	1.34	1.04	1.05	0.73
Static 48h	1.03	0.27	1.25	0.94	1.25	1.09	1.04	0.46
10% 24h	0.92	0.82	1.59	2.39	2.17	1.60	1.20	0.82
10% 48h	0.61	1.48	1.22	1.96	1.88	1.13	0.86	0.87
15% 24h	1.20	1.84	1.82	1.38	2.40	1.38	1.40	1.10
15% 48h	1.97	2.81	1.74	2.35	2.64	1.43	1.50	1.32
20% 24h	1.33	1.78	2.05	1.59	2.17	1.09	1.24	0.97
20% 48h	0.67	0.65	1.02	0.79	1.39	0.75	0.88	0.57

TIMP-1 Western Data (Figure 5-14)								
	Valve 1	**Valve 2**	**Valve 3**	**Valve 4**	**Valve 5**	**Valve 6**	**Valve 7**	**Valve 8**
Fresh	1.00	1.00	1.00	1.00	1.00	1.00	1.00	1.00
Static 24h	0.77	0.80	0.90	0.87	0.81	0.76	0.78	0.79
Static 48h	0.68	0.73	0.87	0.54	0.60	0.75	0.66	0.75
10% 24h	0.30	0.63	0.51	0.76	0.53	0.71	0.51	0.23
10% 48h	0.64	0.38	0.76	0.13	0.49	0.61	0.43	0.65
15% 24h	0.49	0.50	0.78	0.23	0.49	0.32	0.44	0.43
15% 48h	0.41	0.29	0.28	0.42	0.40	0.39	0.24	0.43
20% 24h	0.75	0.60	0.83	0.63	0.38	0.50	0.88	0.56
20% 48h	0.61	0.47	0.55	0.37	0.20	0.55	0.23	0.33

Specific Aim 1: Cathepsin Immunohistochemistry Semi-quantitative Data (Figure 5-11)

Cathepsin L								
	Valve 1	**Valve 2**	**Valve 3**	**Valve 4**	**Valve 5**	**Valve 6**	**Valve 7**	**Valve 8**
Fresh	0.022642	0.022777	0.021194	0.018038	0.01738	0.02032	0.02465	0.03487
10% 48h	0.012684	0.016498	0.014121	0.01581	0.01495	0.015469	0.012384	0.01324
15% 48h	0.004288	0.002141	0.003872	0.003153	0.001092	0.00259	0.002672	0.003653
20% 48h	0.003976	0.002565	0.00164	0.003183	0.001816	0.001601	0.000759	0.002434

Cathepsin S								
	Valve 1	**Valve 2**	**Valve 3**	**Valve 4**	**Valve 5**	**Valve 6**	**Valve 7**	**Valve 8**
Fresh	0.007249	0.003305	0.003412	0.007827	0.0023	0.00251	0.00465	0.00531
10% 48h	0.001074	0.000995	0.003361	0.002867	0.00267	0.001176	0.00096	0.001374
15% 48h	0.016384	0.014028	0.011686	0.015274	0.02843	0.022189	0.020778	0.012008
20% 48h	0.003976	0.002565	0.00164	0.003183	0.001816	0.00284	0.00387	0.00234

Cathepsin K								
	Valve 1	**Valve 2**	**Valve 3**	**Valve 4**	**Valve 5**	**Valve 6**	**Valve 7**	**Valve 8**
Fresh	0.000425	0.00574	0.005983	0.003549	0.003719	0.00423	0.00652	0.00354
10% 48h	0.004892	0.005272	0.002004	0.004675	0.003045	0.001361	0.003885	0.00264
15% 48h	0.020819	0.061207	0.058685	0.029044	0.01182	0.046315	0.051928	0.004148
20% 48h	0.019498	0.008963	0.012048	0.009473	0.020575	0.01048	0.01968	0.0164

Specific Aim 1: Proliferation and Apoptosis Data

BrdU Proliferation Immunoassay (Figure 5-22)								
	Valve 1	**Valve 2**	**Valve 3**	**Valve 4**	**Valve 5**	**Valve 6**	**Valve 7**	**Valve 8**
Static 24h	0	1.080249	1.096171	0	1.735697	0	1.123	1.0304
Static 48h	1.061436	1.080249	2.192342	1.031136	1.735697	1.4758	1.2398	1.8984
10% 24h	3.184309	2.160498	2.192342	2.062272	1.735697	2.0938	2.8903	2.9487
10% 48h	3.427496	2.607926	14.02723	5.196127	6.438127	4.669315	6.222885	7.1239
15% 24h	5.434788	13.63771	10.08578	3.2309	6.972453	8.329912	11.26855	9.1239
15% 48h	56.33941	31.99155	42.48561	20.96199	32.37921	36.7695	32.214	28.2389
20% 24h	45.51743	26.82139	20.07816	23.11811	22.3199	24.2974	23.14972	25.23981
20% 48h	22.9186	67.65055	98.26613	38.56701	45.33529	24.57263	55.2313	82.1284

TUNEL Apoptosis Immunoassay (Figure 5-24)								
	Valve 1	**Valve 2**	**Valve 3**	**Valve 4**	**Valve 5**	**Valve 6**	**Valve 7**	**Valve 8**
Static 48h	74.30624	84.17143	52.95308	67.81106	62.06314	72.24539	69.3542	71.6575
Fresh	1.01927	5	6	4	7	2	3.567498	1.687496
10% 48h	8.339021	2.06681	17.95402	13.49876	8	10.2309	8.98741	9.9841
15% 48h	20	31	30	27	20	36.48641	19.567	18.6576
20% 48h	79.85149	90.27081	63.54369	56.33534	64.8842	67.93223	71.6987	81.68741

Specific Aim 2: Calcium Arsenazo Assay Data (Figure 5-34)

Calcium Arsenazo Assay								
	Valve 1	**Valve 2**	**Valve 3**	**Valve 4**	**Valve 5**	**Valve 6**	**Valve 7**	**Valve 8**
10% 0	0.394424	0.394878	0.468454	0.482488	0.400571	0.501722	0.455168	0.454828
15% 0	1.945202	2.224382	3.204653	3.317657	2.679285	2.837263	2.167459	2.242772
10% 1	0.345596	0.35374	0.508979	0.453639	0.375413	0.352729	0.363508	0.297203
15% 1	2.607908	2.673528	1.259455	1.361717	2.218691	2.335904	0.921887	0.945449
10% 10	0.338147	0.320671	0.301116	0.292129	0.340587	0.27969	0.325897	0.350372
15% 10	0.94064	0.974173	1.031198	1.035517	1.116564	1.117648	0.744248	0.746256
10% 100	0.178005	0.263299	0.223116	0.243766	0.165104	0.164116	0.156877	0.153116
15% 100	0.23735	0.263489	0.445447	0.454091	0.327445	0.328979	0.454471	0.463933

Specific Aim 2: BMP-2 and BMP-4 Immunohistochemistry Semi-quantitative Data (Figure 5-30)

BMP-2	**Valve 1**	**Valve 2**	**Valve 3**	**Valve 4**	**Valve 5**	**Valve 6**
Fresh	1	1	1	1	1	1
10%	3.402125	3.671122	3.267442	6.895416	6.431354	3.079721
15%	5.641843	5.827349	3.584937	9.329872	10.31545	4.541252
BMP-4	**Valve 1**	**Valve 2**	**Valve 3**	**Valve 4**	**Valve 5**	**Valve 6**
Fresh	0.000886	0.001298	0.001626	0.002008	0.0012	0.00092
10%	0.014087	0.012934	0.006474	0.003809	0.00198	0.00234
15%	0.015853	0.009211	0.019284	0.031198	0.02384	0.016999

Specific Aim 2: TUNEL Apoptosis Immunoassay Data (Figure 5-28)

TUNEL								
	Valve 1	**Valve 2**	**Valve 3**	**Valve 4**	**Valve 5**	**Valve 6**	**Valve 7**	**Valve 8**
Fresh	1.01927	5	6	4	7	2	3	5
10%	14.66779	37.79399	33.87641	9.442577	19.17078	13	13.26902	38.06272
10% + N	1.045433	6.8154	7.047602	4.908659	1.43744	2.25607	0	2.391707
15%	476.5679	111.1291	312.4845	99.11179	86.31821	108.5202	109.4279	141.1557
15% + N	14.98428	20.54725	7.138638	12.22269	10.00842	11.05437	13.2451	11.09832

Specific Aim 2: Runx2 and Osteocalcin Western Blotting Data

Osteocalcin Data (Figure 5-32)						
	Valve 1	**Valve 2**	**Valve 3**	**Valve 4**	**Valve 5**	**Valve 6**
Fresh	1	1	1	1	1	1
10%	1.857216	5.171664	3.203433	1.167233	1.943386	2.668586
15%	8.367049	13.03946	5.044973	7.129567	7.658322	8.247875
10% + N	0.671591	2.581494	1.290787	1.105633	1.019387	1.333778
15% + N	1.466388	3.876753	1.371048	1.327724	1.49688	1.907759
Runx2 Data (Figure 5-31)						
	Valve 1	**Valve 2**	**Valve 3**	**Valve 4**	**Valve 5**	**Valve 6**
Fresh	1	1	1	1	1	1
10%	1.831763	1.000111	1.37194	1.16835	1.343041	1.176868
15%	1.804361	2.45853	1.915629	2.795498	2.243505	1.956406
10% + N	1.175335	1.185403	1.0766	0.971858	1.102299	1.045199
15% + N	1.482789	1.381135	1.476767	1.361462	1.425538	1.316699

Specific Aim 3: Collagen Assay Data (Figure 5-35 and Figure 5-36)

	10% Stretch	15% Stretch	10% Stretch	15% Stretch	10% Stretch	15% Stretch
Fresh	**Control**		**1 µM 5-HT**		**10 µM 5-HT**	
25.43414	28.26181276	43.503975	20.15718973	33.02112413	23.44422313	43.7544878
27.61053	14.54727184	35.65867617	21.09136074	22.73256443	41.82022606	39.28384142
26.41972	12.43651427	33.48333984	36.81572571	32.58053407	55.66459269	26.52372794
27.69644	40.38881454	42.79857353	20.15718973	36.6565683	24.78155382	41.69539522
10.30362	48.31500955	36.4666126	21.09136074	33.07506029	28.86758221	48.90164063
20.29598	20.39995557	33.17230155	36.81572571	32.27182205	46.85878876	56.0851301
23.25581	18.01037258	28.46175922		65.92443684	53.1706798	73.7428839
25.07663	29.32956429	39.28901868		54.30089012		40.08440799
23.95731	35.16191215			67.20370856		34.51489412
18.18966				37.02017685		43.14361765
29.40613						52.38867857
20.97179						59.87277551

10% Stretch	15% Stretch	10% Stretch	15% Stretch	10% Stretch	15% Stretch
100 µM 5-HT		**5-HT + ketanserin**		**5-HT + SB204741**	
22.06163115	13.25147241	26.64682867	29.60758741	29.88155323	59.76310645
7.43177976	17.28085188	18.91396552	21.01551724	28.2555	56.511
21.95462207	19.32639027	26.23878571	29.15420635	9.850096552	19.7001931
9.550460133	11.14393721	25.35711639	28.17457377	31.19803571	62.39607143
12.4333085	29.35529326	41.03169231	45.59076923	38.23741935	76.47483871
8.881403173	33.57039678	33.0930031	36.77000345	24.79832636	49.59665272
25.40648829	31.05900997	31.04514286	34.49460317	13.62482759	27.24965517
14.253537	40.58541956	19.43213115	21.59125683	31.35873016	62.71746032
	24.88812643				
	30.88250831				

Specific Aim 3: Mechanical Testing Data (Figure 5-39 and Figure 5-40)

Fresh Control							
Tension (N/m)		**F1**	**F2**	**F3**	**F4**	**F5**	**F6**
0		0	0	0	0	0	0
5		0.1986	0.1963	0.1945	0.2072	0.2027	0.1985
10		0.2029	0.2001	0.2029	0.2075	0.2018	0.2068
20		0.2052	0.2029	0.2062	0.2042	0.2033	0.2038
30		0.2057	0.2003	0.2057	0.2057	0.2042	0.2039
40		0.2068	0.2031	0.2068	0.2058	0.2055	0.2043
50		0.2077	0.2001	0.2078	0.2066	0.2077	0.2064
60		0.2101	0.2081	0.2083	0.209	0.2109	0.2101

10% Stretch Data

No 5-HT Control							
Tension (N/m)		**C1**	**C2**	**C3**	**C4**	**C5**	**C6**
0		0	0	0	0	0	0
5		0.1334	0.138	0.152	0.1525	0.1535	0.1574
10		0.1458	0.1524	0.1525	0.1526	0.1552	0.1577
20		0.1523	0.1524	0.1572	0.1573	0.1552	0.1578
30		0.152	0.1527	0.1603	0.1608	0.1596	0.1601
40		0.1531	0.1551	0.1607	0.1608	0.1613	0.1603
50		0.151	0.1511	0.1619	0.1621	0.1623	0.1633
60		0.15	0.1511	0.1611	0.1628	0.1627	0.1644

5-HT							
Tension (N/m)		**1**	**2**	**3**	**4**	**5**	**6**
0		0	0	0	0	0	0
5		0.1045	0.1047	0.1111	0.1121	0.1235	0.1279
10		0.1078	0.1082	0.1162	0.118	0.1303	0.1309
20		0.1108	0.1109	0.1198	0.12	0.1307	0.1311
30		0.1121	0.1128	0.1205	0.1207	0.1308	0.1317
40		0.1125	0.1131	0.1205	0.1209	0.1309	0.1313
50		0.1125	0.1133	0.1207	0.1207	0.1304	0.1315
60		0.1127	0.1137	0.1208	0.1222	0.1305	0.1317

5-HT-2A Inhibitor							
Tension (N/m)		**1**	**2**	**3**	**4**	**5**	**6**
0		0	0	0	0	0	0
5		0.1373	0.142	0.1518	0.152	0.1527	0.1528
10		0.1511	0.1524	0.152	0.1525	0.1528	0.1552
20		0.1522	0.1525	0.158	0.1581	0.1584	0.1586
30		0.1522	0.1518	0.1588	0.1598	0.158	0.1599
40		0.1526	0.1571	0.1586	0.1593	0.1593	0.1583
50		0.151	0.1577	0.1586	0.1594	0.1599	0.1601
60		0.1566	0.1578	0.1588	0.1594	0.1601	0.1599

5-HT-2B Inhibitor							
Tension (N/m)		**1**	**2**	**3**	**4**	**5**	**6**
0		0	0	0	0	0	0
5		0.1288	0.142	0.146	0.1453	0.1482	0.1507
10		0.1446	0.1456	0.152	0.1525	0.1524	0.1545
20		0.1498	0.1506	0.158	0.1581	0.1584	0.1575
30		0.1534	0.1578	0.1581	0.1588	0.1591	0.1582
40		0.1525	0.158	0.1586	0.162	0.1591	0.1615
50		0.1525	0.1574	0.1591	0.162	0.1599	0.1625
60		0.1527	0.1577	0.1591	0.1623	0.1601	0.1628

15% Stretch Data

No 5-HT Control								
Tension (N/m)		**C1**	**C2**	**C3**	**C4**	**C5**	**C6**	
0		0	0	0	0	0	0	
5		0.1259	0.139	0.1289	0.1277	0.1299	0.132	
10		0.1319	0.1437	0.1321	0.1299	0.131	0.1411	
20		0.1369	0.1444	0.1339	0.1301	0.134	0.1467	
30		0.1379	0.1458	0.1341	0.131	0.1371	0.149	
40		0.1389	0.1454	0.1351	0.1307	0.1391	0.151	
50		0.139	0.142	0.1401	0.1321	0.1411	0.1522	
60		0.1391	0.1436	0.1402	0.1333	0.1408	0.1598	

5-HT							
Tension (N/m)		**1**	**2**	**3**	**4**	**5**	**6**
0		0	0	0	0	0	0
5		0.0454	0.0668	0.0672	0.0659	0.0736	0.0611
10		0.0556	0.0686	0.0726	0.0686	0.0771	0.0717
20		0.0597	0.0705	0.0755	0.0705	0.0796	0.072
30		0.0648	0.0711	0.0756	0.0707	0.0806	0.0742
40		0.0661	0.0719	0.0767	0.0718	0.0804	0.0772
50		0.0694	0.0717	0.0771	0.0719	0.0806	0.0782
60		0.0686	0.0711	0.0758	0.0713	0.081	0.079

5-HT-2A Inhibitor							
Tension (N/m)		**1**	**2**	**3**	**4**	**5**	**6**
0		0	0	0	0	0	0
5		0.1207	0.1263	0.1297	0.1256	0.1292	0.1307
10		0.133	0.1362	0.1351	0.1355	0.1369	0.1343
20		0.1393	0.1398	0.1399	0.1398	0.1399	0.1426
30		0.1411	0.1411	0.1472	0.1433	0.1488	0.1493
40		0.1408	0.1413	0.1508	0.1436	0.1506	0.1509
50		0.141	0.1414	0.1532	0.1439	0.1532	0.1533
60		0.1411	0.1539	0.1544	0.1444	0.1563	0.1566

5-HT-2B Inhibitor							
Tension (N/m)		**1**	**2**	**3**	**4**	**5**	**6**
0		0	0	0	0	0	0
5		0.0848	0.0891	0.0935	0.099	0.0991	0.0888
10		0.0862	0.0866	0.0946	0.1012	0.1023	0.0901
20		0.0892	0.0917	0.0964	0.103	0.1031	0.0923
30		0.0875	0.096	0.0972	0.1035	0.1037	0.0945
40		0.089	0.0968	0.0987	0.1025	0.104	0.0999
50		0.0889	0.096	0.0999	0.1019	0.1041	0.1011
60		0.0914	0.099	0.0993	0.1028	0.1043	0.1034

Specific Aim 3: Mechanical Testing Data (Figure 5-41)

10% Stretch Samples

Fresh					
F1	**F2**	**F3**	**F4**	**F5**	**F6**
25.17623364	25.47121752	25.70694087	24.13127413	24.66699556	25.18891688
Control					
C1	**C2**	**C3**	**C4**	**C5**	**C6**
37.48125937	36.23188406	32.89473684	32.78688525	32.5732899	31.76620076
5-HT					
1	**2**	**3**	**4**	**5**	**6**
47.84688995	47.75549188	45.00450045	44.60303301	40.48582996	39.09304144
5-HT-2A Inhibitor					
1	**2**	**3**	**4**	**5**	**6**
36.41660597	35.21126761	32.93807642	32.89473684	32.74394237	32.72251309
5-HT-2B Inhibitor					
1	**2**	**3**	**4**	**5**	**6**
38.81987578	35.21126761	34.24657534	34.41156228	33.73819163	33.17850033

15% Stretch Samples

Fresh					
F1	**F2**	**F3**	**F4**	**F5**	**F6**
25.17623364	25.47121752	25.70694087	24.13127413	24.66699556	25.18891688
Control					
C1	**C2**	**C3**	**C4**	**C5**	**C6**
39.71405878	35.97122302	38.7897595	39.15426782	38.49114704	37.87878788
5-HT					
1	**2**	**3**	**4**	**5**	**6**
110.1321586	74.8502994	74.4047619	75.87253414	67.93478261	81.83306056
5-HT-2A Inhibitor					
1	**2**	**3**	**4**	**5**	**6**
41.42502071	39.58828187	38.55050116	39.8089172	38.6996904	38.25554705
5-HT-2B Inhibitor					
1	**2**	**3**	**4**	**5**	**6**
58.96226415	56.11672278	53.47593583	50.50505051	50.45408678	56.30630631

APPENDIX D MATLAB CODES

ANALYSIS OF PICROSIRIUS RED IMAGES

File name: Analysis_LATEST.m

```
      % This program reads in picrosirius red image files and
calculates
      % percentage of red, orange, yellow and green fibers in the
      % image.


      stain=imread('xxx.jpg'); %Image file name
      stain_cropped=imcrop(stain);
      figure;
% Magnifies image to simplify the selection of area of intest
      imshow(stain_cropped)
      stain_cropped=double(stain_cropped);
      stain_cropped_norm = stain_cropped./255;
      stain_cropped_thres= stain_cropped_norm > 0.1;
      stain_cropped_thres=double(stain_cropped_thres);
      stain1=stain_cropped_norm.*stain_cropped_thres;
      stain_hsv=rgb2hsv(stain1);
      hue_mat=stain_hsv(:,:,1);
      hue_mat1= hue_mat .* 255;
      [height width]=size(hue_mat1);
% Defines the hue values for a particular color
      H1=double(hue_mat1 > 2 & hue_mat1 < 9) + double(hue_mat1
>230 & hue_mat1 <256);
      H2=double(hue_mat1 > 10 & hue_mat1 < 38);
      H3= double(hue_mat1 > 39 & hue_mat1 < 51);
      H4= double(hue_mat1 > 52 & hue_mat1 < 128);
      figure;
% Shows the individual red, orange, yellow, green images based on
the above mentioned criteria
      imshow(H1)
      figure;
      imshow (H2)
      figure;
      imshow (H3)
      figure;
      imshow (H4)
      num_red=0;
      num_orange=0;
      num_yellow=0;
      num_green=0;
      num_total = height .* width;
      for i=1:height
          for j=1:width
              if(hue_mat1(i,j) > 2) && (hue_mat1(i,j) < 9)
```

```
                num_red = num_red + 1;
            elseif(hue_mat1(i,j)  >  230)  &&  (hue_mat1(i,j)  <
256)
                num_red = num_red + 1;
            elseif(hue_mat1(i,j) > 10) && (hue_mat1(i,j) < 38)
                num_orange = num_orange + 1;
            elseif(hue_mat1(i,j) > 39) && (hue_mat1(i,j) < 51)
                num_yellow = num_yellow + 1;
            elseif(hue_mat1(i,j) > 52) && (hue_mat1(i,j) < 128)
                num_green = num_green + 1;
            end
        end
    end
% Displays the percentage of fibers that are red, orange, yellow,
or green
    (num_red/num_total).*100
    (num_orange/num_total).*100
    (num_yellow/num_total).*100
    (num_green/num_total).*100
```

AUTOMATED MARKER TRACKING CODE

The following marker tracking code was developed by Yap Choon Hwai from the Cardiovascular Fluid Mechanics Laboratory.

File name: automarkertrack5.m

```
function automarkertrack5

% This program automatically tracks 1 marker over multiple
% consequtive high speed camera images, provided the marker
% does not traverse too far between the images.
% This program has a re-click function that allows you to
% bring the tracking point back to the marker if the marker
% 'strays away' between images.

%instructions:
%1. change path and file name to retrieve images
%2. change "ind". This is the starting and ending image #.
%3. change output file name: out1
%3b. change the number of markers to track, n=??;
%4. run program
%5. click on point to track
%6. press enter to go to the next image, or 1 to repeat clicking
%7. resultant data is stored in txt file you named

path1='C:\xxx'; %path where image files are stored
name1='image'; %name (leader) for the images
out1='C:\yyy'; %path where output files for marker coordinates go

% This is to specify the number of markers to track
n=8;

% Specify the number for the images
ind=[000:999];
[s1 s2]=size(ind);

pathnfile1=[path1 '\' name1 sprintf('%3.3d',ind(1)) '.tif'];
M1=imread(pathnfile1,'tif');
        %M1=1./(1+exp(-(double(M1)-90)/20));
        %M1=uint8(M1*255);
imshow(M1);
zoom=ginput(1);
zoomcenter(zoom(1),zoom(2),2)
N=ginput(n);

for i=1:n
    NN{i}=[];
end
```

```
      for i=1:s2

          pathnfile1=[path1 '\' name1 sprintf('%3.3d',ind(i)) '.tif'];
          M1=imread(pathnfile1,'tif');
              %M2=1./(1+exp(-(double(M1(zoom(2)-
200:zoom(2)+200,zoom(1)-200:zoom(1)+200))-90)/20));
              %M2=uint8(M2*255);
              %M1(zoom(2)-200:zoom(2)+200,zoom(1)-200:zoom(1)+200)=M1;

          for j=1:n
              N(j,:)=automarkertrack(M1,N(j,:));
              N(j,:)=automarkertrack(M1,N(j,:));
              N(j,:)=automarkertrack(M1,N(j,:));
          end

          imshow(M1);
          zoomcenter(zoom(1),zoom(2),2)
          hold on
          plot(N(:,1),N(:,2),'r*');
          hold off
          ind(i)

          %rep=0;
          %rep=input('enter 0 to repeat  ');
          %while rep==0
          %    imshow(M1);
          %    zoomcenter(zoom(1),zoom(2),2)
          %    N=ginput(n);
          %    for j=1:n
          %        N(j,:)=automarkertrack(M1,N(j,:));
          %        N(j,:)=automarkertrack(M1,N(j,:));
          %        N(j,:)=automarkertrack(M1,N(j,:));
          %    end
          %    hold on
          %    plot(N(:,1),N(:,2),'r*');
          %    hold off
          %    ind(i)
          %    rep=[];
          %    rep=input('enter 0 to repeat');
          %end

          for j=1:n
              NN{j}=[NN{j};N(j,:)];
          end

      %    for j=1:9
      %        out2=[out1 num2str(j) '.txt'];
      %               dlmwrite(out2,NN{j},  'delimiter',  '','newline',
'pc','precision','%15.10f');
      %    end

      end

      for j=1:n
```

```
        out2=[out1 num2str(j) '.txt'];
        dlmwrite(out2,NN{j},        'delimiter',        '','newline',
'pc','precision','%15.10f');
    end
```

File name: automarkertrack.m

```
    function N=automarkertrack(M,N)

    %figure(1)
    %imshow(M)
    pixel=25;
    num=16;

    %N=ginput(1);
    distance=[-pixel:pixel]';

    count=1;
    for angle=0:pi/num:pi/num*(num-1)
        p=[distance*cos(angle)+N(1), distance*sin(angle)+N(2)];
        p=round(p);
        [s1 s2]=size(p);
        int=[];
        for i=1:s1
            int(i)=M(p(i,2),p(i,1));
        end

        %figure
        %plot(distance,int,'r*')
        %hold on

        fitpol=leastsq(distance,int',8);
        int2=fitpol{1};
        %plot(distance,int2)
        %hold off

        beta=fitpol(269);
        beta=flipud(beta);
        s1=length(beta);
        index=flipud([1:s1-1]');
        p=beta(1:s1-1).*index;
        r=roots(p);

        %this portion has been changed due to difficulty in tracking
        a=find(abs(r)==min(abs(r)));
        if length(a)>1
            a=a(1);
        end
        centroid(count)=real(r(a));
    %    centroid(count)=r(find(abs(r)==min(abs(r))));
```

```
    count=count+1;
end

angle=[0:pi/num:pi/num*(num-1)]';
cosine=cos(angle);
sine=sin(angle);
centroid2=[centroid'.*cosine, centroid'.*sine];
[s1 s2]=size(centroid2);
centroid3=sum(centroid2)/s1;
N=N+centroid3;
%figure(1)
%hold on
%plot(N(1),N(2),'r*');
%hold off
```

File name: leastsq.m

```
function results=leastsq(z,G,ord)

%least square fit to find Gfit.
%z is unvaried x-axis parameter
%ord is the order of the polynomial used for the fit

% Basic principles:
% fitted values {Gfit}=[X]*{beta}
% {beta} is vector of coefficients
% For least square, [X]*{beta}-{G} is orthogonal to [X]
% thus [X]'*([X]*{beta}-{G})=0

zz=ones(length(z),1);
X=[zz];

for i=1:ord
    zz=z.*zz;
    X=[X zz];
end

beta=inv(X'*X)*X'*G;

Gfit=X*beta;

results={Gfit beta};
```

APPENDIX E ALIZARIN RED IMAGES

As mentioned in the Discussion chapter, calcification was only achievable by both cyclic stretch and osteogenic medium. This appendix compiles representative micrographs of valves that were either (i) only stretched, or (ii) only exposed to osteogenic medium under static culture conditions.

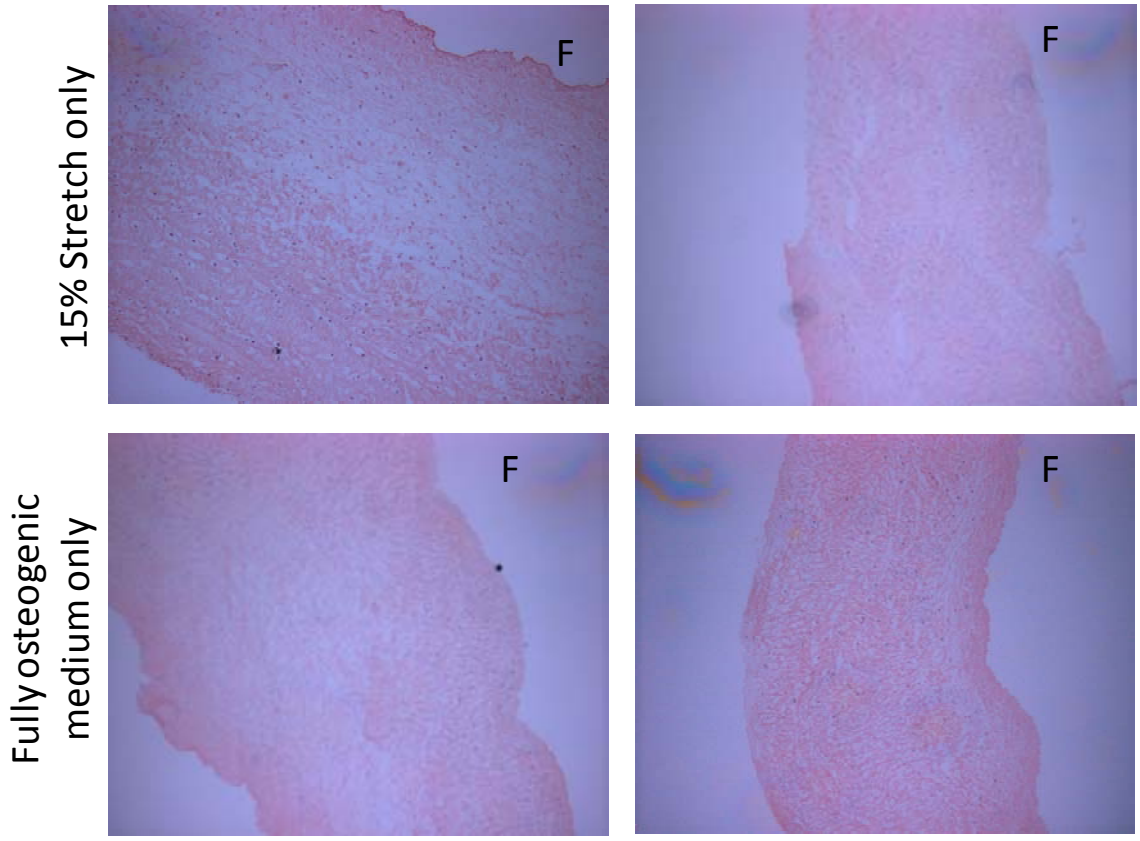

Figure E-1: Representative micrographs of valves stretch to 15% and valves cultured in fully osteogenic medium. Samples show no evidence of positive Alizarin Red staining.

APPENDIX F RADIAL STRETCH EXPERIMENTS

This thesis only studied the effects of circumferential stretch on aortic valve cusp samples. As mentioned in the Discussion chapter, based on Thubrikar's experiments, *in vivo* radial stretches are well within the loading regime of the aortic valve cusp. Uniaxial cyclic stretch experiments on radially aligned strips were therefore not considered to be of crucial importance. To verify this, we conducted pilot experiments in the following manner. Radially aligned 5x15mm rectangular sections were stretched to 30% for 48 hours in the tensile stretch bioreactor. These samples were then assayed for collagen content. The results demonstrated that there were no significant differences in collagen content between fresh, static and stretched samples. A decreasing trend can be observed in the plot below, but the p-value was large ($p>0.1$). This result demonstrates that cyclic stretch was unable to result in increased collagen content as was observed in circumferentially aligned tissue samples.

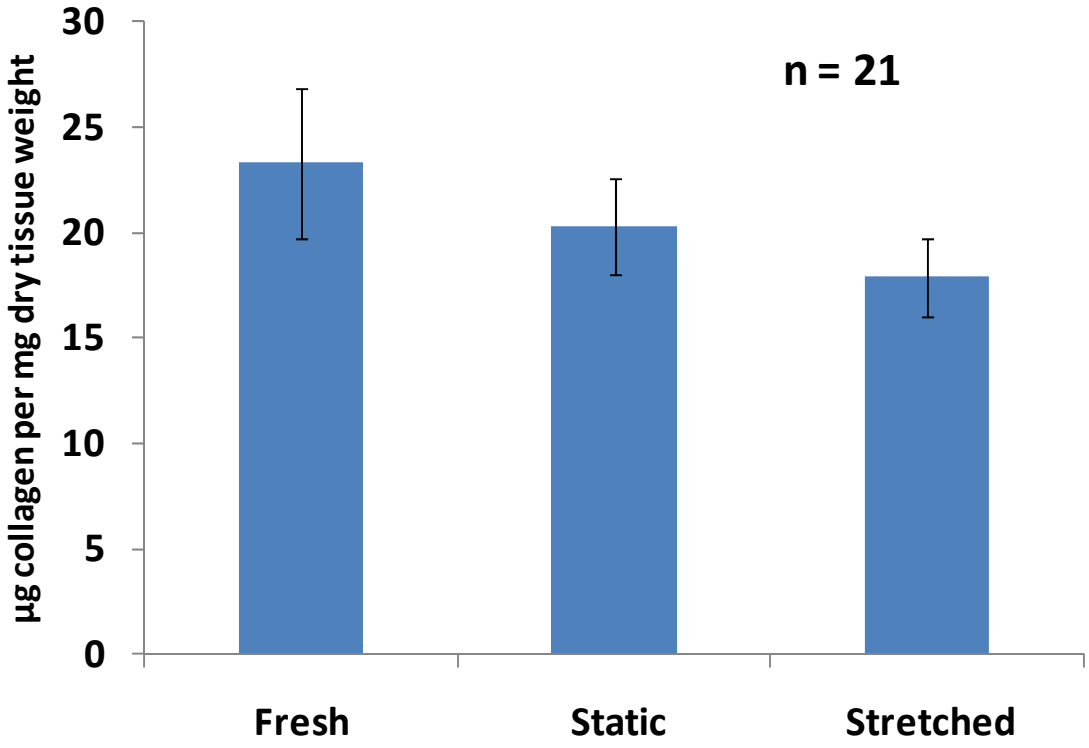

Figure F-1: There was no significant difference in collagen content between fresh, static and radially stretched samples.

REFERENCES

1. **Aggarwal M, and Khan IA**. Hypertensive crisis: hypertensive emergencies and urgencies. *Cardiol Clin* 24: 135-146, 2006.

2. **Aikawa E, Aikawa M, Libby P, Figueiredo JL, Rusanescu G, Iwamoto Y, Fukuda D, Kohler RH, Shi GP, Jaffer FA, and Weissleder R**. Arterial and aortic valve calcification abolished by elastolytic cathepsin S deficiency in chronic renal disease. *Circulation* 119: 1785-1794, 2009.

3. **Aikawa E, Whittaker P, Farber M, Mendelson K, Padera RF, Aikawa M, and Schoen FJ**. Human semilunar cardiac valve remodeling by activated cells from fetus to adult: implications for postnatal adaptation, pathology, and tissue engineering. *Circulation* 113: 1344-1352, 2006.

4. **Akhtar M, Tuzcu EM, Kapadia SR, Svensson LG, Greenberg RK, Roselli EE, Halliburton S, Kurra V, Schoenhagen P, and Sola S**. Aortic root morphology in patients undergoing percutaneous aortic valve replacement: evidence of aortic root remodeling. *J Thorac Cardiovasc Surg* 137: 950-956, 2009.

5. **Arora PD, and McCulloch CA**. Dependence of collagen remodelling on alpha-smooth muscle actin expression by fibroblasts. *J Cell Physiol* 159: 161-175, 1994.

6. **Baaijens F, Bouten C, Hoerstrup S, Mol A, Driessen N, and Boerboom R**. Functional tissue engineering of the aortic heart valve. *Clin Hemorheol Microcirc* 33: 197-199, 2005.

7. **Balachandran K, Konduri S, Sucosky P, Jo H, and Yoganathan AP**. An ex vivo study of the biological properties of porcine aortic valves in response to circumferential cyclic stretch. *Ann Biomed Eng* 34: 1655-1665, 2006.

8. **Balachandran K, Sucosky P, Jo H, and Yoganathan AP**. Elevated Cyclic Stretch Alters Matrix Remodeling in Aortic Valve Cusps - Implications for Degenerative Aortic Valve Disease? *Am J Physiol Heart Circ Physiol* 2009.

9. **Barron V, Lyons E, Stenson-Cox C, Mchugh PE, and Pandit A**. Bioreactors for cardiovascular cell and tissue growth: A review. *Annals of Biomedical Engineering* 31: 1017-1030, 2003.

10. **Bartlett D, Wright M, Yayanos A, and Silverman M**. Interstitial cells of the heart valves possess characteristics similar to smooth muscle cells. *Nature* 342: 572-574, 1989.

11. **Baxley WA**. Aortic valve disease. *Current opinion in cardiology* 9: 152-157, 1994.

12. **Bernheim AM, Connolly HM, Hobday TJ, Abel MD, and Pellikka PA**. Carcinoid heart disease. *Prog Cardiovasc Dis* 49: 439-451, 2007.

13. **Bernheim AM, Connolly HM, and Pellikka PA**. Carcinoid heart disease. *Curr Treat Options Cardiovasc Med* 9: 482-489, 2007.

14. **Bernheim AM, Connolly HM, and Pellikka PA**. Carcinoid heart disease in patients without hepatic metastases. *The American journal of cardiology* 99: 292-294, 2007.

15. **Billiar KL, and Sacks MS**. Biaxial mechanical properties of the native and glutaraldehyde-treated aortic valve cusp: Part II--A structural constitutive model. *J Biomech Eng* 122: 327-335, 2000.

16. **Billiar KL, and Sacks MS**. Biaxial mechanical properties of the natural and glutaraldehyde treated aortic valve cusp--Part I: Experimental results. *J Biomech Eng* 122: 23-30, 2000.

17. **Bosman FT, and Stamenkovic I**. Functional structure and composition of the extracellular matrix. *The Journal of pathology* 200: 423-428, 2003.

18. **Bostrom K, Watson KE, Horn S, Wortham C, Herman IM, and Demer LL**. Bone morphogenetic protein expression in human atherosclerotic lesions. *The Journal of clinical investigation* 91: 1800-1809, 1993.

19. **Brattelid T, Qvigstad E, Birkeland JA, Swift F, Bekkevold SV, Krobert KA, Sejersted OM, Skomedal T, Osnes JB, Levy FO, and Sjaastad I**. Serotonin responsiveness through 5-HT2A and 5-HT4 receptors is differentially regulated in hypertrophic and failing rat cardiac ventricle. *J Mol Cell Cardiol* 43: 767-779, 2007.

20. **Braverman AC**. Bicuspid aortic valve and associated aortic wall abnormalities. *Current opinion in cardiology* 11: 501-503, 1996.

21. **Braverman AC, Guven H, Beardslee MA, Makan M, Kates AM, and Moon MR**. The bicuspid aortic valve. *Curr Probl Cardiol* 30: 470-522, 2005.

22. **Brewer RJ, Mentzer RM, Jr., Deck JD, Ritter RC, Trefil JS, and Nolan SP**. An in vivo study of the dimensional changes of the aortic valve leaflets during the cardiac cycle. *J Thorac Cardiovasc Surg* 74: 645-650, 1977.

23. **Butcher JT, and Nerem RM**. Valvular endothelial cells and the mechanoregulation of valvular pathology. *Philosophical transactions of the Royal Society of London* 362: 1445-1457, 2007.

24. **Butcher JT, Penrod AM, Garcia AJ, and Nerem RM**. Unique morphology and focal adhesion development of valvular endothelial cells in static and fluid flow environments. *Arterioscler Thromb Vasc Biol* 24: 1429-1434, 2004.

25. **Butcher JT, Simmons CA, and Warnock JN**. Mechanobiology of the aortic heart valve. *J Heart Valve Dis* 17: 62-73, 2008.

26. **Butcher JT, Tressel S, Johnson T, Turner D, Sorescu G, Jo H, and Nerem RM**. Transcriptional profiles of valvular and vascular endothelial cells reveal phenotypic differences: influence of shear stress. *Arterioscler Thromb Vasc Biol* 26: 69-77, 2006.

27. **Carew EO, Garg A, Barber JE, and Vesely I**. Stress relaxation preconditioning of porcine aortic valves. *Ann Biomed Eng* 32: 563-572, 2004.

28. **Carpentier A, Deloche A, Relland J, Fabiani JN, Forman J, Camilleri JP, Soyer R, and Dubost C**. Six-year follow-up of glutaraldehyde-preserved heterografts. With particular reference to the treatment of congenital valve malformations. *J Thorac Cardiovasc Surg* 68: 771-782, 1974.

29. **Cataloglu A, Clark RE, and Gould PL**. Stress analysis of aortic valve leaflets with smoothed geometrical data. *J Biomech* 10: 153-158, 1977.

30. **Chambers JC, Somerville J, Stone S, and Ross DN**. Pulmonary autograft procedure for aortic valve disease: long-term results of the pioneer series. *Circulation* 96: 2206-2214, 1997.

31. **Chang K, Weiss D, Suo J, Vega JD, Giddens D, Taylor WR, and Jo H**. Bone morphogenic protein antagonists are coexpressed with bone morphogenic protein 4 in endothelial cells exposed to unstable flow in vitro in mouse aortas and in human coronary arteries: role of bone morphogenic protein antagonists in inflammation and atherosclerosis. *Circulation* 116: 1258-1266, 2007.

32. **Chesler NC, Ku DN, and Galis ZS**. Transmural pressure induces matrix-degrading activity in porcine arteries ex vivo. *Am J Physiol* 277: H2002-2009, 1999.

33. **Chester AH, Misfeld M, Sievers HH, and Yacoub MH**. Influence of 5-hydroxytryptamine on aortic valve competence in vitro. *J Heart Valve Dis* 10: 822-825; discussion 825-826, 2001.

34. **Chester AH, Misfeld M, and Yacoub MH**. Receptor-mediated contraction of aortic valve leaflets. *J Heart Valve Dis* 9: 250-254; discussion 254-255, 2000.

35. **Chester AH, and Taylor PM**. Molecular and functional characteristics of heart-valve interstitial cells. *Philosophical transactions of the Royal Society of London* 362: 1437-1443, 2007.

36. **Chiu JJ, Chen CN, Lee PL, Yang CT, Chuang HS, Chien S, and Usami S**. Analysis of the effect of disturbed flow on monocytic adhesion to endothelial cells. *J Biomech* 36: 1883-1895, 2003.

37. **Chiu JJ, Chen LJ, Lee CI, Lee PL, Lee DY, Tsai MC, Lin CW, Usami S, and Chien S**. Mechanisms of induction of endothelial cell E-selectin expression by smooth muscle cells and its inhibition by shear stress. *Blood* 110: 519-528, 2007.

38. **Chiu JJ, Lee PL, Chen CN, Lee CI, Chang SF, Chen LJ, Lien SC, Ko YC, Usami S, and Chien S**. Shear stress increases ICAM-1 and decreases VCAM-1 and E-selectin expressions induced by tumor necrosis factor-[alpha] in endothelial cells. *Arterioscler Thromb Vasc Biol* 24: 73-79, 2004.

39. **Chong M, Eng M, and Missirlis YF**. Aortic valve mechanics. Part II: a stress analysis of the porcine aortic valve leaflets in diastole. *Biomater Med Devices Artif Organs* 6: 225-244, 1978.

40. **Christie GW**. Anatomy of aortic heart valve leaflets: the influence of glutaraldehyde fixation on function. *Eur J Cardiothorac Surg* 6 Suppl 1: S25-32; discussion S33, 1992.

41. **Christie GW, and Barratt-Boyes BG**. Age-dependent changes in the radial stretch of human aortic valve leaflets determined by biaxial testing. *Ann Thorac Surg* 60: S156-158; discussion S159, 1995.

42. **Christie GW, and Barratt-Boyes BG**. Biaxial mechanical properties of explanted aortic allograft leaflets. *Ann Thorac Surg* 60: S160-164, 1995.

43. **Christie GW, and Barratt-Boyes BG**. Mechanical properties of porcine pulmonary valve leaflets: how do they differ from aortic leaflets? *Ann Thorac Surg* 60: S195-199, 1995.

44. **Cipriani A, Brambilla P, Furukawa T, Geddes J, Gregis M, Hotopf M, Malvini L, and Barbui C**. Fluoxetine versus other types of pharmacotherapy for depression. *Cochrane Database Syst Rev* CD004185, 2005.

45. **Clark-Greuel JN, Connolly JM, Sorichillo E, Narula NR, Rapoport HS, Mohler ER, 3rd, Gorman JH, 3rd, Gorman RC, and Levy RJ**. Transforming growth factor-beta1 mechanisms in aortic valve calcification: increased alkaline phosphatase and related events. *Ann Thorac Surg* 83: 946-953, 2007.

46. **Connolly HM, Crary JL, McGoon MD, Hensrud DD, Edwards BS, Edwards WD, and Schaff HV**. Valvular heart disease associated with fenfluramine-phentermine. *The New England journal of medicine* 337: 581-588, 1997.

47. **Connolly HM, Schaff HV, Mullany CJ, Rubin J, Abel MD, and Pellikka PA**. Surgical management of left-sided carcinoid heart disease. *Circulation* 104: I36-40, 2001.

48. **Corden J, David T, and Fisher J**. Determination of the curvatures and bending strains in open trileaflet heart valves. *Proc Inst Mech Eng H* 209: 121-128, 1995.

49. **Csiszar A, Ahmad M, Smith KE, Labinskyy N, Gao Q, Kaley G, Edwards JG, Wolin MS, and Ungvari Z**. Bone morphogenetic protein-2 induces proinflammatory endothelial phenotype. *Am J Pathol* 168: 629-638, 2006.

50. **Csiszar A, Smith KE, Koller A, Kaley G, Edwards JG, and Ungvari Z**. Regulation of bone morphogenetic protein-2 expression in endothelial cells: role of nuclear factor-kappaB activation by tumor necrosis factor-alpha, H2O2, and high intravascular pressure. *Circulation* 111: 2364-2372, 2005.

51. **Dale L, and Jones CM**. BMP signalling in early Xenopus development. *Bioessays* 21: 751-760, 1999.

52. **David TE, and Feindel CM**. An aortic valve-sparing operation for patients with aortic incompetence and aneurysm of the ascending aorta. *J Thorac Cardiovasc Surg* 103: 617-621; discussion 622, 1992.

53. **Davies PF, Passerini AG, and Simmons CA**. Aortic valve: turning over a new leaf(let) in endothelial phenotypic heterogeneity. *Arterioscler Thromb Vasc Biol* 24: 1331-1333, 2004.

54. **Deck JD**. Endothelial cell orientation on aortic valve leaflets. *Cardiovasc Res* 20: 760-767, 1986.

55. **Deutscher S, Rockette HE, and Krishnaswami V**. Diabetes and hypercholesterolemia among patients with calcific aortic stenosis. *J Chronic Dis* 37: 407-415, 1984.

56. **Dhore CR, Cleutjens JP, Lutgens E, Cleutjens KB, Geusens PP, Kitslaar PJ, Tordoir JH, Spronk HM, Vermeer C, and Daemen MJ**. Differential expression of bone matrix regulatory proteins in human atherosclerotic plaques. *Arterioscler Thromb Vasc Biol* 21: 1998-2003, 2001.

57. **Dollery CM, McEwan JR, and Henney AM**. Matrix metalloproteinases and cardiovascular disease. *Circ Res* 77: 863-868, 1995.

58. **Durbin A, Nadir NA, Rosenthal A, and Gotlieb AI**. Nitric oxide promotes in vitro interstitial cell heart valve repair. *Cardiovasc Pathol* 14: 12-18, 2005.

59. **Durbin AD, and Gotlieb AI**. Advances towards understanding heart valve response to injury. *Cardiovasc Pathol* 11: 69-77, 2002.

60. **Duwel P, Jungling E, Westhofen M, and Luckhoff A**. Potassium currents in vestibular type ii hair cells activated by hydrostatic pressure. *Neuroscience* 116: 963-972, 2003.

61. **Einav S, Stolero D, Avidor JM, Elad D, and Talbot L**. Wall shear stress distribution along the cusp of a tri-leaflet prosthetic valve. *J Biomed Eng* 12: 13-18, 1990.

62. **El-Hamamsy I, Balachandran K, Yacoub MH, Stevens LM, Sarathchandra P, Taylor PM, Yoganathan AP, and Chester AH**. Endothelium-dependent regulation of the mechanical properties of aortic valve cusps. *J Am Coll Cardiol* 53: 1448-1455, 2009.

63. **El-Hamamsy I, Yacoub MH, and Chester AH**. Neuronal regulation of aortic valve cusps. *Curr Vasc Pharmacol* 7: 40-46, 2009.

64. **Engelmayr GC, Jr., Hildebrand DK, Sutherland FW, Mayer JE, Jr., and Sacks MS**. A novel bioreactor for the dynamic flexural stimulation of tissue engineered heart valve biomaterials. *Biomaterials* 24: 2523-2532, 2003.

65. **Engelmayr GC, Jr., Rabkin E, Sutherland FW, Schoen FJ, Mayer JE, Jr., and Sacks MS**. The independent role of cyclic flexure in the early in vitro development of an engineered heart valve tissue. *Biomaterials* 26: 175-187, 2005.

66. **Engelmayr GC, Jr., Soletti L, Vigmostad SC, Budilarto SG, Federspiel WJ, Chandran KB, Vorp DA, and Sacks MS**. A novel flex-stretch-flow bioreactor for the study of engineered heart valve tissue mechanobiology. *Ann Biomed Eng* 36: 700-712, 2008.

67. **Fainsod A, Deissler K, Yelin R, Marom K, Epstein M, Pillemer G, Steinbeisser H, and Blum M**. The dorsalizing and neural inducing gene follistatin is an antagonist of BMP-4. *Mech Dev* 63: 39-50, 1997.

68. **Ferraro JT, Daneshmand M, Bizios R, and Rizzo V**. Depletion of plasma membrane cholesterol dampens hydrostatic pressure and shear stress-induced mechanotransduction pathways in osteoblast cultures. *Am J Physiol Cell Physiol* 286: C831-839, 2004.

69. **Fishman AP**. Aminorex to fen/phen: an epidemic foretold. *Circulation* 99: 156-161, 1999.

70. **Fitzgerald LW, Burn TC, Brown BS, Patterson JP, Corjay MH, Valentine PA, Sun JH, Link JR, Abbaszade I, Hollis JM, Largent BL, Hartig PR, Hollis GF, Meunier PC, Robichaud AJ, and Robertson DW**. Possible role of valvular serotonin 5-HT(2B) receptors in the cardiopathy associated with fenfluramine. *Mol Pharmacol* 57: 75-81, 2000.

71. **Fondard O, Detaint D, Iung B, Choqueux C, Adle-Biassette H, Jarraya M, Hvass U, Couetil JP, Henin D, Michel JB, Vahanian A, and Jacob MP**. Extracellular matrix remodelling in human aortic valve disease: the role of matrix metalloproteinases and their tissue inhibitors. *European heart journal* 26: 1333-1341, 2005.

72. **Fox CS, Guo CY, Larson MG, Vasan RS, Parise H, O'Donnell CJ, D'Agostino RB, Sr., Keaney JF, Jr., and Benjamin EJ**. Relations of inflammation and

novel risk factors to valvular calcification. *The American journal of cardiology* 97: 1502-1505, 2006.

73. **Frater RW, Gong G, Hoffman D, and Liao K**. Endothelial covering of biological artificial heart valves. *Ann Thorac Surg* 53: 371-372, 1992.

74. **Freeman RV, and Otto CM**. Spectrum of calcific aortic valve disease: pathogenesis, disease progression, and treatment strategies. *Circulation* 111: 3316-3326, 2005.

75. **Frishman WH, and Grewall P**. Serotonin and the heart. *Ann Med* 32: 195-209, 2000.

76. **Frishman WH, Huberfeld S, Okin S, Wang YH, Kumar A, and Shareef B**. Serotonin and serotonin antagonism in cardiovascular and non-cardiovascular disease. *J Clin Pharmacol* 35: 541-572, 1995.

77. **Furchgott RF, and Vanhoutte PM**. Endothelium-derived relaxing and contracting factors. *FASEB J* 3: 2007-2018, 1989.

78. **Garvey W, Fathi A, Bigelow F, Carpenter B, and Jimenez C**. Improved Movat pentachrome stain. *Stain Technol* 61: 60-62, 1986.

79. **Ge L, Leo HL, Sotiropoulos F, and Yoganathan AP**. Flow in a mechanical bileaflet heart valve at laminar and near-peak systole flow rates: CFD simulations and experiments. *J Biomech Eng* 127: 782-797, 2005.

80. **Gerosa G, McKay R, and Ross DN**. Replacement of the aortic valve or root with a pulmonary autograft in children. *Ann Thorac Surg* 51: 424-429, 1991.

81. **Gershon MD**. Review article: roles played by 5-hydroxytryptamine in the physiology of the bowel. *Aliment Pharmacol Ther* 13 Suppl 2: 15-30, 1999.

82. **Ghaisas NK, Foley JB, O'Briain DS, Crean P, Kelleher D, and Walsh M**. Adhesion molecules in nonrheumatic aortic valve disease: endothelial expression, serum levels and effects of valve replacement. *J Am Coll Cardiol* 36: 2257-2262, 2000.

83. **Grande-Allen KJ, Cochran RP, Reinhall PG, and Kunzelman KS**. Mechanisms of aortic valve incompetence: finite-element modeling of Marfan syndrome. *J Thorac Cardiovasc Surg* 122: 946-954, 2001.

84. **Grande-Allen KJ, Griffin BP, Ratliff NB, Cosgrove DM, and Vesely I**. Glycosaminoglycan profiles of myxomatous mitral leaflets and chordae parallel the severity of mechanical alterations. *J Am Coll Cardiol* 42: 271-277, 2003.

85. **Grande-Allen KJ, Mako WJ, Calabro A, Shi Y, Ratliff NB, and Vesely I**. Loss of chondroitin 6-sulfate and hyaluronan from failed porcine bioprosthetic valves. *J Biomed Mater Res A* 65: 251-259, 2003.

86. **Grande-Allen KJ, Osman N, Ballinger ML, Dadlani H, Marasco S, and Little PJ**. Glycosaminoglycan synthesis and structure as targets for the prevention of calcific aortic valve disease. *Cardiovasc Res* 76: 19-28, 2007.

87. **Grashow JS, Sacks MS, Liao J, and Yoganathan AP**. Planar biaxial creep and stress relaxation of the mitral valve anterior leaflet. *Ann Biomed Eng* 34: 1509-1518, 2006.

88. **Grashow JS, Yoganathan AP, and Sacks MS**. Biaixal stress-stretch behavior of the mitral valve anterior leaflet at physiologic strain rates. *Ann Biomed Eng* 34: 315-325, 2006.

89. **Griffith LG, and Naughton G**. Tissue engineering--current challenges and expanding opportunities. *Science* 295: 1009-1014, 2002.

90. **Gustafsson BI, Hauso O, Drozdov I, Kidd M, and Modlin IM**. Carcinoid heart disease. *International journal of cardiology* 2008.

91. **Gustafsson BI, Tommeras K, Nordrum I, Loennechen JP, Brunsvik A, Solligard E, Fossmark R, Bakke I, Syversen U, and Waldum H**. Long-term serotonin administration induces heart valve disease in rats. *Circulation* 111: 1517-1522, 2005.

92. **Haase J, Killian AM, Magnani F, and Williams C**. Regulation of the serotonin transporter by interacting proteins. *Biochem Soc Trans* 29: 722-728, 2001.

93. **Hafizi S, Taylor PM, Chester AH, Allen SP, and Yacoub MH**. Mitogenic and secretory responses of human valve interstitial cells to vasoactive agents. *J Heart Valve Dis* 9: 454-458, 2000.

94. **Hakuno D, Kimura N, Yoshioka M, and Fukuda K**. Molecular mechanisms underlying the onset of degenerative aortic valve disease. *J Mol Med* 87: 17-24, 2009.

95. **Harasaki H, Hanano H, Tanaka J, Tokunaga K, and Torisu M**. Surface structure of the human cardiac valve. A comparative study of normal and diseased valves. *J Cardiovasc Surg (Torino)* 19: 281-290, 1978.

96. **Harken DE, Taylor WJ, Lefemine AA, Lunzer S, Low HB, Cohen ML, and Jacobey JA**. Aortic valve replacement with a caged ball valve. *The American journal of cardiology* 9: 292-299, 1962.

97. **Hauso O, Gustafsson BI, Loennechen JP, Stunes AK, Nordrum I, and Waldum HL**. Long-term serotonin effects in the rat are prevented by terguride. *Regul Pept* 143: 39-46, 2007.

98. **Helmke B, and Davies P**. The cytoskeleton under esternal fluid mechanical forces: hemodynamic forces acting on the endothelium. *Annals of Biomedical Engineering* 30: 284-296, 2002.

99. **Helske S, Syvaranta S, Lindstedt KA, Lappalainen J, Oorni K, Mayranpaa MI, Lommi J, Turto H, Werkkala K, Kupari M, and Kovanen PT**. Increased expression of elastolytic cathepsins S, K, and V and their inhibitor cystatin C in stenotic aortic valves. *Arterioscler Thromb Vasc Biol* 26: 1791-1798, 2006.

100. **Hilbert SL, Luna RE, Zhang J, Wang Y, Hopkins RA, Yu ZX, and Ferrans VJ**. Allograft heart valves: the role of apoptosis-mediated cell loss. *J Thorac Cardiovasc Surg* 117: 454-462, 1999.

101. **Hoekstra F, Knoop C, Aghai Z, Jutte N, Mochtar B, Bos E, and Weimar W**. Stimulation of immune-competent cells in vitro by human cardiac valve-derived endothelial cells. *Ann Thorac Surg* 60: S131-133; discussion S133-134, 1995.

102. **Hoerstrup SP, Zund G, Ye Q, Schoeberlein A, Schmid AC, and Turina MI**. Tissue engineering of a bioprosthetic heart valve: stimulation of extracellular matrix assessed by hydroxyproline assay. *ASAIO J* 45: 397-402, 1999.

103. **Hogan BL**. Bone morphogenetic proteins in development. *Curr Opin Genet Dev* 6: 432-438, 1996.

104. **Hopkins RA**. Aortic valve leaflet sparing and salvage surgery: evolution of techniques for aortic root reconstruction. *Eur J Cardiothorac Surg* 24: 886-897, 2003.

105. **Horschitz S, Hummerich R, and Schloss P**. Structure, function and regulation of the 5-hydroxytryptamine (serotonin) transporter. *Biochem Soc Trans* 29: 728-732, 2001.

106. **Horvath J, Fross RD, Kleiner-Fisman G, Lerch R, Stalder H, Liaudat S, Raskoff WJ, Flachsbart KD, Rakowski H, Pache JC, Burkhard PR, and Lang AE**. Severe multivalvular heart disease: a new complication of the ergot derivative dopamine agonists. *Mov Disord* 19: 656-662, 2004.

107. **Hurst JW**. *The Heart, arteries and veins*. New York: McGraw-Hill, 1986.

108. **Hwang J, Saha A, Boo YC, Sorescu GP, McNally JS, Holland SM, Dikalov S, Giddens DP, Griendling KK, Harrison DG, and Jo H**. Oscillatory shear stress stimulates endothelial production of O2- from p47phox-dependent NAD(P)H oxidases, leading to monocyte adhesion. *J Biol Chem* 278: 47291-47298, 2003.

109. **Ikhumetse JD, Konduri S, Warnock JN, Xing Y, and Yoganathand AP**. Cyclic aortic pressure affects the biological properties of porcine pulmonary valve leaflets. *J Heart Valve Dis* 15: 295-302, 2006.

110. **Jaffee OC**. The development of the arterial outflow tract in the chick embryo heart. *Anat Rec* 158: 35-42, 1967.

111. **Jaffer FA, Kim DE, Quinti L, Tung CH, Aikawa E, Pande AN, Kohler RH, Shi GP, Libby P, and Weissleder R**. Optical visualization of cathepsin K activity in atherosclerosis with a novel, protease-activatable fluorescence sensor. *Circulation* 115: 2292-2298, 2007.

112. **Jian B, Jones PL, Li Q, Mohler ER, 3rd, Schoen FJ, and Levy RJ**. Matrix metalloproteinase-2 is associated with tenascin-C in calcific aortic stenosis. *Am J Pathol* 159: 321-327, 2001.

113. **Jian B, Narula N, Li QY, Mohler ER, 3rd, and Levy RJ**. Progression of aortic valve stenosis: TGF-beta1 is present in calcified aortic valve cusps and promotes aortic valve interstitial cell calcification via apoptosis. *Ann Thorac Surg* 75: 457-465; discussion 465-456, 2003.

114. **Jian B, Xu J, Connolly J, Savani RC, Narula N, Liang B, and Levy RJ**. Serotonin mechanisms in heart valve disease I: serotonin-induced up-regulation of transforming growth factor-beta1 via G-protein signal transduction in aortic valve interstitial cells. *The American journal of pathology* 161: 2111-2121, 2002.

115. **Jo H, Sipos K, Go YM, Law R, Rong J, and McDonald JM**. Differential effect of shear stress on extracellular signal-regulated kinase and N-terminal Jun kinase in endothelial cells. Gi2- and Gbeta/gamma-dependent signaling pathways. *The Journal of biological chemistry* 272: 1395-1401, 1997.

116. **Jo H, Song H, and Mowbray A**. Role of NADPH oxidases in disturbed flow- and BMP4- induced inflammation and atherosclerosis. *Antioxid Redox Signal* 8: 1609-1619, 2006.

117. **Jo H, Song H, and Mowbray A**. Role of NADPH oxidases in disturbed flow- and BMP4-induced inflammation and atherosclerosis. *Antioxidants and Reactive Oxygen Species* In press: 2006.

118. **Junqueira LC, Bignolas G, and Brentani RR**. Picrosirius staining plus polarization microscopy, a specific method for collagen detection in tissue sections. *Histochem J* 11: 447-455, 1979.

119. **Kaden JJ, Dempfle CE, Grobholz R, Fischer CS, Vocke DC, Kilic R, Sarikoc A, Pinol R, Hagl S, Lang S, Brueckmann M, and Borggrefe M**. Inflammatory regulation of extracellular matrix remodeling in calcific aortic valve stenosis. *Cardiovasc Pathol* 14: 80-87, 2005.

120. **Kim KM, Valigorsky JM, Mergner WJ, Jones RT, Pendergrass RF, and Trump BF**. Aging changes in the human aortic valve in relation to dystrophic calcification. *Hum Pathol* 7: 47-60, 1976.

121. **Kimmel SE, Keane MG, Crary JL, Jones J, Kinman JL, Beare J, Sammel M, Sutton MS, and Strom BL**. Detailed examination of fenfluramine-phentermine users with valve abnormalities identified in Fargo, North Dakota. *The American journal of cardiology* 84: 304-308, 1999.

122. **Kitamoto S, Sukhova GK, Sun J, Yang M, Libby P, Love V, Duramad P, Sun C, Zhang Y, Yang X, Peters C, and Shi GP**. Cathepsin L deficiency reduces diet-induced atherosclerosis in low-density lipoprotein receptor-knockout mice. *Circulation* 115: 2065-2075, 2007.

123. **Knowles ID, and Ramage AG**. Evidence that activation of central 5-HT(2B) receptors causes renal sympathoexcitation in anaesthetized rats. *Br J Pharmacol* 129: 177-183, 2000.

124. **Konduri S, Xing Y, Warnock JN, He Z, and Yoganathan AP**. Normal physiological conditions maintain the biological characteristics of porcine aortic heart valves: an ex vivo organ culture study. *Ann Biomed Eng* 33: 1158-1166, 2005.

125. **Ku CH, Johnson PH, Batten P, Sarathchandra P, Chambers RC, Taylor PM, Yacoub MH, and Chester AH**. Collagen synthesis by mesenchymal stem cells and aortic valve interstitial cells in response to mechanical stretch. *Cardiovasc Res* 2006.

126. **Ku CH, Johnson PH, Batten P, Sarathchandra P, Chambers RC, Taylor PM, Yacoub MH, and Chester AH**. Collagen synthesis by mesenchymal stem cells and aortic valve interstitial cells in response to mechanical stretch. *Cardiovasc Res* 71: 548-556, 2006.

127. **Ku DN, Giddens DP, Zarins CK, and Glagov S**. Pulsatile flow and atherosclerosis in the human carotid bifurcation. Positive correlation between plaque location and low oscillating shear stress. *Arteriosclerosis* 5: 293-302, 1985.

128. **Langer R, and Vacanti JP**. Tissue engineering. *Science* 260: 920-926, 1993.

129. **Lee JM, Courtman DW, and Boughner DR**. The glutaraldehyde-stabilized porcine aortic valve xenograft. I. Tensile viscoelastic properties of the fresh leaflet material. *J Biomed Mater Res* 18: 61-77, 1984.

130. **Lee YS, and Chou YY**. Pathogenetic mechanism of senile calcific aortic stenosis: the role of apoptosis. *Chin Med J (Engl)* 111: 934-939, 1998.

131. **Leskinen Y, Paana T, Saha H, Groundstroem K, Lehtimaki T, Kilpinen S, Huhtala H, and Airaksinen J**. Valvular calcification and its relationship to atherosclerosis in chronic kidney disease. *J Heart Valve Dis* 18: 429-438, 2009.

132. **Lester WM, Damji AA, Gedeon I, and Tanaka M**. Interstitial cells from the atrial and ventricular sides of the bovine mitral valve respond differently to denuding endocardial injury. *In Vitro Cell Dev Biol* 29A: 41-50, 1993.

133. **Lester WM, Damji AA, Tanaka M, and Gedeon I**. Bovine mitral valve organ culture: role of interstitial cells in repair of valvular injury. *J Mol Cell Cardiol* 24: 43-53, 1992.

134. **Levy FO, Qvigstad E, Krobert KA, Skomedal T, and Osnes JB**. Effects of serotonin in failing cardiac ventricle: signalling mechanisms and potential therapeutic implications. *Neuropharmacology* 55: 1066-1071, 2008.

135. **Levy RJ**. Serotonin transporter mechanisms and cardiac disease. *Circulation* 113: 2-4, 2006.

136. **Li RH, and Wozney JM**. Delivering on the promise of bone morphogenetic proteins. *Trends Biotechnol* 19: 255-265, 2001.

137. **Liang YJ, Lai LP, Wang BW, Juang SJ, Chang CM, Leu JG, and Shyu KG**. Mechanical stress enhances serotonin 2B receptor modulating brain natriuretic peptide through nuclear factor-kappaB in cardiomyocytes. *Cardiovasc Res* 72: 303-312, 2006.

138. **Liu AC, and Gotlieb AI**. Characterization of cell motility in single heart valve interstitial cells in vitro. *Histology and histopathology* 22: 873-882, 2007.

139. **Liu AC, and Gotlieb AI**. Transforming growth factor-beta regulates in vitro heart valve repair by activated valve interstitial cells. *The American journal of pathology* 173: 1275-1285, 2008.

140. **Liu AC, Joag VR, and Gotlieb AI**. The emerging role of valve interstitial cell phenotypes in regulating heart valve pathobiology. *The American journal of pathology* 171: 1407-1418, 2007.

141. **Lo D, and Vesely I**. Biaxial strain analysis of the porcine aortic valve. *Ann Thorac Surg* 60: S374-378, 1995.

142. **Lomashvili K, Garg P, and O'Neill WC**. Chemical and hormonal determinants of vascular calcification in vitro. *Kidney international* 69: 1464-1470, 2006.

143. **Lomashvili KA, Cobbs S, Hennigar RA, Hardcastle KI, and O'Neill WC**. Phosphate-induced vascular calcification: role of pyrophosphate and osteopontin. *J Am Soc Nephrol* 15: 1392-1401, 2004.

144. **MacDonald A**. Ion channels under high pressure. *Comp Biochem Physiol A Mol Integr Physiol* 131: 587-593, 2002.

145. **Manduteanu I, Popov D, Radu A, and Simionescu M**. Calf cardiac valvular endothelial cells in culture: production of glycosaminoglycans, prostacyclin and fibronectin. *J Mol Cell Cardiol* 20: 103-118, 1988.

146. **Massague J**. How cells read TGF-beta signals. *Nat Rev Mol Cell Biol* 1: 169-178, 2000.

147. **Massague J**. TGF-beta signal transduction. *Annu Rev Biochem* 67: 753-791, 1998.

148. **Mayne AS, Christie GW, Smaill BH, Hunter PJ, and Barratt-Boyes BG**. An assessment of the mechanical properties of leaflets from four second-generation porcine bioprostheses with biaxial testing techniques. *J Thorac Cardiovasc Surg* 98: 170-180, 1989.

149. **Mekontso-Dessap A, Brouri F, Pascal O, Lechat P, Hanoun N, Lanfumey L, Seif I, Benhaiem-Sigaux N, Kirsch M, Hamon M, Adnot S, and Eddahibi S**. Deficiency of the 5-hydroxytryptamine transporter gene leads to cardiac fibrosis and valvulopathy in mice. *Circulation* 113: 81-89, 2006.

150. **Merryman WD, Huang HY, Schoen FJ, and Sacks MS**. The effects of cellular contraction on aortic valve leaflet flexural stiffness. *J Biomech* 39: 88-96, 2006.

151. **Merryman WD, Lukoff HD, Long RA, Engelmayr GC, Jr., Hopkins RA, and Sacks MS**. Synergistic effects of cyclic tension and transforming growth factor-beta1 on the aortic valve myofibroblast. *Cardiovasc Pathol* 16: 268-276, 2007.

152. **Merryman WD, Youn I, Lukoff HD, Krueger PM, Guilak F, Hopkins RA, and Sacks MS**. Correlation between heart valve interstitial cell stiffness and transvalvular pressure: Implications for collagen biosynthesis. *Am J Physiol Heart Circ Physiol* 2005.

153. **Metzler SA, Pregonero CA, Butcher JT, Burgess SC, and Warnock JN**. Cyclic strain regulates pro-inflammatory protein expression in porcine aortic valve endothelial cells. *J Heart Valve Dis* 17: 571-577; discussion 578, 2008.

154. **Miriyala S, Gongora Nieto MC, Mingone C, Smith D, Dikalov S, Harrison DG, and Jo H**. Bone morphogenic protein-4 induces hypertension in mice: role of noggin, vascular NADPH oxidases, and impaired vasorelaxation. *Circulation* 113: 2818-2825, 2006.

155. **Mirnajafi A, Raymer JM, McClure LR, and Sacks MS**. The flexural rigidity of the aortic valve leaflet in the commissural region. *J Biomech* 39: 2966-2973, 2006.

156. **Missirlis YF, and Armeniades CD**. Stress analysis of the aortic valve during diastole: important parameters. *J Biomech* 9: 477-480, 1976.

157. **Missirlis YF, and Chong M**. Aortic valve mechanics--Part I: material properties of natural porcine aortic valves. *J Bioeng* 2: 287-300, 1978.

158. **Mohler ER, 3rd**. Are atherosclerotic processes involved in aortic-valve calcification? *Lancet* 356: 524-525, 2000.

159. **Mohler ER, 3rd**. Mechanisms of aortic valve calcification. *The American journal of cardiology* 94: 1396-1402, A1396, 2004.

160. **Mohler ER, 3rd, Chawla MK, Chang AW, Vyavahare N, Levy RJ, Graham L, and Gannon FH**. Identification and characterization of calcifying valve cells from human and canine aortic valves. *J Heart Valve Dis* 8: 254-260, 1999.

161. **Mohler ER, 3rd, Gannon F, Reynolds C, Zimmerman R, Keane MG, and Kaplan FS**. Bone formation and inflammation in cardiac valves. *Circulation* 103: 1522-1528, 2001.

162. **Mohler ER, Sheridan MJ, Nichols R, Harvey WP, and Waller BF**. Development and progression of aortic valve stenosis: atherosclerosis risk factors--a causal relationship? A clinical morphologic study. *Clin Cardiol* 14: 995-999, 1991.

163. **Movat HZ**. Demonstration of all connective tissue elements in a single section; pentachrome stains. *AMA Arch Pathol* 60: 289-295, 1955.

164. **Mulholland DL, and Gotlieb AI**. Cell biology of valvular interstitial cells. *Can J Cardiol* 12: 231-236, 1996.

165. **Nebigil CG, Hickel P, Messaddeq N, Vonesch JL, Douchet MP, Monassier L, Gyorgy K, Matz R, Andriantsitohaina R, Manivet P, Launay JM, and Maroteaux L**. Ablation of serotonin 5-HT(2B) receptors in mice leads to abnormal cardiac structure and function. *Circulation* 103: 2973-2979, 2001.

166. **Nemecek GM, Coughlin SR, Handley DA, and Moskowitz MA**. Stimulation of aortic smooth muscle cell mitogenesis by serotonin. *Proc Natl Acad Sci U S A* 83: 674-678, 1986.

167. **Niklason LE, Abbott W, Gao J, Klagges B, Hirschi KK, Ulubayram K, Conroy N, Jones R, Vasanawala A, Sanzgiri S, and Langer R**. Morphologic and mechanical characteristics of engineered bovine arteries. *J Vasc Surg* 33: 628-638, 2001.

168. **Niklason LE, Gao J, Abbott WM, Hirschi KK, Houser S, Marini R, and Langer R**. Functional arteries grown in vitro. *Science* 284: 489-493, 1999.

169. **Niklason LE, and Langer RS**. Advances in tissue engineering of blood vessels and other tissues. *Transplant immunology* 5: 303-306, 1997.

170. **Nishimura RA**. Cardiology patient pages. Aortic valve disease. *Circulation* 106: 770-772, 2002.

171. **O'Brien KD**. Pathogenesis of calcific aortic valve disease: a disease process comes of age (and a good deal more). *Arterioscler Thromb Vasc Biol* 26: 1721-1728, 2006.

172. **O'Brien KD, Reichenbach DD, and Marcovina SM**. Apolipoproteins B, (a), and E accumulate in the morphologically early lesion of 'degenerative' valvular aortic stenosis. *Arterioscel Thromb Vasc Biol* 16: 523-532, 1996.

173. **O'Brien KD, Reichenbach DD, Marcovina SM, Kuusisto J, Alpers CE, and Otto CM**. Apolipoproteins B, (a), and E accumulate in the morphologically early lesion of 'degenerative' valvular aortic stenosis. *Arterioscler Thromb Vasc Biol* 16: 523-532, 1996.

174. **O'Brien MF, McGiffin DC, Stafford EG, Gardner MA, Pohlner PF, McLachlan GJ, Gall K, Smith S, and Murphy E**. Allograft aortic valve replacement: long-term comparative clinical analysis of the viable cryopreserved and antibiotic 4 degrees C stored valves. *Journal of cardiac surgery* 6: 534-543, 1991.

175. **O'Brien MF, Stafford EG, Gardner MA, Pohlner PG, Tesar PJ, Cochrane AD, Mau TK, Gall KL, and Smith SE**. Allograft aortic valve replacement: long-term follow-up. *Ann Thorac Surg* 60: S65-70, 1995.

176. **Oshinski JN, Ku DN, Mukundan S, Jr., Loth F, and Pettigrew RI**. Determination of wall shear stress in the aorta with the use of MR phase velocity mapping. *J Magn Reson Imaging* 5: 640-647, 1995.

177. **Osman L, Chester AH, Amrani M, Yacoub MH, and Smolenski RT**. A novel role of extracellular nucleotides in valve calcification: a potential target for atorvastatin. *Circulation* 114: I566-572, 2006.

178. **Osman L, Chester AH, Sarathchandra P, Latif N, Meng W, Taylor PM, and Yacoub MH**. A novel role of the sympatho-adrenergic system in regulating valve calcification. *Circulation* 116: I282-287, 2007.

179. **Osman L, Yacoub MH, Latif N, Amrani M, and Chester AH**. Role of human valve interstitial cells in valve calcification and their response to atorvastatin. *Circulation* 114: I547-552, 2006.

180. **Otto CM**. Calcific aortic stenosis--time to look more closely at the valve. *The New England journal of medicine* 359: 1395-1398, 2008.

181. **Otto CM**. Calcification of bicuspid aortic valves. *Heart* 88: 321-322, 2002.

182. **Otto CM, Kuusisto J, and Reichenbach DD**. Characterization of the early lesion of 'degenerative' valvular aortic stenosis. Histological and immunohistochemical studies. *Circulation* 90: 844-853, 1994.

183. **Otto CM, Kuusisto J, Reichenbach DD, Gown AM, and O'Brien KD**. Characterization of the early lesion of 'degenerative' valvular aortic stenosis. Histological and immunohistochemical studies. *Circulation* 90: 844-853, 1994.

184. **Pai RG**. Degenerative valve disease. *J Am Coll Cardiol* 48: 2601; author reply 2602, 2006.

185. **Park SZ, and Reardon MJ**. Current status of stentless aortic xenografts. *Current opinion in cardiology* 15: 74-81, 2000.

186. **Pena-Silva RA, Miller JD, Chu Y, and Heistad DD**. Serotonin produces monoamine oxidase-dependent oxidative stress in human heart valves. *Am J Physiol Heart Circ Physiol* 297: H1354-1360, 2009.

187. **Platt MO, Ankeny RF, and Jo H**. Laminar shear stress inhibits cathepsin L activity in endothelial cells. *Arterioscler Thromb Vasc Biol* 26: 1784-1790, 2006.

188. **Platt MO, Ankeny RF, Shi GP, Weiss D, Taylor WR, Vega JD, and Jo H**. Expression of cathepsin K is regulated by shear stress in cultured endothelial cells and is increased in endothelium in human atherosclerosis. *Am J Physiol Heart Circ Physiol* 2006.

189. **Platt MO, Xing Y, Jo H, and Yoganathan AP**. Cyclic pressure and shear stress regulate matrix metalloproteinases and cathepsin activity in porcine aortic valves. *J Heart Valve Dis* 15: 622-629, 2006.

190. **Poggianti E, Venneri L, Chubuchny V, Jambrik Z, Baroncini LA, and Picano E**. Aortic valve sclerosis is associated with systemic endothelial dysfunction. *J Am Coll Cardiol* 41: 136-141, 2003.

191. **Rabkin E, Aikawa M, Stone JR, Fukumoto Y, Libby P, and Schoen FJ**. Activated interstitial myofibroblasts express catabolic enzymes and mediate matrix remodeling in myxomatous heart valves. *Circulation* 104: 2525-2532, 2001.

192. **Rabkin E, Hoerstrup SP, Aikawa M, Mayer JE, Jr., and Schoen FJ**. Evolution of cell phenotype and extracellular matrix in tissue-engineered heart valves during in-vitro maturation and in-vivo remodeling. *J Heart Valve Dis* 11: 308-314; discussion 314, 2002.

193. **Rabkin SW**. The association of hypertension and aortic valve sclerosis. *Blood Press* 14: 264-272, 2005.

194. **Rajamannan NM, Caplice N, Anthikad F, Sebo TJ, Orszulak TA, Edwards WD, Tajik J, and Schwartz RS**. Cell proliferation in carcinoid valve disease: a mechanism for serotonin effects. *J Heart Valve Dis* 10: 827-831, 2001.

195. **Rajamannan NM, Gersh B, and Bonow RO**. Calcific aortic stenosis: from bench to the bedside--emerging clinical and cellular concepts. *Heart* 89: 801-805, 2003.

196. **Rajamannan NM, Sangiorgi G, Springett M, Arnold K, Mohacsi T, Spagnoli LG, Edwards WD, Tajik AJ, and Schwartz RS**. Experimental hypercholesterolemia induces apoptosis in the aortic valve. *J Heart Valve Dis* 10: 371-374, 2001.

197. **Rajamannan NM, Subramaniam M, Rickard D, Stock SR, Donovan J, Springett M, Orszulak T, Fullerton DA, Tajik AJ, Bonow RO, and Spelsberg T**. Human aortic valve calcification is associated with an osteoblast phenotype. *Circulation* 107: 2181-2184, 2003.

198. **Rajamannan NM, Subramaniam M, Springett M, Sebo TC, Niekrasz M, McConnell JP, Singh RJ, Stone NJ, Bonow RO, and Spelsberg TC**. Atorvastatin inhibits hypercholesterolemia-induced cellular proliferation and bone matrix production in the rabbit aortic valve. *Circulation* 105: 2660-2665, 2002.

199. **Rajamannan NM, Subramaniam M, Stock SR, Stone NJ, Springett M, Ignatiev KI, McConnell JP, Singh RJ, Bonow RO, and Spelsberg TC**. Atorvastatin inhibits calcification and enhances nitric oxide synthase production in the hypercholesterolaemic aortic valve. *Heart* 91: 806-810, 2005.

200. **Regan KL**. Depression treatment with selective serotonin reuptake inhibitors for the postacute coronary syndrome population: a literature review. *J Cardiovasc Nurs* 23: 489-496, 2008.

201. **Renkiewicz R, Qiu L, Lesch C, Sun X, Devalaraja R, Cody T, Kaldjian E, Welgus H, and Baragi V**. Broad-spectrum matrix metalloproteinase inhibitor marimastat-induced musculoskeletal side effects in rats. *Arthritis Rheum* 48: 1742-1749, 2003.

202. **Roberts WC**. The congenitally bicuspid aortic valve. A study of 85 autopsy cases. *Am J Cardiol* 26: 72-83, 1970.

203. **Robicsek F, and Thubrikar MJ**. Mechanical stress as cause of aortic valve disease. Presentation of a new aortic root prosthesis. *Acta chirurgica Belgica* 102: 1-6, 2002.

204. **Robicsek F, Thubrikar MJ, Cook JW, and Fowler B**. The congenitally bicuspid aortic valve: how does it function? Why does it fail? *Ann Thorac Surg* 77: 177-185, 2004.

205. **Rose AG**. Etiology of valvular heart disease. *Current opinion in cardiology* 11: 98-113, 1996.

206. **Rothman RB, Baumann MH, Savage JE, Rauser L, McBride A, Hufeisen SJ, and Roth BL**. Evidence for possible involvement of 5-HT(2B) receptors in the cardiac

valvulopathy associated with fenfluramine and other serotonergic medications. *Circulation* 102: 2836-2841, 2000.

207. **Roy A, Brand NJ, and Yacoub MH**. Expression of 5-hydroxytryptamine receptor subtype messenger RNA in interstitial cells from human heart valve. *Journal of Heart Valve Disease* 9: 256-260, 2000.

208. **Sackin H**. Stretch-activated ion channels. *Kidney international* 48: 1134-1147, 1995.

209. **Sacks MS, David Merryman W, and Schmidt DE**. On the biomechanics of heart valve function. *J Biomech* 42: 1804-1824, 2009.

210. **Sacks MS, and Schoen FJ**. Collagen fiber disruption occurs independent of calcification in clinically explanted bioprosthetic heart valves. *J Biomed Mater Res* 62: 359-371, 2002.

211. **Sacks MS, Smith DB, and Hiester ED**. The aortic valve microstructure: effects of transvalvular pressure. *J Biomed Mater Res* 41: 131-141, 1998.

212. **Sacks MS, and Yoganathan AP**. Heart valve function: a biomechanical perspective. *Philosophical transactions of the Royal Society of London* 362: 1369-1391, 2007.

213. **Salwen S, Szarowski D, Turner J, and Bizios R**. Three-dimentional changes of the cytoskeleton of vascular endothelial cells exposed to sustained hydrostatic pressure. *Transplant Proceedings* 33: 66-68, 2001.

214. **Sarsam MA, and Yacoub M**. Remodeling of the aortic valve anulus. *J Thorac Cardiovasc Surg* 105: 435-438, 1993.

215. **Schneider PJ, and Deck JD**. Tissue and cell renewal in the natural aortic valve of rats: an autoradiographic study. *Cardiovasc Res* 15: 181-189, 1981.

216. **Schnitzler MMY, Storch U, Meibers S, Nurwakagari P, Breit A, Essin K, Gollasch M, and Gudermann T**. G(q)-coupled receptors as mechanosensors mediating myogenic vasoconstriction. *Embo Journal* 27: 3092-3103, 2008.

217. **Schoen FJ**. Aortic valve structure-function correlations: role of elastic fibers no longer a stretch of the imagination. *J Heart Valve Dis* 6: 1-6, 1997.

218. **Schoen FJ, and Levy RJ**. Founder's Award, 25th Annual Meeting of the Society for Biomaterials, perspectives. Providence, RI, April 28-May 2, 1999. Tissue heart valves: current challenges and future research perspectives. *J Biomed Mater Res* 47: 439-465, 1999.

219. **Schwartz E, Bizios R, Medow M, and Gerritsen M**. Exposure of human vascular endothelial cells to sustained hydrostatic pressure stimulates proliferation: Involvement of the α-v integrins. *Circulation Research* 84: 315-322, 1999.

220. **Scott M, and Vesely I**. Aortic valve cusp microstructure: the role of elastin. *Ann Thorac Surg* 60: S391-394, 1995.

221. **Shao JS, Cai J, and Towler DA**. Molecular mechanisms of vascular calcification: lessons learned from the aorta. *Arterioscler Thromb Vasc Biol* 26: 1423-1430, 2006.

222. **Shappell SD**. Valvular heart diseases http://www.heartcenteronline.com/myheartdr/common/articles.cfm?ARTID=187. (12/09)

223. **Shin H, Smith M, TOY K, WILLIAMS P, Bizios R, and Gerritsen M**. VEGF-C mediates cyclic pressure-induced endothelial cell proliferation. *Physiol Genomics* 11: 245-251, 2002.

224. **Shum-Tim D, Stock U, Hrkach J, Shinoka T, Lien J, Moses MA, Stamp A, Taylor G, Moran AM, Landis W, Langer R, Vacanti JP, and Mayer JE, Jr.** Tissue engineering of autologous aorta using a new biodegradable polymer. *Ann Thorac Surg* 68: 2298-2304; discussion 2305, 1999.

225. **Shyy J, and Chien S**. Role of integrins in endothelial mechanosensing of shear stress. *Circulation Research* 91: 2002.

226. **Simmons CA, Grant GR, Manduchi E, and Davies PF**. Spatial heterogeneity of endothelial phenotypes correlates with side-specific vulnerability to calcification in normal porcine aortic valves. *Circ Res* 96: 792-799, 2005.

227. **Simmons CA, Grant GR, Manduchi E, and Davies PF**. Spatial heterogeneity of endothelial phenotypes correlates with side-specific vulnerability to calcification in normal porcine aortic valves. *Circ Res* 96: 792-799, 2005.

228. **Simmons CA, Zilberberg J, and Davies PF**. A rapid, reliable method to isolate high quality endothelial RNA from small spatially-defined locations. *Ann Biomed Eng* 32: 1453-1459, 2004.

229. **Simon A, Wilhelmi M, Steinhoff G, Harringer W, Brucke P, and Haverich A**. Cardiac valve endothelial cells: relevance in the long-term function of biologic valve prostheses. *J Thorac Cardiovasc Surg* 116: 609-616, 1998.

230. **Siney L, and Lewis MJ**. Nitric oxide release from porcine mitral valves. *Cardiovasc Res* 27: 1657-1661, 1993.

231. **Sodian R, Sperling JS, Martin DP, Egozy A, Stock U, Mayer JE, Jr., and Vacanti JP**. Fabrication of a trileaflet heart valve scaffold from a polyhydroxyalkanoate biopolyester for use in tissue engineering. *Tissue Eng* 6: 183-188, 2000.

232. **Sodian R, Sperling JS, Martin DP, Stock U, Mayer JE, Jr., and Vacanti JP**. Tissue engineering of a trileaflet heart valve-early in vitro experiences with a combined polymer. *Tissue Eng* 5: 489-494, 1999.

233. **Somero G**. *Environmental and metabolic animal physiology*. New York: Wiley Liss, 1991, p. 167-204.

234. **Sorescu GP, Song H, Tressel SL, Hwang J, Dikalov S, Smith DA, Boyd NL, Platt MO, Lassegue B, Griendling KK, and Jo H**. Bone morphogenic protein 4 produced in endothelial cells by oscillatory shear stress induces monocyte adhesion by stimulating reactive oxygen species production from a nox1-based NADPH oxidase. *Circ Res* 95: 773-779, 2004.

235. **Sorescu GP, Sykes M, Weiss D, Platt MO, Saha A, Hwang J, Boyd N, Boo YC, Vega JD, Taylor WR, and Jo H**. Bone morphogenic protein 4 produced in endothelial cells by oscillatory shear stress stimulates an inflammatory response. *J Biol Chem* 278: 31128-31135, 2003.

236. **Spies C, Madison JR, and Schatz IJ**. Infective endocarditis in patients with end-stage renal disease: clinical presentation and outcome. *Arch Intern Med* 164: 71-75, 2004.

237. **Steinhoff G, Stock U, Karim N, Mertsching H, Timke A, Meliss RR, Pethig K, Haverich A, and Bader A**. Tissue engineering of pulmonary heart valves on allogenic acellular matrix conduits: in vivo restoration of valve tissue. *Circulation* 102: III50-55, 2000.

238. **Stella JA, Liao J, and Sacks MS**. Time-dependent biaxial mechanical behavior of the aortic heart valve leaflet. *J Biomech* 40: 3169-3177, 2007.

239. **Stella JA, and Sacks MS**. On the biaxial mechanical properties of the layers of the aortic valve leaflet. *J Biomech Eng* 129: 757-766, 2007.

240. **Stephens EH, de Jonge N, McNeill MP, Durst CA, and Grande-Allen KJ**. Age-Related Changes in Material Behavior of Porcine Mitral and Aortic Valves and Correlation to Matrix Composition. *Tissue Eng Part A* 2009.

241. **Stewart BF, Siscovick D, Lind BK, Gardin JM, Gottdiener JS, Smith VE, Kitzman DW, and Otto CM**. Clinical factors associated with calcific aortic valve disease. Cardiovascular Health Study. *J Am Coll Cardiol* 29: 630-634, 1997.

242. **Stock UA, and Schenke-Layland K**. Performance of decellularized xenogeneic tissue in heart valve replacement. *Biomaterials* 27: 1-2, 2006.

243. **Sucosky P, Balachandran K, Elhammali A, Jo H, and Yoganathan AP**. Altered shear stress stimulates upregulation of endothelial VCAM-1 and ICAM-1 in a BMP-4- and TGF-beta1-dependent pathway. *Arterioscler Thromb Vasc Biol* 29: 254-260, 2009.

244. **Sukhova GK, Shi GP, Simon DI, Chapman HA, and Libby P**. Expression of the elastolytic cathepsins S and K in human atheroma and regulation of their production in smooth muscle cells. *The Journal of clinical investigation* 102: 576-583, 1998.

245. **Sukhova GK, Zhang Y, Pan JH, Wada Y, Yamamoto T, Naito M, Kodama T, Tsimikas S, Witztum JL, Lu ML, Sakara Y, Chin MT, Libby P, and Shi GP**. Deficiency of cathepsin S reduces atherosclerosis in LDL receptor-deficient mice. *J Clin Invest* 111: 897-906, 2003.

246. **Tanaka K, Sata M, Fukuda D, Suematsu Y, Motomura N, Takamoto S, Hirata Y, and Nagai R**. Age-associated aortic stenosis in apolipoprotein E-deficient mice. *J Am Coll Cardiol* 46: 134-141, 2005.

247. **Taylor PM, Allen SP, and Yacoub MH**. Phenotypic and functional characterization of interstitial cells from human heart valves, pericardium and skin. *J Heart Valve Dis* 9: 150-158, 2000.

248. **Taylor PM, Batten P, Brand NJ, Thomas PS, and Yacoub MH**. The cardiac valve interstitial cell. *Int J Biochem Cell Biol* 35: 113-118, 2003.

249. **Taylor PM, Sachlos E, Dreger SA, Chester AH, Czernuszka JT, and Yacoub MH**. Interaction of human valve interstitial cells with collagen matrices manufactured using rapid prototyping. *Biomaterials* 27: 2733-2737, 2006.

250. **Thubrikar M**. *The aortic valve*. Boca Raton, Fla.: CRC Press, 1990, p. 221 p.

251. **Thubrikar M, Bosher LP, and Nolan SP**. The mechanism of opening of the aortic valve. *J Thorac Cardiovasc Surg* 77: 863-870, 1979.

252. **Thubrikar M, Nolan SP, Bosher LP, and Deck JD**. The cyclic changes and structure of the base of the aortic valve. *Am Heart J* 99: 217-224, 1980.

253. **Thubrikar M, Piepgrass WC, Shaner TW, and Nolan SP**. The design of the normal aortic valve. *Am J Physiol* 241: H795-801, 1981.

254. **Thubrikar MJ, Aouad J, and Nolan SP**. Comparison of the in vivo and in vitro mechanical properties of aortic valve leaflets. *J Thorac Cardiovasc Surg* 92: 29-36, 1986.

255. **Thubrikar MJ, Heckman JL, and Nolan SP**. High speed cine-radiographic study of aortic valve leaflet motion. *J Heart Valve Dis* 2: 653-661, 1993.

256. **Thubrikar MJ, Nolan SP, Aouad J, and Deck JD**. Stress sharing between the sinus and leaflets of canine aortic valve. *Ann Thorac Surg* 42: 434-440, 1986.

257. **Thubrikar MJ, Skinner JR, Eppink RT, and Nolan SP**. Stress analysis of porcine bioprosthetic heart valves in vivo. *J Biomed Mater Res* 16: 811-826, 1982.

258. **Tokuhiro A, Maekawa M, Iizuka K, Hishida K, and M. M**. Turbulent flow past a bubble and an ellipsoid using shadow-image and PIV techniques. *International Journal of Multiphase Flow* 24: 1383-1406, 1998.

259. **Tokunaga O, and Watanabe T**. Properties of endothelial cell and smooth muscle cell cultured in ambient pressure. *In Vitro Cell Dev Biol* 23: 528-534, 1987.

260. **Vesely I**. The role of elastin in aortic valve mechanics. *J Biomech* 31: 115-123, 1998.

261. **Vesely I, and Lozon A**. Natural preload of aortic valve leaflet components during glutaraldehyde fixation: effects on tissue mechanics. *J Biomech* 26: 121-131, 1993.

262. **Vesely I, and Noseworthy R**. Micromechanics of the fibrosa and the ventricularis in aortic valve leaflets. *J Biomech* 25: 101-113, 1992.

263. **Vlessis AA, Khaki A, Grunkemeier GL, Li HH, and Starr A**. Risk, diagnosis and management of prosthetic valve endocarditis: a review. *J Heart Valve Dis* 6: 443-465, 1997.

264. **Vouyouka AG, Jiang Y, and Basson MD**. Pressure alters endothelial effects upon vascular smooth muscle cells by decreasing smooth muscle cell proliferation and increasing smooth muscle cell apoptosis. *Surgery* 136: 282-290, 2004.

265. **Vouyouka AG, Salib SS, Cala S, Marsh JD, and Basson MD**. Chronic high pressure potentiates the antiproliferative effect and abolishes contractile phenotypic changes caused by endothelial cells in cocultured smooth muscle cells. *The Journal of surgical research* 110: 344-351, 2003.

266. **Walker GA, Masters KS, Shah DN, Anseth KS, and Leinwand LA**. Valvular myofibroblast activation by transforming growth factor-beta: implications for pathological extracellular matrix remodeling in heart valve disease. *Circ Res* 95: 253-260, 2004.

267. **Warnock JN, Burgess SC, Shack A, and Yoganathan AP**. Differential immediate-early gene responses to elevated pressure in porcine aortic valve interstitial cells. *J Heart Valve Dis* 15: 34-41; discussion 42, 2006.

268. **Weber KT, Sun Y, Katwa LC, Cleutjens JP, and Zhou G**. Connective tissue and repair in the heart. Potential regulatory mechanisms. *Ann N Y Acad Sci* 752: 286-299, 1995.

269. **Weston MW, Goldstein S, Epting RE, 2nd, He S, Mauldin JM, and Yoganathan AP**. Establishing a protocol to quantify leaflet fibroblast responses to physiologic flow through a viable heart valve. *Asaio J* 43: M377-382, 1997.

270. **Weston MW, LaBorde DV, and Yoganathan AP**. Estimation of the shear stress on the surface of an aortic valve leaflet. *Ann Biomed Eng* 27: 572-579, 1999.

271. **Weston MW, and Yoganathan AP**. Biosynthetic activity in heart valve leaflets in response to in vitro flow environments. *Ann Biomed Eng* 29: 752-763, 2001.

272. **Willems IE, Havenith MG, Smits JF, and Daemen MJ**. Structural alterations in heart valves during left ventricular pressure overload in the rat. *Lab Invest* 71: 127-133, 1994.

273. **Wu B, Elmariah S, Kaplan FS, Cheng G, and Mohler ER, 3rd**. Paradoxical effects of statins on aortic valve myofibroblasts and osteoblasts: implications for end-stage valvular heart disease. *Arterioscler Thromb Vasc Biol* 25: 592-597, 2005.

274. **Xing Y**. Effects of mechanical forces on the biological properties of porcine aortic valve leaflets. 2004.

275. **Xing Y, He Z, Warnock JN, Hilbert SL, and Yoganathan AP**. Effects of constant static pressure on the biological properties of porcine aortic valve leaflets. *Ann Biomed Eng* 32: 555-562, 2004.

276. **Xing Y, Warnock JN, He Z, Hilbert SL, and Yoganathan AP**. Cyclic pressure affects the biological properties of porcine aortic valve leaflets in a magnitude and frequency dependent manner. *Ann Biomed Eng* 32: 1461-1470, 2004.

277. **Xu J, Jian B, Chu R, Lu Z, Li Q, Dunlop J, Rosenzweig-Lipson S, McGonigle P, Levy RJ, and Liang B**. Serotonin mechanisms in heart valve disease II: the 5-HT2 receptor and its signaling pathway in aortic valve interstitial cells. *The American journal of pathology* 161: 2209-2218, 2002.

278. **Yacoub MH, and Cohn LH**. Novel approaches to cardiac valve repair: from structure to function: Part I. *Circulation* 109: 942-950, 2004.

279. **Yacoub MH, and Takkenberg JJ**. Will heart valve tissue engineering change the world? *Nature clinical practice* 2: 60-61, 2005.

280. **Yap CH, Kim HS, Balachandran K, Weiler MJ, Haj-Ali R, and Yoganathan AP**. Dynamic Deformation Characteristics of Porcine Aortic Valve Leaflet under Normal and Hypertensive Conditions. *Am J Physiol Heart Circ Physiol* 2009.

281. **Yip CY, Chen JH, Zhao R, and Simmons CA**. Calcification by Valve Interstitial Cells Is Regulated by the Stiffness of the Extracellular Matrix. *Arterioscler Thromb Vasc Biol* 2009.

282. **Yoganathan AP, Chandran KB, and Sotiropoulos F**. Flow in prosthetic heart valves: state-of-the-art and future directions. *Ann Biomed Eng* 33: 1689-1694, 2005.

283. **Zanettini R, Antonini A, Gatto G, Gentile R, Tesei S, and Pezzoli G**. Valvular heart disease and the use of dopamine agonists for Parkinson's disease. *The New England journal of medicine* 356: 39-46, 2007.

284. **Zarins CK, Zatina MA, Giddens DP, Ku DN, and Glagov S**. Shear stress regulation of artery lumen diameter in experimental atherogenesis. *J Vasc Surg* 5: 413-420, 1987.

285. **Zimmerman LB, De Jesus-Escobar JM, and Harland RM**. The Spemann organizer signal noggin binds and inactivates bone morphogenetic protein 4. *Cell* 86: 599-606, 1996.